

ULTRAMAFIC ROCKS AND ASSOCIATED
COPPER-NICKEL SULPHIDE ORES,
GORDON LAKE, ONTARIO

A Dissertation
Presented to
The Faculty of Graduate Studies
The University of Manitoba

In Partial Fulfillment
of the Requirements for the Degree
Doctor of Philosophy

by
REGINALD FRANCIS JON SCOATES
May, 1972



ABSTRACT

A series of small ultramafic bodies occur along a fault zone for approximately ten miles. The fault zone lies within and is approximately twelve miles south of the northern contact of the English River gneissic belt in northwestern Ontario. A detailed study of one ultramafic body indicates a crude concentric zonal arrangement of lithologic units ranging from peridotitic hornblendite at the margin to peridotite at the core. Cryptic zoning, displayed by the primary silicate minerals, appears to be a function of their position relative to the margin of the ultramafic body; an increase in the $Mg/(Mg + Fe)$ ratio from margin to centre being observed. The primary ultramafic mineral assemblage displays abundant reaction textures. The ultramafic rocks are olivine tholeiites in composition.

Two stages of recrystallization of the primary assemblage are recognized; a first stage incipient to complete autometamorphic alteration of olivine and orthopyroxene to α serpentine (chrysotile) and bastite respectively; and a second, later stage incipient to complete alteration of the primary assemblage minerals and the first stage recrystallization products by γ serpentine (antigorite), talc, phlogopite and chlorite group minerals.

The second stage recrystallization is caused by metamorphism and limited metasomatism of the ultramafic rocks by late crosscutting pegmatite dykes.

Sulphide-silicate textures of the disseminated sulphide ores in the ultramafic rocks are indicative of an immiscible sulphide-silicate magma. The breccia sulphide ore is characterized by subrounded inclusions of quartz, microcline and plagioclase (sodic andesine). The sulphide assemblage of the breccia ore is considered to represent exsolution from a monosulphide solid solution.

The ultramafic rocks and associated sulphide ores are products of magmatic crystallization. Flowage differentiation is invoked to explain the concentric zoning of rock types and the concentric cryptic zoning of the silicate minerals observed in one of the peridotite bodies. The breccia ore zone formed by gravity settling of nickel-rich sulphide liquid in the silicate-sulphide magma and intrusion of this liquid into a zone of brecciated pegmatite.

ACKNOWLEDGEMENTS

The writer was ably assisted by S.S. Tan during the 1969 field season. The cooperation and hospitality extended the writer by officials of the Consolidated Canadian Faraday Limited (formerly Metal Mines Limited) and in particular former manager C.D.N. Taylor is gratefully acknowledged.

Professor H.D.B. Wilson of the University of Manitoba is extended special thanks for the guidance and constructive criticism during the course of the study.

The writer acknowledges the Geological Survey of Canada who sponsored the project and officers of the G.S.C. for many fruitful discussions, particularly T.N. Irvine, D.C. Findlay and W.J. Wolfe.

Special thanks is extended to Dr. C.H. Smith of the G.S.C. under whose direction the field work and much of the project was conducted.

Staff members of the Geological Division of the Manitoba Mines Branch, in particular I. Haugh and W.D. McRitchie are acknowledged for their interest, criticism and suggestions.

TABLE OF CONTENTS

	<u>Page</u>
ABSTRACT	iii
ACKNOWLEDGEMENTS	v
CHAPTER I - INTRODUCTION	1
Field Work	1
Analytical Work and Laboratory Studies	2
Location and Access	3
Previous Work	3
Property History	4
CHAPTER II - REGIONAL AND MINE GEOLOGY	6
The English River Gneissic Belt	6
Metasedimentary Rocks	8
Ultramafic Rocks	11
Mineralogical Classification	14
Mineral Banding in Ultramafic Rocks	16
Granitic Rocks and Pegmatites	19
Structural Setting	26
Problem of Relative Age Relationships	28
CHAPTER III - MINERALOGICAL AND CHEMICAL VARIATIONS ACROSS THE A-PERIDOTITE	31
Modal Variations	31

CHAPTER III (Continued)	<u>Page</u>
Olivine	33
Orthopyroxene	36
Clinopyroxene	38
Hornblende	43
Hornblende Compositions	45
Disseminated Chrome Spinel	56
Chemical Variations across the A-peridotite	60
Ternary Plot 5 CaO - 2(FeO + Fe ₂ O ₃) - MgO	66
Summary of Mineralogical and Chemical Variations across the A-peridotite	72
 CHAPTER IV - COEXISTING PRIMARY MINERALS AND CRYSTALLIZATION CHEMISTRY	 74
Olivine-orthopyroxene Textures	74
Olivine-orthopyroxene Compositions	76
Chemistry of Coexisting Primary Minerals	83
Trace Elements in Coexisting Ferromagnesian Minerals	94
Nickel	94
Copper	94
Chromium	96
Vanadium	96
Flowage Differentiation	97
Classification of the Ultramafic Rocks	99

	<u>Page</u>
CHAPTER V - SECONDARY RECRYSTALLIZATION OF THE PRIMARY ASSEMBLAGE	102
Distribution of Serpentinization	102
First Stage Recrystallization	104
Second Stage Recrystallization	107
Contact Reaction Zones	112
Chemical Variations across Contact Reaction Zones	116
Chemistry of Altered Ultramafic Rocks	122
Ternary Plot $5(\text{Na}_2\text{O} + \text{K}_2\text{O}) -$ $2(\text{FeO} + \text{Fe}_2\text{O}_3) - \text{MgO}$	123
CHAPTER VI - COPPER-NICKEL SULPHIDE ORES	128
Disseminated Sulphide Ores	128
Sulphide Silicate Textures and Mineragraphy of the Disseminated Sulphide Ores	129
Globular sulphides, poikiliti- cally included in early ferromagnesian silicates	129
Interstitial sulphides	131
Effect of Recrystallization of the Primary Silicate Assemblage on Sulphide-silicate Textures	136
Mineragraphy of the Breccia Ore	146
Massive Sulphide Lenses in Ultramafic Rocks	153
Sulphide-sulphide Textures and Crystallization of the Sulphide Magma	155
The Association of Pegmatite	160
Cu-Ni Distribution in the Sulphide Ores	164

CHAPTER VI (Continued)	<u>Page</u>
Genesis of the Sulphide Ores	169
Sulphur Isotope Ratios - Breccia Sulphide Ore	173
CHAPTER VII - CONCLUSIONS	181
REFERENCES CITED	186
APPENDIX I	195
APPENDIX II	204

LIST OF TABLES

<u>Table</u>		<u>Page</u>
I	Modal compositions of amphibolites and quartzo-feldspathic rocks.	10
II	Modal compositions of granitic rocks.	21
III	Modal compositions of pegmatites.	23
IV	Chemical analysis and CIPW norm of alkali-granite pegmatite.	25
V	Table of Formations.	30
VI	Orthopyroxene compositions.	39
VII	Chemical analysis and structural formula of clinopyroxene.	42
VIII	Chemical analyses and structural formulae of A-peridotite hornblendes.	46
IX	Hornblende optical properties.	49
X	Relation between $100\text{Mg}/(\text{Mg} + \text{Fe}^{3+} + \text{Fe}^{2+} + \text{Mn})$ ratio, $[\text{Al}]^4$ and n_z in the primary hornblendes.	50
XI	Chrome spinel cell edge determinations.	57
XII	Chemical analyses - A-peridotite series.	61
XIII	MgO/MgO + FeO and mineral compositions - A-peridotite series.	67
XIV	Trace element data - A-peridotite series.	71
XV	Distribution constants for coexisting olivine and orthopyroxene	78
XVI	Chemical analyses of coexisting minerals - A-peridotite.	84

<u>Table</u>	<u>Page</u>	
XVII	Modal analyses of the ultramafic rocks corresponding with the analyzed mineral pairs.	85
XVIII	Primary hornblendes - CIPW norms.	88
XIX	Trace elements in coexisting minerals.	95
XX	Suite of analyzed specimens across a contact reaction zone.	117
XXI	Chemical analyses of altered ultramafic rocks.	124
XXII	Modal analysis and estimated modes of altered ultramafic rocks.	125
XXIII	Analyses of breccia sulphide ores.	158
XXIV	Average composition of B-breccia sulphide zone sulphide ore.	159
XXV	Cu/(Cu + Ni) ratios for disseminated and associated massive Cu-Ni ores in basic rocks.	171
XXVI	Sulphur isotope determinations - breccia ore.	174

LIST OF FIGURES

<u>Figure</u>	<u>Page</u>
1. Generalized regional geology.	7
2. Composite plan of levels showing dip and plunge of ultramafic rocks and ore bodies.	13
3. Ternary plot, olivine-hornblende-pyroxene, ultramafic rocks.	15
4. Modal compositions of granitic rocks and pegmatites.	22
5. Geology of the A-peridotite.	in pocket
6. Modal variations across the A-peridotite.	32
7. Olivine compositions.	34
8. Distribution of olivine compositions by rock type.	35
9. Distribution of olivine compositions across the A-peridotite.	37
10. Distribution of orthopyroxene compositions by rock type.	40
11. Orthopyroxene-hornblende-chrome spinel compositional variations across the A-peridotite, 1595 sub level.	42
12. Al _Z substitution in clinopyroxene from the A-peridotite.	44
13. Chemical variation of the analysed amphiboles.	47
14. Relation between Mg/Mg + Fe and n _Z -hornblende.	51
15. Hornblende-olivine-orthopyroxene compositional relationships	53

<u>Figure</u>	<u>Page</u>
16. Plot of octahedral Al against Si in the unit cell of the analysed amphiboles.	55
17. Distribution of chrome spinel cell edges.	58
18. Colour variations vs. unit cell - chrome spinel.	59
19. Modal composition - A-peridotite series.	62
20. Chemical variations - A-peridotite series	63
21. $5Ca - 2(FeO + Fe_2O_3) - MgO$, A-peridotite series.	69
22. A-peridotite series, plotted on base of basalt tetrahedron.	70
23. Olivine-orthopyroxene reaction relation.	77
24. Coexisting olivine and orthopyroxene.	81
25. Silica variation diagrams - analysed hornblendes.	87
26. Analysed hornblendes, plotted on base of basalt tetrahedron.	90
27. $5(Na_2O + K_2O) - 2(FeO + Fe_2O_3) - MgO$, analysed hornblendes.	92
28. Variation in degree of serpentinization across the A-peridotite.	103
29. Serpentine structures commonly associated with first stage recrystallization.	106
30. Monominerallic contact reaction zones associated with pegmatite cutting serpentinized peridotite.	109
31. Chemical variations across a contact reaction zone, 300 level.	118
32. Chemical variations across contact reaction zones	119
33. $5(Na_2O + K_2O) - 2(FeO + Fe_2O_3) - MgO$, A-peridotite series.	126
34. B-breccia sulphide zone.	143

<u>Figure</u>		<u>Page</u>
35.	Longitudinal section-showing relation between A-peridotite and B-breccia sulphide zone.	144
36.	X-ray diffractograms, B-breccia sulphide zone pyrrhotites.	149
37.	Sulphide assemblages - sulphide ores.	156
38.	Fe-Ni-S system.	161
39.	Frequency distribution of copper and nickel.	165
40.	Log-cum curves for disseminated sulphide and B-breccia sulphide ore bodies.	166
41.	Plot of median Cu/Cu + Ni ratios with depth.	168
42.	Variation of $\delta S^{34} \text{‰}$ with depth, B-breccia sulphide zone.	175
43.	Sulphur isotopes, ultramafic-mafic rocks, nickel sulphide ores and meteorites.	178

LIST OF PLATES

<u>Plate</u>		<u>Page</u>
I	Hornblende peridotite.	17
II	Detail of serpentinized olivine seen in Plate I.	17
III	Orthopyroxenite.	18
IV	Peridotitic hornblendite.	18
V	Sulphide blebs wholly enclosed within a single olivine grain.	130
VI	Sulphide blebs wholly enclosed in a single orthopyroxene grain.	130
VII	Sulphide interstitial to serpentinized olivine grains.	132
VIII	Interstitial sulphide.	132
IX	Chromite-sulphide relationships.	134
X	Pyrrhotite-pentlandite-chalcOPYrite.	134
XI	Cubanite exsolution blades in chalcOPYrite.	137
XII	Cubanite exsolution blades in chalcOPYrite and blebs in pentlandite.	137
XIII	Pyrrhotite and chalcOPYrite stringers in serpentine.	139
XIV	Recrystallized pyrrhotite in serpentine.	139
XV	Pyrrhotite grain displaying β component concentrated about rims.	140
XVI	Twinned pyrrhotite.	148
XVII	Pentlandite exsolution flames in pyrrhotite.	148

<u>Plate</u>		<u>Page</u>
XVIII	Pentlandite exsolution flames in pyrrhotite.	151
XIX	Pentlandite in pyrrhotite.	151
XX	Pentlandite-pyrrhotite.	152
XXI	Chalcopyrite-pyrrhotite.	152
XXII	Pyrite-pyrrhotite.	154
XXIII	Chalcopyrite-pyrrhotite-pentlandite.	154

CHAPTER I

INTRODUCTION

The Gordon Lake operation of the Consolidated Canadian Faraday Limited has provided the opportunity of studying small Precambrian ultramafic bodies and associated copper-nickel sulphide ores in detail. The underground mapping and sampling has provided basic material from which petrological, mineralogical and geochemical data could be obtained, so that a hypothesis concerning the genesis of the ultramafic rocks and associated sulphide ores could be constructed. Particular attention is directed towards the petrology and geochemistry of the ultramafic rocks, the comparative compositions of coexisting silicate minerals, sulphide-silicate textures and the mineragraphy of the sulphide ores.

Field Work

Field work, involving an underground mapping and sampling program, began in the fall of 1960 and concluded during the summer of 1961. Level plans, at a scale of one inch equals twenty feet, were used for mapping. The 450, 750, 1050, 1200 and a portion of the 300 level were

mapped and sampled. The eastern portion of the 300 level was not accessible at the time of the study. The 1350, 1500 and 1650 levels were examined in the fall of 1960 but were not accessible for detailed examination in 1961. The ultramafic bodies encountered underground were sampled in detail. Available diamond drill core was logged and sampled and proved suitable for differentiating ultramafic lithologies. A considerable number of copper and nickel assays were obtained from company assay plans and provided basic data for a metal ratio study of the ore bodies (Scoates, 1963).

Analytical Work and Laboratory Studies

Analytical work and laboratory studies were conducted in the laboratories of the Petrological Sciences Division of the Geological Survey of Canada during the summer of 1964 and winter of 1964-1965, and in the laboratories of the Department of Geology, University of Manitoba during the 1963-1964 academic year. Chemical analyses of 15 rocks and 6 mineral concentrates were supplied by the Rock Analysis Laboratory of the G.S.C. One mineral concentrate was analyzed by K. Ramlal at the University of Manitoba. Trace element analyses of rocks and minerals were provided by the Optical Spectrographic Laboratory of the G.S.C. The X-ray determinations of olivine compositions and chrome spinel cell edges were made

by R.N. Delabio at the G.S.C. X-ray Laboratory. Eight sulphur isotope determinations were made by A. Sasaki of the Isotope Geology Section of the G.S.C. Twenty analyses of sulphide ores were made by G. Faye of the Mineral Sciences Division, Mines Branch. Photomicrographs were supplied by the Photographic Section of the G.S.C. and the Photographic Laboratory of the Department of Earth Sciences, University of Manitoba. Petrographic studies were conducted by the writer at the G.S.C. laboratories and the laboratories of the Department of Earth Sciences, University of Manitoba.

Location and Access

The Gordon Lake operation of Consolidated Canadian Faraday Limited (latitude $50^{\circ}30'$; longitude $95^{\circ}00'$), located in northwestern Ontario, is 53 air miles north-northwest of Kenora, Ontario, and 8 miles east of the Ontario-Manitoba provincial boundary. It is accessible via Manitoba Provincial Roads 313 and 315 from Lac du Bonnet, Manitoba, and by a 12 mile all weather road from the Ontario-Manitoba provincial boundary to the mine site.

Previous Work

The area is included in Ontario Department of Mines Map 39G, Minaki to Sydney Lake (Derry, 1931), and in the Kenora Sheet, G.S.C. Map 266A, compiled by Tanton (1939).

Carlson (1958) mapped the Werner-Rex Lake area, and included a description of the mine property. His report is found in Ontario Department of Mines, Volume LXVI, Part 4. E.R. Rose visited the Gordon Lake operation and his description is reported in G.S.C. Paper 58-6.

Descriptions of the mine property are also included in three unpublished thesis studies: Taylor (1950), Anderson (1959) and Scoates (1963).

The regional geological aspects have been studied by Wilson and Brisbin (1963a, 1963b) and by Dwibedi (1966).

Property History

Carlson (op. cit.) has provided a comprehensive survey of the history of development of the Gordon Lake property. A condensation, with additions, of Carlson's report follows.

Nickel-copper mineralization in peridotite was discovered by H. Byberg and A. Vanderbrink in 1942, near the southwest corner of Gordon Lake. Prospectors working for Dome Exploration (Canada) Limited, made a similar discovery near the east end of Werner Lake. A considerable amount of trenching and diamond drilling was done on the Gordon Lake showing during the war years by Noranda Mines Limited. Later this property was acquired by Rexora Mining Corporation Limited. The International Nickel Company of Canada Limited optioned the property in 1946

and Falconbridge Nickel Mines Limited optioned the ground in 1948 and further explored it by means of geophysical surveys and an extensive diamond drilling program. Surface trenching and some diamond drilling were done on the Dome property in 1944 and 1945. During the period 1948-1949, geological and geophysical surveys were carried out in the Werner Lake-Rex Lake area by International Nickel Company of Canada Limited, Frederick Mining and Development Limited, Radio-active Minerals Limited, Rexora Mining Corporation Limited, and Toburn Gold Mines Limited.

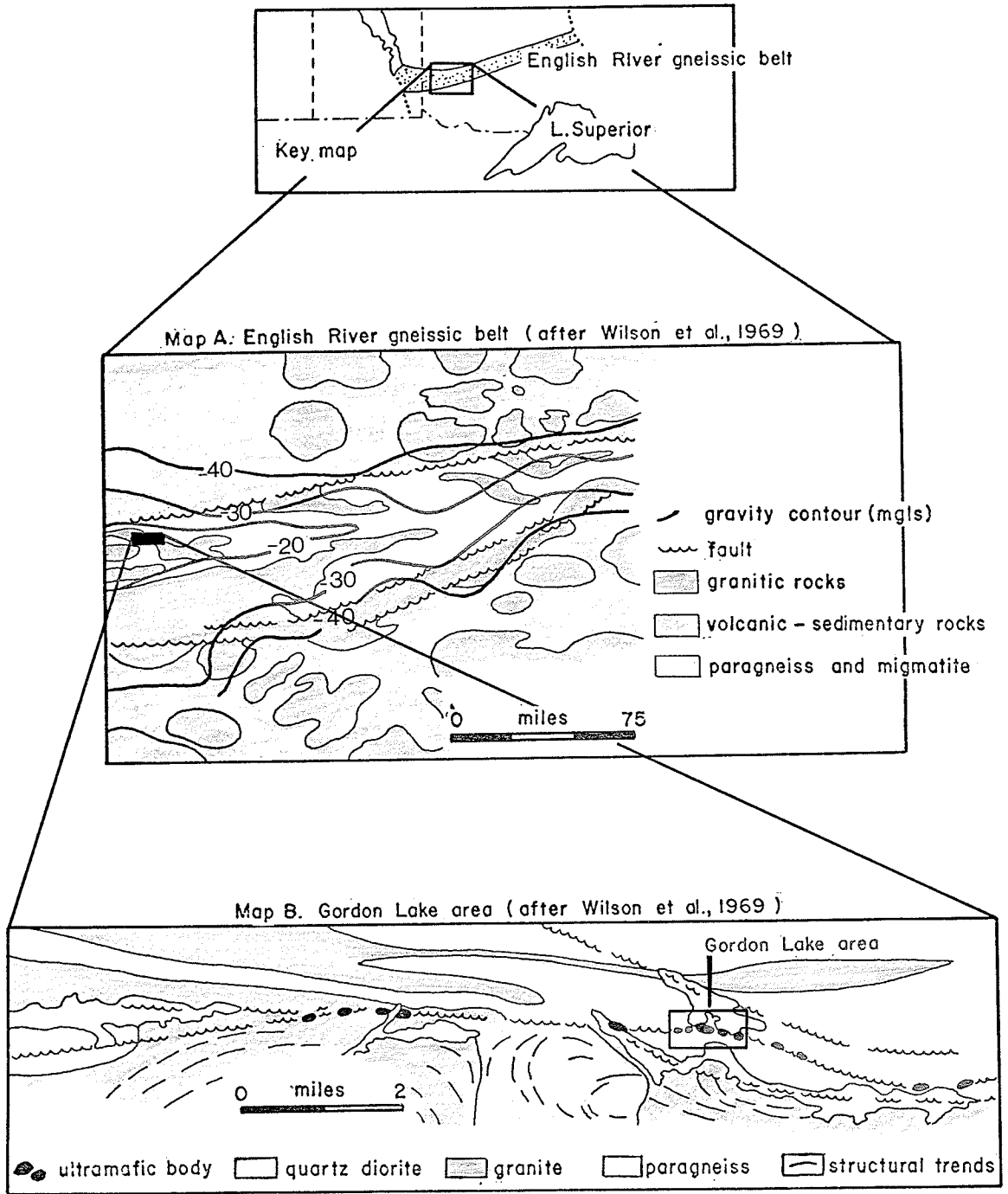
In 1952, Quebec Nickel Corporation acquired all the ground in this area which had formerly been explored by Noranda, Rexora, Falconbridge and International Nickel. Eastern Mining and Smelting Corporation Limited was formed in December, 1955 and in March, 1958, the name was changed to Nickel Mining and Smelting Corporation Limited. A reorganization in December, 1963, resulted in the formation of Metal Mines Limited. Consolidated Canadian Faraday Limited was formed in May, 1967. Milling operations were begun on September 20, 1962.

CHAPTER II

REGIONAL AND MINE GEOLOGY

The English River Gneissic Belt

The Gordon Lake copper-nickel deposit of the Consolidated Canadian Faraday Company Limited, lies within the northwestern portion of the English River gneissic belt in northwestern Ontario (Wilson and Brisbin, 1963a), approximately twelve miles south of the north boundary fault (Figure 1). The gneissic belt is characterized by moderately to highly metamorphosed sedimentary and granitic rocks. The rocks north and south of the gneissic belt consist of metamorphosed and migmatized greenstones, and typical greenstone-granite complexes. A regional Bouguer gravity high (Innes, 1960; Wilson and Brisbin, 1963b) coincides with the gneissic belt. The coincidence of intermediate to high grade metamorphic assemblages and a gravity high led Wilson and Brisbin (op. cit.) to propose a working hypothesis that regional geologic changes in this part of the Superior Province may be a reflection of the different levels of erosion of the granitic crust. A lower level of the granitic



GENERALIZED REGIONAL GEOLOGY

FIGURE 1

crust is thus represented by the English River gneissic belt, and an intermediate level by the metamorphosed and migmatized greenstone rocks found in areas north and south of the belt. The typical greenstone areas, farther north and south of the belt, are considered to represent the normal Superior Province crustal level. Exposure of the lower crustal level is believed to be due to major block faulting in the crust with subsequent erosion of the upfaulted crustal segment.

Dwivedi (1966) studied the physical and chemical characteristics of the metasedimentary and associated rocks of the gneissic belt and classified the rocks of the belt into three broad groups: metasedimentary rocks, amphibolites, and granitic rocks. He variously describes gradations between the above types as banded gneiss, *lit-par-lit* gneiss and migmatite.

Metasedimentary Rocks

Regionally, schists, gneisses and granulites are the most abundant metasedimentary rock types. Greywacke, arkose, conglomerate, chert and iron formation represent the least metamorphosed sedimentary rocks. These latter rock types are found in increasing abundance, passing from east to west along the gneissic belt. The change in rock types from east to west and coincident change in the grade of metamorphism, indicates that the schists, gneisses and

granulites are the metamorphic equivalents of the unaltered sedimentary rocks.

The gneissic rocks examined underground at Gordon Lake fall into two broad groups, amphibolites and quartzofeldspathic rocks, of which the former is the dominant gneissic rock type. Biotite-quartz gneiss and its garnetiferous equivalent occur in minor amounts. The amphibolites and quartzofeldspathic rocks appear to correspond to Carlson's (op. cit.) classifications of amphibolite and quartz-feldspar-hornblende-biotite granulites, gneisses and schists. Pyroxene, garnet and epidote bearing amphibolites have been observed.

Foliation in the amphibolite is marked by alternating light and dark layers and is further enhanced in the biotite-rich varieties by arrangement of the biotite parallel to the light and dark layers.

Hornblende and plagioclase (calcic andesine to sodic labradorite) are the dominant minerals, and biotite and quartz are generally present. Epidote, chlorite and calcite occur as minor constituents. Sericite alteration of plagioclase is common. Orthopyroxene, which is found in two specimens, forms isolated, optically continuous crystals in the equidimensional groundmass. Modal compositions of seven amphibolites are listed in Table I.

Amphibolite, adjacent to ultramafic bodies, generally displays some recrystallization of the hornblende,

Table I

Modal Compositions of Amphibolites and Quartzo-feldspathic Rocks

	<u>Amphibolites</u>						
	<u>707</u>	<u>180</u>	<u>245</u>	<u>155</u>	<u>241</u>	<u>308</u>	<u>303</u>
Quartz	1.6	4.0	4.4	3.6	3.8	2.2	3.1
Plagioclase	26.3	33.7	20.4	38.4	36.4	26.4	24.2
Hornblende	34.1	47.1	70.1	42.8	52.6	62.6	47.6
Biotite	37.6	-	2.6	11.9	0.4	0.2	13.5
Orthopyroxene	-	-	-	-	-	2.8	6.5
Epidote	-	2.9	-	-	0.1	-	-
Sericite	0.4	12.2	1.8	0.4	0.7	2.0	2.0
Chlorite	-	-	-	0.1	-	-	-
Calcite	-	0.1	-	0.1	-	-	-
Zircon	-	-	-	0.1	-	-	-
Sulphide	-	0.7	-	2.6	3.7	3.3	2.4
Magnetite	-	-	-	-	2.3	0.5	0.7
Total	100.0	100.0	100.0	100.0	100.0	100.0	100.0

	<u>Quartzo-feldspathic Rocks</u>		
	<u>181</u>	<u>205</u>	<u>202</u>
Quartz	26.4	25.3	18.9
Microcline	34.2	33.0	20.0
Plagioclase	25.4	39.8	36.5
Biotite	10.2	1.8	20.5
Orthopyroxene	2.9	-	4.1
Sericite	0.9	0.1	-
Total	100.0	100.0	100.0

and the plagioclase is commonly altered to sericite. Diopside has been noted in several of these amphibolites. The development of diopside and the recrystallization of hornblende in some amphibolite adjacent to ultramafic bodies could be indicative of the hornblende-hornfels facies (Turner and Verhoogen, 1960) of contact metamorphism.

The quartzo-feldspathic rocks form thin (1 to 4 feet) layers in the amphibolite. They have a poorly defined foliation and correspond to Carlson's (op. cit.) quartzite and quartz-feldspar granulite. Plagioclase (sodic andesine), microcline and quartz are the dominant minerals; biotite and chlorite are minor constituents (Table I). Two specimens contain large areas of isolated, optically continuous orthopyroxene similar to that described from the amphibolites.

The dominant assemblage hornblende-plagioclase in the amphibolites is characteristic of the almandine-amphibolite facies of regional metamorphism. The limited occurrence of orthopyroxene in both the amphibolite and quartzo-feldspathic rocks could indicate slightly higher conditions of regional metamorphism.

Ultramafic Rocks

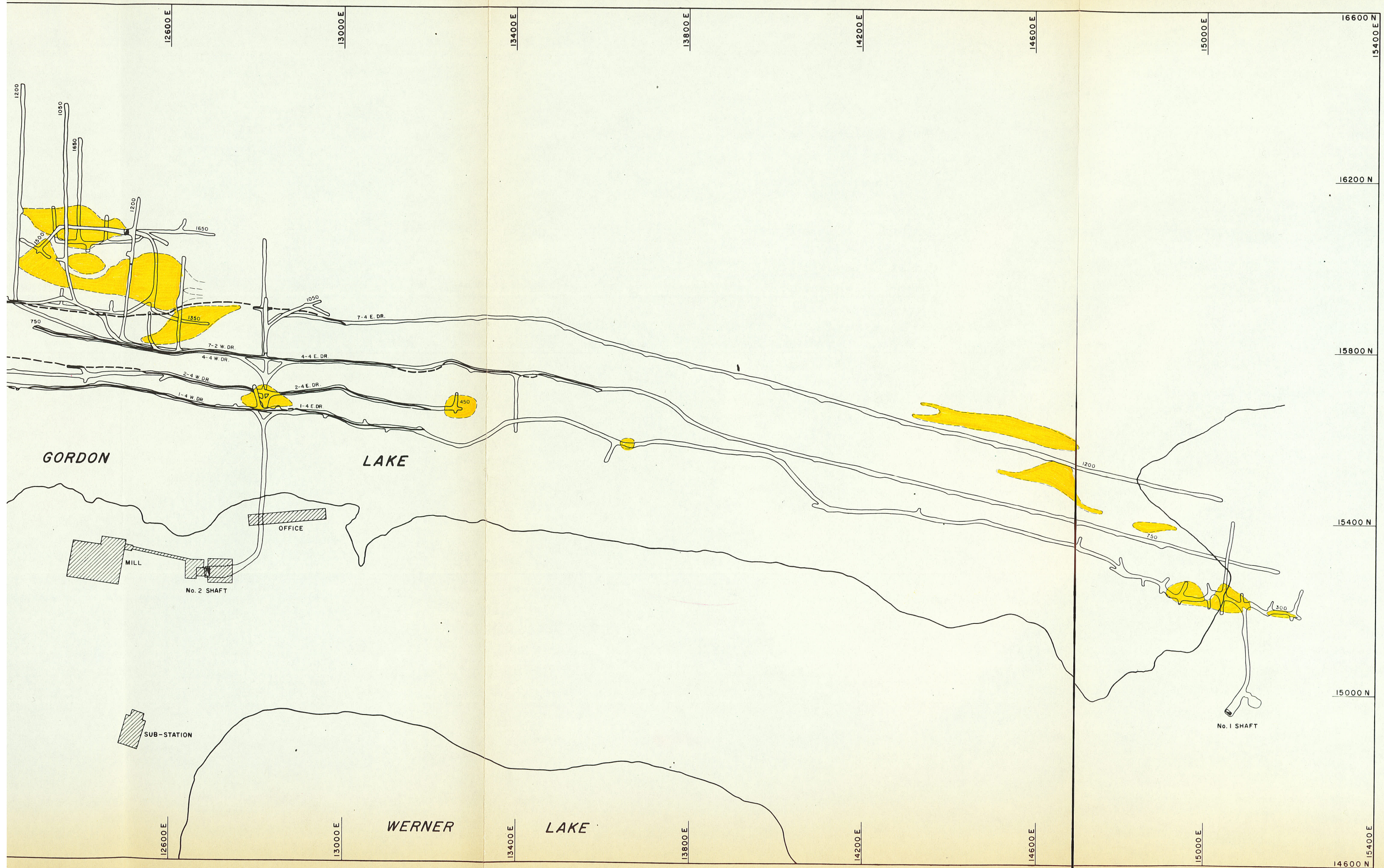
The ultramafic rocks examined underground at Gordon Lake are part of a series of small bodies occurring along an easterly-trending fault zone (Figure 1). Carlson

(op. cit.) has noted ultramafic rocks for approximately ten miles along the fault zone. The ultramafic bodies are enclosed by gneisses and granitic rocks of the English River gneissic belt.

The individual bodies examined range in size from football-shaped pods (10 x 5 x 10 feet) to bodies up to 600 x 150 x 600 feet in size. The latter body is termed the A-peridotite and contains disseminated copper-nickel sulphide ore of the A-peridotite ore body. The bodies are elongate in an easterly direction, dip steeply to the north, and plunge steeply to the northwest (Figure 2). The bodies are generally lens or pod shaped, however in detail the larger bodies tend to pinch and swell and display an irregular outline.

The ultramafic rocks are generally massive and well jointed, the joint spacing ranging from several inches to several feet. Faults, which cut across ultramafic bodies are accompanied by the development of chlorite-biotite schist. The schist is characterized by smooth and highly polished slickensided surfaces.

The ultramafic rocks consist of serpentinized olivine, orthopyroxene and hornblende as the dominant silicate minerals. Clinopyroxene, magnetite and chrome spinel are also present. Serpentine, talc, phlogopite, chlorite, tremolite, anthophyllite, clinocllore and calcite occur as alteration products and are described in Chapter V.



GORDON

LAKE

WERNER

LAKE

OFFICE

MILL

No. 2 SHAFT

SUB-STATION

No. 1 SHAFT

12600 E

13000 E

13400 E

13800 E

14200 E

14600 E

15000 E

15400 E

16200 N

15800 N

15400 N

15000 N

14600 N

12600 E

13000 E

13400 E

13800 E

14200 E

14600 E

15000 E

15400 E

1200

1050

1650

1200

1650

1050

7-4 E. DR.

7-2 W. DR.

4-4 W. DR.

4-4 E. DR.

2-4 W. DR.

2-4 E. DR.

1-4 W. DR.

1-4 E. DR.

450

1200

750

300

12600 E

13000 E

13400 E

13800 E

14200 E

14600 E

15000 E

15400 E

1200

1050

1650

1200

1650

1050

7-4 E. DR.

7-2 W. DR.

4-4 W. DR.

4-4 E. DR.

2-4 W. DR.

2-4 E. DR.

1-4 W. DR.

1-4 E. DR.

450

1200

750

300

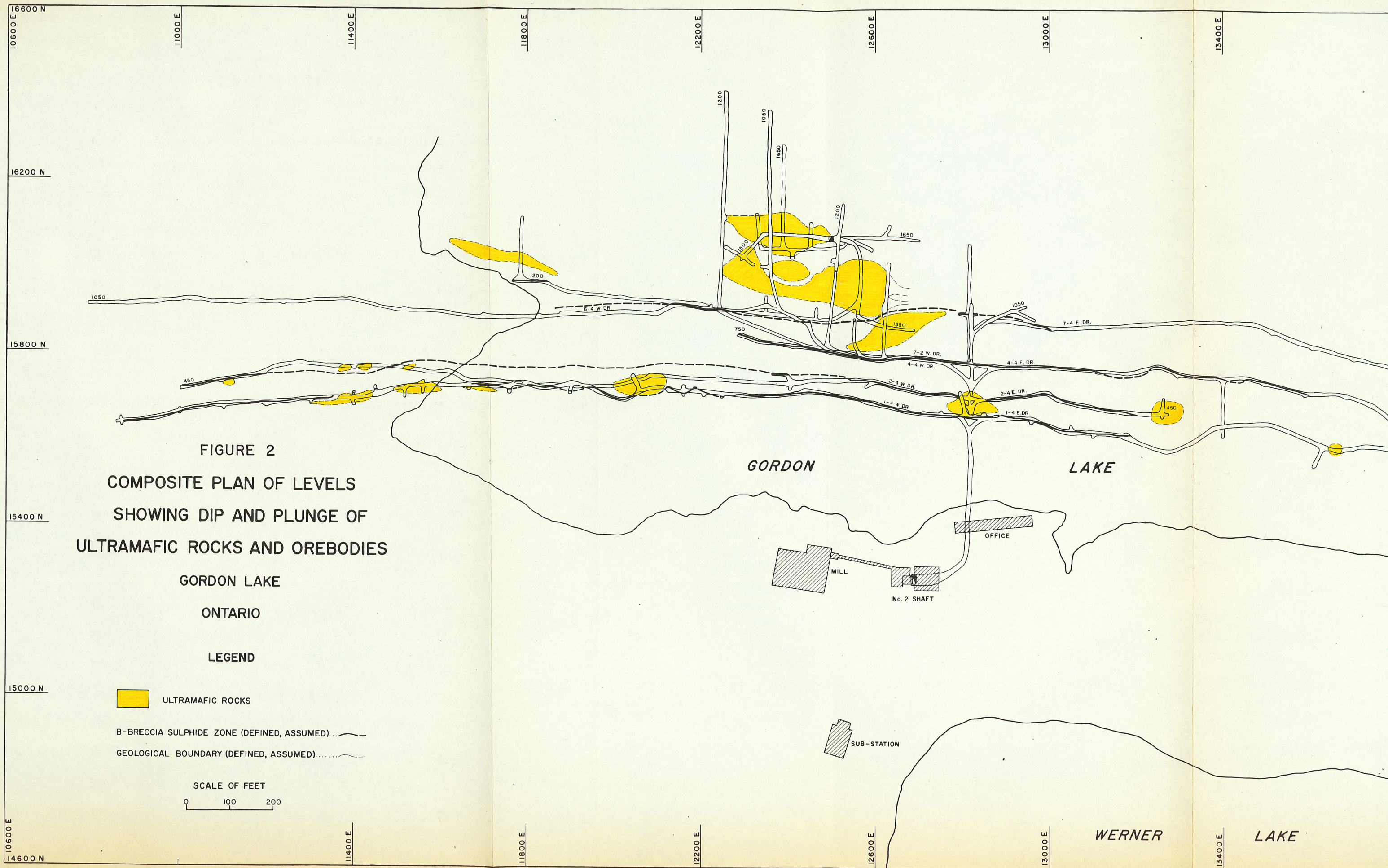


FIGURE 2
 COMPOSITE PLAN OF LEVELS
 SHOWING DIP AND PLUNGE OF
 ULTRAMAFIC ROCKS AND OREBODIES
 GORDON LAKE
 ONTARIO

LEGEND

ULTRAMAFIC ROCKS

B-BRECCIA SULPHIDE ZONE (DEFINED, ASSUMED).....

GEOLOGICAL BOUNDARY (DEFINED, ASSUMED).....

SCALE OF FEET

0 100 200

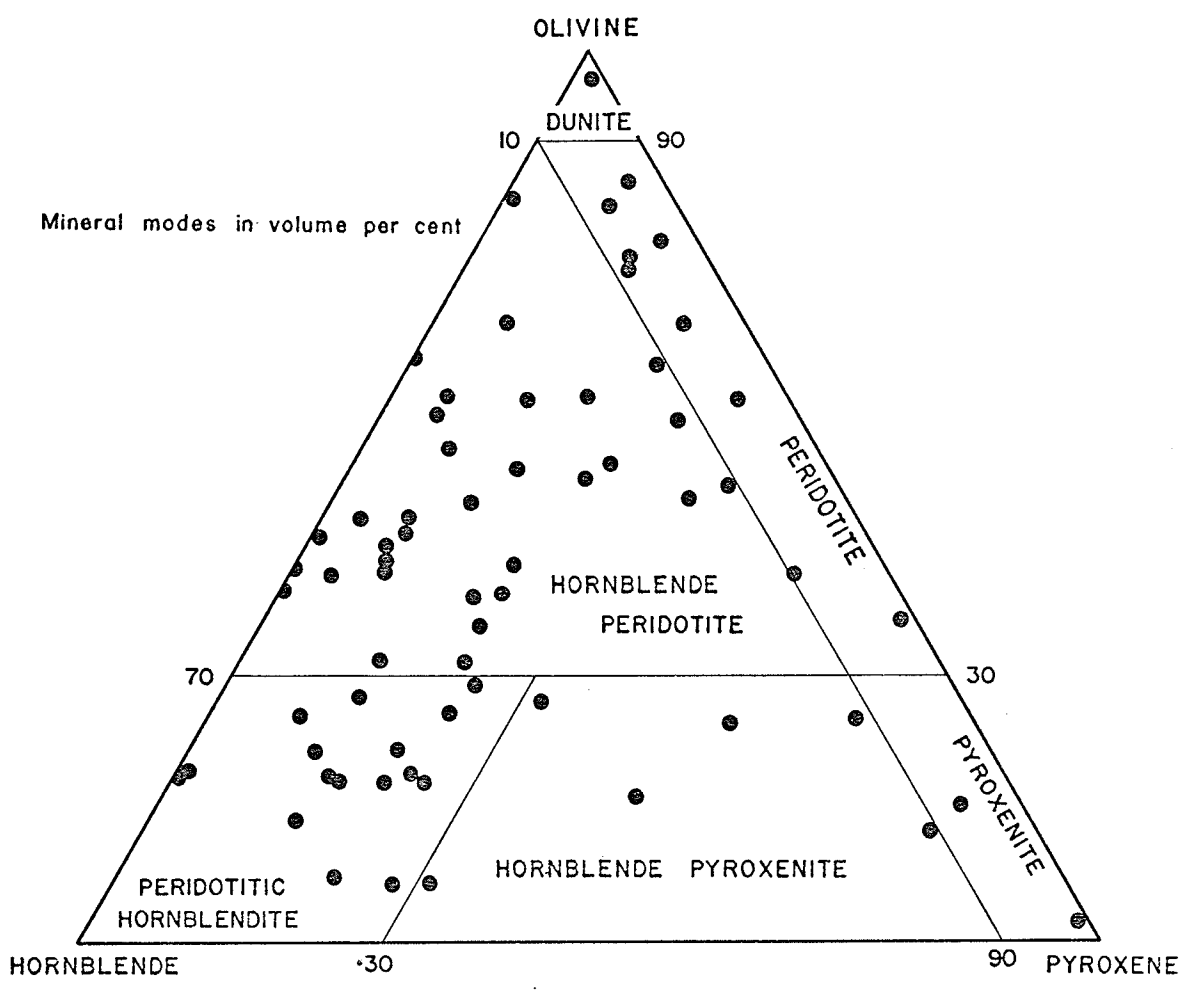
WERNER LAKE

Sulphide minerals which are common are described in Chapter VI.

The overall texture of the ultramafic rocks is hypidiomorphic granular and is typically igneous and non-directed, with a tendency for serpentized olivine and orthopyroxene to form the larger crystals. Serpentized olivine forms medium-sized (2 mm) equidimensional to elongate grains, the elongate grains displaying no tendency toward preferred orientation. Poikilitic orthopyroxenes, commonly containing optically continuous remnants of serpentized olivine are characteristic of the ultramafic rocks. Hornblende occurs as clusters of smaller equidimensional grains, interstitial to olivine and/or orthopyroxene. Lenses of fine grained equidimensional clinopyroxene are observed but are not common. Reaction textures between the primary silicate minerals are common.

Mineralogical Classification

A six fold classification of the ultramafic rocks is made on the basis of three end members: olivine, total pyroxene and hornblende (Figure 3). The plot is a modification of Watkinson and Irvine's (1964) double ternary plot for the Quetico and Shebandowan ultramafic rocks. The modifications involve the extension of the peridotite field, the addition of a pyroxenite and hornblende pyroxenite field, and the reduction in size of



TERNARY PLOT, OLIVINE - HORNBLLENDE - PYROXENE, ULTRAMAFIC ROCKS

the peridotitic hornblendite field. The reduction in size of this latter field is made to accommodate rocks containing greater than 50 per cent combined olivine and pyroxene in the hornblende peridotite field. The fact that plagioclase does not occur in the Gordon Lake ultramafic rocks means that only the olivine, total pyroxene, hornblende portion of the diagram need be used. Alteration products of olivine and orthopyroxene are added to the total for these minerals. The difficulty in determining the difference between magnetite associated with the serpentinization of olivine, and magnetite associated with the oxidation of sulphides and chrome spinel in some thin sections may lead to small errors in the calculated modal analyses. A total of 67 modal analyses have been determined. The modal analyses are listed in Appendix I. The general character of the major ultramafic rock types is illustrated in Plates I to IV.

Mineral Banding in Ultramafic Rocks

Very fine mineral banding is observed in drill core and thin sections of ultramafic rocks. The banding is most commonly developed near the margins of the bodies. It occurs at high angles to the core axis, measured in core from horizontal holes cutting the long axes of the ultramafic bodies. The banding thus approximately parallels the long axis of the bodies and the strike of the layering



Plate I Hornblende peridotite. Note euhedral to subhedral chrome spinel in partially serpentinized olivine and interstitial finer-grained hornblende. Note orthopyroxene with chrome spinel inclusions at lower central portion of photomicrograph. Crossed nicols, X6.5. (538)

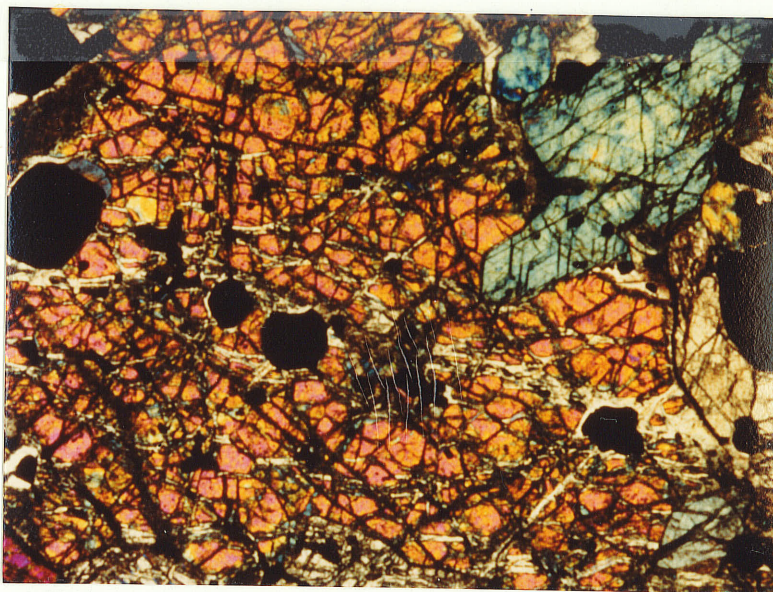


Plate II Detail of serpentinized olivine seen in Plate I. Note inclusions of subhedral chrome spinel and interstitial hornblende in upper right hand corner. Crossed nicols, X10.8. (538)

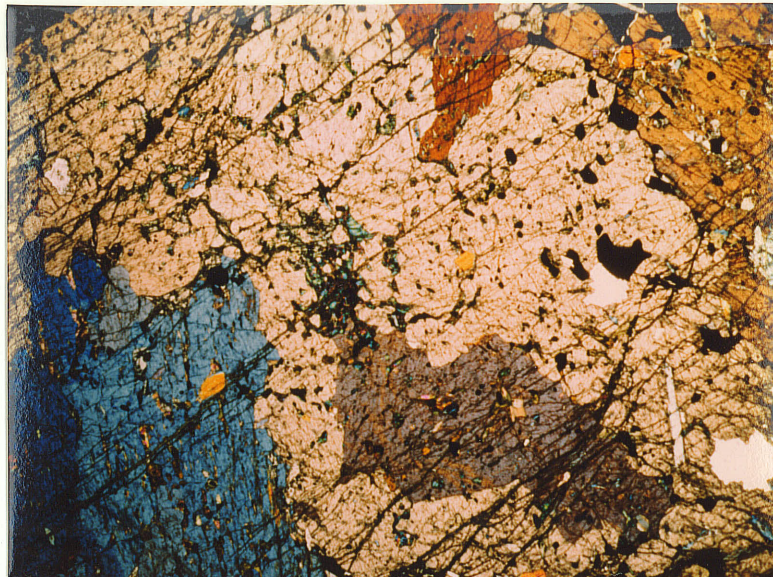


Plate III Orthopyroxenite displaying fine-grained inclusions of optically continuous olivine (central). Opaque minerals are chrome spinel and sulphide. Crossed nicols, X6.5. (675)



Plate IV Peridotitic hornblendite consisting of a fine-grained mosaic of hornblende and discontinuous lenses of olivine (central to upper left hand corner). Opaques are emerald green chrome spinel and sulphide. Crossed nicols, X6.5. (588)

and foliation of the paragneiss group rocks. A number of features contribute to the banding:

- (i) Subparallel serpentine stringers with associated magnetite;
- (ii) Lenses of chromite-serpentine;
- (iii) Elongate lenses of serpentinized olivine alternating with bands of hornblende;
- (iv) Elongate lenses of equidimensional clinopyroxene alternating with bands of hornblende.

The lenses and bands described above seldom exceed 1 cm in width and there is a general absence of cataclastic textures associated with the banding. The banding probably reflects late stage movement of the bodies after crystallization was complete, the movement being taken up by the marginal areas.

Granitic Rocks and Pegmatites

Quartz diorite, granodiorite, quartz monzonite and granite comprise the most abundant rock types exposed in the area. Regionally, granodiorite is the dominant rock type.

The granitic rocks examined underground are medium grained and grey to greyish pink. They display a well-developed gneissosity in the vicinity of the granite-paragneiss contact and this gneissosity becomes less prominent south of the contact. The granite-paragneiss

contact is generally irregular and gradational with tongues of granite protruding into the paragneiss.

The granitic rocks within the mine area are dominantly granites, with quartz monzonite and granodiorite phases, and consist of microcline perthite, quartz and plagioclase. The plagioclase (calcic oligoclase) generally displays slight alteration to sericite. Hornblende, biotite and chlorite are common ferromagnesian constituents. Partially uralitized clinopyroxene was identified in one granite specimen. Apatite, zircon, magnetite and sulphide are rare constituents. String, rod and patch perthites are characteristic and myrmekitic and granophyric intergrowths are common features of the granitic rocks.

Modal compositions of five granitic rocks are listed in Table II and are plotted on the ternary diagram, potash feldspar-quartz-plagioclase, in Figure 4.

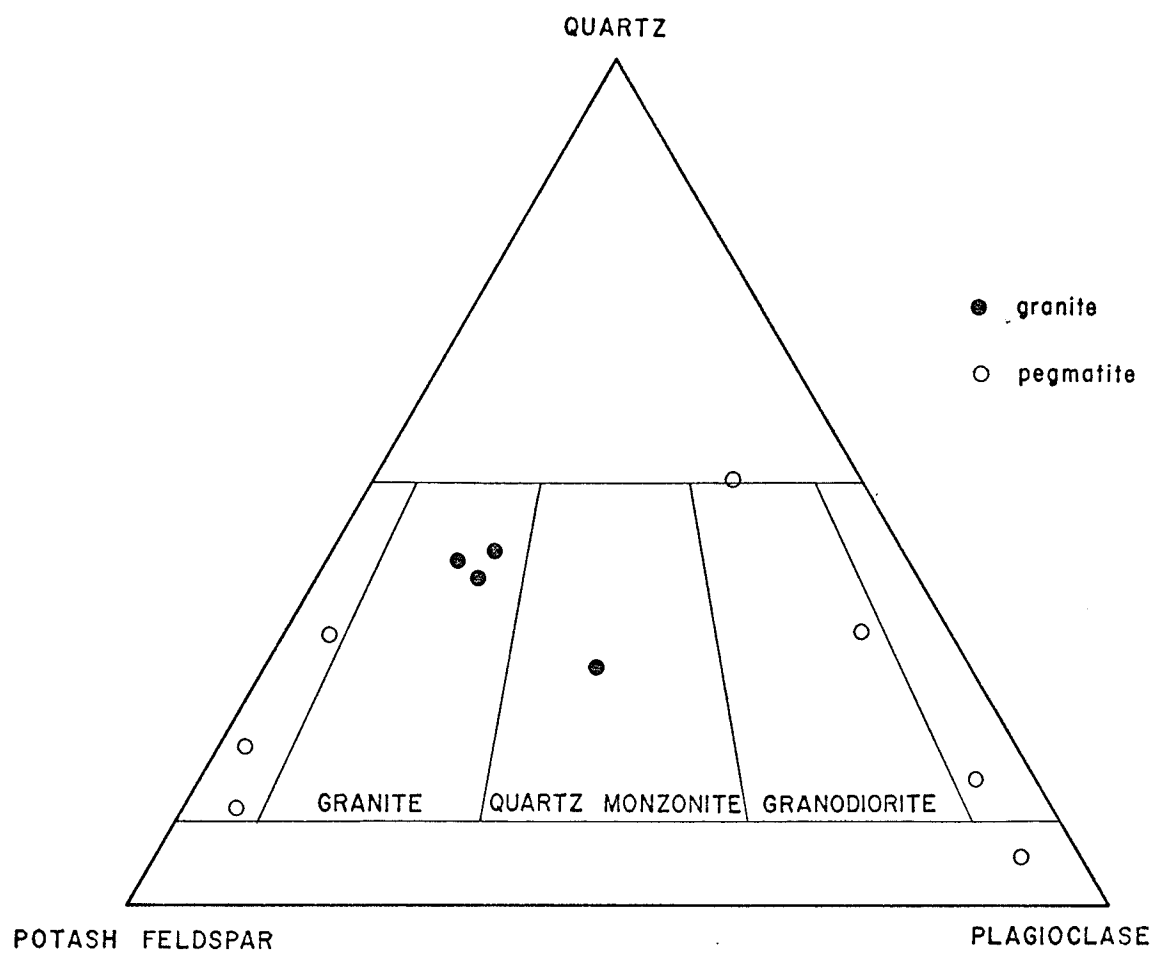
Pegmatites are of two types: alkali granite pegmatites in which microcline perthite and quartz are dominant, and granodiorite-quartz diorite pegmatites in which highly altered plagioclase (sodic andesine), and quartz are the dominant assemblage. Biotite and chlorite are rare constituents of the former, and biotite, chlorite, apatite and zircon are minor constituents of the latter type.

Modal compositions of six pegmatites are listed in Table III and are plotted on the ternary diagram, potash

Table II

Modal Compositions of Granitic Rocks

	<u>Granitic Rocks</u>				
	<u>235</u>	<u>233</u>	<u>111</u>	<u>197</u>	<u>203</u>
Quartz	47.2	25.0	37.8	37.1	39.9
Microcline	13.3	33.6	42.8	44.5	38.7
Plagioclase	33.0	30.4	12.6	16.2	15.6
Hornblende	-	4.5	0.7	-	-
Biotite- chlorite	5.0	6.0	5.8	1.9	5.8
Pyroxene	-	0.3	-	-	-
Sericite	0.6	-	-	-	-
Zircon	-	-	0.2	-	-
Sulphide	-	-	-	0.2	-
Magnetite	-	0.2	0.1	0.1	-
Total	<u>100.0</u>	<u>100.0</u>	<u>100.0</u>	<u>100.0</u>	<u>100.0</u>
<i>Modal Ternary Ratios</i>					
Quartz	50.0	28.1	40.6	37.9	42.3
Microcline	14.1	37.7	45.9	45.5	41.1
Plagioclase	35.9	34.2	13.5	16.6	16.6
Total	<u>100.0</u>	<u>100.0</u>	<u>100.0</u>	<u>100.0</u>	<u>100.0</u>



MODAL COMPOSITIONS OF GRANITIC ROCKS AND PEGMATITES

feldspar-quartz-plagioclase, in Figure 4.

A chemical analysis and CIPW norm of an alkali granite pegmatite are provided in Table IV. The norm and ternary ratio calculation show that the amount of plagioclase is considerably greater than was found by modal analysis of similar rocks (Table III). This is undoubtedly due to the presence of submicroscopic perthitic albite in the microcline.

Dwivedi (op. cit.) suggests, on the basis of triclinicity measurements made on selected granitic rocks, that the results are consistent with amphibolite facies conditions. He also indicates that these rocks are not strictly of magmatic origin but have been influenced by metasomatic processes. A probable origin for most of the granitic rocks of the gneissic belt by anatexis and palingenesis of metasedimentary rocks is suggested.

Unlike Dwivedi (op. cit.), who states that rock types representing all stages of transition from paragneiss to granite were observed in the area, Carlson (op. cit.) finds little field evidence to suggest that either the granitic rocks or the quartz diorite were developed as a result of alteration and replacement of the older metasedimentary rocks. He suggests, however, that the granitic rocks developed as a result of potash metasomatism of the quartz diorite rocks and that this process is closely related to the formation of the granite pegmatite dykes

Table IV

Chemical Analysis and CIPW norm of alkali-granite pegmatite

	<u>24*</u>		<u>CIPW Norm</u>
SiO ₂	72.8	Quartz	31.7
Al ₂ O ₃	16.8	Corundum	5.1
Fe ₂ O ₃	0.6	Orthoclase	38.2
FeO	0.9	Albite	17.5
CaO	0.6	Anorthnite	2.9
MgO	1.0	Enstatite	2.5
Na ₂ O	2.1	Ferrosilite	1.0
K ₂ O	6.56	Magnetite	0.9
TiO ₂	0.09	Ilmenite	0.2
MnO	0.01		
Total	<u>101.46</u>		<u>100.0</u>
		<u><i>Ternary ratio</i></u>	
		Quartz	35.1
		Orthoclase	42.3
		Plagioclase	22.6

* Analysis made by the Analytical Chemistry Division, G.S.C.

in both major rock types.

As noted previously, a distinct gneissosity is found in the granite, where the paragneiss-granite contact is exposed underground. The gneissosity is marked by a parallel development of biotite, and both the biotite content and the intensity of the gneissosity decrease farther into the granite. The paragneiss, adjacent to the contact contain granite *lit* and numerous irregular patches of granite. These observations can fit either an igneous or metasomatic origin for the granitic rocks and are consequently of little value in unequivocally solving the problem of the origin of the granite.

Structural Setting

The regional structural geology has not received the same intensity of study as other aspects of the gneissic belt, and the existing information is of a reconnaissance nature. Carlson (op. cit.), suggests that primary sedimentary structures are completely destroyed as a result of metamorphism, except that layering in the paragneiss sequence may represent original sedimentary bedding. Foliation is found to be coincident with layering in the paragneiss sequence. Tight isoclinal squeezing of the original strata, broad warps in the terrain or several periods of folding are presented by Carlson as possible mechanisms producing the steep dips common in the layers

of the paragneiss sequence.

Derry (1931) points out that fold axes strike easterly to northeasterly and thus parallel the regional foliation directions. Carlson states that the long axes of the quartz diorite masses are roughly parallel to the paragneiss belts and the layering of the various members therein.

A fold just north of Davidson Lake along the Ontario-Manitoba interprovincial boundary may represent the eastward extension of the Bird River anticline in Manitoba (Davies, 1956). On the Ontario side of the boundary the anticlinal structure is overturned, and the axial plane strikes easterly, dipping steeply to the north.

A second fold just north of the east end of Trapline Lake is considered by Carlson to be a syncline, the axis of which strikes easterly and dips vertically.

A large number of narrow topographic lineaments have been interpreted by Carlson as faults. Discordance of geology on either side of the fault and evidence of fault gouge in some diamond drill holes and underground at the Gordon Lake mine are used by Carlson as fault indicators.

The layering and foliation of the gneissic rocks at Gordon Lake strike approximately easterly and dip steeply to the north.

The major structural feature at Gordon Lake is an

easterly trending fault zone which has a slight arcuate shape (concave to the south) and follows along the south shore of Gordon Lake (Figure 1). Where it is exposed underground, the fault is marked by a band of chlorite schist, ranging in width from 1 to 15 feet. As the fault is parallel to the layering of the gneissic rocks, it is not possible to determine the displacement along the fault. Slickensides indicate that the last movement was essentially horizontal.

Rinds composed of chloritized biotite have been observed selvaging many of the ultramafic bodies. Highly polished and slickensided surfaces associated with these rinds indicate that some faulting was post-ultramafic intrusion.

Several small scale folds were noted in the amphibolite rocks. Since these folds were observed on the backs of the drifts, measurement of axes was not possible. Both dextral and sinistral folds were observed.

Problem of Relative Age Relationships

The relative age relationships between faulting, intrusion of ultramafic bodies and the intrusion or formation of quartz diorite, granodiorite and granite have not been unequivocally determined. Carlson (op. cit.) and Derry (op. cit.) both consider the paragneiss as representing the the oldest rocks of the area. Derry lumps the acid

intrusive rocks (granodiorite, quartz monzonite and granite) together under the Algoman intrusive series. Carlson places the ultramafic rocks later than the quartz diorite and earlier than the granite. Dwibedi (op. cit.) and Carlson both consider that metasomatic processes were active in the formation of the granitic rocks although differing in the selection of a source rock type.

It was noted that alkali granite pegmatite and granodiorite-quartz diorite pegmatite cut all rock types including the ultramafic rocks. The compositions of the two types of pegmatites correspond with the composition of the two major types of granitic rocks in the area, granodiorite-quartz diorite and granite. If the pegmatites are related to the formation of these rocks, as seems reasonable, then both the granodiorite-quartz diorite and granite can be considered to be, in part, later than the ultramafic rocks (Table V).

A detailed evaluation of the age relationships of pegmatite, ultramafic rocks and sulphide mineralization is made in Chapter VI.

Table V

Table of Formations

P	Granite-granodiorite group
R	and related pegmatites
E	
C	<i>Intrusive contact</i>
A	Ultramafic rocks
M	
B	<i>Intrusive contact</i>
R	Metasedimentary group
I	
A	Amphibolite, biotite
N	Amphibolite, biotite-quartz gneiss
	Quartzo-feldspathic rocks

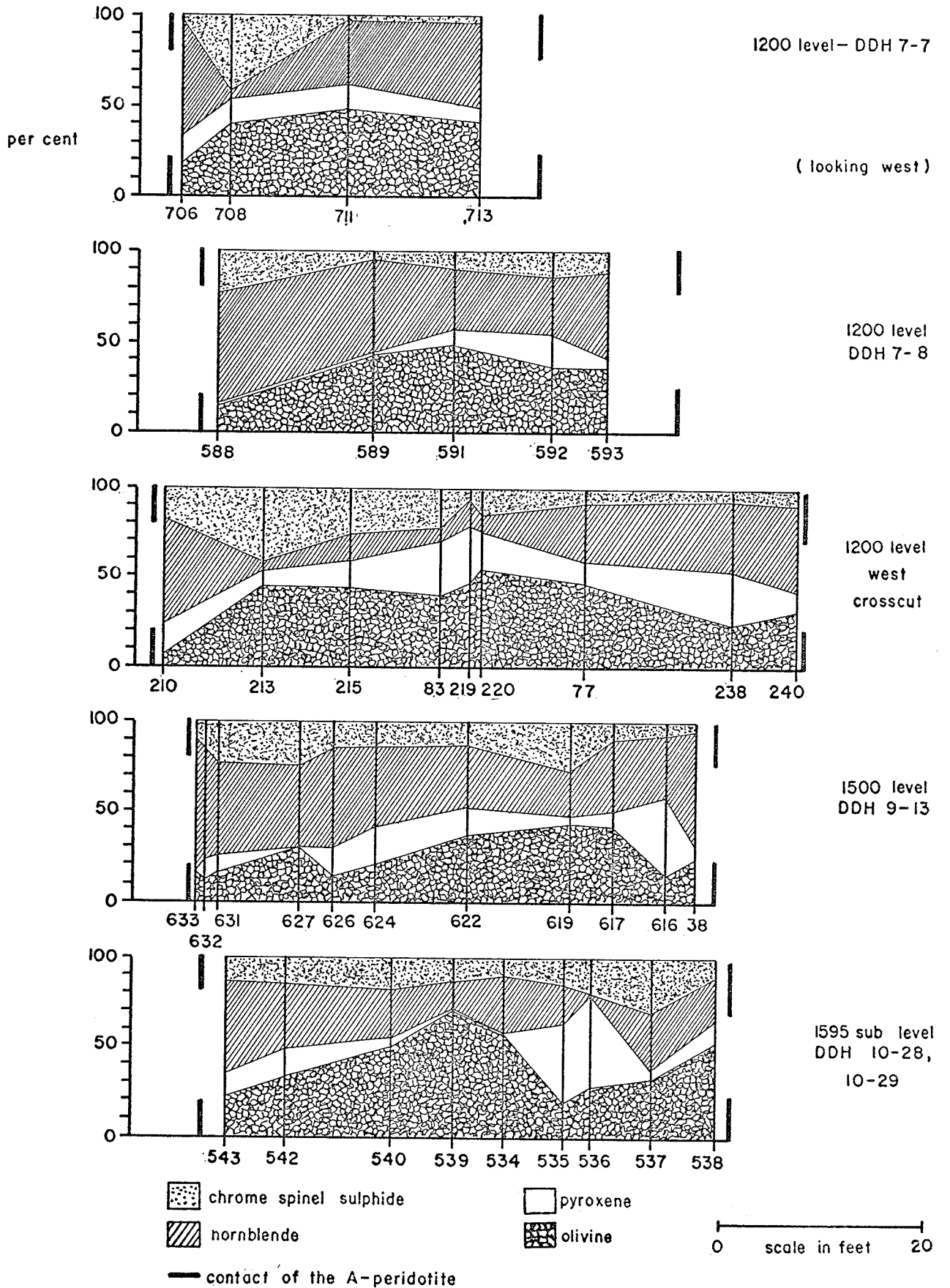
CHAPTER III

MINERALOGICAL AND CHEMICAL VARIATIONS ACROSS THE A-PERIDOTITE

The A-peridotite is the largest body studied and its position relative to other ultramafic bodies is shown in Figure 2. The A-peridotite was chosen for detailed study because of the availability of core from diamond drill holes which cut across the body on six levels. Underground sampling of the body was carried out on five levels. The geology of the body is illustrated in Figure 5 (map pocket).

Modal Variations

Modal analyses made on samples collected from diamond drill holes and one cross-cut have been used in constructing the five cross sections shown in Figure 6. In each cross section, olivine is more abundant in the centre of the body, whereas hornblende is more abundant toward the margins. The increase in pyroxene content between the centre and north margin which can be seen in three of the five cross sections reflects the abundance of orthopyroxene in those areas. Clinopyroxene is for the



MODAL VARIATIONS ACROSS THE A - PERIDOTITE

FIGURE 6

most part a minor constituent (see modal analyses, Appendix I).

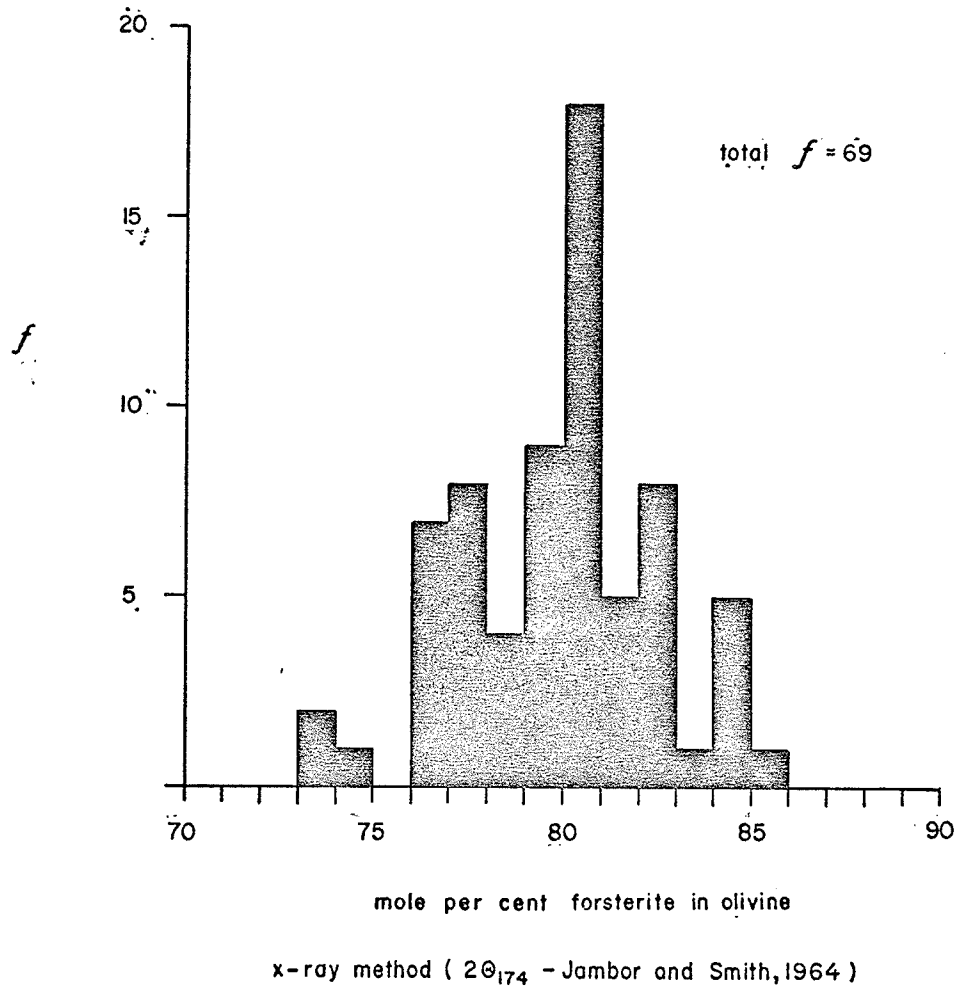
There is consequently a crude zonation of the primary silicate minerals which gives rise to olivine-rich rocks in the central part of the A-peridotite and hornblende-rich rocks at its marginal area. Pyroxene-rich rocks tend to occur between the central and marginal areas, however the distribution of pyroxene is quite irregular.

Olivine

Olivine occurs as optically continuous, remnant grains in serpentine and associated magnetite. It is the earliest formed silicate mineral and displays reaction textures with orthopyroxene and hornblende.

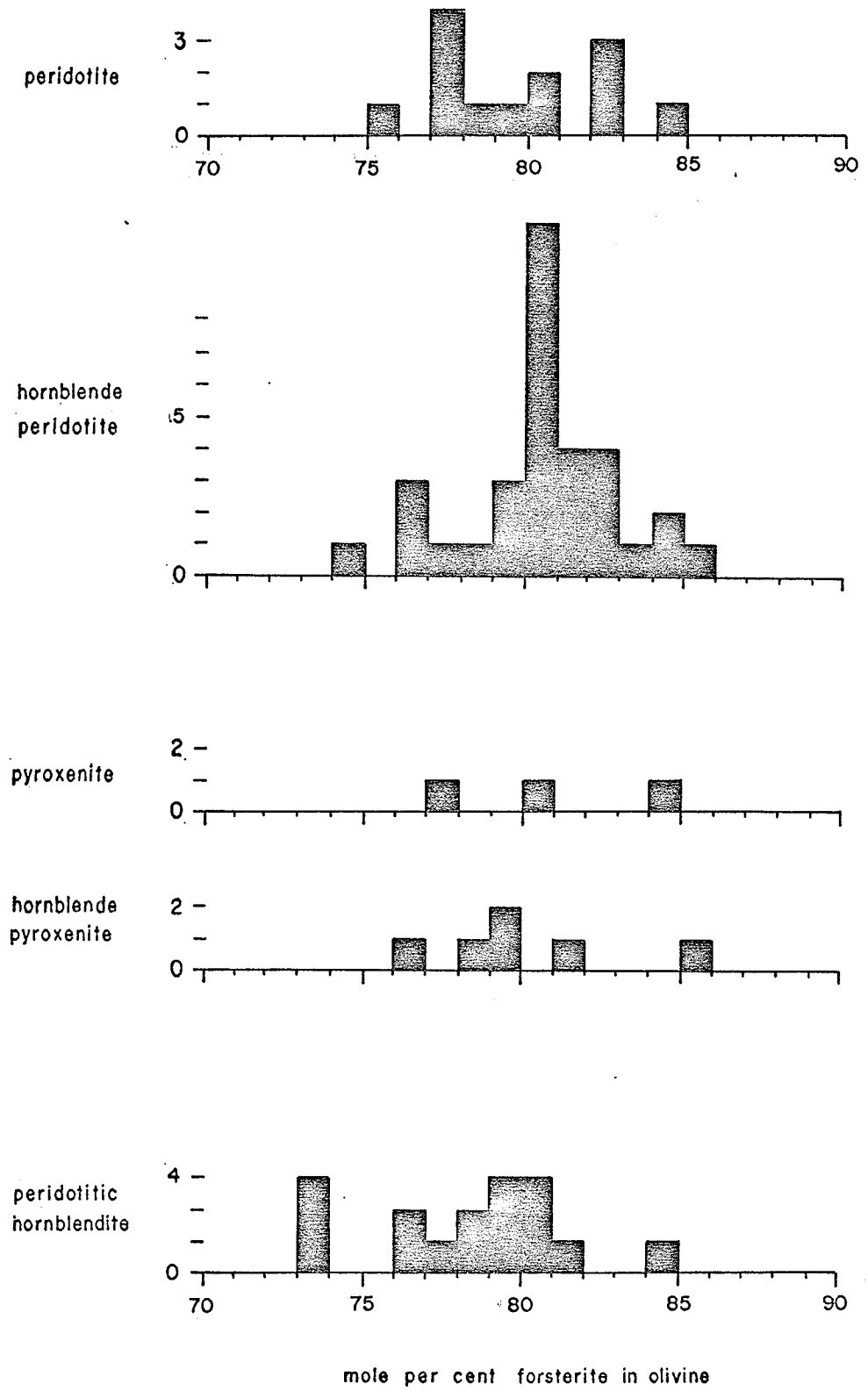
Olivine compositions range from Fo_{73.8} to Fo_{85.1}, the average being Fo_{79.8} (Figure 7). The overall distribution of olivine compositions is similar to that described for Precambrian ultramafic rocks by Smith (1961). He pointed out that olivines with a forsterite content of greater than 90 per cent are confined to the Cordillera and Appalachian belts and are generally absent from ultramafic rocks of the Precambrian Shield.

The compositions, grouped according to rock type (Figure 8), display a slight increase in forsterite content from peridotitic hornblendite through hornblende pyroxenite



OLIVINE COMPOSITIONS

FIGURE 7



DISTRIBUTION OF OLIVINE COMPOSITIONS
BY ROCK TYPE

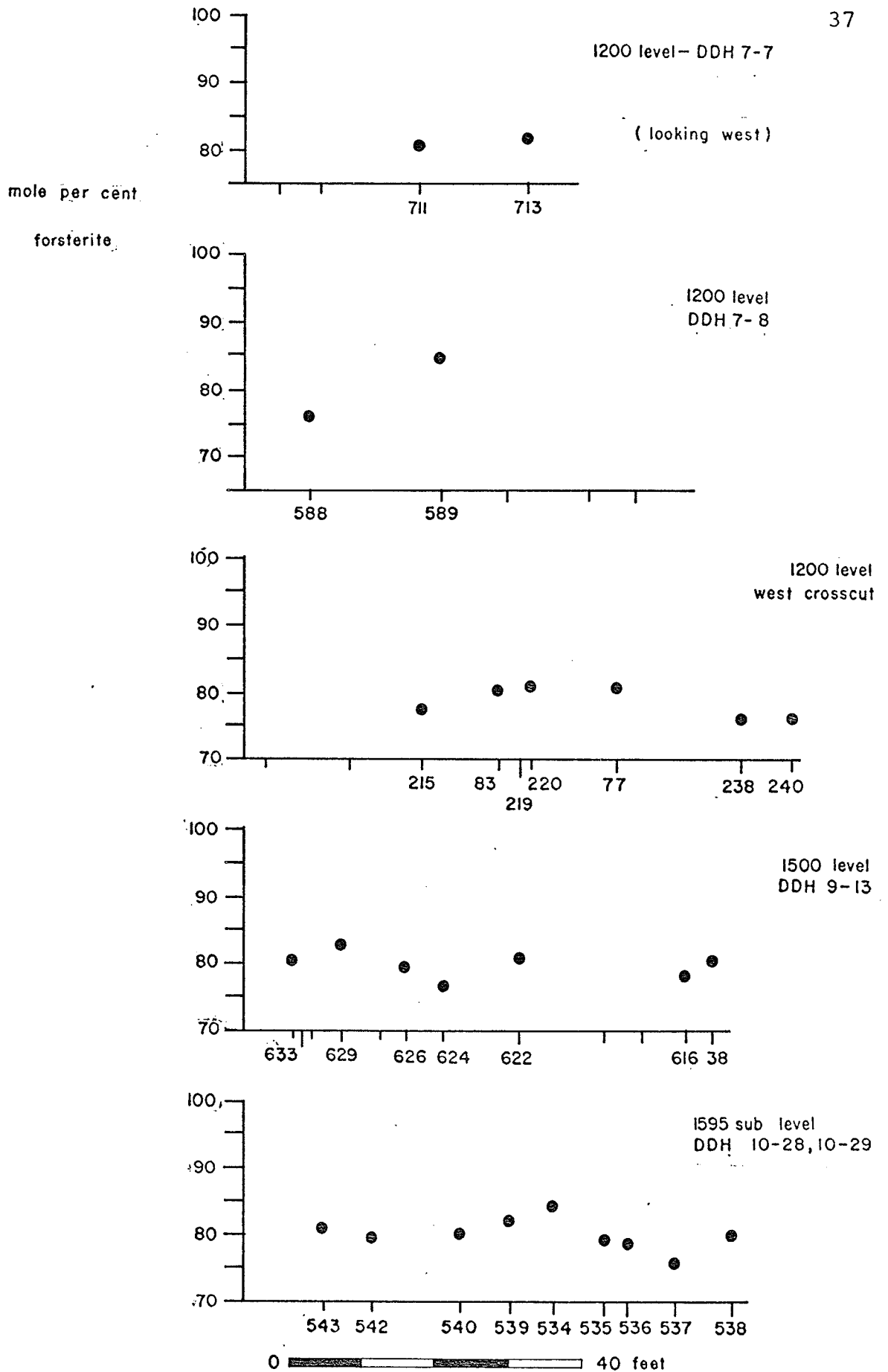
and pyroxenite to hornblende peridotite. There is no apparent change in composition from hornblende peridotite to peridotite. The distribution of olivine compositions across the A-peridotite (Figure 9) is not perfectly regular, however a trend toward increasing forsterite content from margin to centre of the body can be seen in three of the cross sections.

It has been noted previously that the modal abundance of olivine increases from the margins to the centre of the A-peridotite. Thus, in a gross way, there is a direct relation between modal abundance and forsterite content of olivine in the A-peridotite.

Orthopyroxene

Orthopyroxene occurs as equidimensional to slightly elongate plates (average grain size, 3 x 2 mm), the shapes of which are substantially modified by reaction textures with olivine and hornblende. Fine ruled line lamellae, forming parallel continuous sheets, characterize many of the orthopyroxene crystals. The lamellae are considered to represent a Ca-rich monoclinic pyroxene and the orthopyroxenes are probably of the Bushveld Type (Hess and Phillips, 1940). Orthopyroxene is altered by serpentine (bastite), talc and chlorite.

Orthopyroxene compositions were estimated from n_z and correlation charts (Hess, 1952; Deer *et al.*, 1962).



DISTRIBUTION OF OLIVINE COMPOSITIONS ACROSS THE A-PERIDOTITE

FIGURE 9

The compositions range from En₇₆ to En₉₂ , and average En_{85.5} (Table VI).

The compositions are grouped according to rock type (Figure 10) and a well-defined trend toward increasing En content is formed from peridotitic hornblendite through to peridotite. A range of 10 per cent En can be noted for three of the groups. A plot of orthopyroxene compositions across the A-peridotite is shown in Figure 11 and a trend toward increasing En content from margins to centre is well developed.

The orthopyroxene compositions thus display a distribution in the A-peridotite similar to that described for olivine.

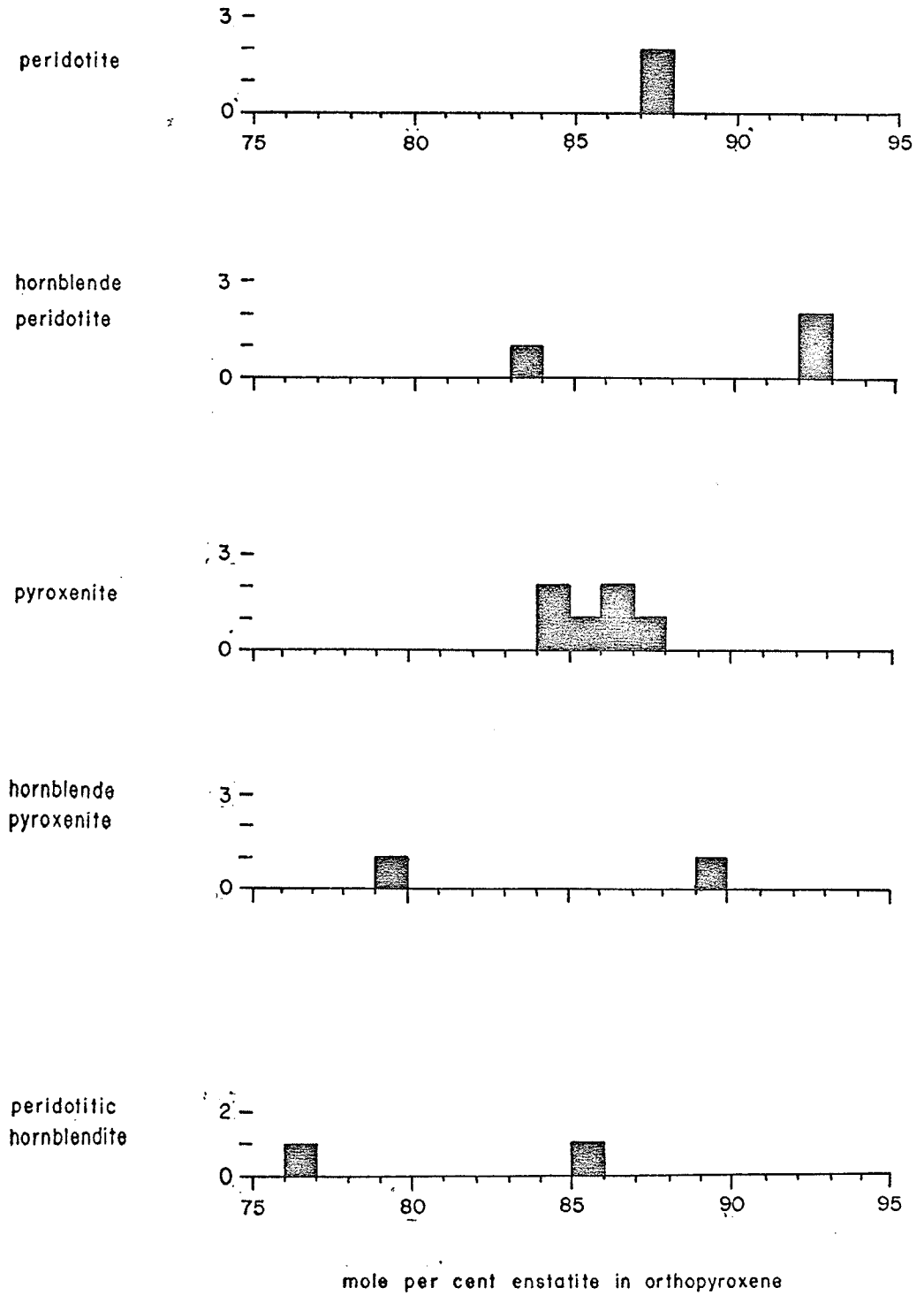
Clinopyroxene

Clinopyroxene, a minor constituent in most ultramafic rocks examined, forms local concentrations in the A-peridotite. These concentrations tend to occur in the areas intermediate between the centre and the margins of the body and form small podiform masses. In other areas, clinopyroxene occurs as small, independent, discrete grains in association with olivine, orthopyroxene and hornblende. Replacement of clinopyroxene by hornblende is common. A chemical analysis of a clinopyroxene concentrate is provided in Table VII.

Table VI

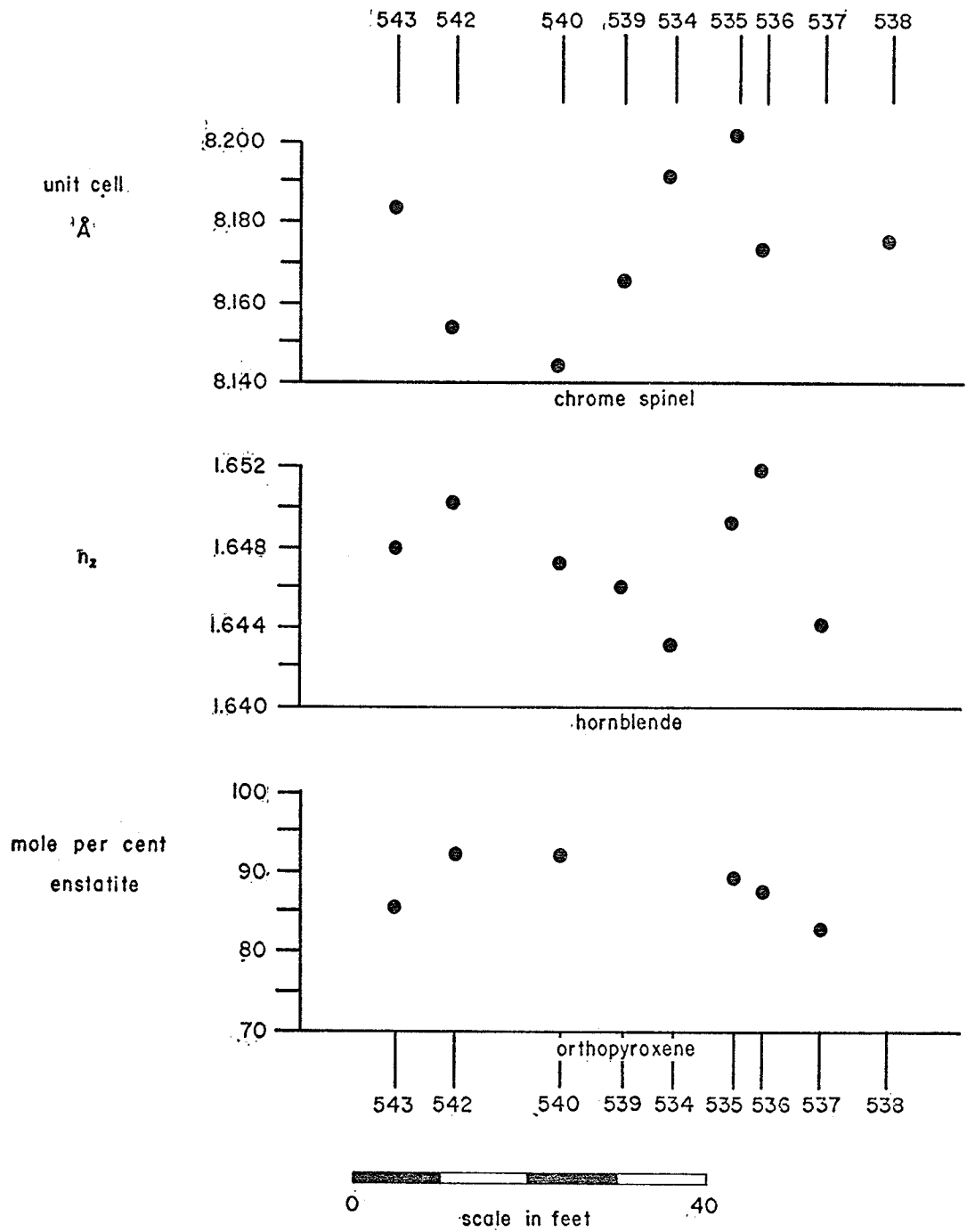
Orthopyroxene Compositions

<u>Sample No.</u>	<u>n_z</u>	<u>En (mole %)</u>
SDG61-613	1.684	85
SDG61-648	1.682	87
SDG61-661	1.679	88
SDG61-663	1.682	87
SDG61-672	1.685	84
SDG61-675	1.683	85
SDG61-536	1.681	87
SDG61-724	1.685	84
SDG61-543	1.684	85
SDG61-642	1.695	76
SDG61-616	1.691	78
SDG61-535	1.678	89
SDG61-540	1.676	92
SDG61-542	1.675	92
SDG61-537	1.686	83



DISTRIBUTION OF ORTHOPYROXENE COMPOSITIONS BY ROCK TYPE

FIGURE 10



ORTHOPYROXENE - HORNBLLENDE - CHROME SPINEL
 COMPOSITIONAL VARIATIONS ACROSS THE A-PERIDOTITE
 1595 SUB LEVEL

FIGURE II

Table VII

Chemical Analysis and Structural
Formula of Clinopyroxene

<u>Analysis*</u>		<u>Structural Formula**</u>		
SiO ₂	52.02	Si	1.917	2.000
Al ₂ O ₃	2.20	Al	0.083	
Fe ₂ O ₃	0.96	Al	0.013	2.024
FeO	2.59	Ti	0.004	
MgO	17.27	Fe ³	0.027	
CaO	23.70	Cr	0.002	
Na ₂ O	0.12	Mg	0.947	
K ₂ O	0.06	Ni	0.001	
TiO ₂	0.14	Fe ²	0.080	
MnO	0.14	Mn	0.004	
Cr ₂ O ₃	0.06	Ca	0.935	
NiO	0.02	Na	0.008	
		K	0.003	
Total	99.28			

* Analysis made by the Analytical Chemistry Division, G.S.C.

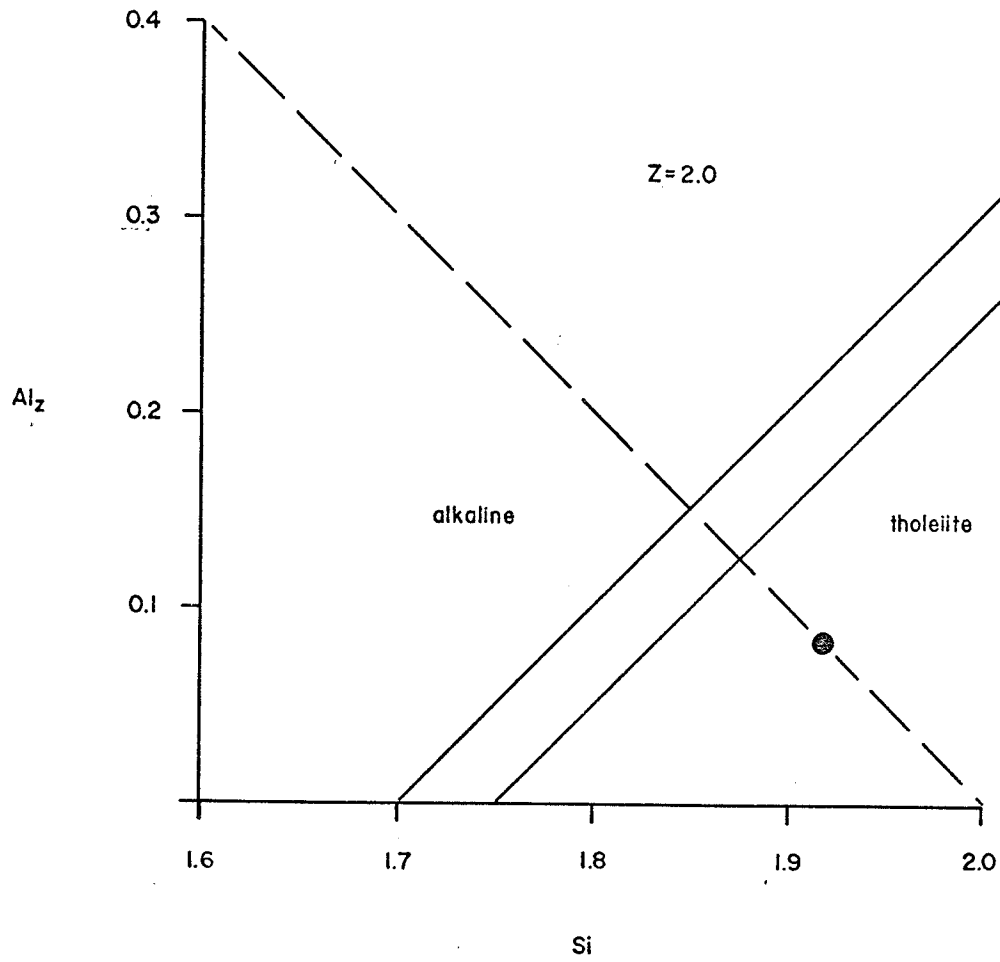
** Formula based on the number of cations/6 anions.

The Al_2 substitution in the analyzed clinopyroxene has been plotted against Si in Figure 12 (after Challis, 1965). This scheme is used to differentiate between clinopyroxene from tholeiitic and alkaline ultramafic assemblages. It can be seen that the clinopyroxene plots in the tholeiitic field.

Hornblende

Hornblende has an almost ubiquitous association with the Gordon Lake suite of ultramafic rocks. The textural relations are dominantly replacement of the earlier formed olivine, orthopyroxene and clinopyroxene, by hornblende occurring as fine equidimensional grains forming an interlocking mosaic. Its average grain size is approximately 0.7 to 1 mm although larger grains up to 2 or 3 mm are not uncommon. The hornblende is dark greenish-black in hand specimen and colourless to pale green in thin section.

In the central and intermediate areas of the A-peridotite, little difficulty is encountered in distinguishing between hornblende which has developed as a result of recrystallization of the ultramafic assemblage due to late crosscutting pegmatite dykes (discussed in Chapter V) and hornblende which represents a primary phase. The former is generally more coarse grained and much greener in colour. However, in the marginal areas the



Al_2 SUBSTITUTION IN CLINOPYROXENE
FROM THE A-PERIDOTITE (after Challis, 1965)

primary hornblende has properties similar to the recrystallized hornblende. Although this problem has not been resolved using optical properties, a slight difference in chemical composition appears to distinguish the recrystallized hornblende from marginal primary hornblende. This point is discussed in the following section.

Hornblende Compositions

Chemical compositions and structural formulae of four A-peridotite hornblendes are listed in Table VIII. Three of the samples (534, 616 and 731) represent primary hornblende and one (331) is a recrystallized hornblende from one of the contact reaction zones. A considerable range in composition exists between the four analyzed hornblendes.

Each of the primary hornblendes is associated with one other dominant primary silicate. Hornblende 534 is from a rock composed essentially of olivine and hornblende, 616 orthopyroxene and hornblende, and 731 clinopyroxene and hornblende.

Figure 13 (after Deer, Howie and Zussman, 1963) shows the variation in composition of the four analyzed hornblendes with respect to $[Al]^4$ and $(Na + K)$ atoms per formula unit, and $([Al]^6 + Fe^{3+} + Ti)$. In Figure 13a and 13b the three primary hornblendes lie close to the field

Table VIII

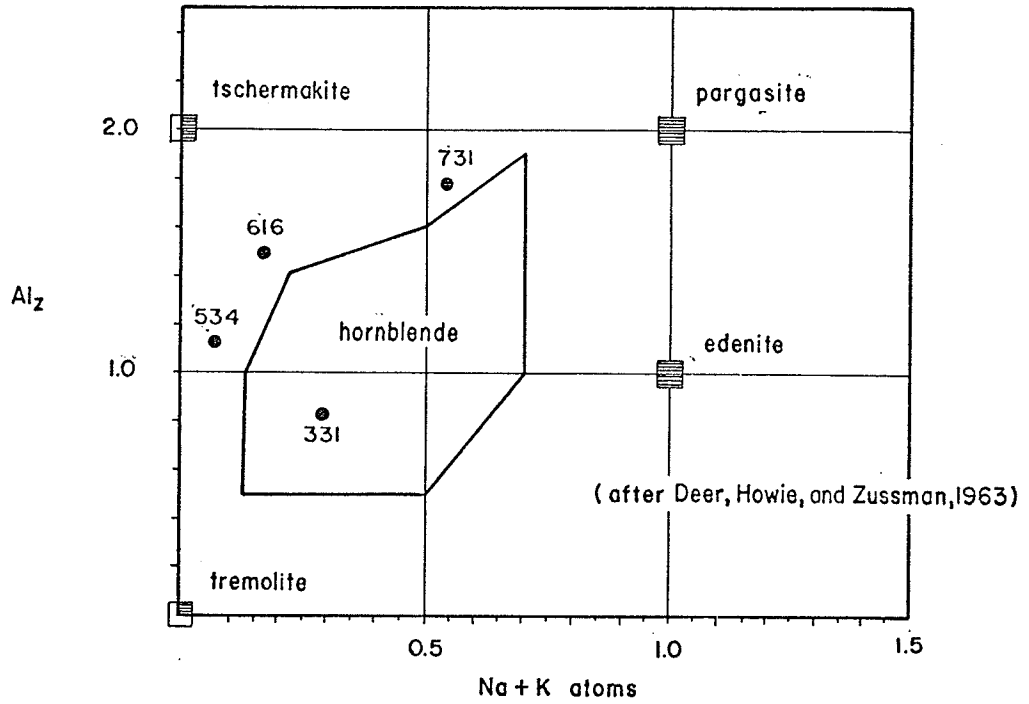
Chemical Analyses and Structural Formulae of A-peridotite Hornblendes

	534*	616*	731*	331**
SiO ₂	49.72	46.14	43.60	48.80
Al ₂ O ₃	6.99	10.59	11.92	7.54
Fe ₂ O ₃	1.57	2.31	4.23	2.92
FeO	2.88	5.09	3.25	8.90
MgO	22.14	18.38	17.43	14.44
CaO	11.74	13.00	14.10	11.18
Na ₂ O	0.17	0.44	1.27	0.80
K ₂ O	0.14	0.26	1.02	0.33
TiO ₂	0.51	0.94	0.59	0.24
MnO	0.10	0.11	0.11	0.11
H ₂ O ⁺	3.44	2.55	2.32	1.80
H ₂ O ⁻	0.06	0.05	0.03	
F ⁻	0.05	-	-	-
Cr ₂ O ₃	0.70	0.15	0.61	0.46
	<u>100.21</u>	<u>100.01</u>	<u>100.48</u>	<u>97.52</u>
$\frac{100 \text{ Mg}}{\text{Mg} + \text{Fe}^{3+} + \text{Fe}^{2+} + \text{Mn}}$	79.6	66.2	65.4	49.1
Si ⁴⁺	6.820	6.515	6.221	7.176
Al ³⁺	1.129	1.485	1.779	0.824
Fe ³⁺	0.051			
	8.000	8.000	8.000	8.000
Al ³⁺	-	0.277	0.225	0.482
Fe ³⁺	0.111	0.246	0.454	0.323
Ti ⁴⁺	0.053	0.100	0.064	0.027
Cr ³⁺	0.076	0.017	0.069	0.053
Fe ²⁺	0.330	0.601	0.387	1.095
Ni ²⁺	0.009	0.008	0.006	0.012
Mg ²⁺	4.523	3.864	3.704	3.163
Mn ²⁺	0.012	0.013	0.013	0.013
Ca ²⁺	1.724	1.965	2.155	1.760
Na ¹⁺	0.045	0.120	0.350	0.228
K ¹⁺	0.025	0.047	0.187	0.062
	1.794	2.132	2.692	2.050
OH ⁻	3.143	2.400	2.208	1.761
F ⁻	0.021			
	3.164	2.400	2.208	1.761
n _Z	1.643	1.655	1.661	1.654
Z _Λ ^c	19°	20°	20°	18°

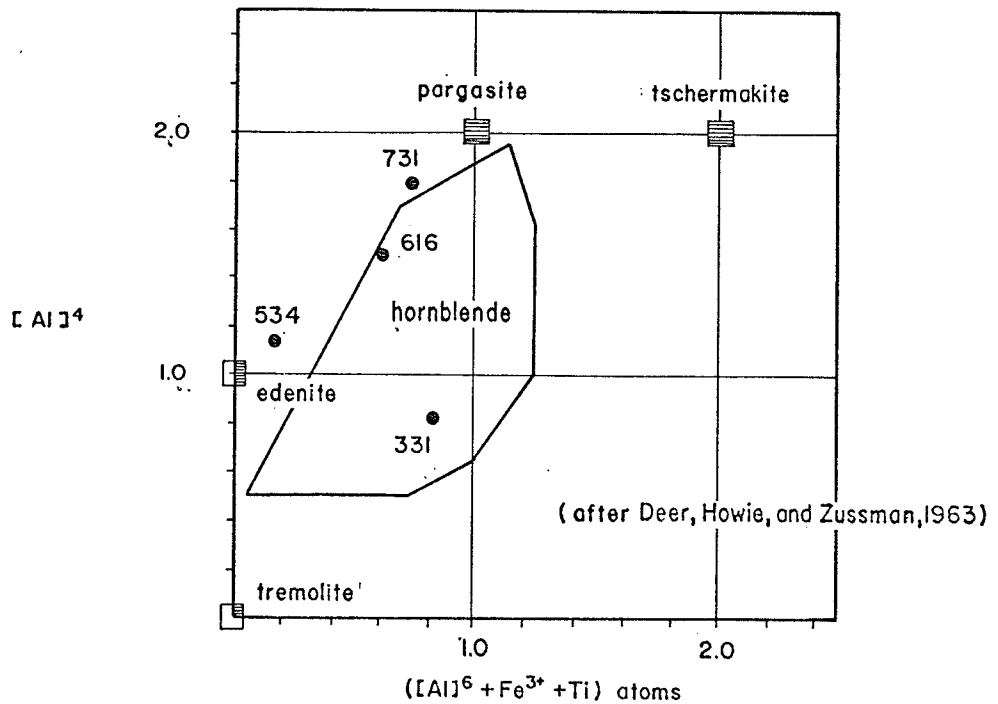
* Analyses made by the Analytical Chemistry Division, G.S.C.

** Analysis made by K. Ramlal, Geology, Department, University of Manitoba

† Structural formulae based on 24 anions



A. Expressed as the number of (Na+K) and $[Al]^{IV}$ atoms per formula unit



B. Expressed as the number of $([Al]^{VI} + Fe^{3+} + Ti)$ and $[Al]^{IV}$ atoms per formula unit

CHEMICAL VARIATION OF THE ANALYSED AMPHIBOLES

for common hornblende and display a wide range with respect to the parameters. In each diagram the recrystallized hornblende lies in the field of common hornblende. The optical properties for hornblende are listed in Table IX.

The substitution of Mg by Fe^{2+} exercises the major control on the refractive indices of the hornblende minerals. An appreciable influence is also exerted on the refractive indices by the amount of Al in tetrahedral coordination, and both substitutions, i.e., Mg by Fe^{2+} and Si by Al, are accompanied by higher refractive indices. Octahedrally coordinated Al does not differ appreciably from Mg in its effect on the optical properties of hornblendes.

The relationship between Mg/(Mg + Fe) ratio, $[\text{Al}]^4$ and n_z is shown in Table X. Attention is drawn to the small decrease in Mg/(Mg + Fe) between 616 and 731. The corresponding increase in refractive index, however, is larger than expected for a small change in Mg/(Mg + Fe). The increase in $[\text{Al}]^4$ between 616 and 731 is approximately the same as that between 534 and 616. Therefore the increase in n_z for 731 is largely due to the increase in $[\text{Al}]^4$.

Therefore, in constructing a relation between Mg/(Mg + Fe) ratio and n_z (Figure 14a), only hornblendes 534 and 616 are used. Hornblende 731 is plotted on Figure 14a and is indicative of the possible error due to Al for

Table IX

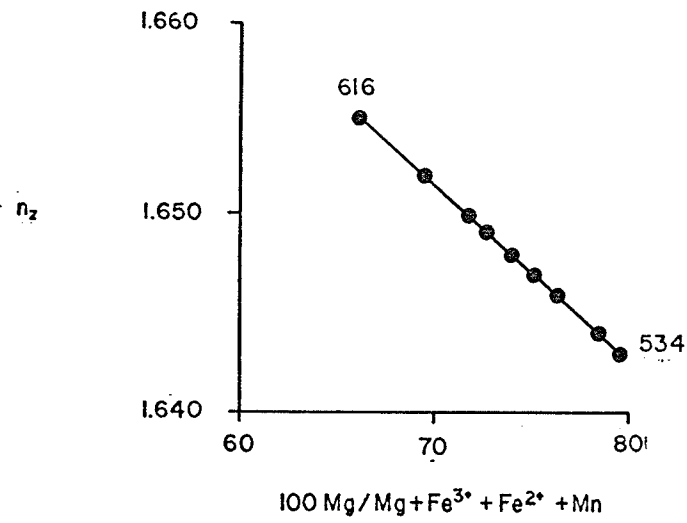
Hornblende Optical Properties

<u>Sample No.</u>	<u>n_z</u>	<u>$\frac{z}{\Lambda} c$</u>
SDG61-535	1.649	17
SDG61-537	1.644	20
SDG61-540	1.647	18
SDG61-543	1.648	19
SDG61-542	1.650	20
SDG61-539	1.646	20
SDG61-536	1.652	19
SDG61-331	1.654	18
SDG61-731	1.661	20
SDG61-642	1.660	19
SDG61-616	1.655	20
SDG61-534	1.643	19

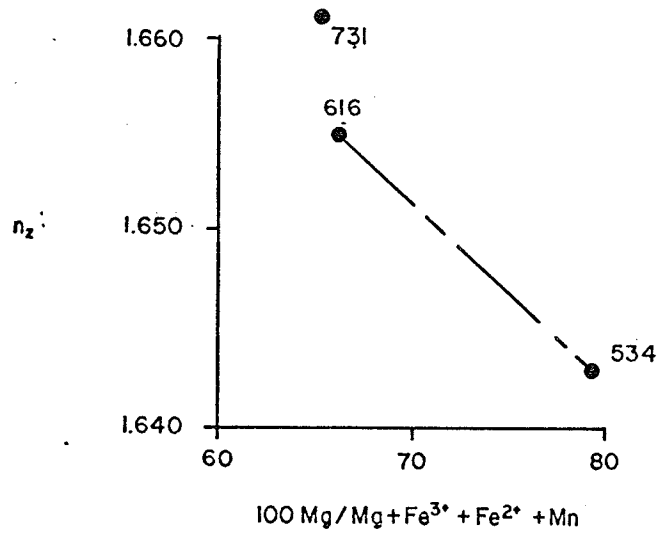
Table X

Relation between $100\text{Mg}/(\text{Mg} + \text{Fe}^{3+} + \text{Fe}^{2+} + \text{Mn})$ Ratio,
 $[\text{Al}]^4$ and n_Z in the Primary Hornblendes

<u>Sample No.</u>	<u>$100\text{Mg}/(\text{Mg} + \text{Fe}^{3+} + \text{Fe}^{2+} + \text{Mn})$</u>	<u>$[\text{Al}]^4$</u>	<u>n_Z</u>
534	79.6	1.129	1.643
616	66.2	1.458	1.655
731	65.4	1.779	1.661



B. Hornblendes plotted by n_z on curve established in A



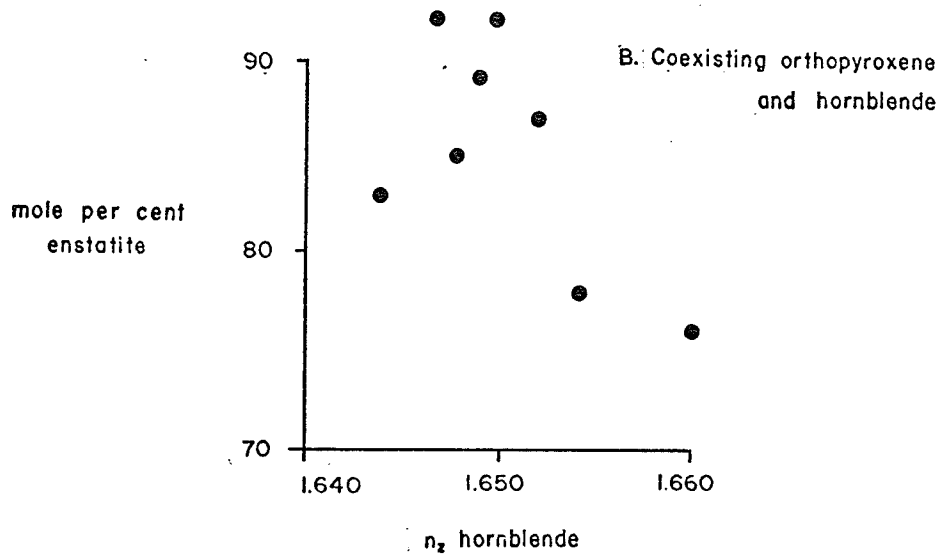
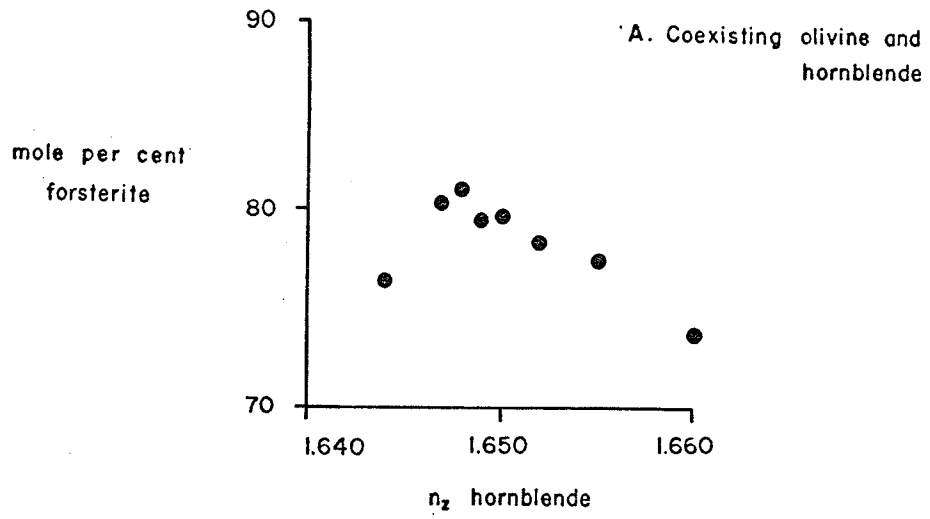
A. Analyzed hornblendes

RELATION BETWEEN $\text{Mg} / (\text{Mg} + \text{Fe})$ AND n_z - HORNBLENDE

Si substitution. In Figure 14b hornblendes 616 and 534 have been joined by a line and other A-peridotite hornblendes are plotted on the line on the basis of their n_z determinations. The plotted hornblendes represent rocks which contain less than one per cent clinopyroxene with the exception of 616 and 738 which contain 4.3 and 58.3 per cent respectively. The position of the hornblendes relative to the margins is indicated on Figure 11, and a general decrease in n_z from margin to centre is indicated. This corresponds to a decrease in the Mg/(Mg + Fe) ratio from the centre to the margins of the A-peridotite.

This trend for hornblende is similar to the trends previously observed for olivine and orthopyroxene. Figure 15 illustrates the relations between hornblende-olivine and hornblende-orthopyroxene compositions. As expected hornblende-olivine and hornblende-orthopyroxene compositions show a direct relation. The hornblende-olivine trend is extremely well defined. The direct relation between hornblende-orthopyroxene compositions is not as well marked.

A plot of octahedrally coordinated Al, ($[Al]^6$), against tetrahedrally coordinated Si, ($[Si]^4$), in the unit cell, calculated on a basis of 24(O, OH, F, Cl) made by Leake (1965) shows that metamorphic amphiboles tend to have higher $[Al]^6$ values than igneous amphiboles, although there is some overlap. The four analyzed hornblendes from



HORNBLende - OLIVINE - ORTHOPYROXENE
COMPOSITIONAL RELATIONSHIPS

FIGURE 15

Gordon Lake are plotted according to the same scheme in Figure 16. It can be seen that the three hornblendes thought to represent primary crystallization by reaction of early formed silicates and interprecipitate liquid, plot in the area of the diagram occupied dominantly by igneous amphiboles. The recrystallized hornblende from a marginal hornblendite plots in the area of the diagram occupied dominantly by metamorphic amphiboles. Therefore, by utilizing Leake's scheme it appears possible to distinguish between those hornblendes representing primary crystallization and those representing recrystallization.

Leake suggests that the higher $[Al]^6$ values for metamorphic amphiboles is partly a reflection of the higher temperatures of crystallization of igneous compared with metamorphic rocks, and that it could also reflect pressure differences during crystallization. This is because the plotted low-grade amphiboles do not contain large amounts of $[Al]^6$, but many of the amphiboles which are associated with kyanite, jadeite or glaucophane, which are indicative of high pressure conditions, plot close to the line on Figure 16. This indicates that they contain nearly the maximum possible amount of $[Al]^6$ for their corresponding silicon values.

Large pressure gradients across small ultramafic bodies, such as those at Gordon Lake, are not likely to be significant and the difference in $[Al]^6$ content of the

recrystallized hornblende (331) compared with the primary hornblendes, presumably reflects its lower temperature of formation.

Disseminated Chrome Spinel

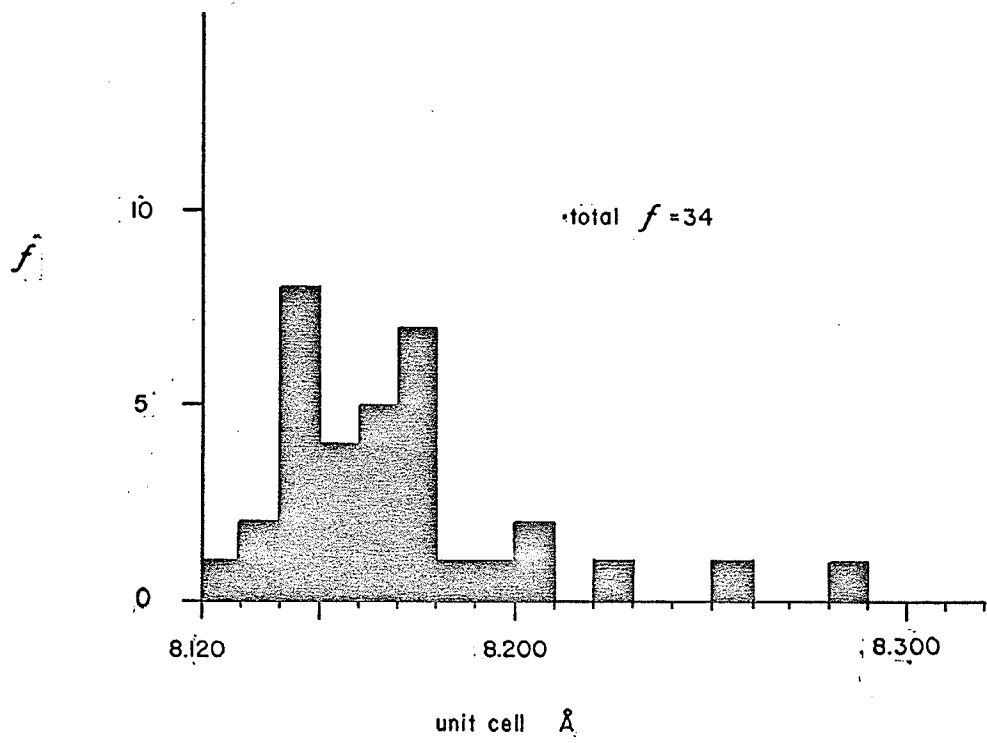
Disseminated chrome spinel is a common constituent of the Gordon Lake ultramafic suite. It occurs in a number of hosts and in a variety of forms and has a considerable range in grain size and composition. In certain areas chrome spinel appears to have been a mobile component during late stage reaction crystallization.

Chrome spinel cell edges, determined using the small diameter X-ray powder camera, were made by R.N. Delabio of the Geological Survey of Canada. Disseminated chrome spinel has a range in cell edge from 8.126 Å to 8.226 Å (Table XI and Figure 17), which corresponds to colour changes from emerald green (8.126 Å) through middle to dark green and dark brown-green to brown (8.226 Å) (Figure 18). Variations in degree of crystallinity accompany the variations in unit cell dimension and colour; the green varieties ranging from anhedral to subhedral and the dark brown-green to brown varieties from subhedral to euhedral. Correlative data on cell edge and colour of the chrome spinels indicate that the compositions lie in the general field of picotites.

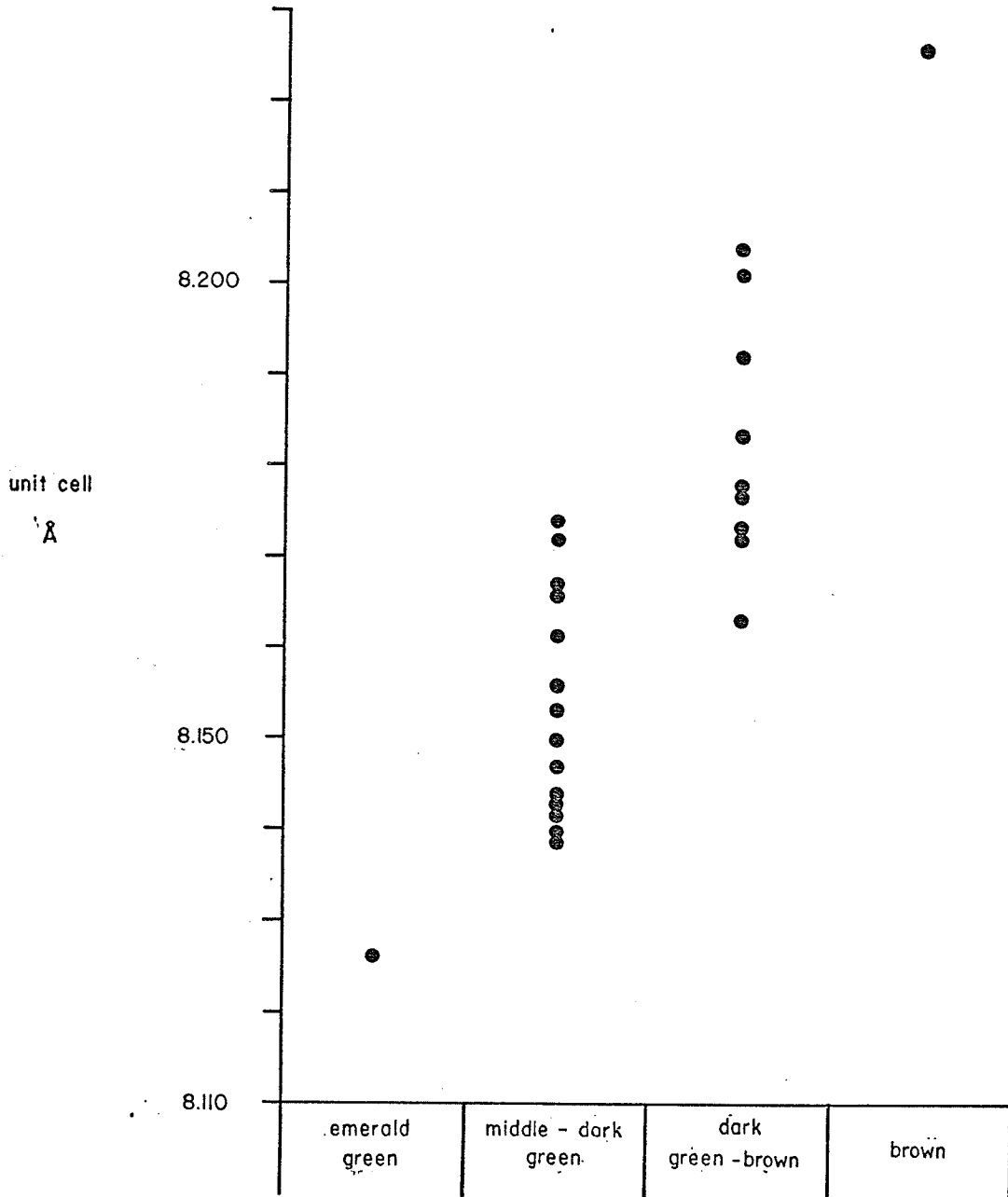
Table XI

Chrome Spinel Cell Edge Determinations

<u>Sample No.</u>	<u>Level</u>	<u>a_o</u>
SDG61-251	300	8.156 Å ± 0.005Å
SDG63-1000	300	8.256
SDG61-442	450	8.226
SDG61-592	1200	8.172
SDG61-591	1200	8.173
SDG61-77A	1200	8.150
SDG61-240	1200	8.172
SDG61-593	1200	8.201
SDG61-219	1200	8.167
SDG61-589	1200	8.163
SDG61-588	1200	8.126
SDG61-596	1200	8.139
SDG61-713	1200	8.161
SDG61-721	1200	8.178
SDG60-5	1350	8.140
SDG60-6	1350	8.144
SDG60-17B	1350	8.142
SDG61-622A	1500	8.285
SDG61-632	1500	8.167
SDG61-624	1500	8.144
SDG61-626	1500	8.144
SDG61-617	1500	8.149
SDG61-616	1500	8.138
SDG61-631	1500	8.170
SDG61-629	1500	8.155
SDG61-536	1595	8.177
SDG61-543	1595	8.183
SDG61-642	1595	8.147
SDG61-535	1595	8.204
SDG61-542	1595	8.153
SDG61-539	1595	8.166
SDG61-538	1595	8.174
SDG61-534	1595	8.192
SDG61-540	1595	8.143



DISTRIBUTION OF CHROME SPINEL CELL EDGES



COLOUR VARIATIONS Vs UNIT CELL - CHROME SPINEL

FIGURE 18

Opaque chrome spinels from the small chromite pods have larger cell dimensions than the disseminated chrome spinels; two measuring 8.265 and 8.285 Å, respectively. Chrome spinel in this association is generally euhedral.

The distribution of chrome spinel cell edges by position within the A-peridotite is shown in Figure 11. The trend toward larger unit cell dimensions (higher Cr₂O₃ content) in the centre of the body is well marked, although there is an anomalously high cell edge at the south margin. The cryptic variation of the chrome spinels is similar to the cryptic variations displayed by olivine, orthopyroxene, and hornblende.

Chemical Variations Across the A-peridotite

A series of analyzed specimens from the A-peridotite is chosen to represent the chemical variation from the centre to the margin of the body. The modal variations of these specimens are listed in Table XII and plotted on Figure 19. It can be seen that the major ultramafic lithologic units are represented by this series. These samples are also selected so that chemical effects due to second stage recrystallization are a minimum. Sample 642, a marginal peridotitic hornblendite, is included in the series, although the hornblende present in this specimen may have been formed by recrystallization.

Figure 20 is a purely diagrammatical representation

Table XIII

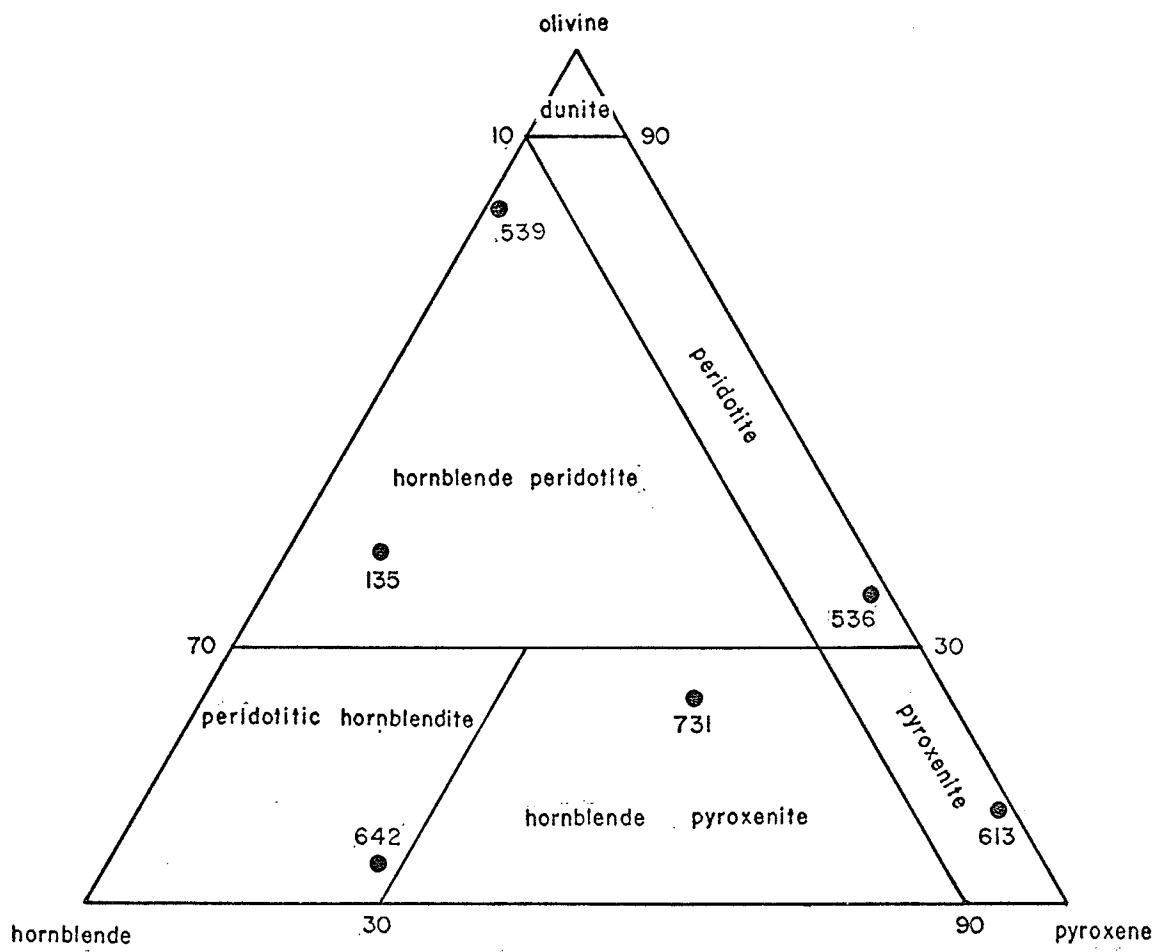
Chemical Analyses* - A-peridotite Series

	<u>539</u>	<u>536</u>	<u>613</u>	<u>135</u>	<u>731</u>	<u>642</u>
SiO ₂	32.0	36.7	49.9	39.8	36.7	41.5
Al ₂ O ₃	8.2	6.9	6.7	7.7	8.9	9.96
Fe ₂ O ₃	0.3	2.4	3.4	6.9	9.2	3.80
FeO	21.3	20.7	12.2	6.8	6.4	8.96
CaO	3.2	0.9	0.6	4.8	5.5	6.40
MgO	25.4	26.9	26.9	24.8	22.6	17.24
Na ₂ O	0.3	0.1	0.1	0.2	0.4	0.92
K ₂ O	0.08	0.08	0.05	0.2	1.5	0.36
TiO ₂	0.09	0.42	0.02	0.16	0.24	0.43
MnO	0.12	0.16	0.18	0.14	0.13	0.23

Modal Analyses - A-peridotite Series

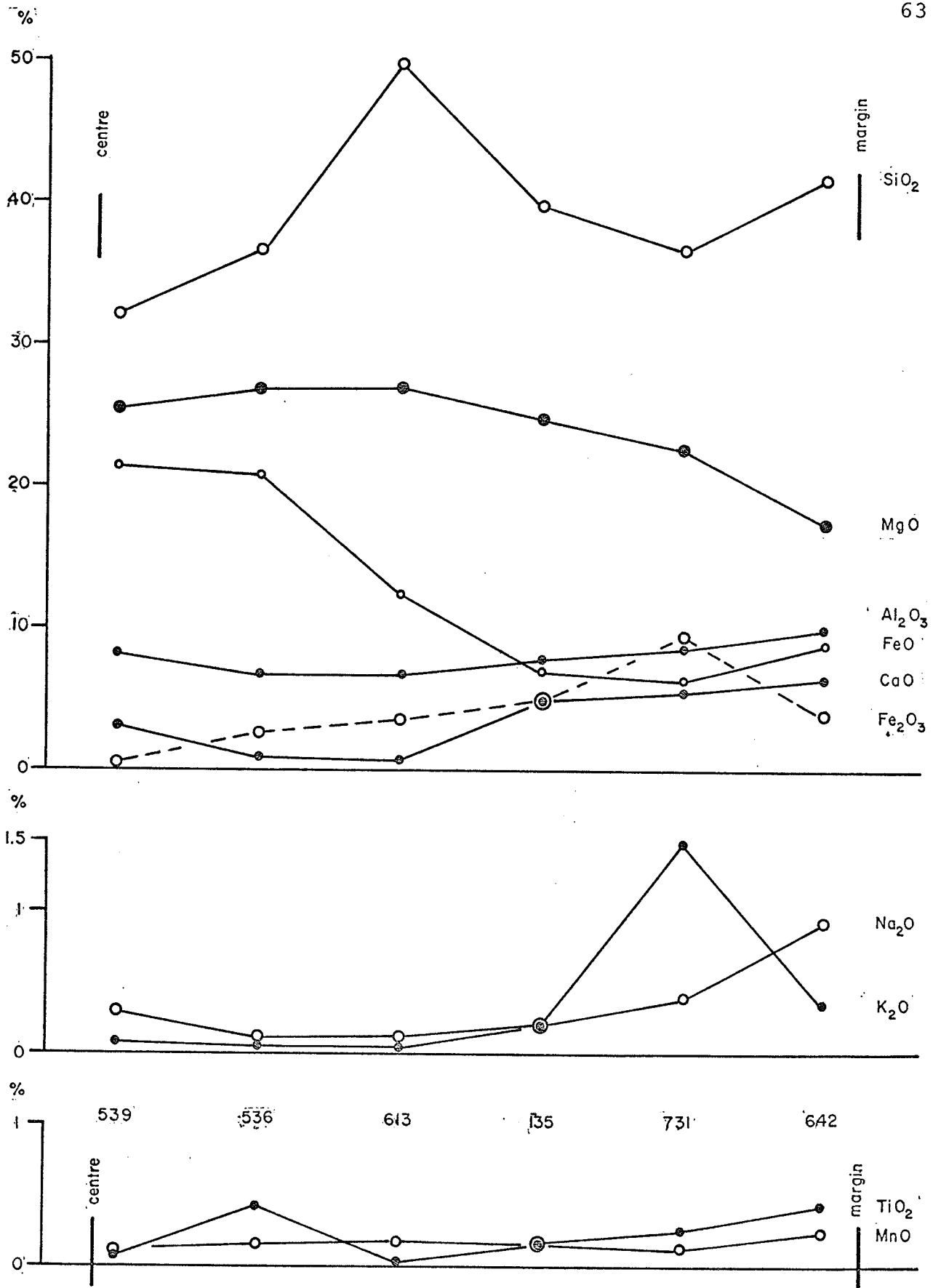
	<u>539</u>	<u>536</u>	<u>613</u>	<u>135</u>	<u>731</u>	<u>642</u>
Olivine	17.2	14.9	3.7	3.6	6.2	2.0
Serp. (ol.)	37.7	7.9	3.4	26.6	12.1	1.1
Mgt. (ol.)	17.4	7.2	0.2	8.0	4.9	2.0
Cpx.	0.5	-	-	-	53.3	-
Opx.	-	50.8	84.0	2.6	-	26.5
Serp. (opx.)	-	-	-	6.4	-	0.6
Hnblde	14.0	2.0	1.9	45.0	10.9	64.7
Chrome sp.	8.7	11.2	3.7	3.7	4.0	2.2
Mgt.	-	-	-	-	-	0.7
Sulphide	4.5	4.9	3.0	4.1	3.6	0.2
Talc	-	0.9	-	-	-	-
Calcite	-	-	-	-	-	-
Chlorite	-	-	0.1	-	-	-
Total	100.0	100.0	100.0	100.0	100.0	100.0

* Analyses made by the Analytical Chemistry Division, G.S.C.



MODAL COMPOSITION - A-PERIDOTITE SERIES

FIGURE 19



CHEMICAL VARIATIONS - A-PERIDOTITE SERIES

FIGURE 20

of the chemical variations in that the specimens from different levels which cut across the A-peridotite are plotted according to an arbitrary scale to represent a sequence from the centre to the margin of the body.

The general observations which can be made from Figure 20 are: an increase in SiO_2 , Al_2O_3 , CaO , Fe_2O_3 , Na_2O , K_2O , MnO , TiO_2 ; and a decrease in MgO and FeO from the centre to the margins of the A-peridotite. The trends in the bulk chemistry are somewhat variable, but in general they reflect the modal variations and cryptic zoning of the primary silicate mineral assemblage as previously described.

SiO_2 displays a general increase from the centre to the margin of the body. The high SiO_2 content of the orthopyroxenite, sample 613, can be seen. The overall trend for SiO_2 is believed to reflect the trend of increasing modal abundance of hornblende and pyroxene at the expense of olivine, from centre to margin of the A-peridotite.

Al_2O_3 displays little variation across the body. This is difficult to explain, especially because the first three specimens contain little hornblende. It is probable, however, that sufficient Al_2O_3 is present in the chrome spinel to account for that present in the first three specimens. Two of the last three specimens contain abundant hornblende and the other (731) contains clino-

pyroxene. The Al_2O_3 content of these three specimens is therefore due to the abundance of hornblende and clinopyroxene.

CaO appears to be directly related to the abundance of hornblende and in sample 731, clinopyroxene.

Fe_2O_3 displays a marked regular increase from the centre to the margin of the A-peridotite. It was previously noted that the Fe_2O_3 content of the analyzed hornblendes also increased from centre to margin of the body, and hornblende probably exercises the main control in the distribution of Fe_2O_3 .

FeO displays a regular decrease across the body and directly reflects the modal abundance of sulphide minerals, chrome spinel and olivine. The decrease in FeO far outweighs the increase in Fe_2O_3 across the body and the trend for total iron ($\text{FeO} + \text{Fe}_2\text{O}_3$) is reversed to that indicated by the cryptic zoning of the primary silicate minerals. However, the distribution of sulphide minerals and chrome spinel probably controls the distribution of FeO in the bulk rock analyses.

MgO is concentrated in the three central specimens and then displays a regular decrease to the margin of the body. This trend reflects the cryptic zoning of the primary assemblage which in turn is due to the sequence and mechanism of crystallization. This latter aspect is discussed in Chapter IV.

Na_2O and K_2O both are minor constituents and both display a slight increase toward the margin of the body. Both are probably controlled by hornblende and minor amounts of phlogopite may affect the distribution of K_2O .

MnO and TiO_2 both display a slight increase toward the margins of the body and are probably controlled by hornblende.

The regular increase of Fe_2O_3 from centre to margin in the A-peridotite is similar to the distribution of Fe_2O_3 in the analyzed primary hornblendes (Table VIII). This could suggest that $p\text{O}_2$ increased during crystallization thereby causing an increase in the Fe_2O_3 contents of the later formed hornblendes. The overall increase in Fe_2O_3 in the bulk rock analyses is therefore considered to be a reflection of the trend of Fe_2O_3 in hornblende which in turn is related to increasing $p\text{O}_2$ during crystallization

The decrease in FeO from centre to margin of the body, due in large measure to the distribution of sulphide minerals and chrome spinel, means that the cryptic zoning, which is well documented in the primary mineral assemblage is not as well displayed in the bulk rock chemistry (Table XIII).

Ternary Plot $5\text{CaO} - 2(\text{FeO} + \text{Fe}_2\text{O}_3) - \text{MgO}$

The sequence of six analyzed A-peridotite rocks are plotted utilizing the scheme $5\text{CaO} - 2(\text{FeO} + \text{Fe}_2\text{O}_3) - \text{MgO}$

Table XIII

MgO/MgO + FeO and Mineral Compositions - A-peridotite Series

<u>Sample No.</u>	<u>MgO/MgO + FeO</u>	<u>% Fo</u>	<u>% En</u>	n_z <u>Hnblde</u>	a_o <u>Chrome Spinel</u>
SDG61-539	66.2	82.2	-	1.646	8.166
SDG61-536	61.7	78.2	87	1.652	8.177
SDG61-613	63.8	-	85	-	-
SDG61-135	67.9	80.9	-	-	-
SDG61-731	62.1	79.5	-	1.661	-
SDG61-642	58.2	73.7	75	1.660	8.147

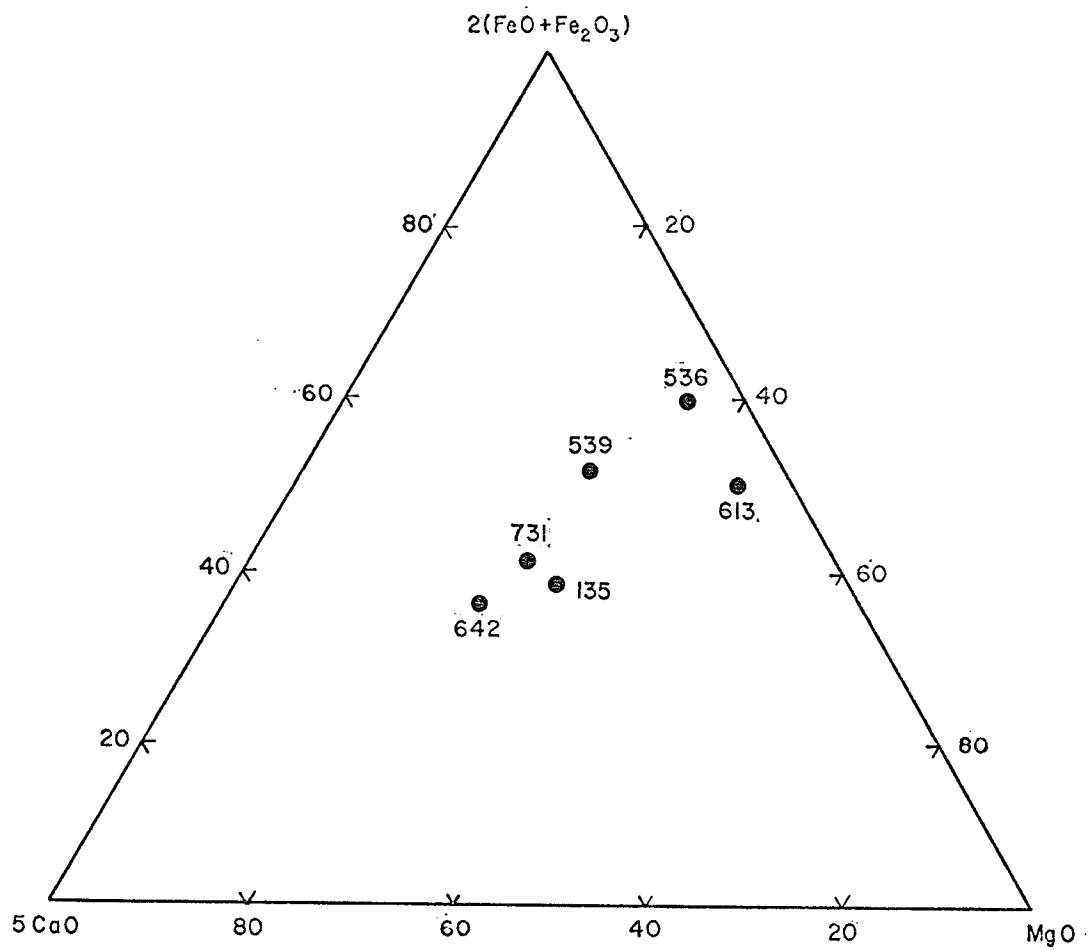
(Figure 21) after Ogura and Kuroda (1967). This scheme appears to have some advantages over the standard CaO - (FeO + Fe₂O₃) - MgO scheme by enhancing the effects of CaO and (FeO + Fe₂O₃). Fluctuations in CaO and (FeO + Fe₂O₃) are therefore more pronounced in this type of diagram.

The series of six A-peridotite rocks produce a trend from the 2(FeO + Fe₂O₃) - MgO join, toward the 5CaO corner (Figure 21). The rocks from the central area plot close to the 2(FeO + Fe₂O₃) - MgO join while the rocks from the marginal areas plot towards the 5CaO corner. The increase in CaO reflects an increase in the modal abundance of amphibole.

The analyzed ultramafic samples are plotted on the base of the basalt tetrahedron (Yoder and Tilley, op. cit.) and all points but one lie in the field of olivine tholeiite (Figure 22). The plotted points form a trend from the 01 corner toward the Opx-Pl join on the diagram.

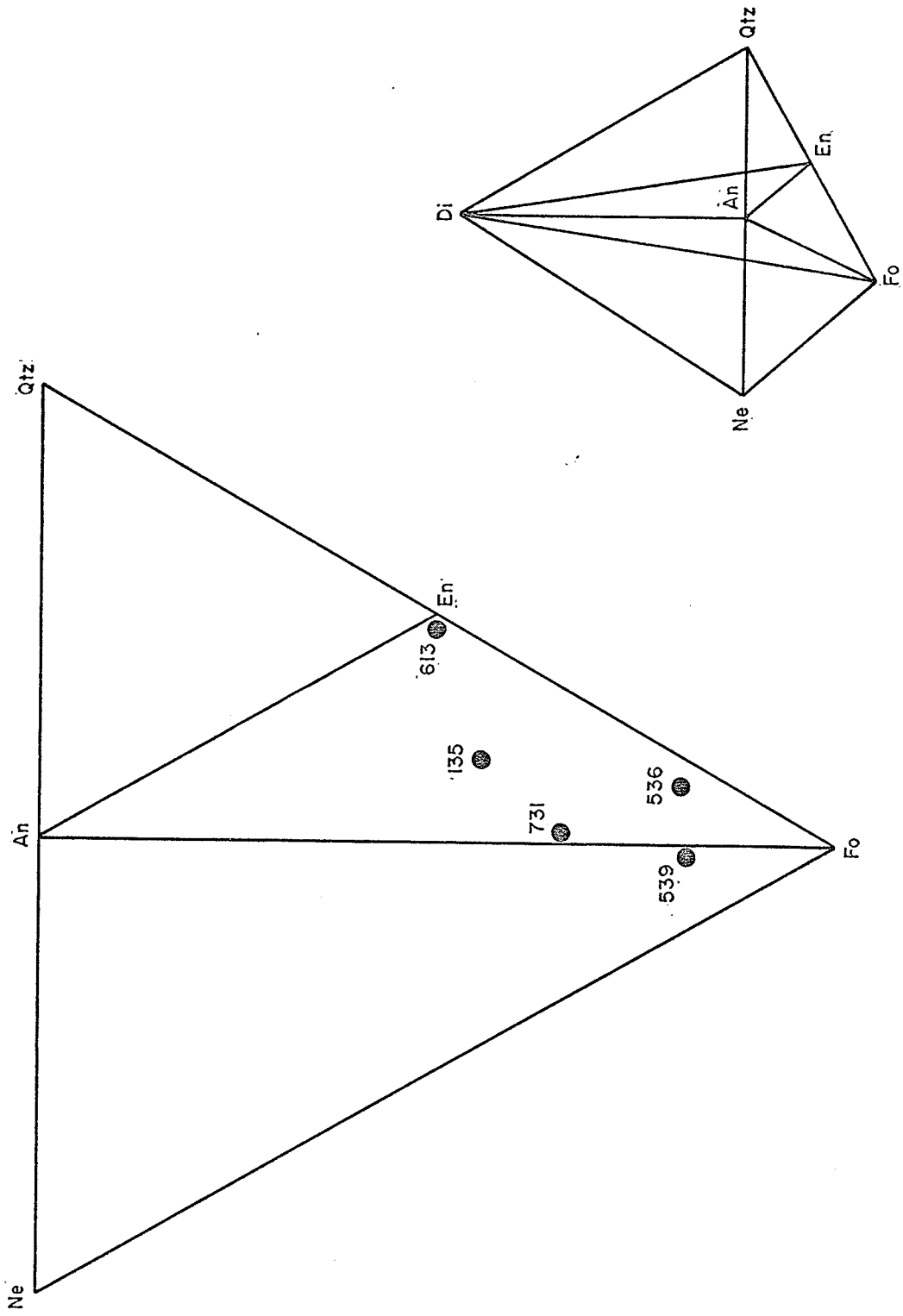
Trace Element Data - A-peridotite Series

The distribution of certain trace elements for the A-peridotite series is shown in Table XIV. Marked trends can be seen for the Ni and Co distributions. Both trends decrease from the centre to the margin and both are totally influenced by the abundance of sulphide minerals. The extremely low values for 613 are due to the lack of



5CaO - 2(FeO+Fe₂O₃) - MgO, A-PERIDOTITE SERIES

FIGURE 21



A-PERIDOTITE SERIES, PLOTTED ON BASE OF BASALT TETRAHEDRON (after Yoder and Tilley, 1962)

Table XIV

Trace Element Data[†] - A-peridotite Series*

	<u>539</u>	<u>536</u>	<u>613</u>	<u>135</u>	<u>731</u>
Sr	N.F.	N.F.	N.F.	0.0036	0.0062
Ba	0.0022	0.003	0.0032	0.0017	0.011
Cr	0.77	0.56	0.29	0.40	1.3
V	0.012	0.022	0.0079	0.011	0.017
Ni	1.1	0.90	0.056	0.57	0.38
Cu	0.7	0.7	0.0089	0.15	0.11
Co	0.046	0.036	0.0057	0.017	0.014
Sc	N.F.	0.01	0.01	0.0048	0.0048

† in per cent

* Analyses by Optical Spectrographic Laboratory of G.S.C.

sulphide in that sample.

Chrome (Cr) displays a decrease from 539 to 613, a slight increase from 613 to 135 and a marked increase for 731. The distribution of Cr should be directly related to the distribution of chrome spinel but as far as can be seen from the modal variations this does not appear to be the case. However, small chromite pods occur toward the marginal areas and it is likely that the high Cr value for 731 is due to one or more of these small pods that was not seen in thin section.

Vanadium (V) displays an erratic distribution and has its greatest concentration in 536 decreasing between 536 and 613 and then increasing toward the margin. Vanadium may be influenced by the modal distribution of magnetite.

Barium (Ba) remains relatively constant across the series and then shows a marked increase in 731 and is probably influenced by the abundance of clinopyroxene.

Summary of Mineralogical and Chemical Variations
Across the A-peridotite

The modal and cryptic variations of the primary mineral assemblage and bulk rock chemical variations define a broad, somewhat irregular concentric zonal arrangement within the A-peridotite. The variations are summarized below:

- (i) increase in modal abundance of olivine from

- the margin to the centre of the body,
- (ii) decrease in modal abundance of hornblende from margin to centre,
 - (iii) irregular distribution of pyroxene with a tendency to concentrate between the centre and the margin of the body,
 - (iv) cryptic zoning of the primary silicate minerals, marked by an increase in $Mg/(Mg + Fe)$ from margin to centre, and
 - (v) trends in bulk rock chemistry which reflect the modal and cryptic variations of the primary mineral assemblage.

CHAPTER IV

COEXISTING PRIMARY MINERALS AND CRYSTALLIZATION CHEMISTRY

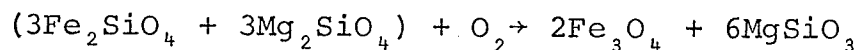
Olivine-orthopyroxene Textures

The dominant texture of coexisting olivine and orthopyroxene is one of optically continuous olivines poikilitically enclosed by orthopyroxene. As orthopyroxene increases in modal abundance, optically continuous olivine grains included in orthopyroxene become more widespread. Inclusions of fine-grained chrome spinel and magnetite (\pm sulphide) as well as coarser-grained (up to 1mm) irregularly shaped chrome spinel are common in orthopyroxene. There is a common association of a rim of olivine surrounding some of the larger irregular chrome spinel inclusions. Orthopyroxene appears to have formed by reaction of olivine with interprecipitate magma. Compositions of coexisting olivine and orthopyroxene indicate that the MgO/FeO ratio is greater in orthopyroxene than in the coexisting olivine. A reaction relationship between early formed olivine and orthopyroxene has been observed in many basic rocks.

Kuno (1950), Muir and Tilley (1957), and Yoder and

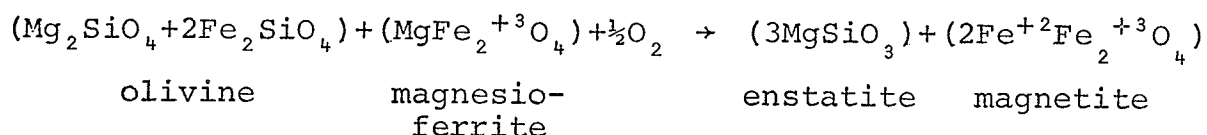
Tilley (1962) have discussed the nature of this relationship. Kuno, in a study of Hakone volcano found that olivine is frequently surrounded by a corona of porphyritic hypersthene and that the hypersthene corona, in some instances, encloses vermicular magnetite. In a more advanced stage of resorption, when the olivine disappears completely, the whole aggregate consists of dense stellate groupings of vermicular magnetite in the centre and a corona of hypersthene in the margin. The resorption of olivine gives rise to separation of magnetite along its margin, which, upon complete disappearance of the olivine, tends to coalesce to form porphyritic grains. Kuno concludes that the reaction rims around crystals of olivine are formed by using materials introduced both from the crystals and from the magma.

Muir and Tilley (1957) outlined the effect of oxygen on the olivine-orthopyroxene reaction relation by the following reaction:



Yoder and Tilley (1962) concur with the above reaction and consider the hypersthene corona and abundant magnetite to represent oxidation of olivine, not resorption by liquid. From a study of a picritic basalt from Hawaii they find that most of the magnetite is concentrated in spheres surrounding what appears to be grains of magnesio-

ferrite rimmed by magnetite. They state that the grains of magnesioferrite have apparently acted as oxidation centres. The magnesioferrite grains rimmed with magnetite are usually separated from the spherical zone containing dispersed magnetite by a sphere of hypersthene. Hypersthene is particularly concentrated where two oxidation spheres coalesce. Yoder and Tilley conclude that the formation of hypersthene probably evolves in the following way:



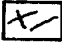




An example of the reaction relationship under discussion is shown in Figure 23. The association of olivine, orthopyroxene, a green spinel and magnetite can be seen. Because chrome spinel crystallizes early in the crystallization sequence it might act as oxidation centres for the formation of magnetite during the reaction. In any event, $p\text{O}_2$ must have been at a critical value to allow the formation of the oxide phase. The consequences of the reaction relation on the compositions of coexisting olivine and orthopyroxene are discussed in the next section.

Olivine-orthopyroxene Compositions

The compositions of ten olivine-orthopyroxene pairs from the A-peridotite are listed in Table XV. One pair is



field is 1.8 mm

-  orthopyroxene
-  optically continuous olivine
-  serpentine
-  magnetite
-  green chrome spinel

OLIVINE - ORTHOPYROXENE REACTION RELATION

FIGURE 23

Table XV

Distribution Constants for Coexisting
Olivine and Orthopyroxene

<u>Sample No.</u>	<u>X_{ol}</u>	<u>X_{opx}</u>	<u>X_m</u>	<u>K¹</u>	
540	80.2	92	86.1	2.840	Centre
535	79.5	89	84.3	2.087	
542	79.6	92.5	86.1	3.157	
663	80.6	87	83.8	1.606	Intermediate
536	78.2	83	80.6	1.362	
648	80.0	87	83.5	1.673	
543	81.0	85	83.0	1.332	
537	76.2	83	79.6	1.523	Margin
642	73.7	76	74.9	1.131	
616	77.4	79	78.2	1.098	

$${}^1 K = \frac{X_{\text{opx}}}{1 - X_{\text{opx}}} \cdot \frac{1 - X_{\text{ol}}}{X_{\text{ol}}} \quad (\text{Ramberg and de Vore, 1951})$$

from the centre of the body, five from an area intermediate between the centre and the margin and four from marginal areas. It can be noted that the orthopyroxenes display a regular decrease in enstatite content from the centre to the margin, while the olivines representing the central and intermediate areas show little variation in forsterite content. Only the marginal olivines show a significant decrease in forsterite content. However, in each case, orthopyroxene is more Mg-rich than the coexisting olivine.

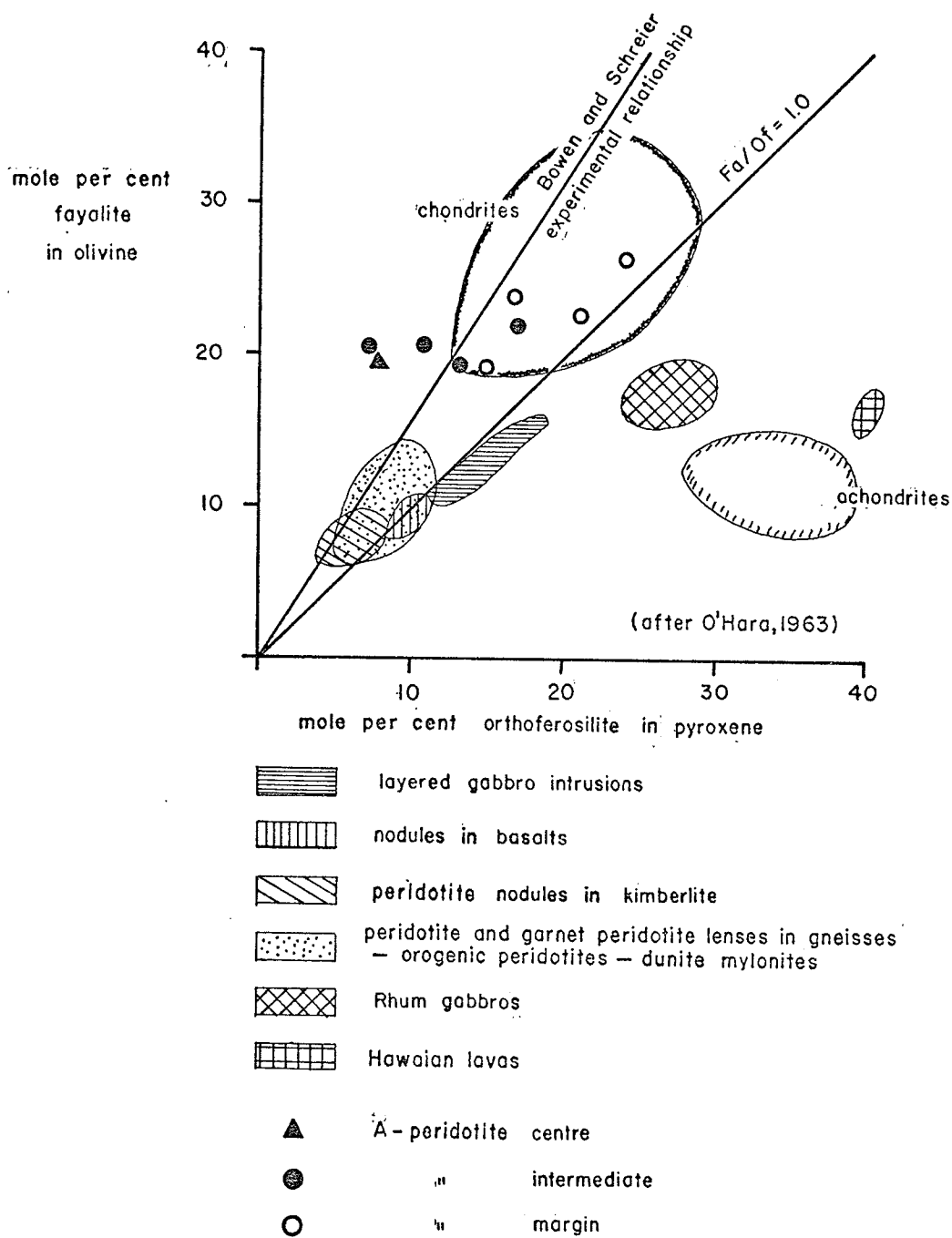
Several workers have investigated the relationships between coexisting olivine and orthopyroxene. Ramberg and de Vore (1951) determined that in natural assemblages olivine contained less Mg than the coexisting orthopyroxene when the average mole fraction was less than approximately 0.65. Within the Mg-rich part of the diagram, olivine was found to be richer in Mg than the coexisting orthopyroxene. The average mole fraction of the olivine-orthopyroxene pairs from the A-peridotite is much greater than 0.65 and their comparative compositions display a reverse relation to that expected from the data of Ramberg and de Vore. It should be noted, however, that very few assemblages from ultramafic rocks are represented in Ramberg and de Vore's work.

O'Hara (1963) presents data for 160 natural assemblages of olivine and Ca-poor pyroxene. The data are grouped according to the differing geologic environments

of the specimens and are reproduced in Figure 24. The data are compared with a curve taken from the data of Bowen and Schairer (1935), which shows the distribution of Fe^{2+} between the two silicates at atmospheric pressure in the artificial system. All the determinations of natural igneous rocks depart from the experimentally determined relationship, and the departure is greatest in those rocks that have crystallized most rapidly.

The olivine-orthopyroxene pairs, which are grouped according to their position in the A-peridotite, are also plotted on Figure 24 for comparison with the data of O'Hara. The olivines of the A-peridotite are more Fe-rich than those of the other assemblages except for the large field occupied by chondrite meteorites. The pairs from the central and intermediate areas of the A-peridotite lie on either side of the line representing the experimental relationship of Bowen and Schairer. Two of the four pairs from the marginal areas of the A-peridotite lie along the line representing $Fa/Of = 1.0$. Each of the three areas of the A-peridotite therefore exhibits a different relationship between olivine-orthopyroxene pairs. The differences are considerable compared with the groupings of the other assemblages and taking into account the small size of the A-peridotite.

If the errors in the determination of the compositions of olivine and orthopyroxene are small and the compositions



COEXISTING OLIVINE AND ORTHOPYROXENE

FIGURE 24

and distribution differences are real, O'Hara suggests two possible explanations for the differences. The first is that the equilibrium distribution is changed by the different temperatures and pressures of crystallization, corresponding to the different environments of formation. Alternatively, it may be assumed that a significant departure from equilibrium could cause a discrepancy between some assemblages. Any factor therefore that hinders free interaction between the early olivine crystals and the liquid will tend to produce disequilibrium assemblages in which $\frac{\text{Fe}^{2+}/\text{Mg}^{2+} \text{ in olivine}}{\text{Fe}^{2+} \text{ Mg}^{2+} \text{ in pyroxene}}$ is less than the equilibrium value.

On this basis the pairs from the central and intermediate areas of the A-peridotite approximate the experimental equilibrium as determined by Bowen and Schairer, and the marginal pairs approach an Fa/Of ratio of 1.0.

Distribution constants calculated for the ten olivine-orthopyroxene pairs are listed in Table XV. They have been calculated utilizing the scheme of Ramberg and de Vore (op. cit.).

The distribution constants calculated display a grouping similar to that shown in Figure 24. The distribution of Mg in olivine and orthopyroxene of the pairs is relatively constant in each of the three groups

and a decrease in the difference between the Mg content of orthopyroxene and olivine is consistent from centre to margin of the A-peridotite. Since large temperature and/or pressure differences are not likely to exist across a body as small as the A-peridotite then some other mechanism must be appealed to in order to explain the changes observed. Separation of early formed olivine from the liquid during crystallization is one such mechanism.

Chemistry of Coexisting Primary Minerals

Analyses of three primary silicate pairs are listed in Table XVI. The pairs, olivine-hornblende, orthopyroxene-hornblende and clinopyroxene-hornblende are from the A-peridotite, and in each case the mineral pair represents the major minerals represented in the rock. Modal analyses of these rocks are listed in Table XVII. The chemical analysis of the orthopyroxene totals 94 per cent, and it is, therefore, only used for comparative purposes.

As previously noted, the observed order of crystallization of the primary silicates is olivine, orthopyroxene clinopyroxene and hornblende; the hornblende being primary and representing reaction between the early silicates and the interprecipitate liquid. Hornblende, therefore, is considered to reflect the compositional change of the liquid during crystallization.

A number of silica variation diagrams have been

Table XVI

Chemical Analyses of Coexisting Minerals - A-peridotite

	Olivine ¹	Hnblde	Opx	Hnblde	Cpx	Hnblde	A ²
	534	534	616	616	731	731	
SiO ₂	39.9	49.72	51.0	46.14	52.02	43.60	49.16
Al ₂ O ₃	1.6	6.99	3.6	10.59	2.20	11.92	13.33
Fe ₂ O ₃	0.4	1.57	1.1	2.31	0.96	4.23	1.31
FeO	13.5	2.88	11.2	5.09	2.59	3.25	9.71
MgO	41.6	22.14	26.6	18.38	17.27	17.43	10.41
CaO	0.2	11.74	0.4	13.00	23.70	14.10	10.93
Na ₂ O	-	0.17	-	0.44	0.12	1.27	2.15
K ₂ O	0.02	0.14	-	0.26	0.06	1.02	0.51
TiO ₂	0.01	0.51	0.09	0.94	0.14	0.59	2.29
MnO	0.22	0.10	0.14	0.11	0.14	0.11	0.16
Cr ₂ O ₃	0.01	0.70	0.03	0.15	0.06	0.61	0.09
NiO	0.25	-	0.032	-	0.02	-	-
CoO	0.01	-	0.0046	-	-	-	-
P ₂ O ₅	-	-	-	-	-	-	0.16
H ₂ O ⁺	-	3.44	-	2.55	-	2.32	0.04
H ₂ O ⁻	-	0.06	-	0.05	-	0.03	0.05
Total	97.72	100.21		100.01	99.28	100.48	100.30

¹ Analyses made by the Analytical Chemistry Division, G.S.C.

² Olivine tholeiite basalt investigated by Yoder and Tilley (1962, Table II, No. 14).

Table XVII

Modal Analyses¹ of the Ultramafic Rocks
Corresponding with the Analyzed Mineral Pairs

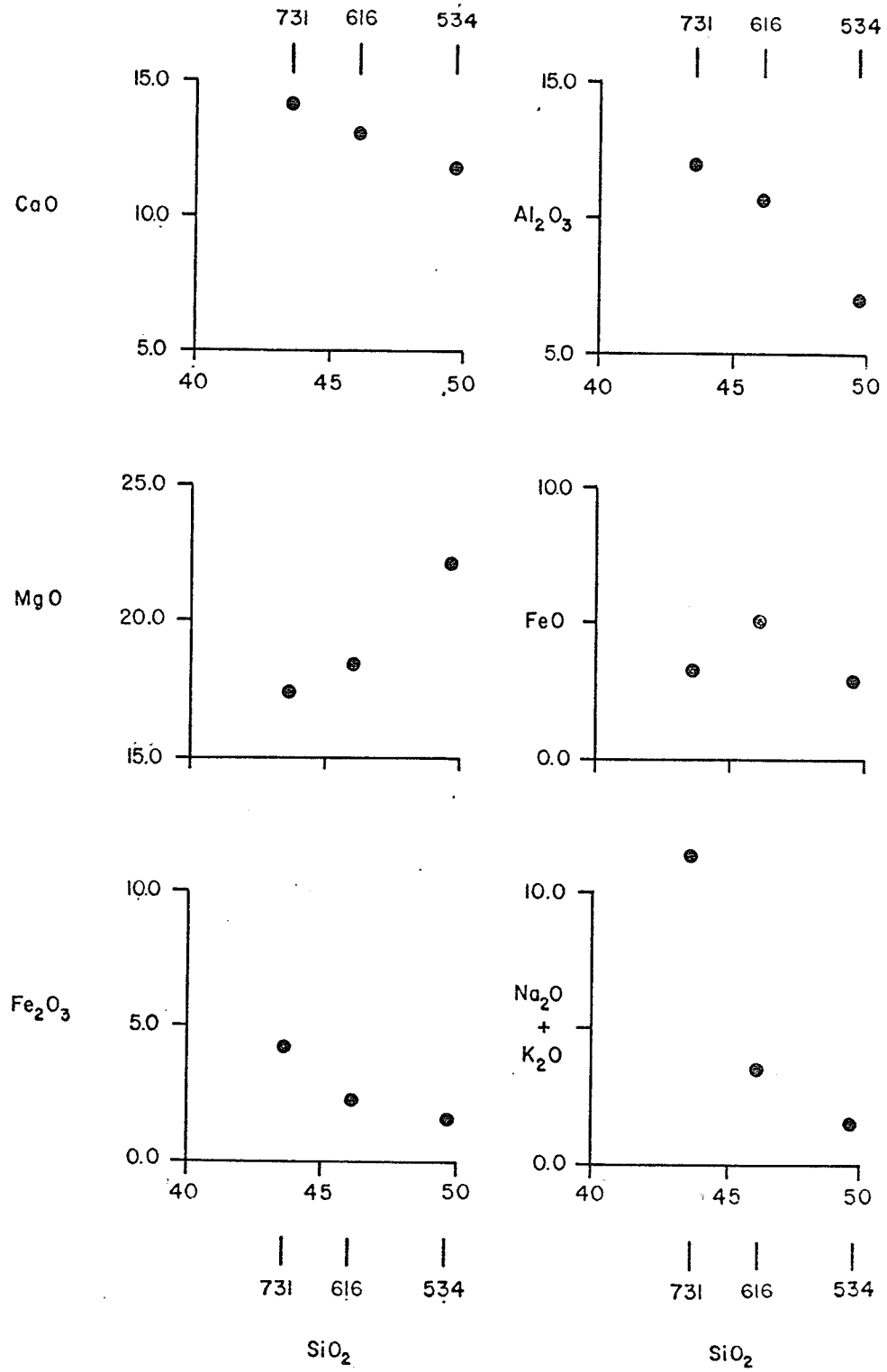
	<u>534</u>	<u>616</u>	<u>731</u>
Olivine	21.6	5.2	6.2
Serpentine (after olivine)	26.8	4.9	12.1
Magnetite	12.1	4.5	4.9
Clinopyroxene	-	4.3	58.3
Orthopyroxene	-	39.0	-
Hornblende	31.0	35.0	10.9
Talc	-	0.1	-
Chrome Spinel	7.8	6.7	4.0
Sulphide	0.7	0.3	3.6
	—	—	—
Total	100.0	100.0	100.0

¹Analyses based on a minimum of 1000 counts per thin section

constructed using the three analysed hornblendes (Figure 25). The apparent reversal in trends is the direct result of SiO_2 , which is greatest in the hornblende associated with olivine 534 and least in the hornblende associated with clinopyroxene 731. This trend of SiO_2 in the three primary hornblendes indicates that at the time of formation of the hornblende associated with olivine, the interprecipitate liquid was still relatively enriched in SiO_2 . This suggests that pyroxene had not yet begun to crystallize to any great extent. The hornblendes associated with orthopyroxene and clinopyroxene show a regular decrease in SiO_2 content which reflects the lower SiO_2 content of the liquid due to the crystallization of pyroxenes. The remainder of the chemical trends of the hornblende series are predictable i.e. the enrichment of the liquid in Al_2O_3 , FeO and Fe_2O_3 , CaO , $\text{Na}_2\text{O} + \text{K}_2\text{O}$, and depletion of the liquid in MgO .

CIPW norms have been calculated for the three hornblendes and they are listed in Table XVIII. Normative anorthite occurs in all specimens and normative enstatite in two of the three hornblendes. The presence of normative plagioclase and hypersthene indicates that the interprecipitate liquid had a composition analogous to that of a tholeiite basalt. Hornblende 731, associated with clinopyroxene, contains normative nepheline and leucite and thus displays alkalic affinities.

The series of three analyzed hornblendes, which are



SILICA VARIATIONS DIAGRAMS - ANALYSED HORNBLENDES

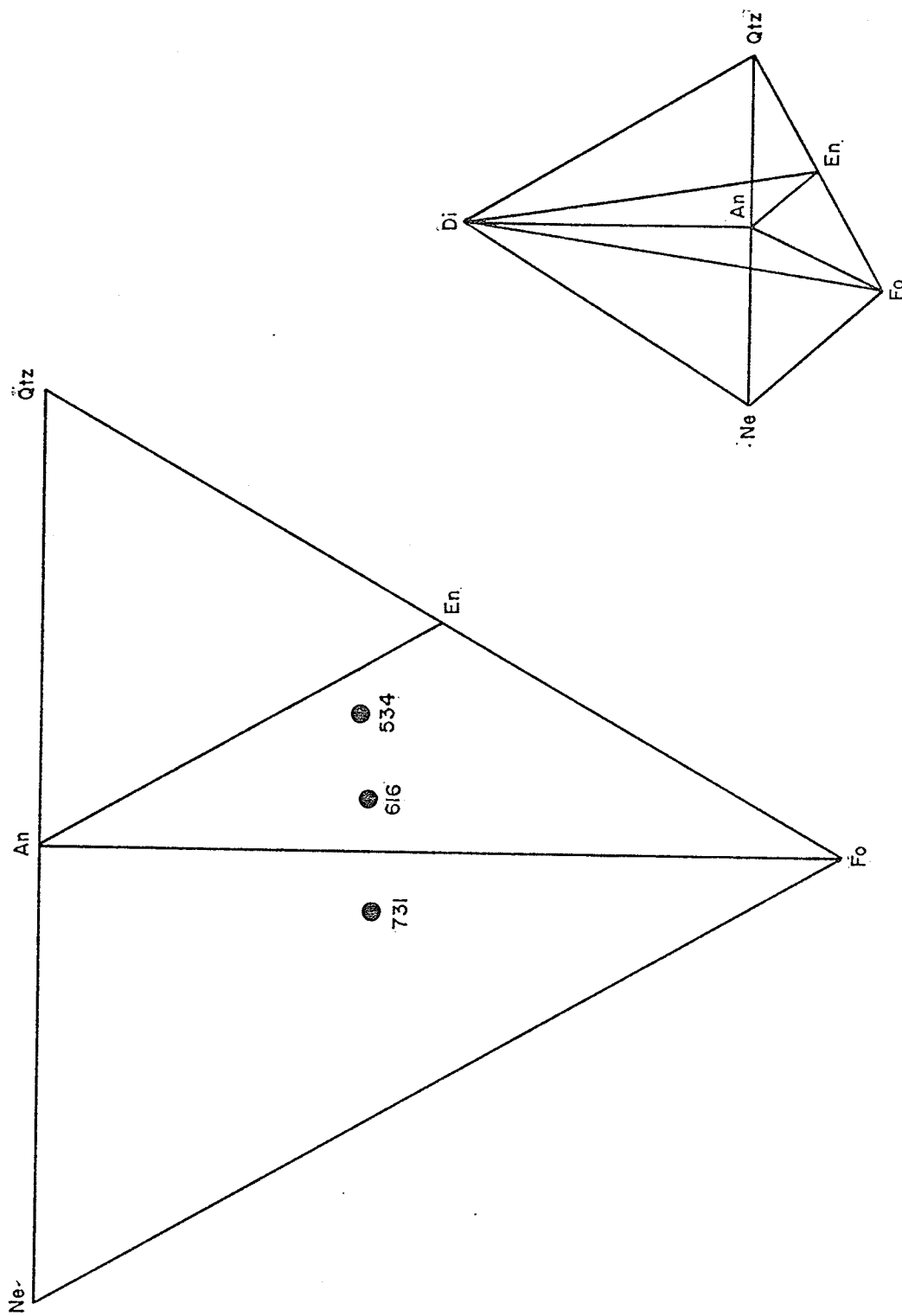
FIGURE 25

Table XVIII

Primary Hornblendes - CIPW Norms

	<u>534</u>	<u>616</u>	<u>731</u>
Lc	-	-	4.20
Ne	-	-	6.74
Or	0.82	1.53	0.69
Ab	1.51	3.94	-
An	17.77	26.12	23.49
Di	31.11	27.89	35.97
He	0.94	2.75	0.43
En	37.11	12.86	-
Fs	1.12	1.26	-
Fo	6.02	17.90	22.10
Fa	0.18	1.76	0.26
Mt	1.63	2.41	4.36
Il	0.70	1.30	0.81
Cr	0.77	0.16	0.67
Total	<u>99.74</u>	<u>99.94</u>	<u>99.78</u>

considered to represent the trend of the liquid from early to later stages of crystallization, are plotted on the base of the basalt tetrahedron in Figure 26. Hornblendes 534 and 616 lie in the field of olivine tholeiite and trend toward the boundary O1-P1, which is the position of the critical plane of silica undersaturation. Hornblende 731 lies in the field of alkali basalt and the three hornblendes form a relatively straight line. The liquid trend in this case appears to cross the critical plane of silica undersaturation. In any event, the liquid appears to become more alkali-rich during crystallization. The fractional crystallization of olivine would produce silica-saturated magmas and, therefore, would have an opposite effect than that observed. The crystallization of orthopyroxene by reaction relation between olivine and liquid and subsequent removal of this assemblage from the liquid would tend to deplete the liquid in SiO_2 and enrich it in alkalis. However, Yoder and Tilley (op. cit.) consider that crystallization and removal of orthopyroxene can have little influence on the ultimate course of a magma. Murata (1960) states that fractional crystallization of clinopyroxene is the general mechanism for converting the tholeiitic magmas into alkalic magmas. However, the nepheline normative hornblende is considered to have formed through reaction between clinopyroxene and liquid. The manner in which the critical plane of silica undersaturation is breached is



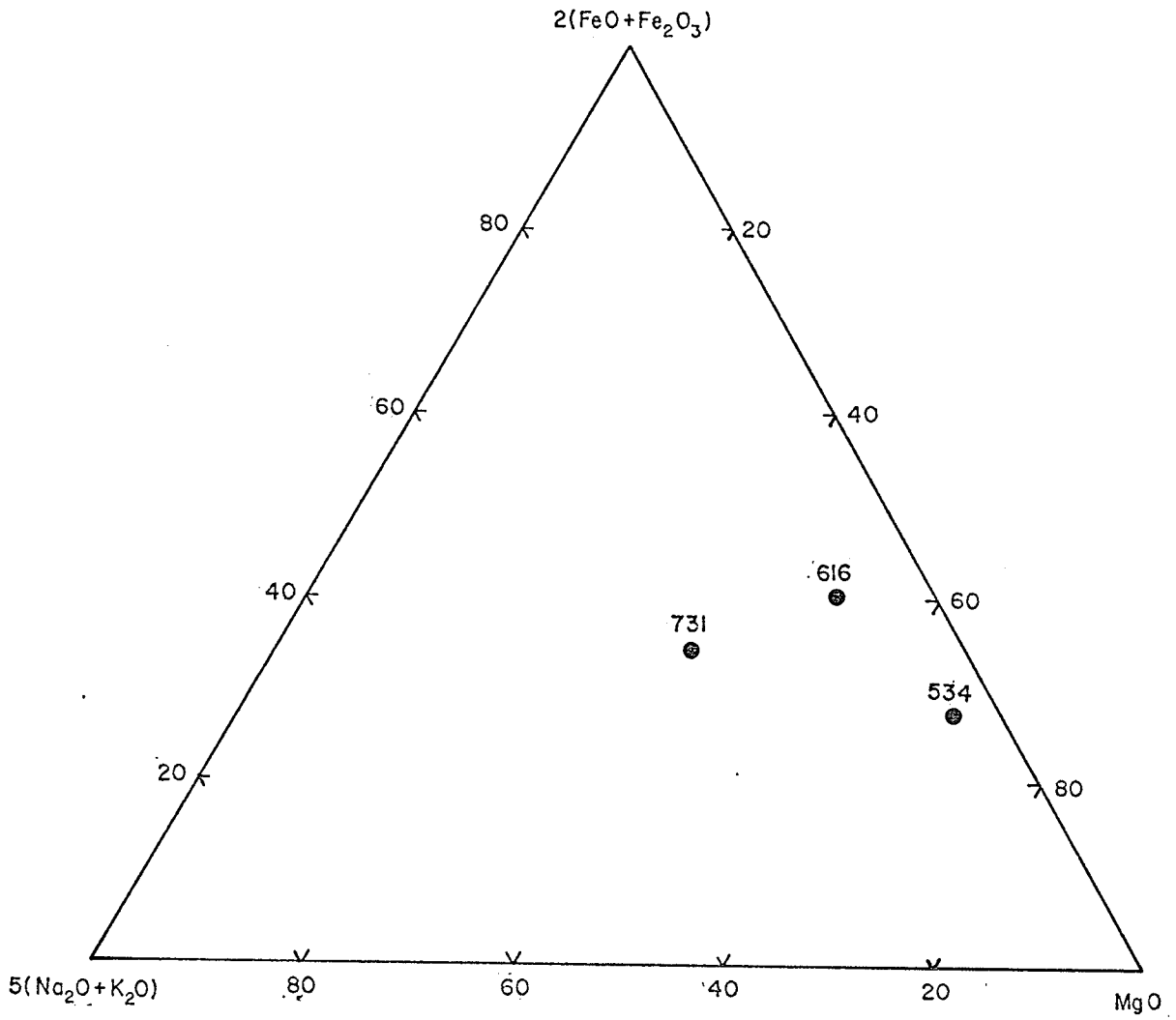
ANALYZED HORNBLENDES, PLOTTED ON BASE OF BASALT TETRAHEDRON (after Yoder and Tilley, 1962)

FIGURE 26

unknown.

The analyzed hornblendes are plotted according to the scheme $5(\text{Na}_2\text{O} + \text{K}_2\text{O}) + 2(\text{FeO}) + \text{MgO}$, which is a modification of the standard FMA diagram (Figure 27). The variations in $\text{Na}_2\text{O} + \text{K}_2\text{O}$ and FeO are therefore enhanced and trends if present may be more readily observed. The hornblendes plot across the field and do not display any Fe-enrichment. The liquid trend of the A-peridotite is akin to the calc-alkalic trend. Therefore, although the rocks display typical tholeiitic associations, the liquid appears to have had a calc-alkalic trend during the course of crystallization.

The observed order of crystallization of the primary silicates is the same as that determined experimentally by Yoder and Tilley (op. cit.) in their investigation of tholeiite olivine basalt, crystallized at a $P_{\text{H}_2\text{O}}$ of 5,000 to 10,000 bars. Their experimental results suggest that the sequence obtains for $P_{\text{H}_2\text{O}}$ greater than 2,500 bars. Watkinson and Irvine (op. cit.) have drawn a parallel observation for the Shebandowan-Quetico ultramafic rock series. The limitations on the analogy between the observed ultramafic assemblages and the experimentally observed assemblages are the same for the Gordon Lake ultramafic rocks as those imposed by Watkinson and Irvine for the Shebandowan-Quetico assemblages. In summary these are:



$5(\text{Na}_2\text{O} + \text{K}_2\text{O}) - 2(\text{FeO} + \text{Fe}_2\text{O}_3) - \text{MgO}$, ANALYZED HORNBLENDES

FIGURE 27

- (i) The Gordon Lake ultramafic assemblages are much more basic than the olivine tholeiite investigated by Yoder and Tilley. An analysis of the investigated olivine tholeiite is listed in Table XVI.
- (ii) The ultramafic lithologic units are the products of fractionation of a magma whose composition therefore changed during crystallization. The experimental assemblages, however, are the result of one fractionation of the same starting liquid at progressively lower temperatures.
- (iii) All the experimental charges crystallized magnetite because of the moderately high pO_2 of the environment. In the natural magma, pO_2 probably varied during crystallization.
- (iv) The experimental melt was saturated with water, and its water content at any stage was determined by its general composition and independently controlled P_{H_2O} . During crystallization the natural magma may have gained or lost water to the wall rocks. The crystallization of olivine, orthopyroxene and clinopyroxene would cause P_{H_2O} to increase during the course of crystallization.

Considering these limitations Watkinson and Irvine conclude from the analogous crystallization sequences of Yoder and Tilley, that P_{H_2O} was probably in excess of 2,500

bars by the time hornblende began to precipitate. A similar conclusion is considered apt for the Gordon Lake assemblage.

Trace Elements in Coexisting Ferromagnesian Minerals

Nickel

There is approximately an order of magnitude more Ni in olivine than in orthopyroxene and clinopyroxene and about a four fold greater abundance than in hornblende (Table XIX). The abundance of Ni in hornblende forms a regular series, decreasing from hornblende with olivine, through hornblende with orthopyroxene to hornblende with clinopyroxene. This series probably reflects the abundance of Ni in the liquid phase during crystallization. The change in abundance of Ni in the hornblende series is not great and probably indicates that the major subtraction of nickel into the sulphide phase took place before the crystallization of hornblende. The abundance of Ni in olivine is approximately equal to the average abundance of Ni in ultramafic rocks. It is interesting to note that not all Ni occurs in the sulphide phase. It would appear that sufficient Ni was present during crystallization to satisfy both the sulphide and silicate phase.

Copper

Copper displays a concentration in clinopyroxene which is from 4 to 10 times the concentration in the other

Table XIX

Trace Elements[†] in Coexisting Minerals*

	<u>Olivine</u> <u>534</u>	<u>Hnblde</u> <u>534</u>	<u>Opx</u> <u>616</u>	<u>Hnblde</u> <u>616</u>	<u>Cpx</u> <u>731</u>	<u>Hnblde</u> <u>731</u>
Sr	-	-	-	-	-	.018
Ba	-	-	-	-	.0019	-
Cr	.0065	.48	.03	.10	.042	.42
V	-	.021	.01	.029	.0064	.028
Ni	.20	.065	.032	.057	.015	.042
Cu	.0089	.017	.0059	.0089	.10	.021
Co	.0089	-	.0046	-	-	-
Mn	.17	.079	.20	.085	.11	.085

† in per cent

* Analyses by Optical Spectrographic Laboratory of G.S.C.

analyzed minerals. The hornblende associated with the clinopyroxene is slightly more enriched in copper than the other hornblendes. As clinopyroxene is considered as the last anhydrous silicate phase to crystallize it appears that there is a slight concentration of copper in the magma toward the latter stages of crystallization.

Chromium

Chromium displays a concentration in hornblende which ranges from 4 to 50 times the concentration in the early formed silicates. As the bulk of the chromium is tied up in the early formed chromite, it seems unlikely that there would be any concentration of chromium in the late fluid phase of the magma. The chromium in the hornblende probably represents chromium derived from chrome spinel which breaks down during the reaction between the late fluid magmatic phase and the primary silicate minerals to form hornblende.

Vanadium

Like chromium, vanadium displays a greater concentration in hornblende and for the same reasons as stated for chromium.

Cobalt is found only in olivine and orthopyroxene, and strontium and barium are restricted to sample 731; barium in clinopyroxene and strontium in hornblende.

Flowage Differentiation

A special mechanism of intrusion that will concentrate Mg-rich olivine in the centre of the body and explain the distribution and the general cryptic zoning of the primary silicate minerals of the A-peridotite is required. Flowage differentiation is considered as a possible mechanism.

Flowage differentiation is an experimentally demonstrable process capable of causing crystal and chemical fractionation in nature. It is a mechanism for forming olivine-rich rocks in a vertical or steeply dipping position without prior concentration on a flat floor. Thus, early-formed Mg-rich olivine may be concentrated closer to the conduit axis than later formed olivine with a lower Mg/Fe ratio. The process of flowage differentiation is intended to explain the distribution of rock types in the feeder of the Muskox Intrusion. The picrite dykes of Skye, described by Drever and Johnson (1958), exhibit features similar to that of the Muskox feeder. The process may also explain concentric zoning in ultramafic gabbro intrusions. Bhattacharji and Smith (1964) state that in flowage differentiation, translation of the fluid takes place together with the simultaneous translation and rotation of the solid particles within it. It can be shown that a spherical particle carried along in a non-uniform velocity

gradient is subjected to a shear couple and a longitudinal force acting in the direction of streaming. This causes rotation in addition to translation along the direction of flow. It is these components of translation, acting in conjunction with the rotation, that give rise to lateral components of translation. The existence of a lateral component of translation normal to the flow direction leads to the conclusion that when a solid-fluid mixture, such as a magma carrying suspended or settling crystals, flows through a conduit there will be a continuous motion of solids toward the centre. As the concentration of particles increases a column of solids with immobilized fluid develops.

In the case of the A-peridotite, flowage explains both the concentration of olivine toward the centre of the body and its cryptic zoning. At the time of intrusion, the first olivines, with the highest F_0 content, started to crystallize. As the magma flowed and cooled these crystals migrated away from the walls leaving the residual fluid depleted in Mg relative to Fe. Succeeding crystals became relatively more rich in Fe as the process proceeded. The chemical evolution is similar in principle to that occurring during normal gravitative crystallization, except that separation of crystals occurs across the gravity field rather than vertically within it. Thus the process may be considered as the flow analogue of gravitative differentiation.

Classification of the Ultramafic Rocks

General reviews of problems concerning the genesis and mode of emplacement of ultramafic rocks are found in the literature (Benson, 1926; Bowen, 1928; Hess, 1938, Thayer, 1960; and Wyllie, 1969) and in unpublished dissertations (Coats, 1966 and Wolfe, 1966). A review concerning the classification of Precambrian ultramafic rocks has recently been published (Scoates, 1971).

Wyllie (1969) includes eleven associations, two of which are considered in further detail.

- (i) The concentrically zoned dunite-peridotite association or Alaska-type ultramafic rocks have been discussed by Thayer (1960, 1967), Taylor (1967) and Irvine (1967). These rocks occur in orogenic belts as small, circular or cylindrical bodies. Most of the bodies are hornblende pyroxenites or hornblendites. The common relationship is a crude zonal arrangement; a core of dunite being surrounded by successive shells of peridotite, olivine pyroxenite, magnetite pyroxenite and hornblende pyroxenite. The pyroxene is typically a diopsidic augite, orthopyroxene being absent.
- (ii) The alpine-type ultramafic rocks, also found along orogenic belts, occur as irregular masses

of dunite and peridotite. Their mineralogy is simple and the common pyroxene is an orthopyroxene. Individual bodies generally display no variation in composition (excluding serpentinization and steatitization) towards the margins.

The modal variations of the primary silicate minerals across the A-peridotite define a broad, crude concentric arrangement. This fact plus the presence of abundant primary hornblende indicates features similar to those described for Alaska-type ultramafic rocks. It should be noted however that the scale of the ultramafic bodies is vastly different; the Gordon Lake bodies being very much smaller in size. The overall composition of the bodies is also vastly different; the difference being marked by the abundance of orthopyroxene in the Gordon Lake rocks and its absence in the Alaska-type assemblages.

Although the presence of orthopyroxene in the Gordon Lake ultramafic rocks can be considered as characteristic of alpine-type ultramafic rocks, the non-uniform composition of the Gordon Lake rocks cannot be accommodated in the alpine-type classification.

The abundant reaction textures among the primary silicate minerals and the presence of orthopyroxene containing well developed clinopyroxene exsolution (Bushveld-type orthopyroxene) indicate that petrographically the Gordon Lake ultramafic rocks resemble differentiates of

stratiform mafic intrusions. Watkinson and Irvine (op. cit.) in describing peridotite intrusions near Quetico and Shebandowan in northwestern Ontario reach a similar conclusion. They state that structurally the intrusions resemble alpine-type peridotite, but chemically and petrographically they are more like the differentiates of stratiform mafic intrusions.

It does not appear possible therefore to rigidly classify the Gordon Lake ultramafic rocks according to existing schemes. The Gordon Lake ultramafic rocks would be classified as *discrete ultramafic bodies* by a recent classification of Precambrian ultramafic rocks (Scoates, op. cit.). This classification is not rigidly bound by compositions or processes of intrusion and accommodates all those linear belts of ultramafic bodies which are common in the Precambrian Shield.

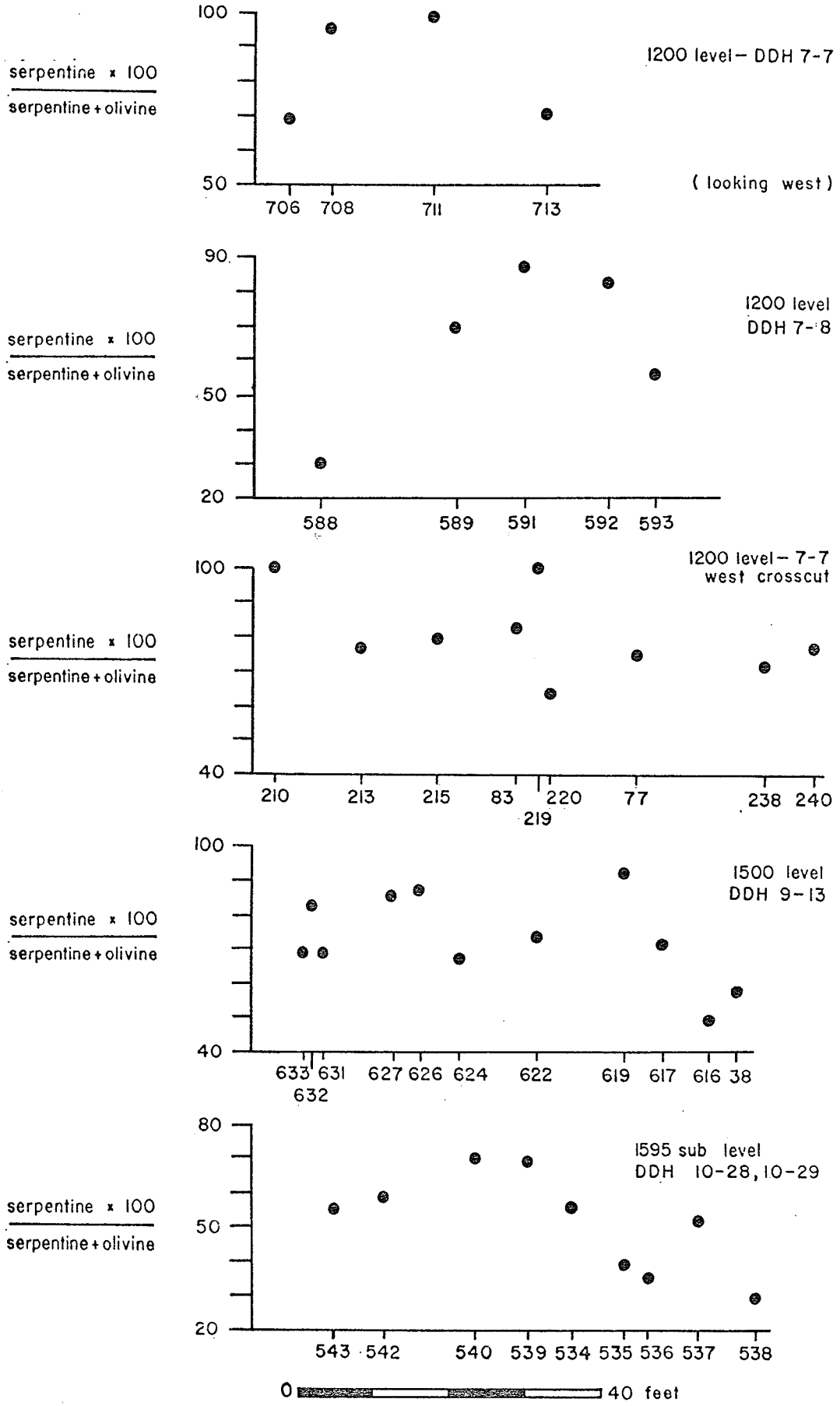
CHAPTER V

SECONDARY RECRYSTALLIZATION OF THE PRIMARY ASSEMBLAGE

Distribution of Serpentinization

The degree of serpentinization of the primary assemblage ranges from 20 to 100 per cent, and averages 70 per cent. The degree of serpentinization tends to increase from the margin to the centre of the A-peridotite (Figure 28). The ratio that is used (serpentine x 100/serpentine + olivine) should be independent of the amount of olivine, however, the trend of increasing serpentinization toward the centre of the body parallels the trend of increasing olivine abundance already described.

Attempts to relate volume per cent serpentine to specific gravity are not possible because the erratic distribution of sulphide minerals in the samples reduces the significance of the specific gravity determinations. The abundant hornblende in the ultramafic rocks makes use of specific gravity as an indicator of the degree of serpentinization somewhat unreliable in any event.



VARIATION IN DEGREE OF SERPENTINIZATION ACROSS THE A-PERIDOTITE

FIGURE 28

First Stage Recrystallization

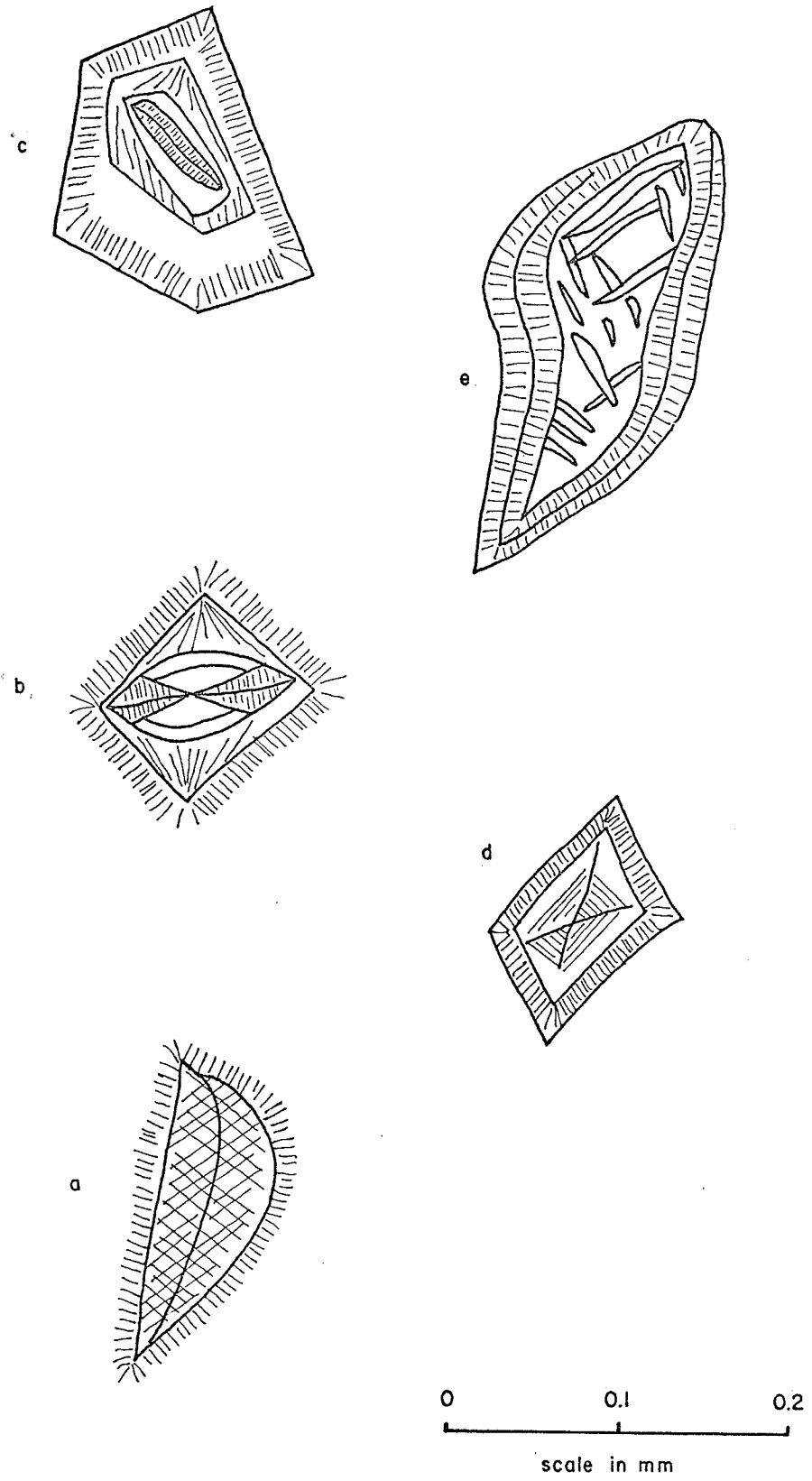
Two fibre types are recognized in optical studies; alpha (α) serpentine with negative elongation and gamma (γ) serpentine with positive elongation. The variable optical orientation of fibrous serpentine has been discussed by Francis (1956).

The dominant serpentine of the recrystallized assemblage is a colourless α serpentine having grey to greyish-white birefringence. It occurs as crossfibre, generally bipartite veinlets forming either a moderately well developed mesh texture or a series of veinlets showing a pronounced parallelism over a wide area. It also occurs as irregular veinlets and as inter-vein serpentine. Its texture and mode of occurrence suggest α chrysotile; however, due to its fine grain size a detailed survey of its optical properties was not possible. The fibres generally grow perpendicular to the vein walls and are joined in the centre of the vein by either continuous or discontinuous magnetite stringers. The α serpentine occurs in areas of incipient alteration of olivine and in areas of complete serpentinization. In most areas, the α serpentine is directly related to the alteration of olivine, however, in areas of intense serpentinization, veinlets of serpentine are found cutting across orthopyroxene and hornblende. In one section small discontinuous lenses of calcite occupy the central area of an α serpentine veinlet.

In the mesh texture variety, the α serpentine cross-fibre veinlets enclose a central area, which is generally coloured in greens, yellows or browns and which can be either fibrous, blade- or plate-like in structure (Figure 29). Some of this material is nearly isotropic and has been termed serpophite (Francis, 1956; Deer, Howie and Zussman, 1962). The serpentine in the non-isotropic areas tends to have a positive elongation and is thus gamma (γ) serpentine. The non-isotropic serpentine of these areas generally displays anomalous birefringence. In plane polarized light a gradual increase in colour intensity from the margins to the mesh centre can be seen. Irregular blades with wavy extinction under high power magnification display two directions of fibre growth which are mutually perpendicular (Figure 29a, 29c). Hourglass structures and groups of square and rectangular plates have also been noted (Figure 29b, 29d). Coats (1966) has suggested that similar coloured areas in certain Manitoba serpentinites may represent an Fe-rich serpentine phase.

Considerable secondary magnetite is associated with the serpentine as stringers, irregular patches and very fine dust-like grains. The magnetite veins primary assemblage minerals and was therefore mobile during the first stage recrystallization.

Partial to complete replacement of orthopyroxene by bastite, a length slow serpentine resembling antigorite,



SERPENTINE STRUCTURES COMMONLY ASSOCIATED WITH FIRST STAGE RECRYSTALLIZATION

FIGURE 29

has been observed. All stages of replacement from incipient alteration by small crossfibre veinlets, to complete bastite pseudomorphs after orthopyroxene occur. The bastite is characterized by elongate fibres having a preferred orientation which parallel the original orthopyroxene cleavage direction. Francis (1956) and Whittaker and Zussman (1956) have identified bastite with chrysotile and lizardite on the basis of X-ray diffraction patterns.

The bulk of the water now present in the ultramafic rocks, excluding that combined in hornblende, is considered to have entered the ultramafic rocks in response to the chemical potential gradients established by the serpentinization reaction. The presence of relatively abundant relict primary olivine suggests that insufficient water vapour was available to drive the serpentinization reaction to completion. The source of the water is considered to be the country rock amphibolites.

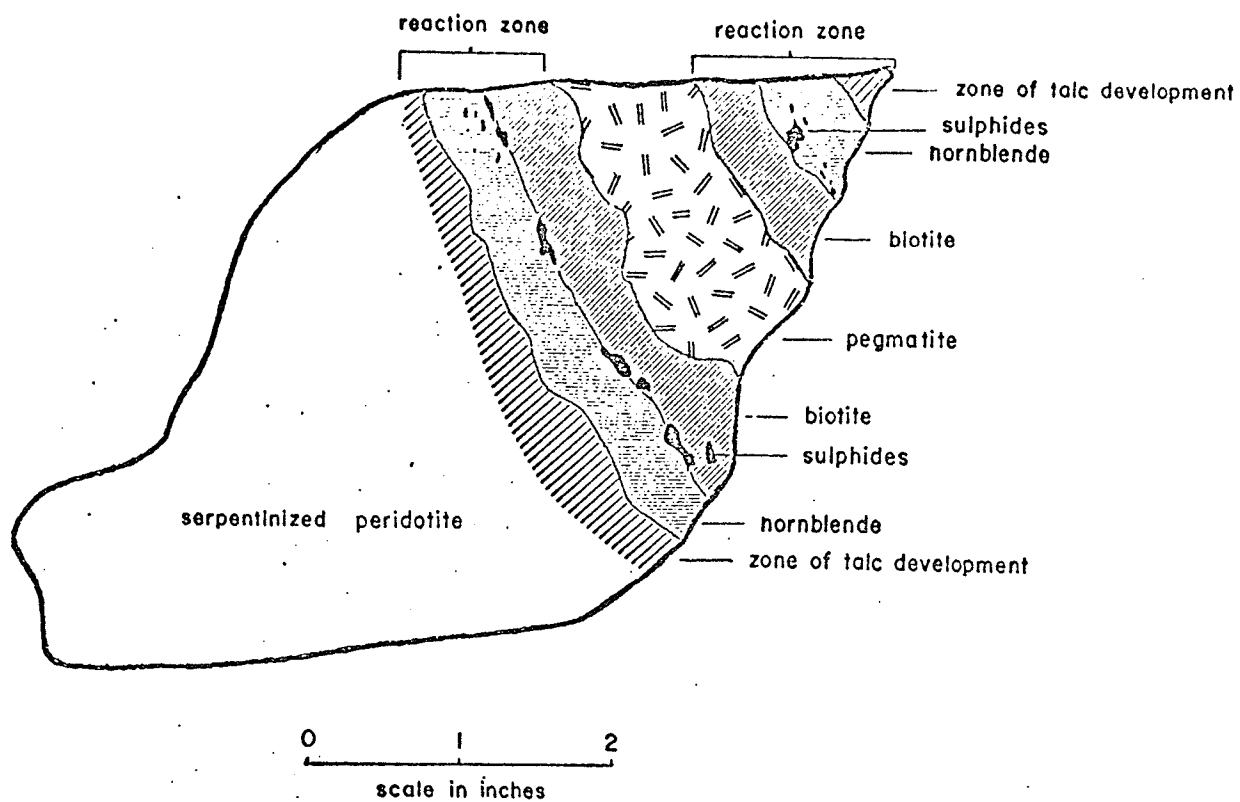
Second Stage Recrystallization

Recrystallization of α serpentine and bastite and the primary assemblage minerals including hornblende to antigorite and talc occurs in areas where later pegmatite dykes intrude the ultramafic bodies. Phlogopite-biotite, chlorite group minerals and green hornblende are commonly associated with this later recrystallization. A regular zonation, progressing outward from the intruding pegmatite,

and consisting of chloritized biotite, recrystallized dark green hornblende, and talc-antigorite has been observed in several areas (Figure 30). This type of zonation is also characteristic of many of the ultramafic contact zones. There does not appear to be a consistent relationship between dyke width and width of associated reaction zones. The small, one-inch dyke, sketched in Figure 30, develops one-inch symmetrical zones of chloritized biotite and recrystallized hornblende on each side.

Antigorite has been found in some of the more highly altered areas of the A-peridotite and in some of the completely serpentized, smaller ultramafic bodies. It is length slow, has negative optic sign, and a moderate $2V$ ($\sim 45^\circ$). Its most common forms are as fine plates and fibro-lamellar stellate groups. Replacement of the primary silicates and α serpentine by blades and flames of antigorite are observed. In some thin sections it occurs in well defined areas with sharp undulating boundaries outlined by a brownish opaque material which also regularly dissects the antigorite into roughly equidimensional areas. In areas of antigorite development relict textures are rare, and considerable redistribution of magnetite is observed.

Talc, like antigorite, occurs in areas of intense alteration. It occurs as fine platy to fibrous aggregates and is most commonly associated with the alteration of orthopyroxene. In incipient alteration of orthopyroxene,



MONOMINERALLIC CONTACT REACTION ZONES ASSOCIATED WITH PEGMATITE
CUTTING SERPENTINIZED PERIDOTITE

talc forms along the cleavage traces and also forms small crudely bipartite veinlets crossing the orthopyroxene crystals. Complete replacement of orthopyroxene leaves a fine grained felted talc mass with continuous to discontinuous magnetite stringers outlining former pyroxene cleavages. In some sections, talc has been found replacing antigorite, and thus it overprints the first stage and early second stage recrystallization.

Biotite-phlogopite, chlorite group minerals, and recrystallized green hornblende are commonly associated with the second stage recrystallization as noted previously. Chloritized biotite always forms closest to the pegmatite; generally forming the contact between the pegmatite and the ultramafic assemblage. Development of green chlorite around biotite margins and along cleavage is common. Adjacent to the zone of biotite which ranges in thickness from one inch to several feet, is a zone of medium to dark green hornblendite forming an interlocking mosaic of stubby equidimensional crystals. This inner zone of hornblendite ranges in width from several inches to several feet.

As noted in the preceding paragraph, medium to dark green chlorite occurs along the edges and cleavages of the marginal biotite. Fine-grained, colourless to very pale green chlorite, some displaying abnormal birefringence, forms irregularly-shaped featureless masses associated with

both antigorite and talc. Colourless clinochlore, poikiloblastically including serpentized olivine and also replacing orthopyroxene is probably associated with the second stage recrystallization. Polysynthetic twinning, and considerable kinking and bending of crystals are characteristic of the clinochlore.

In areas outside of the symmetrical reaction zones, phlogopite is found associated with antigorite and talc and also replacing the primary assemblage. Phlogopite is replaced by talc but largely unaffected by antigorite.

Magnetite is further remobilized during the later recrystallization to form large irregular patches and discontinuous veinlets while the bulk of the antigorite and talc are generally free of the dust-like magnetite inclusions which characterize the formation of α serpentine.

Hornblende associated with the symmetrical reaction zones takes the form of large (2 to 3mm) equidimensional crystals having a pronounced green colouration in plane polarized light. Gradations between the primary hornblende and this secondary recrystallized hornblende in grain size and colour intensity are common. Contacts between the biotitite zones and hornblendite zones are generally sharp.

Tremolite and anthophyllite are rare in the recrystallized assemblage. In some areas, where these two minerals are associated, they form localized zones

of alteration in rocks which are otherwise not highly altered. Tremolite forms highly elongate to acicular crystals, commonly forming bundles of radiating acicular crystals as an alteration of the primary assemblage. Considerable redistribution of magnetite and sulphide by tremolite occurs. Anthophyllite forms long lath-like crystals and irregularly shaped and bent crystals with feathery terminations. It is generally associated with localized areas of intense talc alteration. In most areas tremolite and anthophyllite appear to be contemporaneous with the development of talc.

The spatial association of second stage recrystallization products and crosscutting pegmatite dykes has been noted. This second stage recrystallization is therefore formed in response to metamorphism and limited metasomatism caused by the intruding pegmatite dykes. The geochemistry of this process is discussed in the following sections.

Contact Reaction Zones

The development of monomineralic contact zones between some of the ultramafic bodies and the country rocks has been noted in the foregoing section. These zones are identical to those already described which are associated with the later pegmatite dykes which cut across some of the ultramafic bodies. Where the contact zones are well

developed, an outer zone of chloritized biotitite forms the contact between the ultramafic assemblage and the surrounding rocks. The biotitite zone, which may range in width from several inches up to a maximum of four feet, has an inner sharp contact with a medium-grained hornblendite which in turn grades into the ultramafic assemblage proper. The hornblendite zone ranges in width from several inches up to a maximum of five feet. The ultramafic assemblages adjacent to these zones generally show signs of second stage recrystallization, manifest in the development of talc and/or antigorite. However, in some areas immediately adjacent to the contact zones, the ultramafic assemblage displays only intense first stage recrystallization with incipient phlogopite and/or clinochlore development.

Partially chloritized biotite generally displaying a crude preferred orientation comprises 95 to 100 per cent of the biotitite zone. The biotite has a small $2V$ ($0 - 5^\circ$ estimated) and is pleochroic in pale to dark reddish brown. Inclusions of the green recrystallized hornblende from the inner zone occur, and rare remnants of orthopyroxene and serpentized olivine of the primary ultramafic assemblage have been observed. These remnants are always highly altered to talc and antigorite. Apatite occurs as an accessory in a few areas and magnetite and sulphide, occurring as fine discrete grains, have been

noted.

Massive, medium-grained, green hornblende comprises 95 to 100 per cent of the hornblendite zone. In thin section it occurs as green, equidimensional crystals, having a pronounced pleochroism in medium to dark green. Highly altered inclusions of the primary ultramafic assemblage are more common in the hornblendite than the biotitite zone; and these inclusions are highly altered to antigorite-talc assemblages. Magnetite and associated sulphide occur as irregular sieve-like grains and as discrete regular crystals.

Incipient recrystallization of the primary ultramafic assemblage to hornblende and biotite is recorded in several areas. Hornblende in these areas forms optically continuous crystals with numerous nuclei over a large area and may involve several primary crystals. These nuclei appear to continue growth until a large (2 - 4 mm) hornblende crystal is formed, which may replace several orthopyroxene plates and olivine crystals. Small biotite laths replacing minerals of the primary ultramafic assemblage and the recrystallized hornblende are commonly associated with the incipient recrystallization. In one thin section, incomplete replacement of an orthopyroxenite by hornblende is associated with the development of quartz.

The development of monomineralic bands similar to those described in the preceding section is well known.

Phillips and Hess (1936) discuss contact effects between serpentinite bodies and siliceous country rocks in the northern Appalachians and have termed such effects *contact reaction zones*. Two main types are distinguished:

- (i) a low temperature type with chlorite developed at the edge of the country rock schist and talc at the edge of the serpentinite and
- (ii) a high temperature type with biotite at the edge of the country rock and actinolite at the edge of the serpentinite.

Read (1934) and Macdonald (1942) have studied small ultramafic bodies which consist of concentrically developed monomineralic zones in the Shetland Islands and California respectively. The zoning in both cases follows a sequence from centre outwards: antigorite, talc, actinolite, chlorite, biotite, country rock. In both studies the zonal development is considered to represent recrystallization of an original serpentinite due to metasomatism and metamorphism by later acid intrusive rocks. Kulp and Brobst (1954) describe dunites intruded by later pegmatite in North Carolina and the progressive development of talc, asbestiform anthophyllite and ferroan phlogopite. Similarly, Wilkinson (1955) has noted that where ultramafic bodies have been intruded by later acid to intermediate igneous rocks, metasomatic changes, evidenced by the development of biotite and tremolite-actinolite rocks, are common.

Chemical Variations Across Contact Reaction Zones

Chemical variations across monomineralic contact reaction zones from the literature are compared with an analyzed series from the 300 level, Gordon Lake (Table XX, Figures 31 and 32). SiO_2 and CaO culminate in the talc (if present) and amphibole-rich zones. Al_2O_3 and K_2O culminate in the outer biotite zone. MgO decreases through the zones; being lowest in the biotite zone. H_2O with one exception, forms a depression in the amphibole-rich zone. Fe_2O_3 and FeO do not form consistent patterns, however, $\text{FeO} + \text{Fe}_2\text{O}_3$ forms a general increase across the zones, with the exception of the North Carolina series. Na_2O is a minor constituent in each series and does not display a consistent pattern.

The exceptions to the patterns described above are associated with the universal zones of North Carolina described by Kulp and Brobst (1954). The different chemistry reflects the different assemblages which in turn are caused by the unaltered nature of the ultramafic rock and the formation of vermiculite at the contact. The formation of the vermiculite is apparently due to weathering of a pre-existing phlogopite.

It is evident from Figures 31 and 32 that the chemical variations are coincident with the assemblage which is stable in the various zones. However, Gordon Lake samples 330 and 331, both from a single hornblendite zone

Table XX

Suite of Analyzed Specimens Across
a Contact Reaction Zone

	<u>328*</u>	<u>330*</u>	<u>331*</u>	<u>332*</u>
SiO ₂	37.60	50.00	46.50	40.10
Al ₂ O ₃	3.70	5.40	7.00	13.20
Fe ₂ O ₃	8.00	3.10	6.30	3.30
FeO	4.45	8.95	9.36	12.52
CaO	1.20	9.40	7.80	0.58
MgO	29.80	17.30	15.20	16.00
Na ₂ O	0.18	0.70	0.76	0.36
K ₂ O	0.92	0.40	0.90	6.90
H ₂ O	10.80	3.10	4.00	4.30
TiO ₂	0.06	0.12	0.17	0.66
MnO	0.11	0.06	0.08	0.03
P ₂ O ₅	0.03	-	0.12	0.19
CO ₂	0.22	-	0.09	0.13
Cr ₂ O ₃	1.40	0.90	2.00	0.03
NiO	0.30	0.10	0.10	0.30
Total	<u>98.77</u>	<u>99.53</u>	<u>100.28</u>	<u>98.60</u>

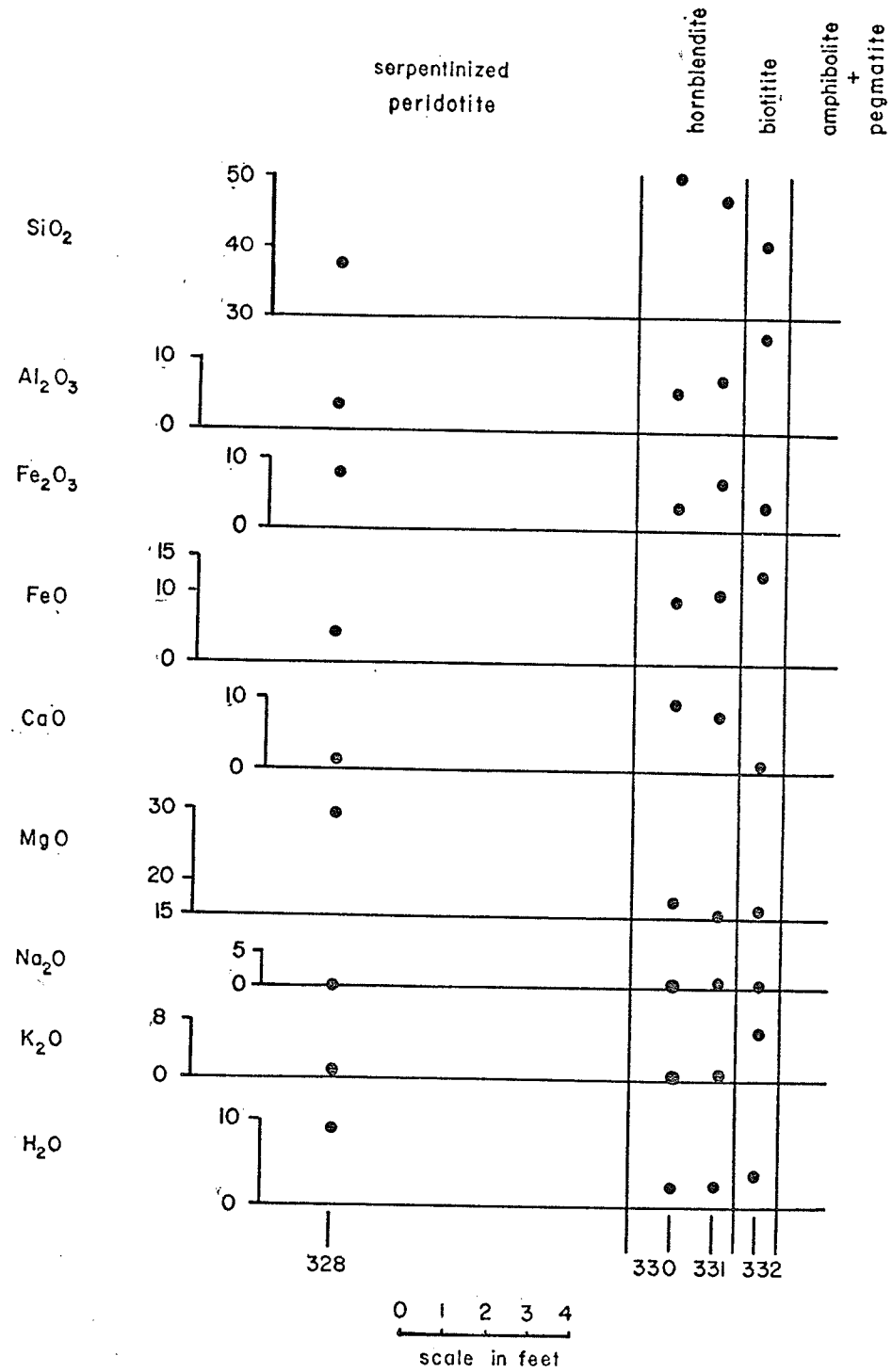
* Analyses made by the Analytical Chemistry Section of the Geological Survey of Canada.

328 - Serpentinized peridotite

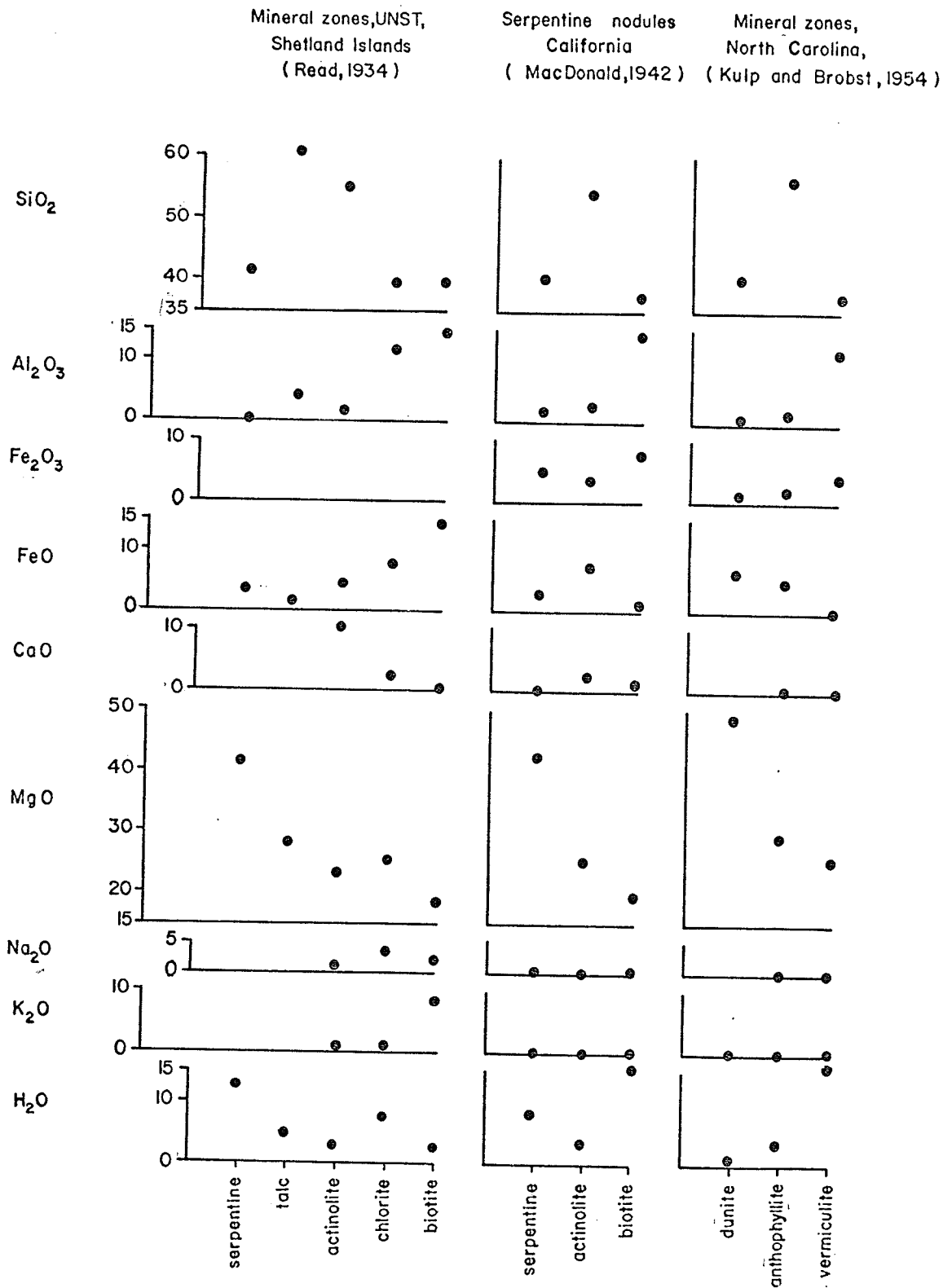
330 - Hornblendite

331 - Hornblendite

332 - Biotitite



CHEMICAL VARIATIONS
ACROSS A CONTACT REACTION ZONE , 300 LEVEL



CHEMICAL VARIATIONS ACROSS CONTACT REACTION ZONES

and 12 inches apart, display considerable difference in bulk chemical composition (Table XX). Brownlow (1961) has demonstrated that considerable chemical variation takes place in individual actinolite and biotite zones surrounding a serpentine-marble in Massachusetts. The chemical variation is accompanied by a range of the $Mg/(Mg + Fe)$ ratio and is interpreted by Brownlow as indicating that general thermodynamic equilibrium had not been reached at the time of formation of the bands. He therefore suggests rapid formation of the bands without time for adjustments in the distribution of elements involved in the reaction.

SiO_2 , which forms a maximum in the amphibole-rich zones, is probably one of the controlling factors influencing the development of talc. It was previously noted that at Gordon Lake there is a general close spatial relation between the development of talc in the ultramafic bodies and the proximity of pegmatites. Kulp and Brobst (1954) recognized the influence of SiO_2 in the formation of reaction zones including talc and described the desilication of pegmatite involved in the formation of the zones. Coats (1966) has similarly concluded that desilication of pegmatites cutting Manitoba nickel belt ultramafic rocks has led to the availability of SiO_2 required for the formation of reaction zones. Desilication of pegmatites in some areas, appears to be a consequence of the development of contact reaction zones.

The formation of reaction zone assemblages appears to be a direct consequence of the intrusion of pegmatite. SiO_2 , Al_2O_3 and K_2O are supplied by the pegmatite with perhaps small quantities of Na_2O and CaO . MgO , $\text{FeO} + \text{Fe}_2\text{O}_3$ and H_2O are available from the serpentinized ultramafic bodies. CaO may also be contributed by the ultramafic rocks. Mobility of elements during the formation of these zones is evident. The development of monomineralic reaction zones is apparently an attempt to establish equilibrium between two rock types of unreconcilably diverse compositions. The magnitude of the diversity in composition precludes the development of hybrid rocks of intermediate composition.

Sørensen (1952) discusses the presence of a "composition gradient" along which the exchange of material between ultramafic masses and country rocks takes place. If the country rocks are granitized, the margins of the ultramafic rocks are changed into aggregates composed of one or more of the following minerals: anthophyllite, actinolite, hornblende, talc, serpentine, chlorite and carbonates. The central parts of the ultramafic bodies are not as highly altered and Sørensen suggests that this is due to the fact that the bodies are incapsulated by reaction rims which, to some extent, protected the inner parts of the ultramafic bodies. Intrusion of pegmatite into the fractured margin of the ultramafic bodies results in reaction between the ultramafic assemblage and the pegmatite. If the reaction

is on a small scale, equilibrium is reached, and the minerals stable at the given pressure and temperature conditions are formed.

The presence of culminations and depressions in the concentrations of certain elements from zone to zone has been noted. Matthews (1967) has made a similar observation from small, zoned ultramafic bodies in the Lewisian of the Moine Nappe in Skye. He suggests that such elements did not diffuse down a simple concentration gradient, but that they were selectively concentrated in zones where minerals containing these elements were stable, and that the diffusion of these elements was sufficiently rapid to allow such concentrations.

It was noted that in general the width of the reaction zones did not appear to vary directly with the width of the pegmatite dyke involved in the reaction. Thompson (1959) pointed out that if a reaction goes to completion, the nature and size of the zones depend on the original amounts of the reactants, but if the reaction is arrested before equilibrium is reached, the size of the zones will be governed by the rates of diffusion of the various elements under the prevailing conditions of metamorphism.

Chemistry of Altered Ultramafic Rocks

Chemical analyses of five ultramafic rocks which

have undergone second stage recrystallization are listed in Table XXI. Modal analyses and visual estimates of modal variations for each of these specimens are also listed in Table XXII. Sample 465 is a marginal hornblendite and its composition is similar to the marginal hornblendites previously discussed. Phlogopite, one of the characteristic minerals of the recrystallized assemblage, has been observed in four of the specimens. Pegmatite dykes are spatially associated with all but one of the specimens. Sample 730 has no apparent pegmatite in association and yet displays development of anthophyllite and minor phlogopite, which are considered characteristic of recrystallized ultramafic rocks. For this reason, sample 730 has been included in the group of analyzed altered ultramafic rocks.

Ternary Plot $5(\text{Na}_2\text{O} + \text{K}_2\text{O}) - 2(\text{FeO} + \text{Fe}_2\text{O}_3) - \text{MgO}$

All analyzed ultramafic rocks are plotted according to the scheme $5(\text{Na}_2\text{O} + \text{K}_2\text{O}) - 2(\text{FeO} + \text{Fe}_2\text{O}_3) - \text{MgO}$ (Figure 33), which is a modification of the standard FMA diagram. The reasons for utilizing this scheme are the same as those for the $5\text{CaO} - 2(\text{FeO} + \text{Fe}_2\text{O}_3) - \text{MgO}$ ternary plot, i.e., variations in $(\text{Na}_2\text{O} + \text{K}_2\text{O})$ and $(\text{FeO} + \text{Fe}_2\text{O}_3)$ are enhanced and trends, if present, may be more readily apparent.

Rocks of the A-peridotite series are plotted for

Table XXI

Chemical Analyses of Altered Ultramafic Rocks

	<u>328*</u>	<u>730*</u>	<u>128*</u>	<u>733*</u>	<u>465*</u>
SiO ₂	37.6	36.9	40.1	41.7	49.4
Al ₂ O ₃	3.7	9.6	7.4	10.1	6.7
Fe ₂ O ₃	8.0	8.4	6.0	5.1	2.9
FeO	4.45	5.5	5.1	7.3	9.2
CaO	1.2	4.7	7.0	3.2	10.5
MgO	29.8	24.4	23.7	24.5	15.9
Na ₂ O	0.18	0.5	0.8	0.3	0.8
K ₂ O	0.92	0.7	0.4	0.1	0.5
TiO ₂	0.06	0.26	0.21	0.33	0.17
MnO	0.11	0.16	0.21	0.15	0.20
P ₂ O ₅	0.03	-	-	-	-
CO ₂	0.22	-	-	-	-
Ca ₂ O ₃	1.4	-	-	-	-
NiO	0.3	-	-	-	-
H ₂ O (total)	10.8	n.d.	n.d.	n.d.	n.d.
<hr/>					
Total	98.8				

*Analyses by the Analytical Chemistry Division, Geological Survey of Canada.

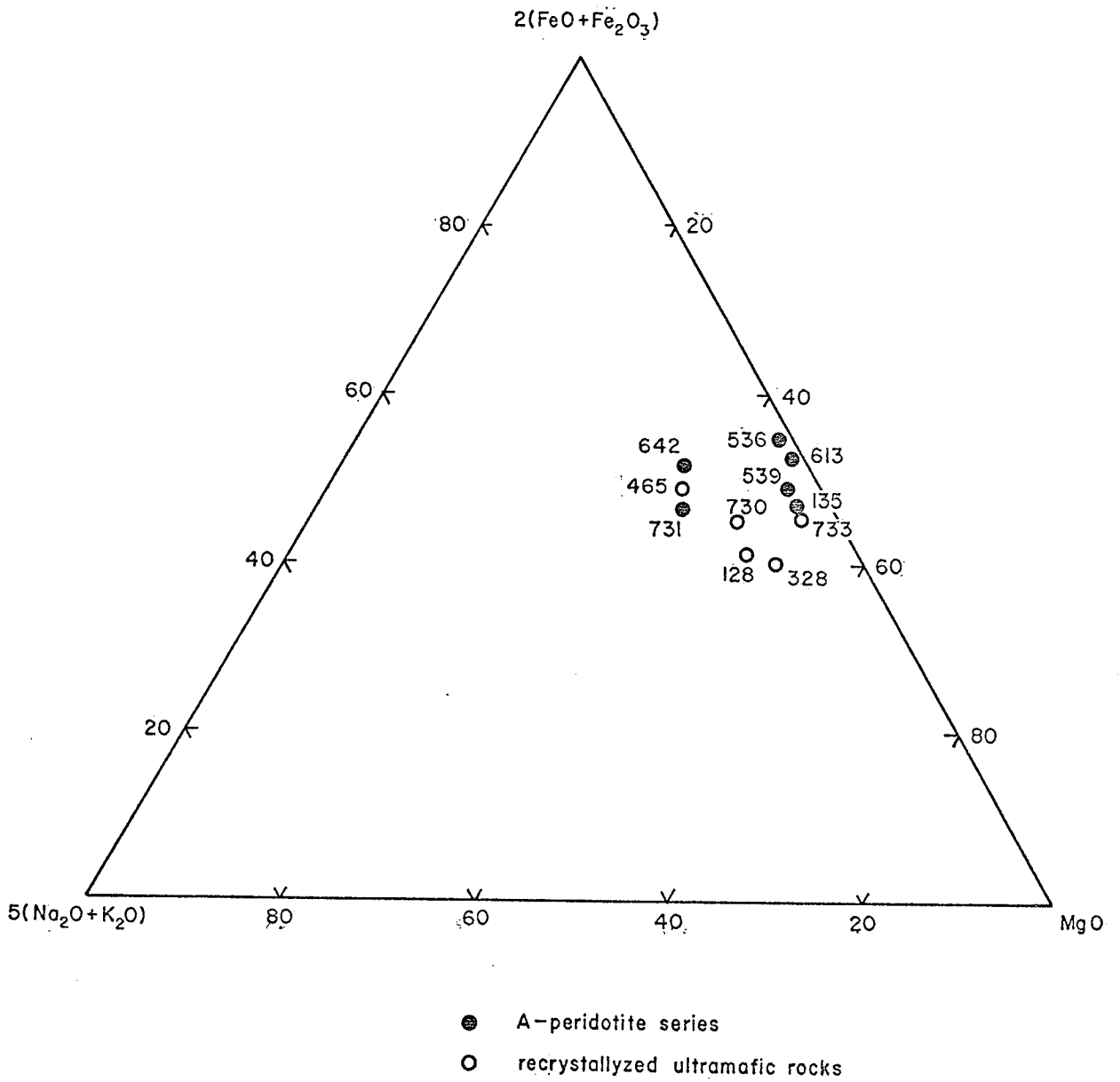
Table XXII

Modal Analysis and Estimated Modes
of Altered Ultramafic Rocks

	<u>328*</u>	<u>730**</u>	<u>128**</u>	<u>733**</u>	<u>465**</u>
Olivine	9.1	10	10	-	-
Serpentine (after olivine)	40.5	15	15	-	-
Magnetite (after olivine)	11.7	10	5	-	-
Clinopyroxene	1.8	-	5	-	-
Orthopyroxene	11.9	-	3	35	-
Hornblende	3.1	35	60	15	80
Serpentine (after orthopyroxene)	-	10	-	10	-
Phlogopite	17.0	15	-	2	20
Chrome Spinel	4.9	5	1	5	-
Sulphide Minerals	-	-	1	3	-
Anthophyllite	-	-	-	20	-
Magnetite	-	-	-	10	-
Total	<u>100.0</u>	<u> </u>	<u> </u>	<u> </u>	<u> </u>

*Modal analyses based on a minimum of 1000 counts.

**Visual estimates.



5(Na₂O+K₂O) - 2(FeO+Fe₂O₃) - MgO, A-PERIDOTITE SERIES

FIGURE 33

comparison. The plotted points form two distinct groups; one group lying along the join $2(\text{FeO} + \text{Fe}_2\text{O}_3) - \text{MgO}$, and the second group paralleling the first group but displaying a slight enrichment in $(\text{Na}_2\text{O} + \text{K}_2\text{O})$. All but one of the rocks lying close to the $2(\text{FeO} + \text{Fe}_2\text{O}_3) - \text{MgO}$ join represent rocks of the A-peridotite series. Two A-peridotite series rocks (642 and 731) display enrichment of $(\text{Na}_2\text{O} + \text{K}_2\text{O})$ and one recrystallized rock (733) does not display any enrichment of $(\text{Na}_2\text{O} + \text{K}_2\text{O})$. This latter rock contains abundant anthophyllite and only minor phlogopite (Table XXII).

The ultramafic rocks which have suffered the second stage of recrystallization thus display some enrichment in $(\text{Na}_2\text{O} + \text{K}_2\text{O})$.

CHAPTER VI

COPPER-NICKEL SULPHIDE ORES

Two distinct types of sulphide mineralization are found at Gordon Lake; (i) disseminated copper-nickel sulphides in ultramafic rocks, and (ii) breccia sulphides in amphibolite. Lenses of massive sulphide have been found in some of the ultramafic bodies. The A-peridotite ore body, characteristic of the disseminated type and the B-breccia sulphide zone, characteristic of the breccia ore are described in the following sections.

Disseminated Sulphide Ores

An example of the disseminated sulphide ores is the A-peridotite ore body (Figure 5, map pocket). The disseminated sulphide mineralization is situated towards the south side of the body on the upper levels and towards the southwest side of the body on the lower levels. The areas outlining the disseminated ore in Figure 5 contain greater than 5 per cent total sulphide, and this is based on visual estimates of drill core and hand specimens.

The disseminated ores range from fine-grained and diffuse sulphides with a ragged irregular outline, to coarse-

grained interstitial sulphide having sharply defined grain boundaries. Some of the coarse sulphide grains attain dimensions of 15 x 5 mm. The medium to coarse-grained interstitial sulphide is found in the central areas of the A-peridotite, and the finer-grained, ragged sulphide is restricted, in general, to the marginal areas. An exception to this general rule occurs in areas adjacent to late pegmatite dykes. In these areas the sulphide is the fine-grained ragged variety.

Sulphide Silicate Textures and Mineragraphy
of the Disseminated Sulphide Ores

Globular sulphides, poikilitically included in early
ferromagnesian silicates

Polished section examination has revealed fine-grained spherical to elongate and club-shaped sulphides occurring as inclusions in olivine and orthopyroxene (Plates V and VI). The boundaries between silicate and included sulphide are generally sharply defined. Partial rims of magnetite form between the included sulphide and the silicate, where olivine is the host, and presumably have developed due to partial serpentinization of olivine. Pyrrhotite and chalcopyrite are the common sulphide minerals of this type; pentlandite and cubanite are much less common. Pyrrhotite and chalcopyrite form both discrete and complex grains. Pentlandite is always associated with pyrrhotite

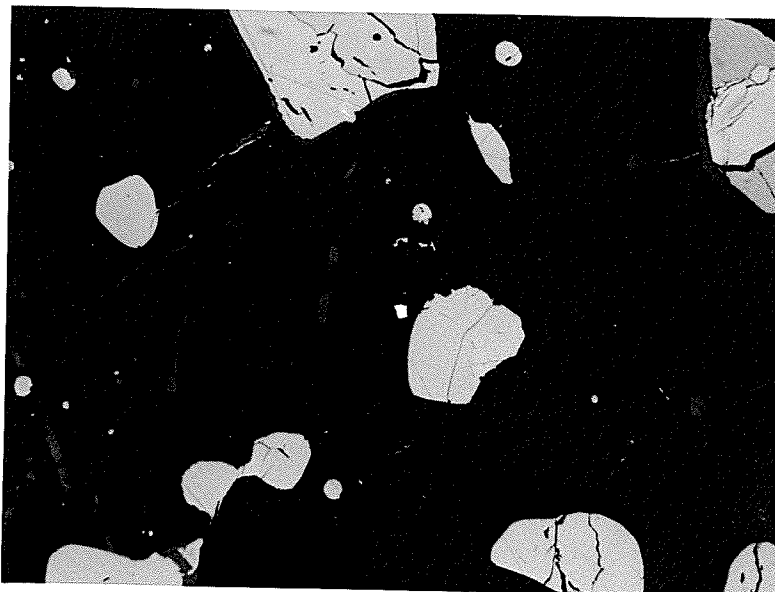


Plate V Sulphide blebs wholly enclosed within a single olivine grain. Grey rims about sulphides are magnetite. Partially crossed nicols, X130. (536)

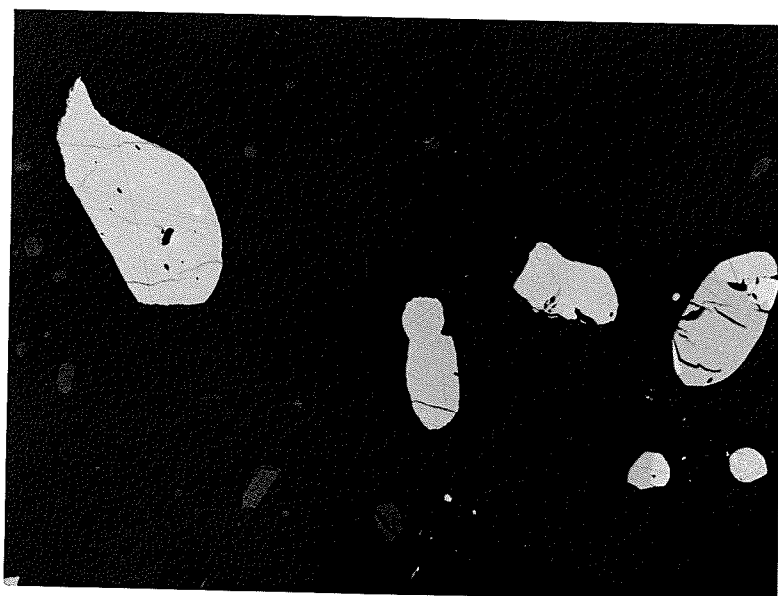


Plate VI Sulphide blebs wholly enclosed in a single orthopyroxene grain. Grey blebs are chrome spinel. Partially crossed nicols, X130. (536)

and cubanite occurs as rare small laths and irregular patches in chalcopyrite and pentlandite.

This type of sulphide-silicate association occurs in the central area of the A-peridotite on the lower levels. The shape and association of the sulphides suggest globules or droplets of sulphide liquid which were trapped during crystallization of the early ferromagnesian silicates. There is, therefore, a strong indication that at the time of crystallization of olivine and orthopyroxene, a sulphide liquid was present; presumably as an immiscible magma type.

Interstitial sulphides

Interstitial sulphide is the most common form of disseminated mineralization. It takes the form of interstitial silicate and in areas of first stage recrystallization (formation of α serpentine) the sulphide-silicate boundaries are sharp and well defined (Plates VII and VIII). In these areas, the sulphides are generally medium grained (1 to 5 mm). Plate VII shows the general silicate-sulphide texture of this type of interstitial sulphide, the sulphide occupying areas interstitial to partially serpentinized olivine. The presence of a narrow rim of magnetite separating the sulphide and silicate in Plate VII is probably due to magnetite released during the incipient formation of α serpentine. Silicate inclusions, as seen in Plates VII and VIII, are common in the medium to coarse-grained interstitial sulphide.

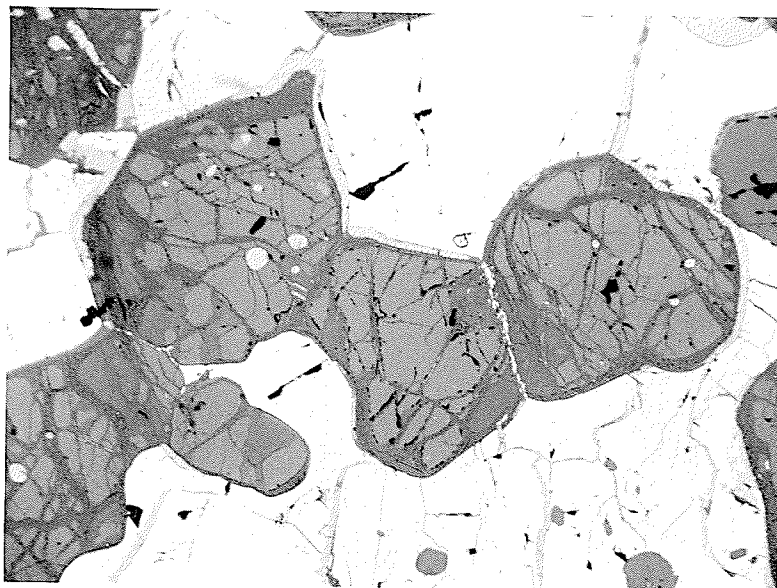


Plate VII Sulphide interstitial to serpentinized olivine grains. Grey is magnetite forming partial rims on sulphides and also veining sulphides. Plane light, X47. (536)

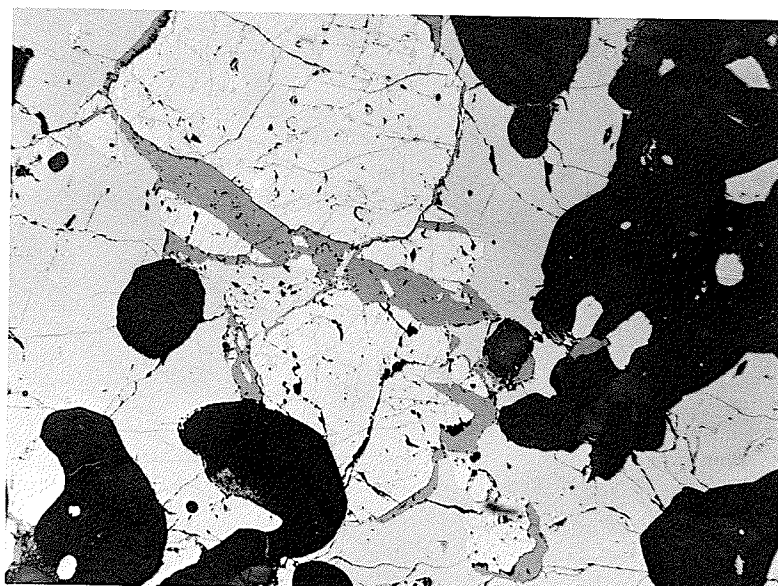


Plate VIII Interstitial sulphide. Magnetite (grey) forms along contact between pyrrhotite and pentlandite. Plane light, X47. (515)

Thin section examination of ultramafic rocks and associated sulphides indicate that the bulk of the sulphide minerals in areas of moderately intense mineralization are interstitial to hornblende, the common interstitial silicate mineral. Textures indicating replacement of silicate by sulphide are rare. As sulphide mineralization increases, the interstitial areas are increasingly occupied by sulphide to the exclusion of the interstitial silicate minerals.

Sulphide-chrome spinel textures are similar to those described above for the medium-grained, interstitial sulphide mineralization. The presence of small, lenticular chromite pods has been previously noted. The association of pyrrhotite interstitial to and included in chromite can be seen in Plate IX. A number of small (0.1 mm) blebs of pyrrhotite are wholly enclosed in chrome spinel grains.

The sulphide-silicate textures indicate that the interstitial sulphides of the disseminated ore display little replacement of the host silicates. The early ferromagnesian silicates retain their subhedral outline which they display in sparsely mineralized areas. The sulphide-silicate boundaries are sharp and smooth. Embayments of sulphide by silicate, and silicate by sulphide are interpreted as indicating coexisting sulphide-silicate assemblages. Thus a sulphide-silicate immiscible magma type is indicated, in which separation of the magmas took place early in the



Plate IX Chromite-sulphide relationships. Sulphide blebs and wholly enclosed by individual chromite grain (lower central). Remainder of sulphide is interstitial. Plane light, X31. (602).

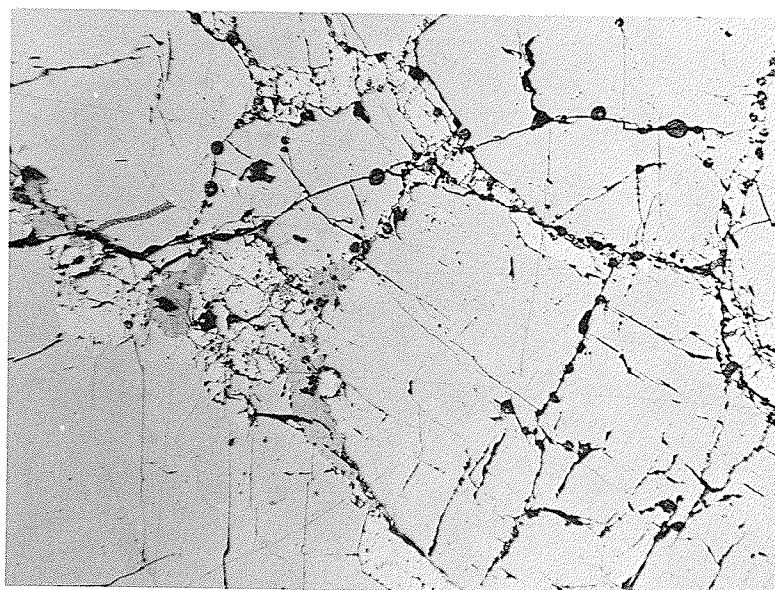


Plate X Pyrrhotite-pentlandite-chalcopyrite. Continuous delicate net pentlandite and associated chalcopyrite (left central) in host pyrrhotite. Plane light, X31. (759)

magma sequence, as evidenced by the sulphide globules poikilitically enclosed in olivine, orthopyroxene and chrome spinel.

Pyrrhotite, the dominant mineral of the sulphide assemblage, occurs as irregular grains in areas of medium to coarse disseminated mineralization. The grains are generally homogeneous and display an even anisotropism except in areas of intense recrystallization of the primary silicates which is discussed in the next section. In areas of heavy dissemination, pyrrhotite forms a partially continuous phase, occupying areas interstitial to primary silicate minerals. Inclusions of silicate minerals in pyrrhotite are common. Partial magnetite rims along pyrrhotite margins and magnetite veins crosscutting pyrrhotite grains are interpreted as being due to magnetite formed during serpentinization. The development of a lamellar intergrowth of twinned pyrrhotite has been noted in a few areas.

Chalcopyrite forms irregular, discrete grains and irregular patches in association with pyrrhotite and pentlandite. A common association is chalcopyrite ± pentlandite forming a partially continuous selvage around large irregular pyrrhotite grains (Plate X). Chalcopyrite generally displays similar textural relations with silicate minerals as pyrrhotite. Cubanite, as blades and laths, is found in association with chalcopyrite in areas displaying

a low degree of serpentinization of the primary silicate assemblage (Plates XI and XII). The cubanite laths generally display several directions of orientation in the chalcopyrite host.

Pentlandite forms irregularly-shaped grains always in association with pyrrhotite. Large irregular pentlandite grains completely surrounded by pyrrhotite are common (Plate VIII). Flames and blades of pentlandite in pyrrhotite, adjacent to larger pentlandite grains have been noted. There is a general association between magnetite and pentlandite, magnetite rimming the contact between pentlandite and pyrrhotite and also filling fractures and cleavages in the pentlandite grains (Plate VIII). Most large pentlandite grains contain many irregular fine-grained patches of pyrrhotite which render a distinctly mottled texture to the pentlandite. Fine-grained rods and blades of cubanite have been noted in association with pentlandite (Plate XII). This association of cubanite is restricted to areas displaying a low degree of serpentinization.

Effect of Recrystallization of the Primary
Silicate Assemblage on Sulphide-silicate Textures

With increasing intensity of recrystallization (intense first stage recrystallization and second stage recrystallization, see Chapter V) the sulphide grain



Plate XI Cubanite exsolution blades in chalcopyrite. Note three directions of orientation of blades, and interstitial nature of chalcopyrite. Crossed nicols, X122. (536).



Plate XII Cubanite exsolution blades in chalcopyrite and blebs in pentlandite. Magnetite (grey) veins pentlandite and part of pentlandite-chalcopyrite contact. Crossed nicols, X130. (536)

boundaries become increasingly irregular until highly serrated and fretted margins are formed (Plates XIII and XIV). Fine, discontinuous sulphide stringers occur in the silicate areas adjacent to the sulphide grains and in some areas a fine, delicate net texture is formed (Plate XIV). The sulphide stringers are dominantly chalcopyrite and pyrrhotite with associated magnetite. Pentlandite also forms serrated margins (Plate XIII) but the development of pentlandite stringers is extremely rare.

In areas of intense recrystallization, a rim of less intense anisotropism commonly selvages some of the pyrrhotite grains (Plate XV). Scholtz (1936) describes dark and light anisotropic properties in pyrrhotites from the Insizwa nickel deposit, Africa and uses the terms α and β pyrrhotite to describe the dark and light phases. Naldrett (1964) describes two phases of pyrrhotite that occur as subparallel lamellae in the massive ore of the Alexo deposit near Timmins, Ontario. The less intense anisotropic material forming the rims is interpreted as being the β -pyrrhotite component; the central darker area the α -pyrrhotite component. These optical phases are generally considered to reflect two crystallographic varieties of pyrrhotite, hexagonal and monoclinic (Naldrett and Kullerud, 1967). X-ray results determined on four breccia sulphide pyrrhotites, which are discussed in the next section, indicate the presence of both hexagonal and monoclinic phases.

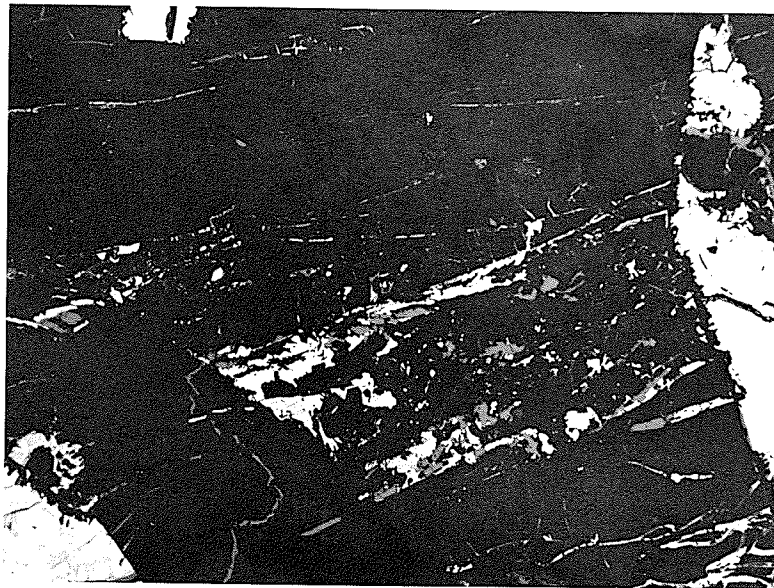


Plate XIII Pyrrhotite and chalcopyrite stringers in serpentine. Note magnetite stringers associated with the recrystallized sulphide and the serrated nature of the margins of the larger grains. Crossed nicols, X130. (542)

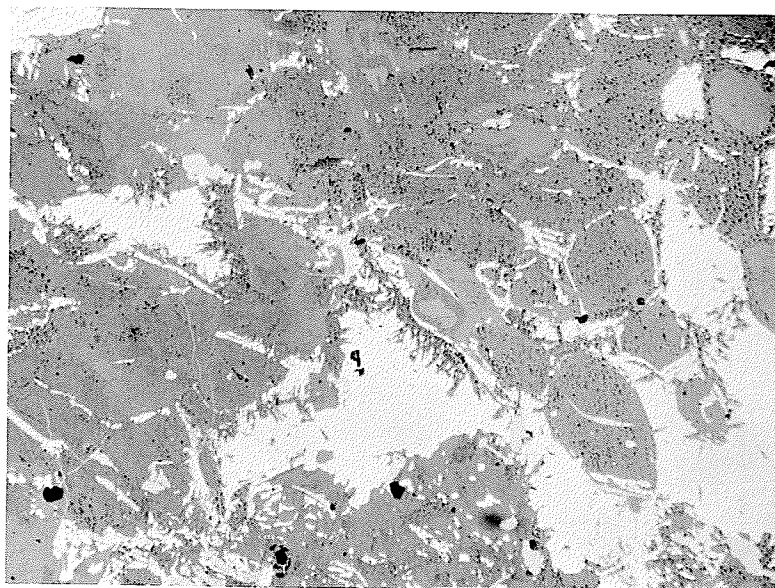


Plate XIV Recrystallized pyrrhotite in serpentine. Note highly serrated nature of larger grains, and association of magnetite with pyrrhotite veinlets. Plane light, X47. (212)

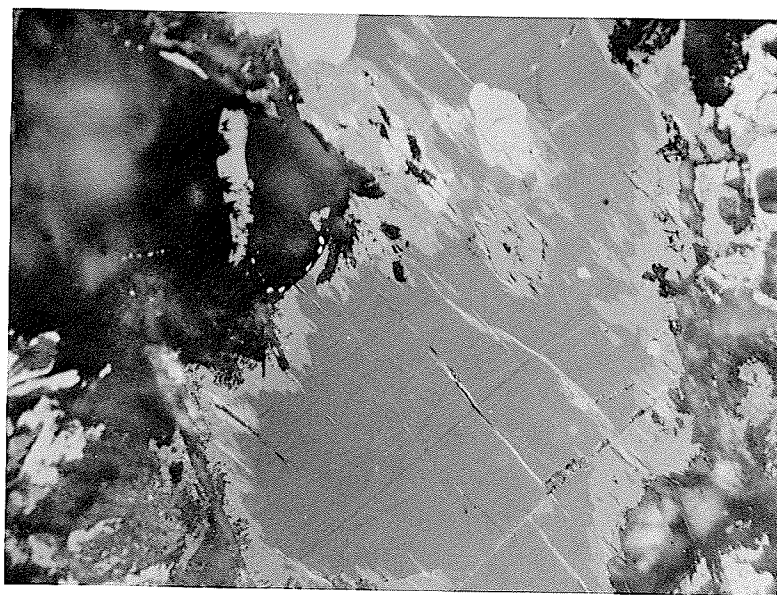


Plate XV Pyrrhotite grain displaying β component concentrated about rims. Central (darker) area is α component. Note serrated nature of margins indicative of recrystallization. Crossed nicols, X122. (212)

The fact that the β pyrrhotite forms rims selvaging the larger pyrrhotite grains, only in areas of intense recrystallization, indicates that the recrystallization is responsible for the development of the β pyrrhotite selvages. In the polished sections of the samples X-rayed, the α - β pyrrhotite relation was not visible. It therefore appears that the β pyrrhotite rims are a marginal concentration of the β pyrrhotite component formed during recrystallization. There does not appear to be an equivocal method for determining which optical phase corresponds to the monoclinic or hexagonal pyrrhotite.

The sulphide-silicate textures reflect the secondary recrystallization of the silicate assemblage. Incipient first stage recrystallization has little effect on the sulphide-silicate textures apart from the molding of magnetite about some of the sulphide grain boundaries. Increasing recrystallization causes serrated and fretted sulphide margins and the development of fine-grained sulphide veinlets. Kilburn *et al.* (1969) have similarly shown that intense serpentinization seriously alters the sulphide-silicate textural patterns of disseminated sulphides in ultramafic rocks.

Breccia Sulphide Ore

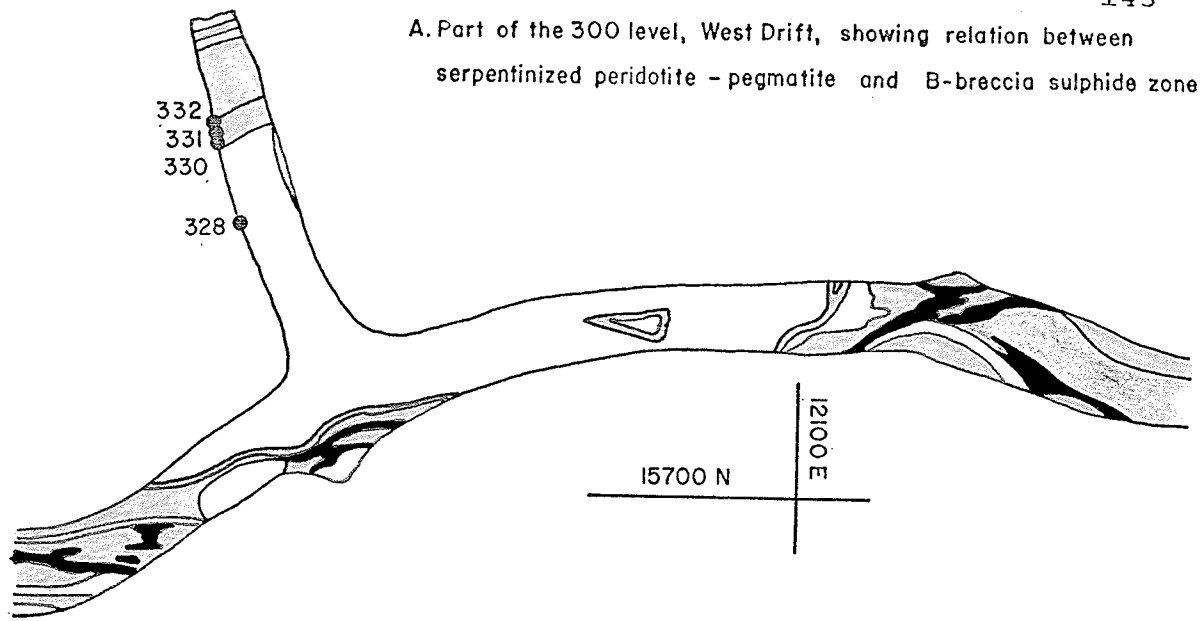
In general the term breccia ore is used for ore containing fragments of any rock. Breccia ores are

essentially bodies containing rounded, subrounded to subangular fragments of a wide variety of rock types in a matrix ranging from almost massive sulphide to varying proportions of sulphide and fine silicate particles of wall rocks and inclusions. Breccia ores are indicative of introduction of sulphides with extensive replacement of any pre-existing matrix and varying degrees of impregnation and replacement of coarser material, especially by chalcopyrite. Hydrothermal alteration is generally lacking.

The above description, condensed from Hawley (1962), is a fitting description for the breccia sulphide ore at Gordon Lake. The B-breccia sulphide zone is a continuous linear, sinuous band of breccia sulphide, which is dominantly enclosed by amphibolite (Figure 34). In longitudinal section (Figure 35) it has a crude wedge shape, the apex of the wedge pointing downward. It has its greatest length, therefore, on the upper levels where it attains a length of approximately 2000 feet. It has a vertical dimension of approximately 1300 feet and is 300 feet in length on the 1650 level. It is not known to continue below the 1650 level. The breccia sulphide zone, parallels the main fault zone and lies from 10 to 40 feet south of the fault.

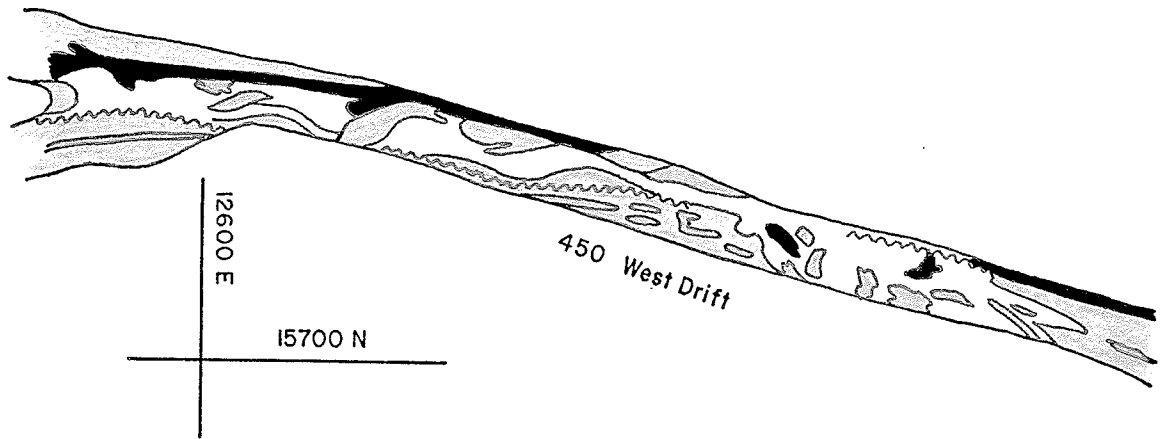
In detail the B-breccia sulphide zone forms a series of partially continuous breccia sulphide zones which range in width from several inches to 10 feet. These zones are

A. Part of the 300 level, West Drift, showing relation between serpentized peridotite - pegmatite and B-breccia sulphide zone











B. B-breccia zone - pegmatite relations, 450 level.

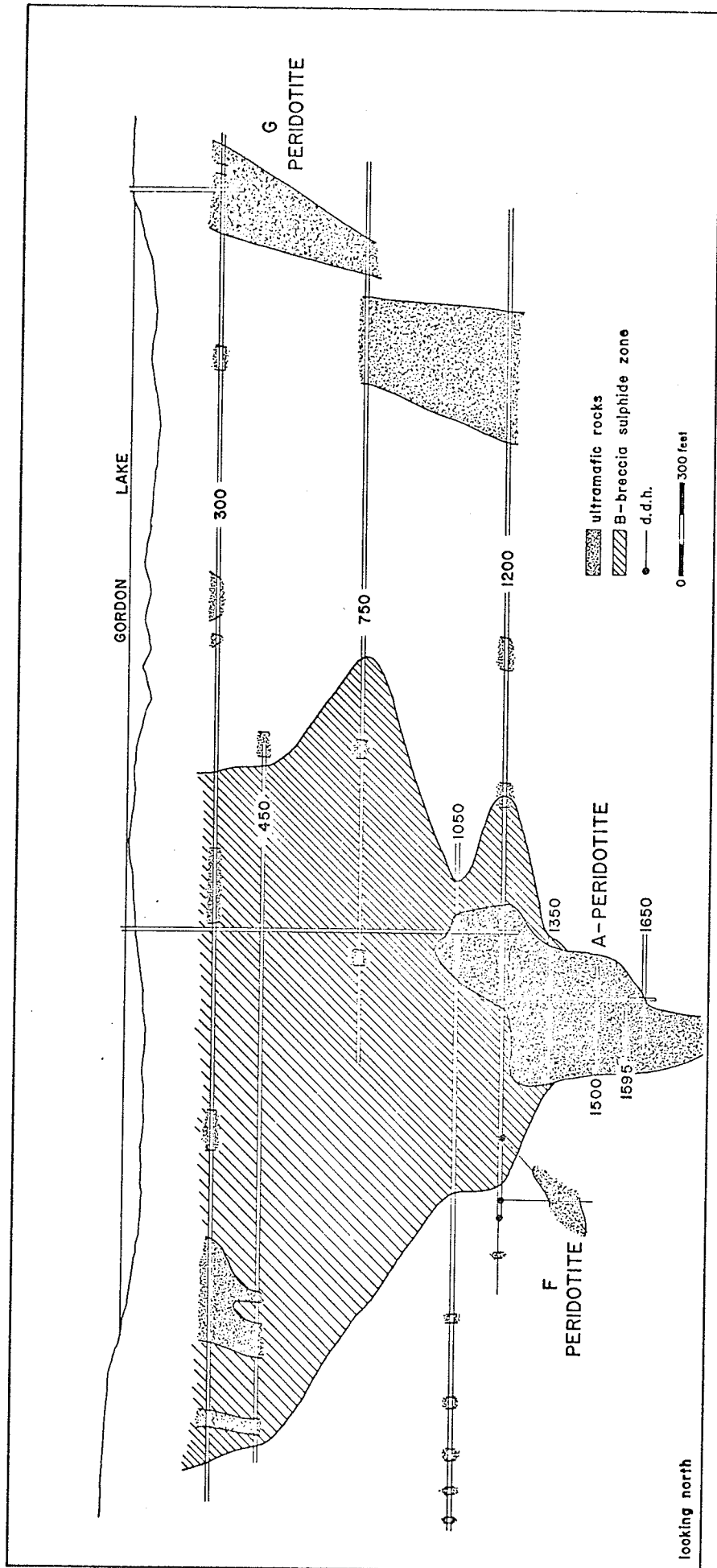
Note inclusions of B-zone sulphide in later pegmatite



Legend

- | | |
|--|---|
|  amphibolite |  biotite -chlorite - hornblende reaction zones |
|  biotite amphibolite |  B-breccia sulphide zone |
|  serpentized peridotite |  d.d.h. |
|  pegmatite | scale in feet 0  20 |

B - BRECCIA SULPHIDE ZONE



LONGITUDINAL SECTION — SHOWING RELATION BETWEEN A-PERIDOTITE AND B-BRECCIA SULPHIDE ZONE

FIGURE 35

generally conformable with the enclosing gneissic rocks and generally display a close spatial relation with pegmatite dykes. The contacts with the enclosing gneisses are sharp and distinct in most areas and are generally marked by a thin selvage of biotite. With the exception of the development of biotite, wall rock alteration is lacking. Contacts between breccia sulphide and pegmatite are both sharp and regular and gradational.

The term, breccia ore, comes from the fact that in many areas the massive sulphides contain rounded to sub-rounded plagioclase (sodic andesine), quartz and microcline inclusions which range from several mm to 4 cm in diameter. Biotite and chlorite occur in minor amounts. The silicate mineral assemblage is mineralogically compatible with the granodiorite-quartz diorite pegmatites described in Chapter II. Replacement of the silicate assemblage by sulphide can be seen megascopically.

Inclusions of amphibolite and pegmatite attaining dimensions of two to three feet in length and one to two feet in width are common in the breccia sulphide. Stringers of fine-grained chalcopyrite form veins which parallel the foliation in some of the amphibolite inclusions. The majority of these inclusions do not appear to have been rotated and their foliation parallels the foliation of the enclosing amphibolite.

In the area of the A-peridotite, the B-breccia

sulphide zone occurs along the north contact of the peridotite body and cuts across the peridotite on two levels (Figure 5). In detail on the 1500 and 1650 levels, tongues of massive sulphide are found protruding from the peridotite into the massive sulphide zone. As previously noted, diamond drill holes failed to intersect the B-breccia sulphide zone below the 1650 level. Thus it is indicated that the B-breccia sulphide zone terminates at the bottom of the A-peridotite. The breccia ore of the B-zone and the disseminated ore of the A-peridotite therefore display a close spatial relation.

Mineragraphy of the Breccia Ore

The sulphide assemblage of the B-breccia sulphide zone is a simple mixture of pyrrhotite, pentlandite and chalcopyrite. Pyrite and marcasite are minor accessory sulphide minerals. The distribution of these sulphide minerals ranges considerably along the length and depth of the ore body. Areas are found which are composed solely of pyrrhotite and pentlandite to the exclusion of chalcopyrite. Chalcopyrite can be the dominant sulphide along with minor pyrrhotite to the total exclusion of pentlandite, in other areas. Generally, however, all three minerals are present in the decreasing order of abundance: pyrrhotite, pentlandite, chalcopyrite.

The breccia ore differs from the disseminated ore

in the following manner:

- (i) overall decrease in the amount of chalcopyrite and corresponding increase in amount of pentlandite,
- (ii) general absence of magnetite,
- (iii) slightly greater abundance of pyrite and associated marcasite,
- (iv) common replacement of silicates by sulphides.

Pyrrhotite, the dominant mineral of the sulphide assemblage, forms large irregular grains, generally displaying an even anisotropism. The grain size ranges from 0.1 mm to greater than 1.5 cm. The smaller grains tend to form an equidimensional mosaic in polished section. The development of a lamellar intergrowth of twinned pyrrhotite has been noted in a few areas (Plate XVI).

Four breccia sulphide pyrrhotites were X-rayed to determine if both the monoclinic and hexagonal phases were present. Figure 36 shows that in each case the presence of a double peak indicates that both monoclinic and hexagonal phases are present. Groves and Ford (1963) state that in the more metal deficient pyrrhotites, monoclinic symmetry is exhibited in varying proportions, and in pyrrhotites containing less than 46.80 atomic per cent metals, it is always present. Formation of the monoclinic phase is considered to be a relatively low-temperature transformation from unstable, metal deficient, hexagonal pyrrhotite,



Plate XVI Twinned pyrrhotite. Note delicate exsolution flames of pentlandite associated with terminations of pyrrhotite lamellae. Crossed nicols, X36, (739)

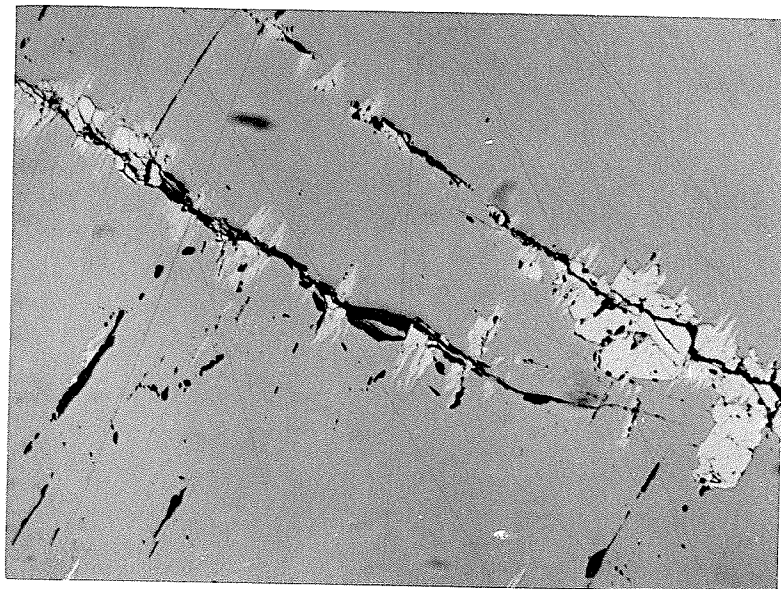
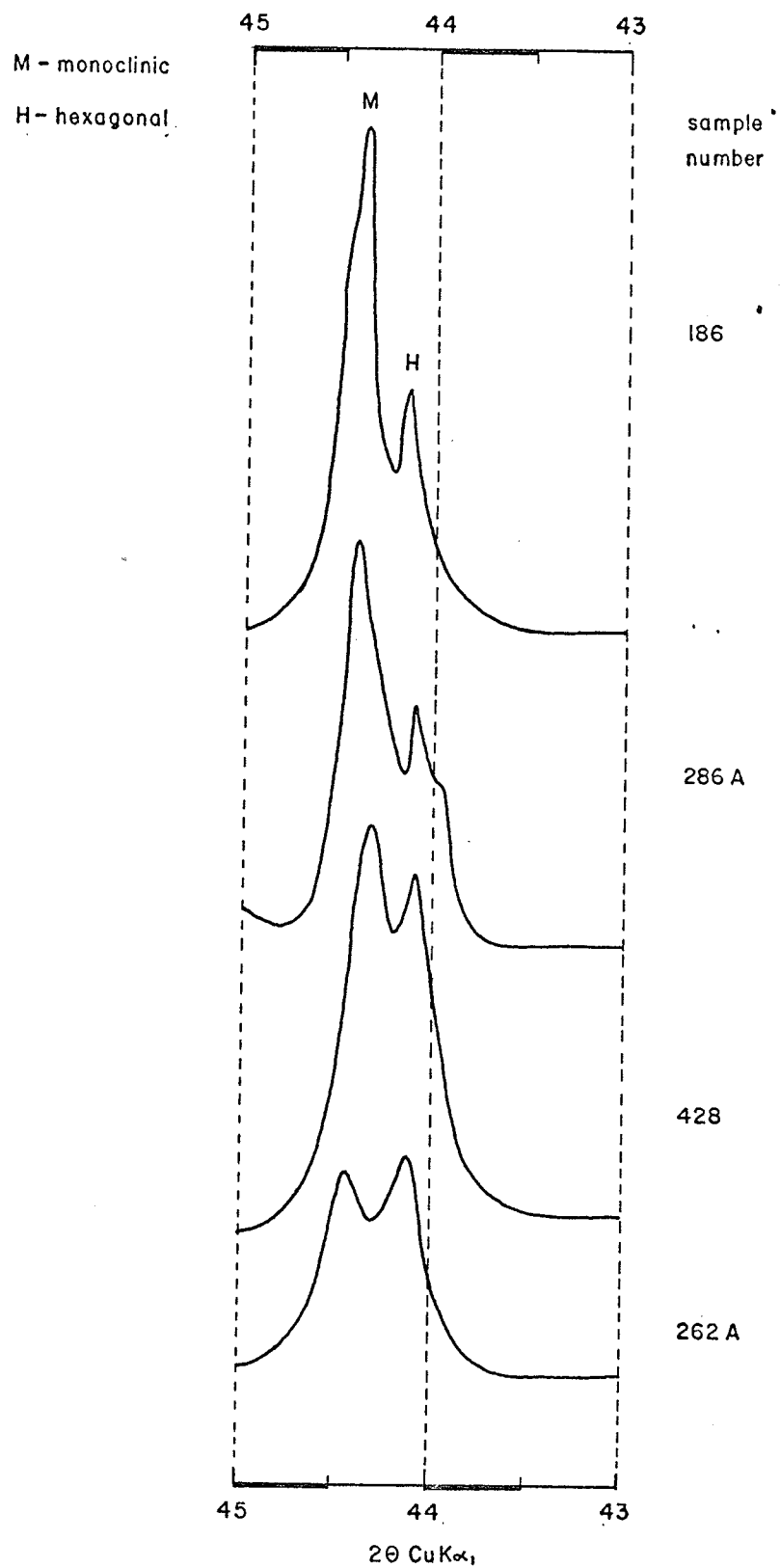


Plate XVII Pentlandite exsolution flames in pyrrhotite. Exsolution appears to be controlled by fractures in the pyrrhotite. Plane light, X130. (1004)



X-RAY DIFFRACTOGRAMS
B - BRECCIA SULPHIDE ZONE PYRRHOTITES

crystallized at high temperatures, to a super-lattice type structure (Kullerud, 1967).

Fine exsolution flames and blades of pentlandite are common along fractures and cleavages in pyrrhotite and along pyrrhotite grain boundaries. Many of these flames and blades have an indefinite shape which is in part due to feathery terminations (Plate XVII). These features have also been noted at the boundary between pyrrhotite lamellae, discussed above (Plate XVIII). As larger grains (0.3 mm to 2 mm) it occupies fractures and pyrrhotite boundaries and its margins with the enclosing pyrrhotite are marked by exsolution flames and blades (Plate XIX). The formation of pentlandite between pyrrhotite grain boundaries leads to the development of a partially continuous and in some areas a continuous net texture (Plate XX). Larger irregular masses of pentlandite (1 mm to 3.5 mm) are either wholly enclosed by a large continuous pyrrhotite grain or by a finer-grained pyrrhotite mosaic. The association of magnetite with pentlandite of the disseminated ores is virtually absent in the breccia sulphide assemblage.

Small (0.1 mm to 0.5 mm) irregularly-shaped grains of chalcopyrite commonly occur along pyrrhotite-pyrrhotite and pyrrhotite-pentlandite grain boundaries. Fine blades associated with exsolution flames of pentlandite along fractures and cleavages in pyrrhotite occur in a few areas. Chalcopyrite is associated with lenticular masses of pent-

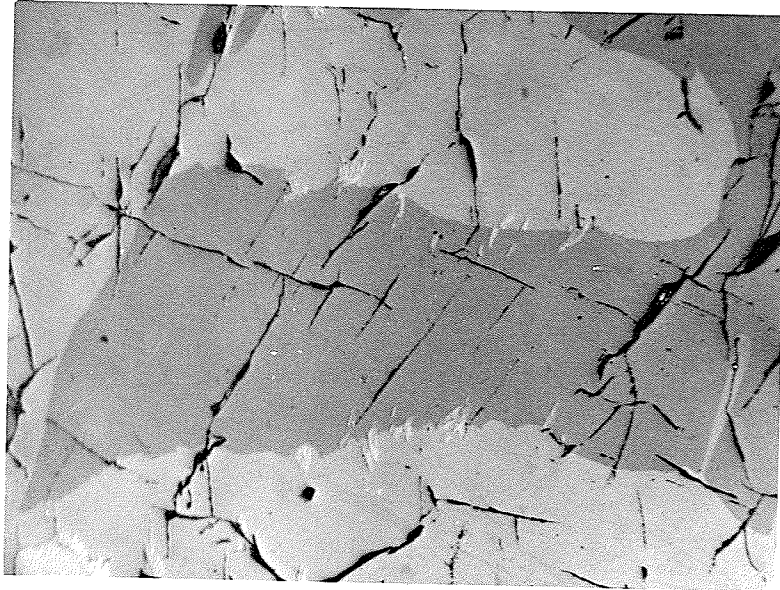


Plate XVIII Pentlandite exsolution flames in pyrrhotite
Exsolution is controlled by pyrrhotite-
pyrrhotite grain boundaries. Crossed
nicols, X36. (739).

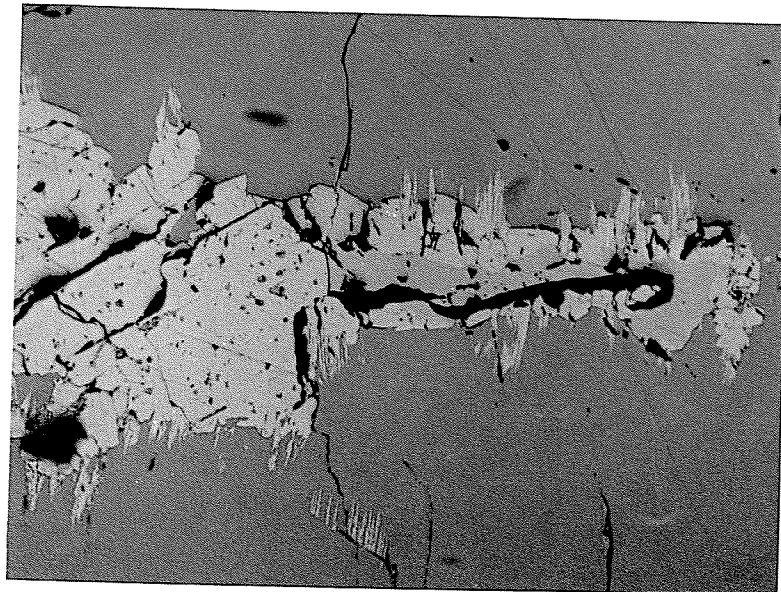


Plate XIX Pentlandite in pyrrhotite. Note exsolution
flames along pentlandite-pyrrhotite boundary.
Note chalcopyrite (on either side of horizontal
fracture) associated with pentlandite. Plane
light, X130. (1004)

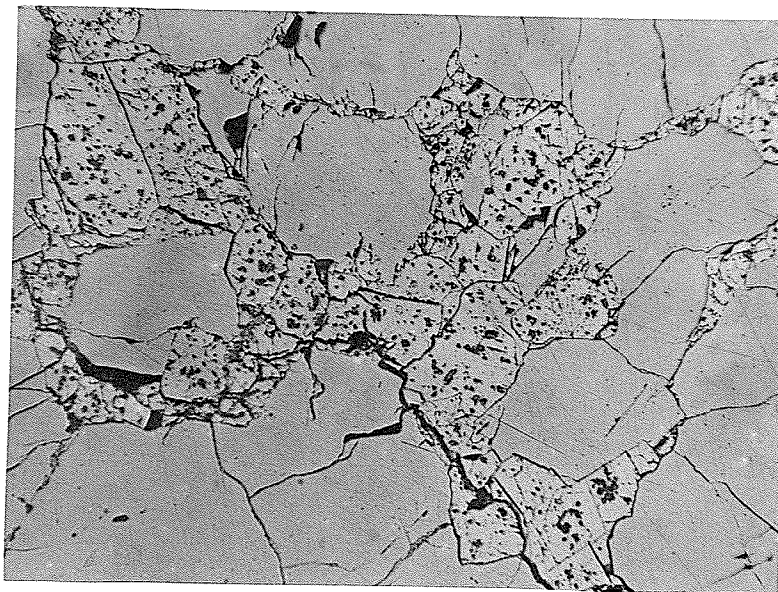


Plate XX Pentlandite-pyrrhotite. Coarser, continuous net-texture pentlandite in pyrrhotite. Plane light, X37. (483)



Plate XXI Chalcopyrite-pyrrhotite. Elongate chalcopyrite grain cutting across pyrrhotite. Small blebs to the right of the chalcopyrite grain in the central part of the photo are chalcopyrite exsolution blades in pyrrhotite. Plane light, X31. (1002)

landite which form along fractures in pyrrhotite and along pyrrhotite grain boundaries. Chalcopyrite follows the same fractures and boundaries as discontinuous veinlets or irregular masses (Plate XXI). Chalcopyrite-rich zones are composed of a continuous phase of chalcopyrite with minor irregular inclusions of pyrrhotite. Silicate inclusions are commonly selvaged and partially replaced by chalcopyrite.

Pyrite is not a common constituent although several small pyrite-rich zones are known. It occurs in pyrrhotite as irregular masses and partially to well-developed cubes (Plate XXII). Small irregular masses of marcasite have been found associated with pyrite.

A small (0.1 mm), soft, white, slightly anisotropic unknown mineral, wholly enclosed by pentlandite, was observed in two polished sections.

Massive Sulphide Lenses in Ultramafic Rocks

Lenses of massive sulphide are known in the G-peridotite and A-peridotite ore bodies, but their general shape and distribution is not known. Samples obtained from drill core indicate that in general, few silicate inclusions are present. The associations and textures of the sulphide minerals are similar to those described for the B-breccia sulphide zone. The ratio of pentlandite plus chalcopyrite to pyrrhotite is slightly greater in the massive lenses compared with the B-breccia sulphide zone. Exsolution blades and

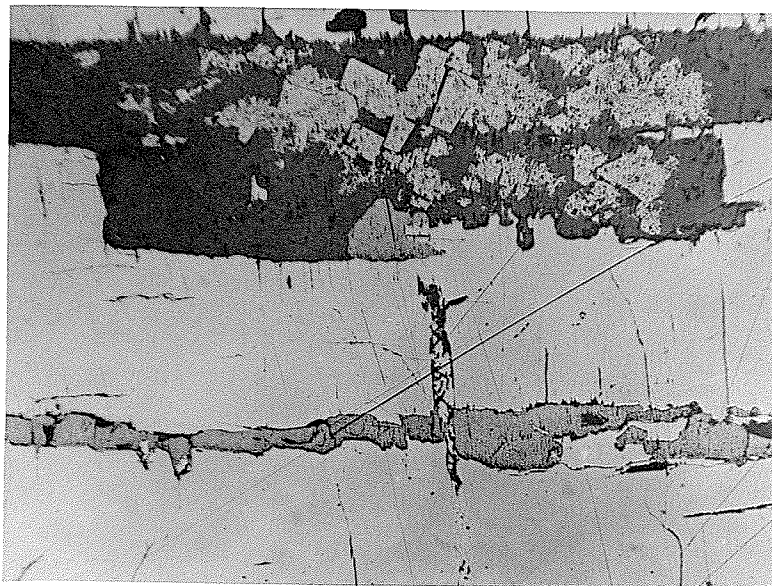


Plate XXII Pyrite-pyrrhotite. Pyrite cubes in silicate host associated with pyrrhotite. Note magnetite vein cut by later pentlandite (central). Plane light, X31. (577)

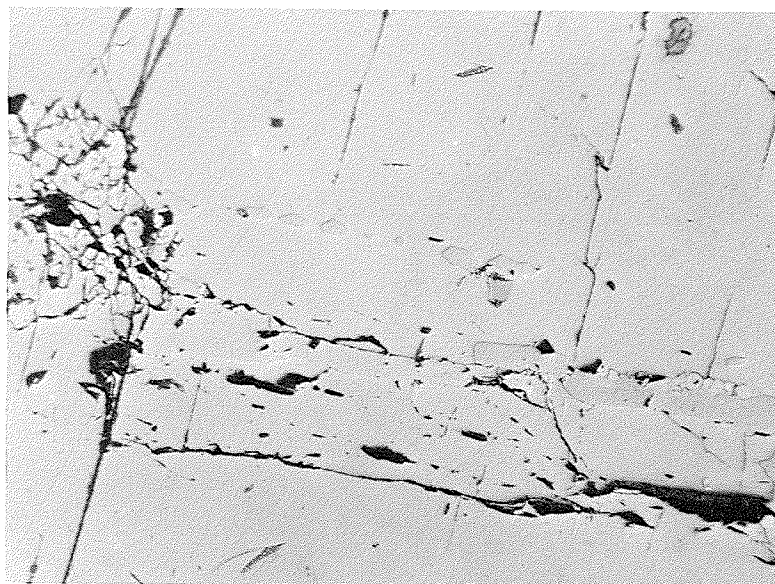


Plate XXIII Chalcopyrite-pyrrhotite-pentlandite. Fine-grained exsolution blebs of chalcopyrite in pyrrhotite (left centre to right centre). Note pentlandite associated with chalcopyrite in left centre. Plane light, X55. (1002)

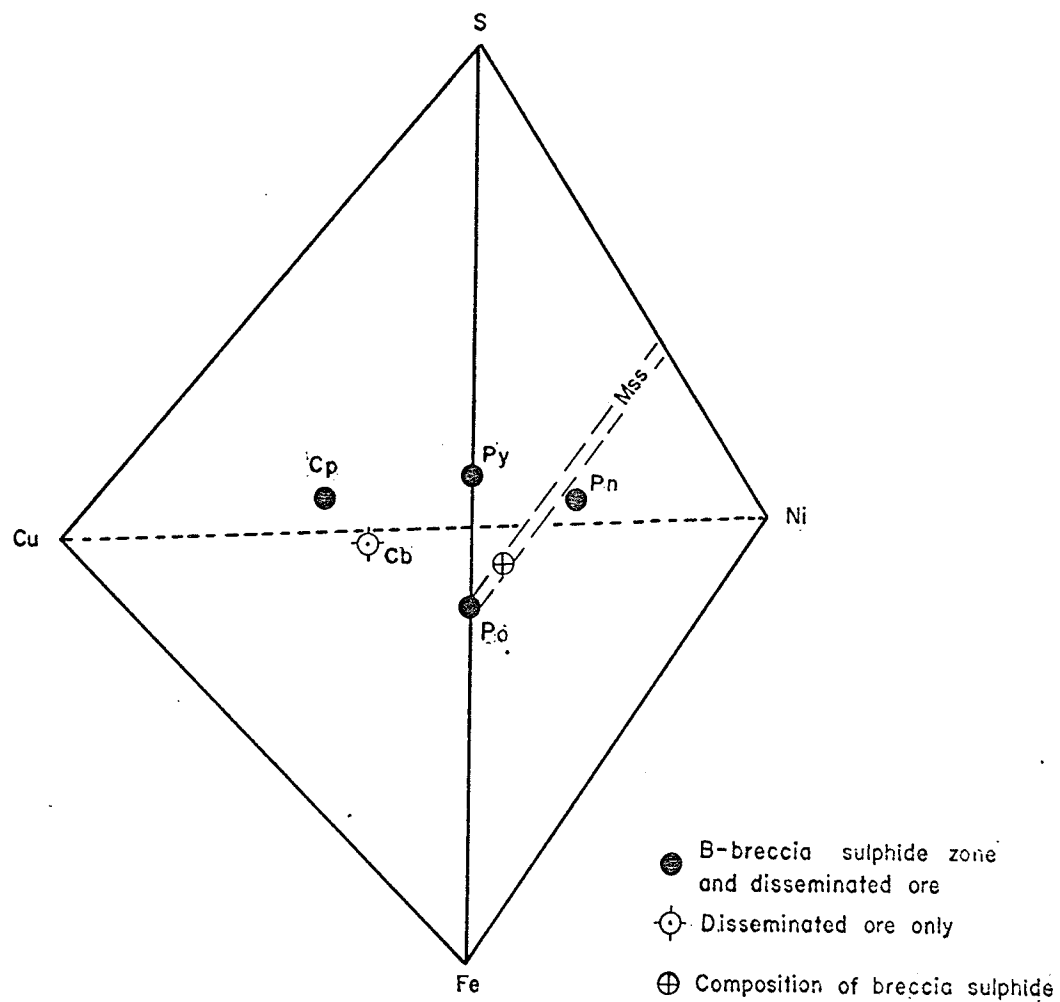
laths of chalcopyrite, similar to and commonly associated with exsolution blades and flames of pentlandite, are found along fractures and cleavages in pyrrhotite (Plate XXIII).

Sulphide-sulphide Textures and Crystallization
of the Sulphide Magma

The sulphide-sulphide textures, described for the disseminated breccia and massive ores, are compatible with exsolution of pentlandite and chalcopyrite from pyrrhotite. The association of chalcopyrite and pentlandite in fractures and cleavages in pyrrhotite, and partially selvaging pyrrhotite grain boundaries in both the disseminated and breccia ores, suggests that in some areas both chalcopyrite and pentlandite exsolved from pyrrhotite at approximately the same time.

The sulphide phases present in the disseminated and breccia ores are plotted in the Cu-Fe-Ni-S system (Figure 37). With the exception of some Cu-rich zones the Gordon Lake ores average less than 2 per cent Cu. Craig and Kullerud (1969), in their discussion of the geological implications of the Cu-Fe-Ni-S system, state that when the Cu content is less than 2 per cent the Cu as well as the Ni will be accommodated within the pyrrhotite structure. The maximum temperature at which chalcopyrite and pentlandite can exsolve together from pyrrhotite is about 575°C.

Analyses of pure sulphide ore, representing the



All points lie on the two upper, facing surfaces

SULPHIDE ASSEMBLAGES - SULPHIDE ORES

FIGURE 37

various types of nickel-copper sulphide ores present at Gordon Lake are not available. However, analyses of B-breccia sulphide zone samples, some of which are very nearly massive are listed in Table XXIII. Four analyses, containing greater than 33 per cent S, represent essentially massive sulphide with minor silicate inclusions. The Gordon Lake breccia ore appears to be similar to the Ni-Cu ores of the Strathcona Mine, Sudbury Basin (Naldrett and Kullerud, 1967) and the Alexo Mine, Timmins (Naldrett, 1964). Analyses of these ores (Naldrett, 1968) indicate consistent values of Fe (55 per cent in both ores) and S (38 per cent Alexo, and 39 per cent Strathcona). A value of 55 per cent for Fe was included with the averaged values for Cu, Ni and S for the four breccia sulphide analyses and the resulting figures were calculated to 100 per cent. The average composition for the sulphide of the breccia ore is listed in Table XXIV.

It would appear that Cu is a minor constituent of the B-breccia sulphide zone ore. However, in Table XXIII, the erratic distribution of Cu is readily apparent. Reference to Figure 39 confirms the fact that Cu is not a major constituent of the B-breccia sulphide ore, however, it can also be seen that high Cu samples do occur. For purposes of the following discussion, Cu is considered a minor constituent and attention is focussed on the Fe-Ni-S system.

A sulphide of the above composition (minus Cu) has been plotted on the Fe-Ni-S system at 1,000° and 650°C

Table XXIII

Analyses of Breccia Sulphide Ores^{*}

		<u>Cu</u>	<u>Ni</u>	<u>Co</u>	<u>S</u>
SDG61-243A ^{**}	300 level	0.033	6.40	0.28	34.60
SDG61-262	300 level	0.13	3.60	0.10	16.56
SDG61-423	300 level	0.15	5.78	0.15	27.13
SDG61-280	300 level	0.16	5.95	0.18	28.20
SDG61-429	450 level	13.02	2.15	0.07	22.42
SDG61-431	450 level	1.48	4.60	0.23	28.32
SDG61-434 ^{**}	450 level	0.15	7.35	0.19	33.03
SDG61-436	450 level	0.08	3.35	0.09	15.11
SDG61-232 ^{**}	750 level	0.05	6.20	0.15	34.07
SDG61-182	750 level	0.06	6.05	0.14	26.52
SDG61-225	750 level	0.12	1.93	0.06	11.04
SDG61-227 ^{**}	750 level	0.06	5.00	0.21	33.80
SDG61-463	750 level	0.12	2.05	0.28	26.60
SDG61-464	750 level	1.54	2.40	0.07	12.31

* Analyses made by the Mineral Sciences Division, Mines Branch, Department of Energy, Mines and Resources, Ottawa, Ontario.

** Analyses used in calculating average composition of sulphide ore.

Table XXIV

Average Composition of B-breccia
Sulphide Zone Sulphide Ore

S	37.93
Ni	6.99
Cu	0.08
Fe	55.00
	<hr/>
Total	100.00

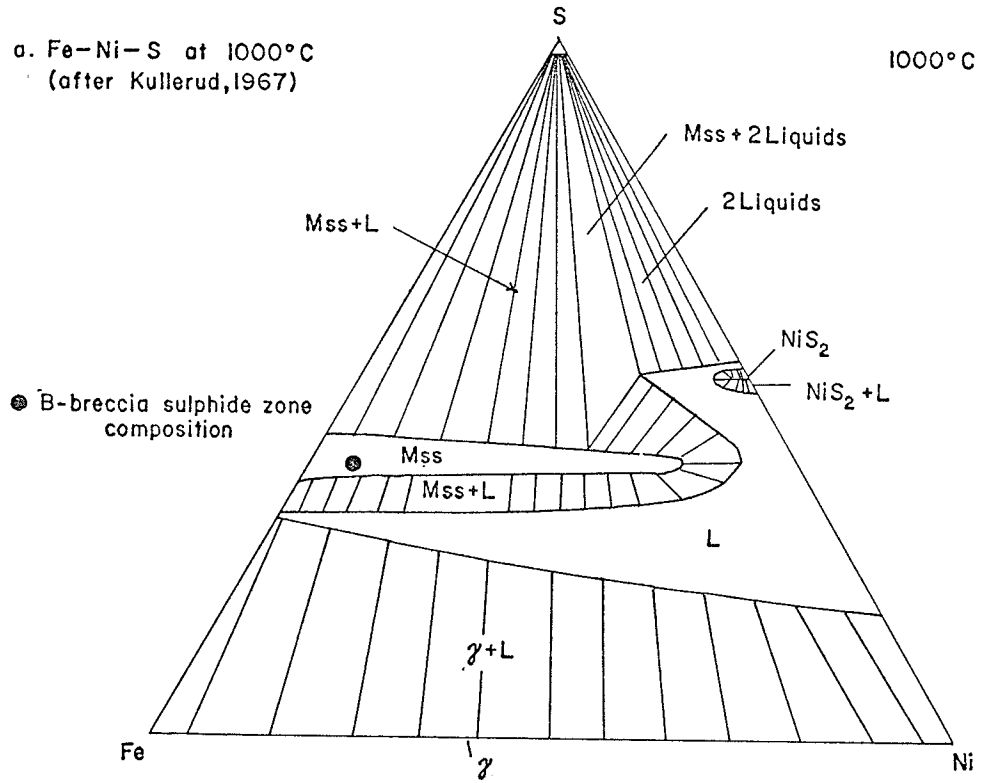
(Figure 38) after Kullerud (1963). In each case the point lies in the field occupied by monosulphide solid solution + vapour. Within the limits of error inherent in the assumptions made for the calculation of the sulphide ore, noted above, it appears that the sulphide of the B-breccia sulphide zone existed as a monosulphide solid solution to at least 650°C. This is compatible with the sulphide-sulphide textures observed in the breccia ore, and in the massive sulphide lenses in the ultramafic bodies.

The presence of Cu-rich areas in the breccia sulphide ore and as thin massive lenses in the amphibolite has been noted. Craig and Kullerud (op. cit.) indicate that separation of sulphide liquid from pyrrhotite at temperatures above 850°C can give rise to chalcopyrite-rich veins and segregations.

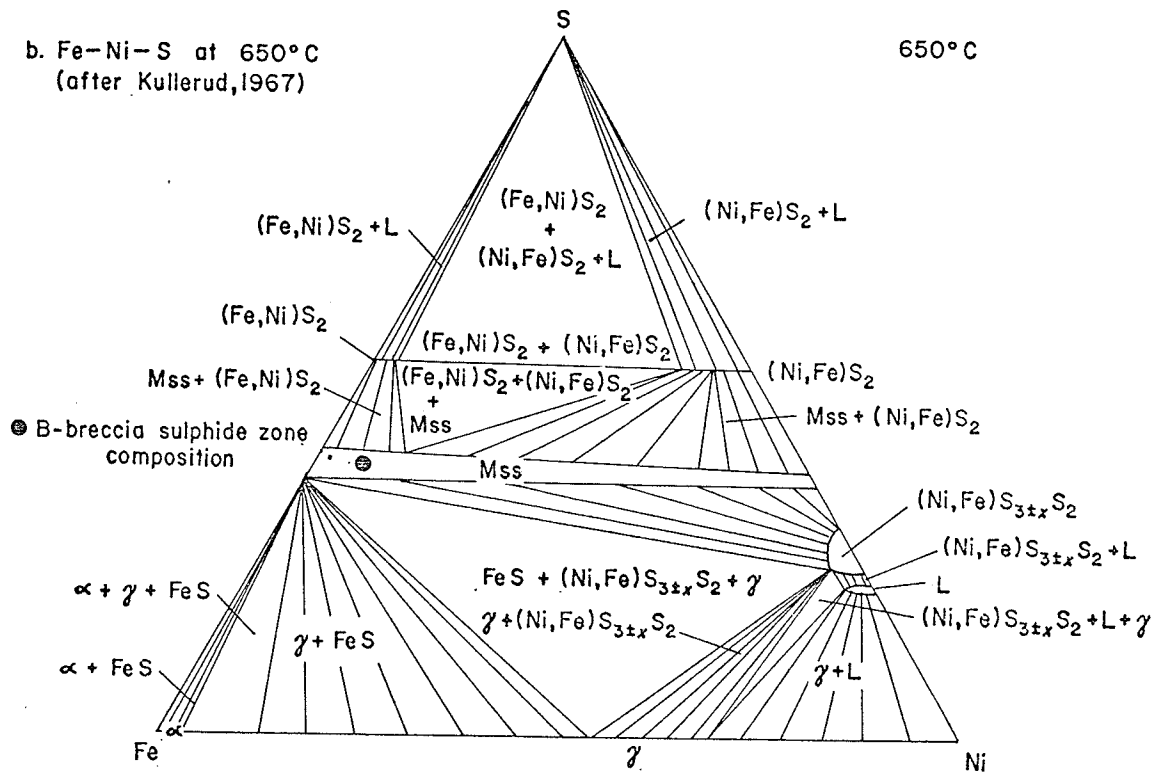
The Association of Pegmatite

The relationship between sulphide mineralization and pegmatite dykes is uncertain. The apparent replacement of pegmatite within the B-zone, and the truncation of some pegmatite dykes by the breccia sulphide zone, leads to the conclusion that the sulphide is later than some pegmatite. Pegmatites clearly cut across peridotite causing some recrystallization of the silicate assemblage and alteration of the silicate-sulphide textural patterns. Attention is drawn to Figure 30 where a small pegmatite dyke cuts across

a. Fe-Ni-S at 1000°C
(after Kullerud, 1967)



b. Fe-Ni-S at 650°C
(after Kullerud, 1967)



Fe-Ni-S SYSTEM

FIGURE 38

serpentinized peridotite. The disseminated sulphide of the serpentinized peridotite is the fine-grained ragged variety. Irregular subrounded grains of sulphide can be seen along the interface between the hornblende and biotite zones of both reaction rims.

If the pegmatite, represented by the inclusions of plagioclase, microcline and quartz of the B-breccia sulphide zone and the pegmatite dykes crosscutting the ultramafic bodies are contemporaneous, then the sulphide of the B-breccia sulphide zone must be later than the pegmatites and therefore later than ultramafic bodies and the disseminated sulphide ore. If, as seems more likely, the disseminated ore and breccia ore are approximately contemporaneous, then two ages of pegmatite are required.

Evidence regarding the relative age relationships between pegmatite dykes and the breccia sulphide ore is not well documented. However, in several areas, pegmatite dykes are found which truncate the B-breccia sulphide zone. An example is found on the 450 level, west drift, where a large pegmatite dyke includes two large pieces of B-breccia sulphide zone material (Figure 34). Inclusions of amphibolite and an inclusion of earlier pegmatite can also be seen.

It appears therefore that there are at least two ages of pegmatite intrusions: an early pre-ore intrusion and a later, post-ore intrusion. It is proposed further

that the breccia sulphide ore and the disseminated ore are genetically related. Further evidence for this is presented in the following sections.

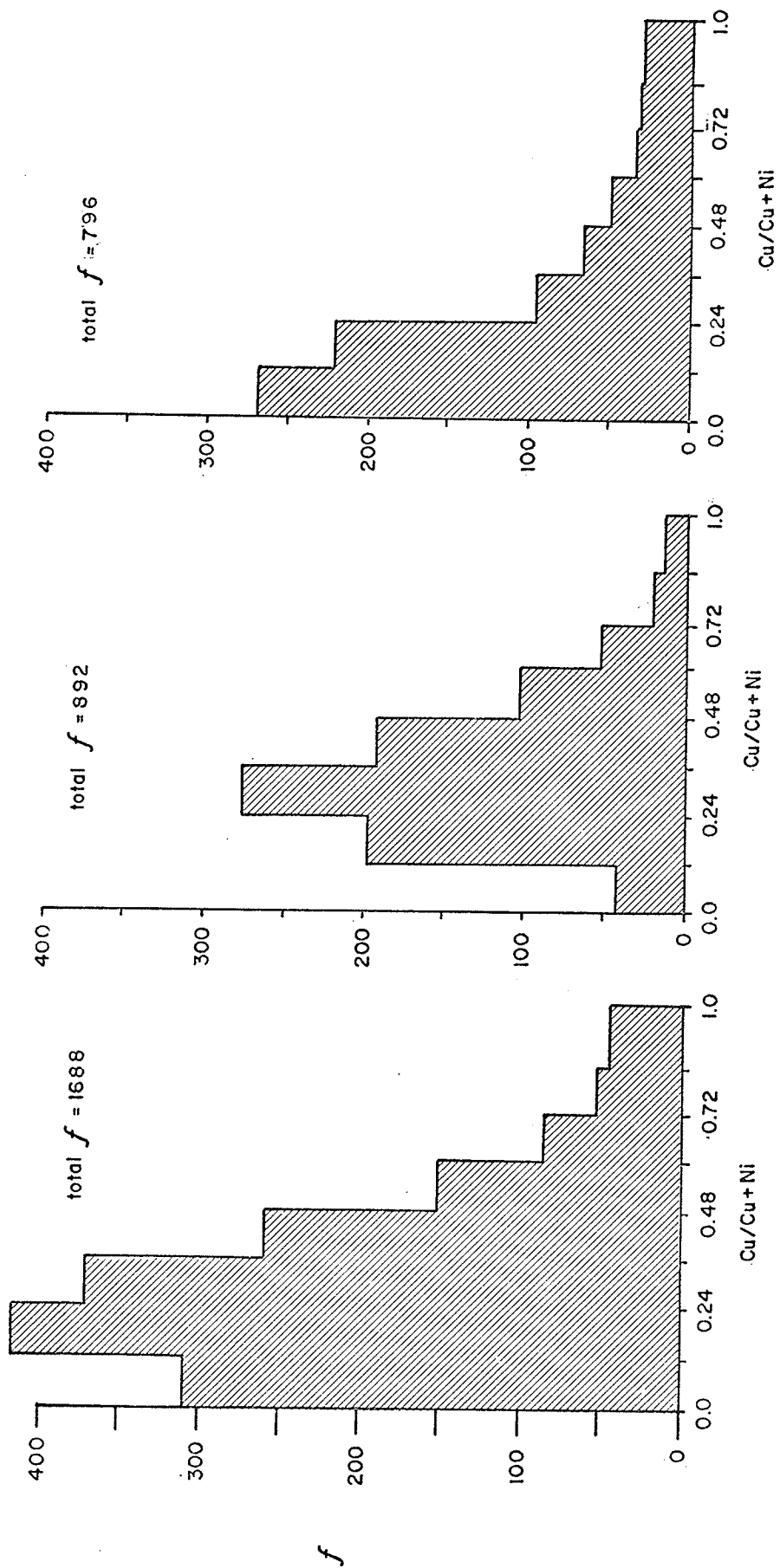
The reasons for the preferential association of sulphide ore and pegmatite are not clear. The inclusions of plagioclase, microcline and quartz are not an ubiquitous association, however, they are present in sufficient quantity to merit attention. It was previously noted that the ratio of the silicate inclusions is compatible with the quartz diorite-granodiorite pegmatite described in Chapter II. The problem of pegmatite association is compounded by the fact that the B-breccia sulphide zone truncates earlier pegmatite dykes without any apparent sulphide replacement of some of the truncated dykes.

Although there is little evidence of brecciation of the silicate inclusions it is probable that movement along the main fault zone caused some brecciation of the pegmatite. The pegmatite, which is generally bounded by amphibolite would be relatively competent compared to the amphibolite. A stress pattern developed along the main fault zone could be taken up, in part, by brecciation of a competent layer like pegmatite. It was previously noted that the B-breccia sulphide zone parallels the main fault and ranges from 10 to 40 feet south of the fault zone. The lack of evidence of brecciation may be due to total replacement of the brecciated matrix by sulphide mineralization.

Cu-Ni Distribution in the Sulphide Ores

A study of the distribution of Cu and Ni in the Gordon Lake ore bodies was previously completed (Scoates, 1963). The basis for the study was the availability of assay plan data for the ore bodies on the various levels of the mine. The assays were grouped according to the type of ore and their spatial position within the mine. Copper-nickel ratios $Cu/(Cu + Ni)$ were calculated and the results were statistically analyzed. The methods used in the study are outlined by Scoates (op. cit.). A summary of the results of this study is provided in this section.

In Figure 39 the distributions of Cu and Ni for the whole mine, the disseminated ores and the breccia ore are shown. The positions of the histograms indicate that there is more Ni relative to Cu in the breccia sulphide ore than in the disseminated ores. Figure 40 shows the logarithmic frequency cumulative curves of the breccia sulphide and disseminated ores. The differences in the slopes of the curves indicate a broad concentration of the values about the median point of the curve of the disseminated ores and virtually no concentration of values about the median point of the curve of the breccia sulphide ore. The curve of the breccia sulphide ore, therefore, indicates the general homogeneous nature of Cu and Ni in the breccia sulphide ore. This is illustrated in another way in Figure



a. All orebodies
 b. Disseminated orebodies
 c. Breccia sulphide zone

FREQUENCY DISTRIBUTION OF COPPER AND NICKEL

FIGURE 39

LOG-CUM CURVES FOR DISSEMINATED SULPHIDE AND B-BRECCIA SULPHIDE OREBODIES

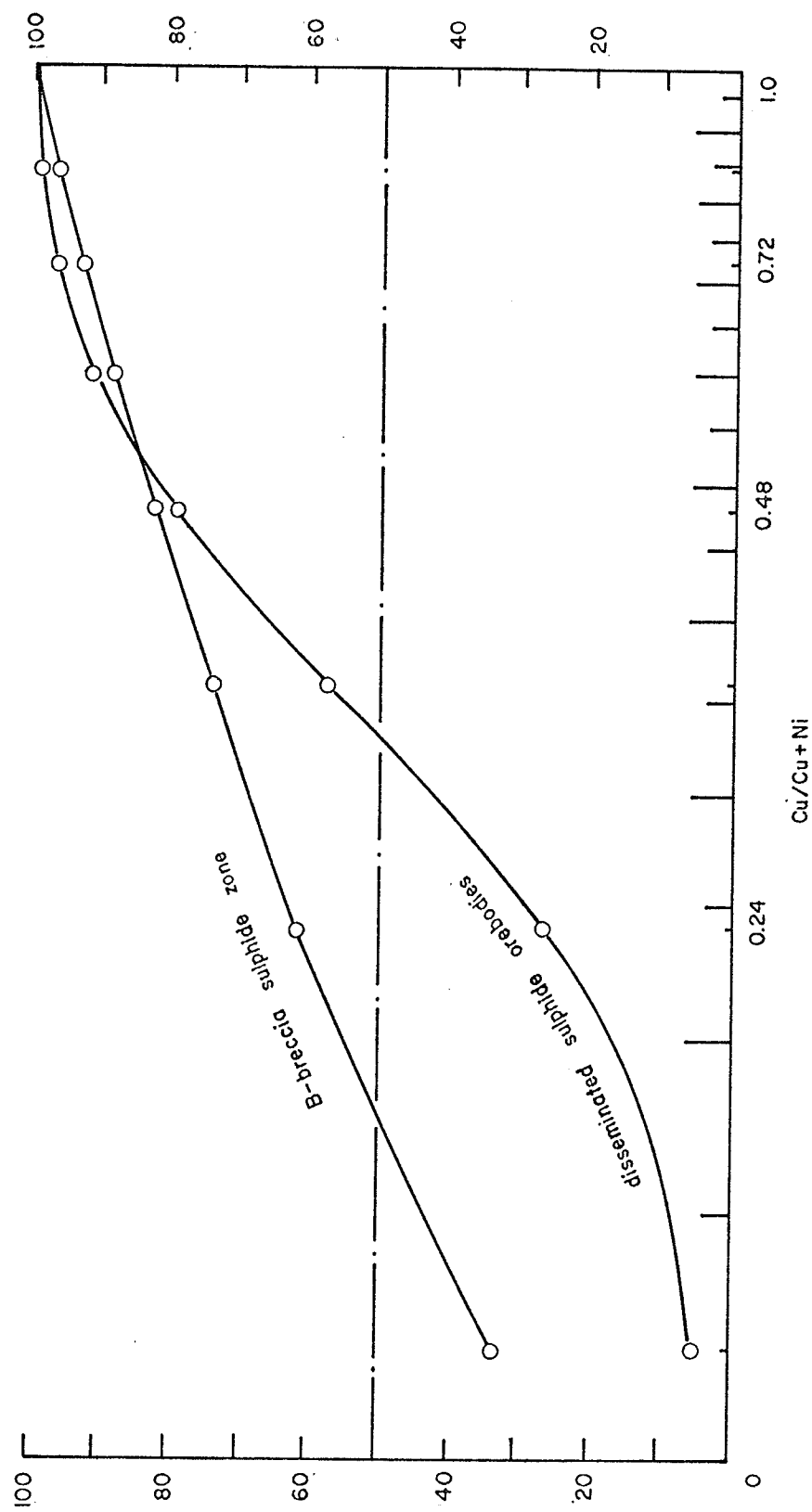
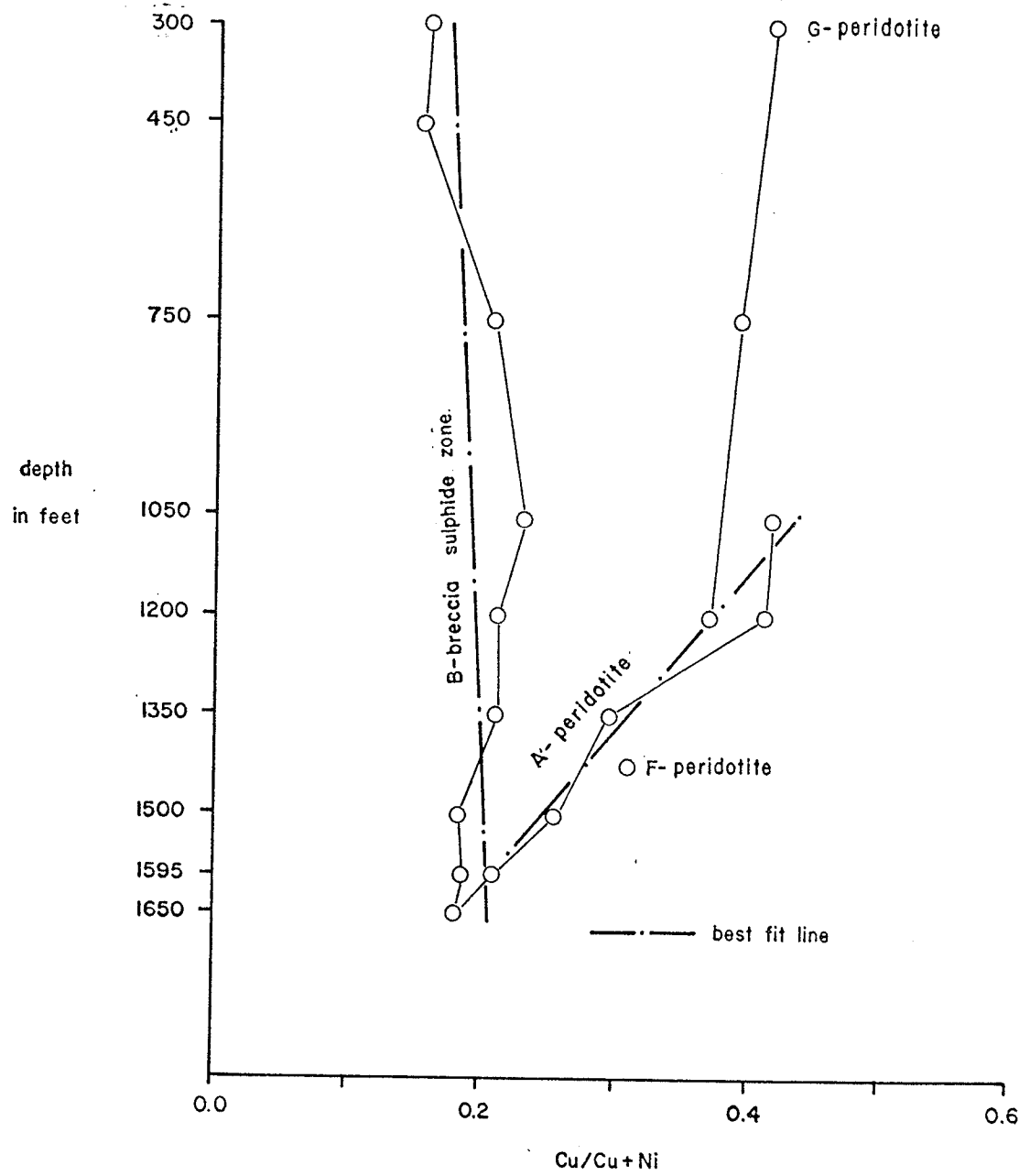


FIGURE 40

41 where the vertical distribution of Ni and Cu in both the breccia and disseminated ores is shown. The distribution of Cu and Ni in the breccia ore displays small-scale fluctuations with depth and is in keeping with the general homogeneous nature of this ore. The distribution of Cu and Ni in the disseminated ores displays a consistent trend of increasing Ni, relative to Cu, with depth. It can be seen that the trend is consistent throughout the mine and in an individual ore body like the A-peridotite. The median value of the F-peridotite ore body is plotted at the approximate centre of its vertical limits, and the position of this point fits the general trend of the disseminated sulphide ores.

Figure 41 shows that on the lowest levels, the distribution of Cu and Ni in the breccia sulphide ore and the disseminated ore of the A-peridotite ore body is virtually the same. It was noted earlier in this chapter that the B-breccia sulphide zone intersects the A-peridotite on the 1200 and 1650 levels, and that tongues of sulphide ore are found protruding into the breccia ore from the A-peridotite on the 1500 and 1650 levels. It was also noted that the B-breccia sulphide zone appears to terminate at or near the base of the A-peridotite. The point of interest is that where the disseminated and breccia ore display a close spatial relation, they also display a similar distribution of Cu and Ni.



PLOT OF MEDIAN Cu/Cu+Ni RATIOS WITH DEPTH

Genesis of the Sulphide Ores

The existence of a silicate-sulphide immiscible magma is indicated by the sulphide-silicate textures. Flowage differentiation has been suggested as the mechanism for explaining the modal concentration of Fo-rich olivine toward the centre of the A-peridotite. Therefore, during intrusion, the magma consisted of olivine crystals, silicate magma and sulphide liquid. Naldrett and Kullerud (op. cit.) have concluded that estimates of the settling rate of sulphide liquid globules in a basic magma, containing 50 per cent crystals in suspension, and magma velocity during intrusion, are compatible with sulphide droplets having been held in suspension during magma intrusion.

The central area of the A-peridotite is estimated to contain approximately 40 per cent olivine and the body as a whole probably contained in excess of 20 per cent olivine crystals in suspension during intrusion. It is considered possible that a magma of the A-peridotite type could transport sulphide droplets in suspension during magma intrusion.

An increase in Ni relative to Cu, with depth has been noted for the disseminated ores. The breccia sulphide ore is enriched in Ni relative to Cu and the distribution of Cu and Ni in the breccia sulphide ore and the disseminated

ore of the A-peridotite is approximately the same on the lower levels. Similar relationships exist between massive and disseminated sulphide ores in mafic and ultramafic sills. The Insizwa sill of South Africa (Scholtz, 1936) has a differentiated basal zone containing Cu-Ni sulphides. The disseminated ores are more Cu-rich than the pyrrhotite-rich massive ores which lie along the basal contact (Table XXV). The Katiniq sill of northern Quebec (Wilson *et al.*, 1969) displays the same relation, the massive basal ore being more Ni-rich than the overlying disseminated sulphides (Table XXV). It should be noted that there is a marked difference in the number of determinations made for the three areas compared. However, the consistency of the results is considered important. Both intrusions are considered to represent gravitative settling of sulphides in a basic silicate magma and concentration of these sulphides at the base of the intrusions. In each case gravitative separation of Ni-rich sulphide occurred during settling, with the consequent formation of Ni-rich basal sulphide ores.

The vertical distribution of Cu and Ni in the disseminated ores of Gordon Lake is thought to be indicative of gravity separation of the denser Ni-rich sulphide liquid during intrusion of the silicate-sulphide magma. It was noted that the sulphide liquid could have been transported in suspension in the silicate magma during intrusion.

Table XXV

Cu/(Cu + Ni) Ratios for Disseminated and
Associated Massive Cu-Ni Ores in Basic Rocks

	<u>Insizwa</u>	<u>Katinig</u>	<u>Gordon Lake</u>
disseminated ores	0.524 ¹	0.338 ³	0.330 ⁵
massive ores	0.319 ²	0.205 ⁴	0.182 ⁶

¹ average - 10 assays

² average - 9 assays

³ 1 analysis

⁴ 1 analysis

⁵ median - 892 assays

⁶ median - 796 assays

The rate of upward movement of the more dense sulphide liquid would be less than that of the intruding silicate magma and the sulphide liquid would tend to lag behind the intruding magma. Progressing from top to bottom in the silicate-sulphide magma, a sequence would exist of silicate magma with olivine crystals and disseminated sulphide liquid near the top, and an increase in the ratio of sulphide liquid to olivine crystals and silicate liquid toward the bottom. The lower regions of this sequence would contain more Ni relative to Cu as well as containing more sulphide liquid.

The mechanism described above is essentially gravitative settling of a sulphide liquid in a silicate magma and the results are essentially the same as those described for the Insizwa sill (Scholtz, *op. cit.*) and the Katiniq sill (Wilson *et al.*, *op. cit.*). The main difference is the addition of the upward movement of intrusion of the magma.

As the rate of intrusion decreases, a point will be reached when the sulphide liquid will begin to move downward or settle. If this liquid collects at or near the base of the intruding magma, a Ni-rich sulphide liquid will be formed and the result would be akin to the sills previously described. If this pool of sulphide liquid were to be mobilized and injected and partially replace a zone of brecciated pegmatite, a breccia sulphide mass would result

which would be more Ni-rich than the disseminated ores of the ultramafic body. The process of intrusion of the sulphide liquid would probably homogenize the distribution of Cu and Ni in the resulting ore body.

Sulphur Isotope Ratios - Breccia Sulphide Ore

Eight sulphur isotope determinations were made on five samples of breccia sulphide ore. The determinations were made on four samples of pyrrhotite, three samples of pentlandite and one sample of chalcopyrite. The determinations were made by A. Sasaki of the Isotope Geology Section of the Geological Survey of Canada.

Sulphur dioxide gases were prepared by direct combustion of sulphides employing the method described by Wanless *et al.*, (1960). The sulphur isotope ratios were determined using techniques described by Wanless and Thode (1953). The troilite from the Canon Diablo meteorite was used as the comparison standard, assuming that it has $S^{32}/S^{34} = 22.220$. The results of the isotopic analyses are given as δS^{34} where

$$\delta S^{34} \text{ ‰} = \frac{(S^{34}/S^{32})_{\text{sample}} - (S^{34}/S^{32})_{\text{standard}}}{(S^{34}/S^{32})_{\text{standard}}} \times 1000$$

Experimental accuracy is $\pm 0.2 \text{ ‰}$.

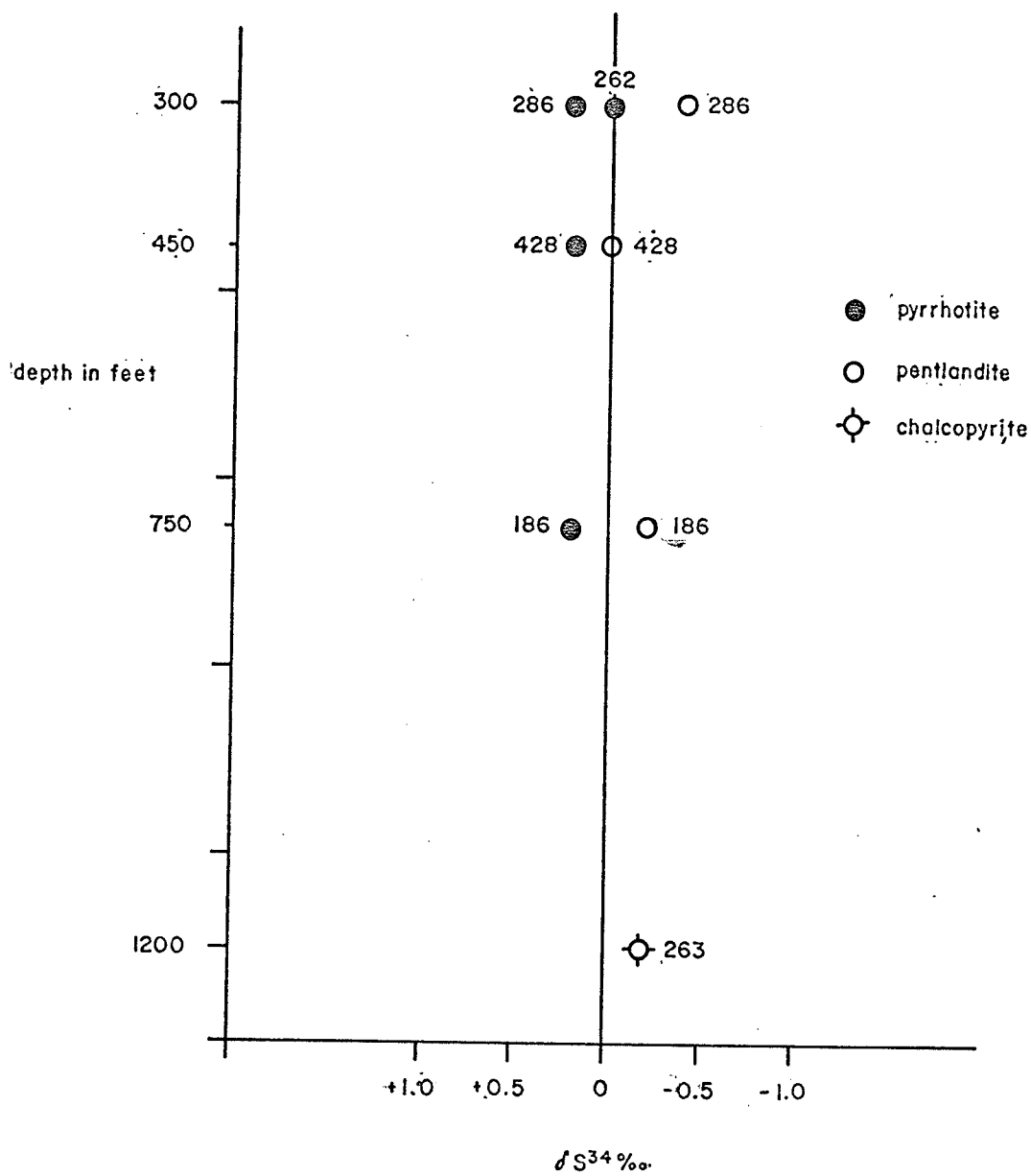
The sulphur isotope determinations are listed in Table XXVI and shown in Figure 42. The determinations

Table XXVI

Sulphur Isotope Determinations* - Breccia Ore

		$\frac{S^{32}}{S^{34}}$	$\delta S^{34} \text{ ‰}$	
SDG61-186a	pyrrhotite	22.217	+0.22	$\pm 0.2 \text{ ‰}$
SDG61-186b	pentlandite	22.227	-0.22	$\pm 0.2 \text{ ‰}$
SDG61-262	pyrrhotite	22.222	0.00	$\pm 0.2 \text{ ‰}$
SDG61-263	chalcopyrite	22.227	-0.22	$\pm 0.2 \text{ ‰}$
SDG61-286a	pyrrhotite	22.217	+0.22	$\pm 0.2 \text{ ‰}$
SDG61-286b	pentlandite	22.232	-0.44	$\pm 0.2 \text{ ‰}$
SDG61-428a	pyrrhotite	22.217	+0.22	$\pm 0.2 \text{ ‰}$
SDG61-428b	pentlandite	22.222	0.00	$\pm 0.2 \text{ ‰}$

* Determinations made by Isotope Geology Division, G.S.C.



VARIATION OF $\delta S^{34}\text{‰}$ WITH DEPTH

B - BRECCIA SULPHIDE ZONE

straddle the line of meteoritic sulphur and are relatively constant from the 300 to the 1200 level, indicating that fractionation of sulphur did not occur in the breccia sulphide ore. It can also be noted that pyrrhotite sulphur is heavier than pentlandite sulphur in three coexisting pyrrhotite-pentlandite pairs.

Several authors have compared data from terrestrial rocks and sulphide ores with meteoritic sulphur data. Macnamara, Fleming, Szabo and Thode (1952) noticed the close agreement between S^{32}/S^{34} ratios for igneous sulphur and meteorites and suggested this as possible evidence in favour of the theory that meteorites and the earth have a common origin. They also found that the majority of sulphide ores appear to be enriched in S^{34} by 0.5 per cent with respect to meteoritic sulphur. Thus, some fractionation of the sulphur isotopes would seem to occur as a result of early fractional crystallization of sulphide minerals.

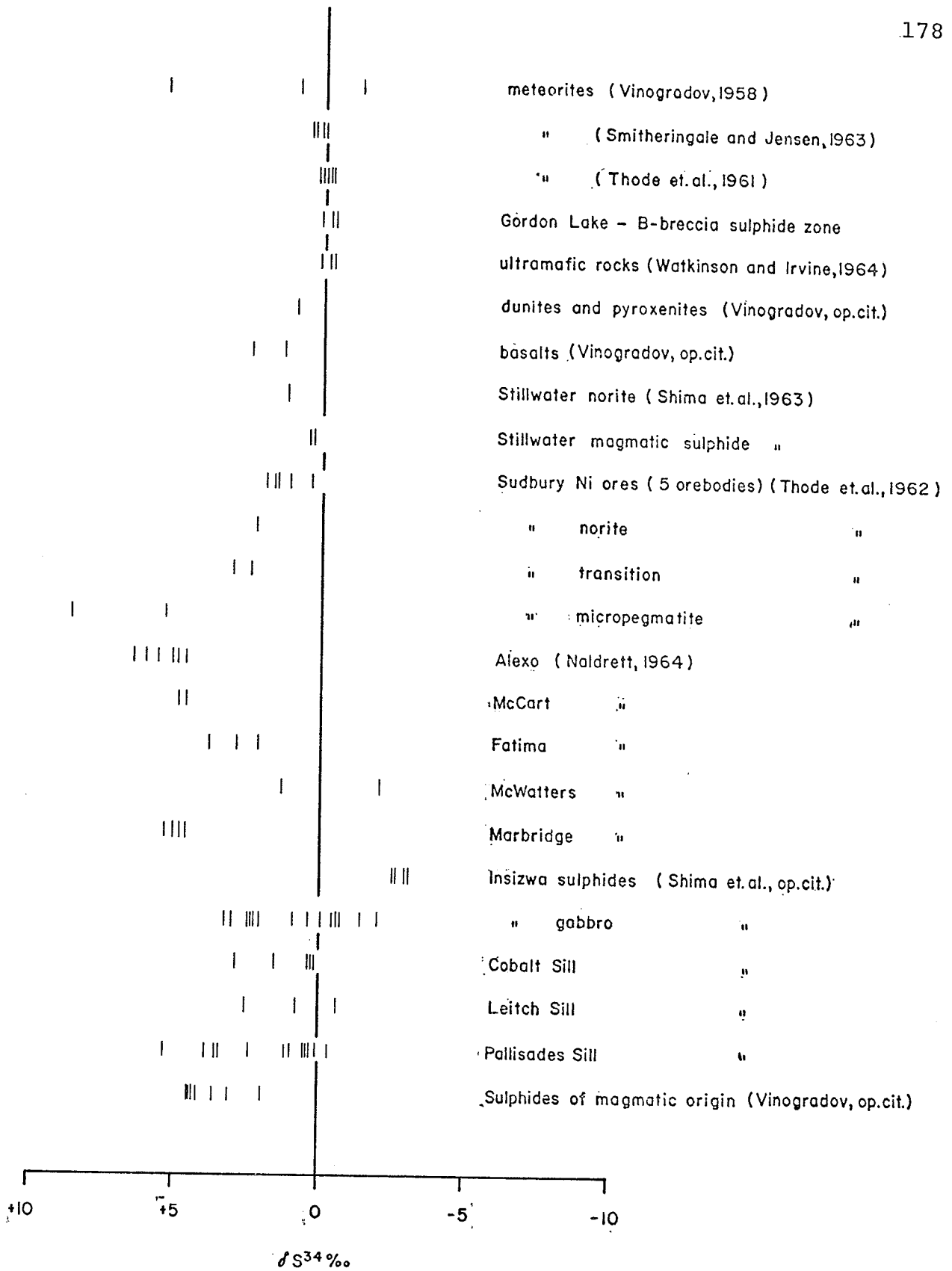
Vinogradov (1958) noticed that high temperature sulphides formed at an early stage of magmatic differentiation differed in their S^{32}/S^{34} ratio with the sulphur of meteorites. Thus, as a consequence of the sulphides being removed at the earliest stage of magmatic differentiation, sulphides are formed with a S^{32}/S^{34} ratio which differs from meteoritic sulphide. He concludes that the isotopic composition of sulphur of iron meteorites, stony

meteorites, iron-stony meteorites, ultramafic rocks and volcanic sulphur is very similar or identical. The isotopic composition of igneous sulphides from pegmatites of contact metamorphic origin, hydrothermal veins and from acid and basic igneous rocks has a wide range of S^{32}/S^{34} ratios, distinguishing it from the isotopic composition of cosmic sulphur.

The sulphur isotope data for the Sudbury nickel irruptive (Thode, Dunford and Shima, 1962) suggest a gradual increase in δS^{34} , passing from ore, through norite into micropegmatite (Figure 43). Results similar to that demonstrated for the sequence at Sudbury have been found for the Stillwater complex and the Insizwa sill (Shima, Gross and Thode, 1963). In each case the sulphide ores are richer in S^{32} compared with the sparsely disseminated sulphides from the upper portions of the bodies.

Smitheringale and Jensen (1962) conclude that the isotopic composition of sulphur in the upper mantle beneath the Newark basins in the late Triassic was identical to the isotopic composition of sulphur in meteorites. They also indicate a different degree of fractionation of sulphur between coexisting sulphide phases.

Watkinson and Irvine (op. cit.) observe that the low δS^{34} value for sulphur in the Shebandowan peridotite ($-0.34 \frac{0}{0}$), indicates that the sulphur was indigenous to the



SULPHUR ISOTOPES, ULTRAMAFIC - MAFIC ROCKS,
NICKEL SULPHIDE ORES AND METEORITES

peridotitic intrusion. Treating their data as a whole, it would seem that a similar conclusion could be reached for the Quetico area ultramafic rocks. They also state that their data are consistent with the notion that sulphur isotopic fractionation can accompany crystallization differentiation in mafic magmas.

The δS^{34} values for the massive breccia ore at Gordon Lake display a marked similarity with results obtained for meteoritic sulphur (Figure 43). They are also similar to the values for the sulphides associated with the Shebandowan peridotites, for which Watkinson and Irvine suggest that the sulphur was indigenous to the peridotite. Other apparently magmatic sulphides, the dunites and pyroxenites investigated by Vinogradov (op. cit.), the Stillwater magmatic sulphides and Sudbury nickel ores (Thode, Dunford and Shima, op. cit.), have somewhat higher S^{34}/S^{32} ratios but otherwise compare closely with the Gordon Lake results. It appears that there has been no enrichment of S^{34} in the breccia ore zone and that no fractionation of sulphur has taken place in the zone.

Unfortunately sulphur isotope determinations were not made for the disseminated sulphide ores in ultramafic rocks and it may be that some fractionation of sulphur has taken place between the disseminated and massive ore. In any event, the results of the sulphur isotope study appear to be in keeping with the magmatic origin of the

sulphide ores as postulated in the preceding section. The sulphur is considered to be indigenous to the ultramafic rocks and may, in fact, represent unaltered mantle sulphur.

CHAPTER VII

CONCLUSIONS

The ultramafic rocks and associated sulphide ores are products of magmatic crystallization. Abundant reaction textures among the primary silicate minerals and the nature of the sulphide-silicate textures attest this conclusion. The tholeiitic character of the silicate magma is borne out by the abundant orthopyroxene in the rocks. The absence of sharp lithologic contacts and crosscutting ultramafic lithologies indicates that the silicate assemblage crystallized from a single magma. The distribution of lithologic units and therefore the primary silicate minerals and the distribution of the cryptic zoning is best explained by flowage differentiation. This process explains the concentration of forsterite-rich olivine in the centre of the A-peridotite. During flowage, reaction between olivine and liquid to form orthopyroxene took place in the area of the contact between the olivine crystals and the liquid. Reaction between olivine and liquid to form orthopyroxene also took place in the central area occupied by olivine, but is much less marked in development. Local variations in the modal distributions of the primary silicates could

have been caused by irregularities in the conduit interrupting and causing turbulence in the flow. The development of olivine and orthopyroxene along the margin of the A-peridotite, which are much less forsterite-rich and enstatite-rich than those of the centre, is indicative of late stage marginal crystallization. The crystallization of hornblende takes place in response to a P_{H_2O} of greater than 2,500 bars and forms by reaction between the magma and olivine and pyroxene.

The development of mineral banding in the A-peridotite and general lack of a metamorphic aureole surrounding the ultramafic bodies indicates that when they reached their present position, they were essentially crystalline. The general lack of cataclastic textures and mineral banding in the central portions of the A-peridotite indicate that late stage movement of the body was taken up by the margins.

The ultramafic rocks do not fit any of the existing classifications for Phanerozoic ultramafic rocks. They appear to belong to the linear belts of discrete bodies (Scoates, 1971) which is a classification that is not dependent on a process or processes of intrusion, nor particular host rock associations.

The chemistry of the primary hornblendes is considered to reflect the composition of the interstitial liquid during crystallization. The indications are that

although the rocks display typical tholeiitic associations, the liquid may have had a calc-alkalic trend during crystallization. The reaction of olivine and liquid to form orthopyroxene would significantly deplete the magma in SiO_2 , and this is considered as a possible explanation of the liquid trend.

Two stages of recrystallization of the primary assemblage have been recognized. The first stage recrystallization involves the formation of chrysotile and bastite and is considered to represent the autometamorphic serpentinization process. Investigation of the chemistry of the serpentinization process has not been made, basically because of the complex nature of the mineralogy. Evidence concerning whether or not the reaction involves a change in composition or an increase in volume is absent. Metasomatism of the country rocks as a result of the expulsion of MgO- and SiO_2 -rich solutions has not been observed. On the other hand evidence of large scale volume increase of the ultramafic bodies has not been observed. In thin sections, systems of radiating serpentine-filled fractures occur in orthopyroxene around some included serpentinized olivine grains.

Antigorite, talc, biotite-phlogopite and chlorite group minerals characterize the second stage recrystallization which is related to metamorphism of the ultramafic assemblage by late pegmatite dykes. Monomineralic contact

reaction zones, which are identical to the second stage recrystallized assemblages, are found selvaging some of the ultramafic bodies. These selvages are also considered to have formed in response to metamorphism of the ultramafic bodies by late pegmatites.

The variations in major element content of the analyzed ultramafic rocks can be explained largely by variations in the mineralogy, hornblende exercising the greatest control on the bulk rock composition. The recrystallized ultramafic rocks display significant additions of $(\text{Na}_2\text{O} + \text{K}_2\text{O})$ in comparison with the unaltered rocks.

A magma composed in excess of 20 per cent olivine crystals in suspension is considered to be compatible with sulphide droplets having been held in suspension during magma intrusion. The sulphide-silicate textures observed in the disseminated ore indicate the existence of a sulphide-silicate immiscible magma type. Second stage recrystallization of the ultramafic rocks causes highly serrated and fretted margins between sulphide grains and the silicate host. Minor redistribution of the sulphide minerals in response to the recrystallization has been observed.

The breccia ore zone is considered to have formed by gravity settling of a Ni-rich sulphide liquid in the sulphide-silicate magma and intrusion of this settled

sulphide liquid into a brecciated pegmatite.

Sulphur isotope ratios of breccia sulphide zone sulphides support the view that the ores are magmatic in origin.

REFERENCES CITED

- Amin, M.S.
1952. Metamorphic differentiation of talc-magnesite-chlorite rocks in Shetland. *Geol. Mag.*, v. 89, pp. 97-105.
1954. Notes on the ultrabasic body of Unst, Shetland Islands. *Geol. Mag.*, v. 91, pp. 339-406.
- Amin, M.S. and Afia, M.S.
1954. Anthophyllite-vermiculite deposit of Hafafit, Eastern Desert, Egypt. *Econ. Geol.*, v. 49, pp. 317-327.
- Anderson, D.T.
1959. The distribution of copper and nickel in magmatic sulphides. Unpubl. M.Sc. thesis, University of Manitoba.
- Bartholomé, P.
1960. L'interprétation petrogenetique des associations d'olivine et d'orthopyroxene. *Ann. Soc. Geol. Belgique*, v. 83, pp. 319-344.
1961. Coexisting pyroxene in igneous and metamorphic rocks. *Geol. Mag.*, v. 98, pp. 346-348.
- Benson, W.N.
1926. The tectonic conditions accompanying the intrusion of basic and ultrabasic igneous rocks. *Mem. Nat. Acad. Sci.*, v. 19, No. 1, pp. 1-90.
- Bhattacharji, S. and Smith, C.H.
1964. Flowage differentiation. *Sci.*, v. 145, pp. 150-153.
- Bowen, N.L.
1928. *The Evolution of the Igneous Rocks*. Princeton Univ. Press, Princeton.
- Brownlow, A.H.
1961. Variation in composition of biotite and actinolite from monomineralic contact bands near Westfield, Massachusetts. *Amer. Jour. Sci.*, v. 259, pp. 353-370.

- Carlson, H.D.
1958. Geology of the Werner Lake-Rex Lake area, Ontario. Ont. Dept. Mines, An. Rep. 66, v. LXVI, Part 4.
- Challis, G.A.
1965. The origin of New Zealand ultramafic intrusions. Jour. Petrol., v. 6, pp. 322-364.
- Chamberlain, J.A.
1967. Sulphides in the Muskox Intrusion. Can. Jour. Earth Sci., v. 4, pp. 105-154.
- Chamberlain, J.A. and Delabio, R.N.
1965. Mackinawite and valleriite in the Muskox Intrusion. Am. Min., v. 50, pp. 682-695.
- Chamberlain, J.A., McLeod, C.R., Traill, R.J. and Lachance, G.R.
1965. Native metals in the Muskox Intrusion. Can. Jour. Earth Sci., v. 2, pp. 188-215.
- Chidester, A.H.
1962. Petrology and geochemistry of selected talc-bearing ultramafic rocks and adjacent country rocks in north-central Vermont. U.S. Geol. Surv. Professional Paper 345.
- Chisholm, E.O.
1949. The copper-nickel-cobalt occurrences in the Rex-Werner Lake area, Ontario. Precambrian, v. 22, pp. 10-15.
- Coats, C.J.A.
1966. Serpentinized ultramafic rocks of the Manitoba nickel belt. Unpubl. Ph.D. thesis, University of Manitoba.
- Craig, J.R. and Kullerud, G.
1969. Phase relations in the Cu-Fe-Ni-S system and their application to magmatic ore deposits. Econ. Geol. Mono. 4.
- Davies, J.F.
1952. Geology of the Booster Lake area. Man. Mines Br. Publ. 55-1.
- Deer, W.A., Howie, R.A. and Zussman, J.
1962. Serpentine. *Rock Forming Minerals*, v. 3, Sheet Silicates. Longmans, London.
1963. Chain Silicates. *Rock Forming Minerals*, v. 2, Longmans, London.

- Dennen, W.H.
1951. Variations in chemical composition across igneous contacts. *Bull. Geol. Soc. Amer.*, v. 62, pp. 547-558.
- Derry, D.R.
1931. Geology of the area from Minaki to Sydney Lake, District of Kenora. *Ont. Dept. Mines, Report*, v. XXXIX, Part 3, pp. 25-41.
- Drever, H.I. and Johnson, R.
1958. The petrology of picritic rocks in minor intrusions - a Hebridean group. *Roy. Soc. Edinburgh Trans.*, v. 63, pp. 459-498.
- Dwibedi, K.
1966. Petrology of the English River Gneissic belt, northwestern Ontario and southeastern Manitoba. Unpubl. Ph.D. dissertation, University of Manitoba.
- Edwards, A.B.
1954. Textures of the Ore Minerals. *Austral. Inst. Min. Met.*, Melbourne.
- Findlay, D.C.
1963. Petrology of the Tulameen ultramafic complex Yale District, British Columbia. Unpubl. Ph.D. dissertation, Queen's University, Kingston, Ontario.
- Findlay, D.C. and Smith, C.H.
1965. The Muskox drilling project. *Geol. Surv. Can. Paper* 64-44.
- Francis, G.H.
1956. The serpentinite mass in Glen, Urquhart, Invernesshire, Scotland. *Amer. Jour. Sci.*, v. 254, pp. 201-226.
- Green, D.H.
1964. The petrogenesis of the high-temperature peridotite intrusion in the Lizard area, Cornwall. *Jour. Petrol.*, v. 5, pp. 134-188.
- Greenwood, H.J.
1963. The synthesis and stability of anthophyllite. *Jour. Petrol.*, v. 4, pp. 317-351.
- Hawley, J.E.
1962. The Sudbury Ores: Their Mineralogy and Origin. *In: Can. Min.*, v. 7, pp. 1-207.

- Hawley, J.E.
1965. Upside-down zoning at Frood, Sudbury, Ontario. *Econ. Geol.*, v. 60, pp. 529-575.
- Hess, H.H. and Phillips, A.H.
1940. Optical properties and chemical compositions of magnesian orthopyroxenes. *Am. Mineral.*, v. 25, pp. 271-285.
1952. Orthopyroxenes of the Bushveld type, ion substitution and changes in unit cell dimensions. *Am. J. Sci.*, Bowen Vol., pp. 173-187.
- Jahns, R.H.
1967. Serpentinites of the Roxbury district, Vermont. *In: Ultramafic and Related Rocks*, (editor, P.J. Wyllie), John Wiley and Sons, Inc., New York.
- Jambor, J.L. and Smith, C.H.
1964. Olivine compositions determined with small diameter X-ray powder cameras. *Min. Mag.*, v. 33, pp. 730-741.
- Kilburn, L.C., Wilson, H.D.B., Graham, A.R., Ogura, Y., Coats, C.J.A. and Scoates, R.F.J.
1969. Nickel sulphide ores related to ultrabasic intrusions in Canada. *Econ. Geol. Mono.* 4.
- Kretz, R.
1961. Some applications of thermodynamics to coexisting minerals of variable composition. Examples: orthopyroxene-clinopyroxene and orthopyroxene-garnet. *Jour. Geol.*, v. 69, pp. 361-387.
- Kullerud, G.
1967. Sulfide studies. *In: Researches in Geochemistry*. v. 2, (Philip H. Abelson, ed.), John Wiley and Sons, Inc., New York.
- Kulp, J.L. and Brobst, D.A.
1954. Notes on the dunite and the geochemistry of vermiculite at the Day Brook dunite deposit Yancey County, North Carolina. *Econ. Geol.*, v. 49, pp. 211-220.
- Kuno, H.
1950. Petrology of Hakone volcano and the adjacent areas, Japan. *Bull. Geol. Soc. Amer.*, v. 61, pp. 957-1020.
- Leake, B.E.
1965. The relationship between composition of calciferous amphibole and grade of metamorphism. *In: Controls of Metamorphism*, editors, W.S. Pitcher and G.W. Flinn, Oliver and Boyd, London.

- Macdonald, G.A.
1941. Progressive metasomatism of serpentine in the Sierra Nevada of California. *Amer. Min.*, v. 26, pp. 276-287.
- MacDonald, J.A.
1960. A petrological study of the Cuthbert Lake ultrabasic and basic dyke swarm; a comparison of the Cuthbert Lake ultrabasic rocks to the Moak Lake - type serpentinite. Unpubl. M.Sc. thesis, University of Manitoba.
- MacGregor, I.D.
1962. Geology, petrology and geochemistry of the Mount Albert and associated ultramafic bodies of central Gaspé, Quebec. Unpubl. M.Sc. thesis, Queen's University, Kingston, Ontario.
- Macnamara, J., Fleming, W.H., Szabo, A. and Thode, H.G.
1952. The isotopic composition of igneous sulphur and the primordial abundances of the terrestrial sulphur isotopes. *Can. J. Chem.*, v. 30, pp. 73-76.
- Matthews, D.W.
1967. Zoned ultrabasic bodies in the Lewisian of the Moine Nappe in Skye. *Scott. Jour. Geol.*, v. 3, pp. 17-33.
- Muir, I.D. and Tilley, C.E.
1957. Contributions to the petrology of Hawaiian basalts: I. The picrite-basalts of Kilauea. *Am. Jour. Sci.*, v. 255, pp. 241-253.
- Naldrett, A.J.
1964. Ultrabasic rocks of the Porcupine and related nickel deposits. Unpubl. Ph.D. dissertation, Queen's University, Kingston, Ontario.

1968. Melting relations over a portion of the Fe-S-O system and their bearing on the temperature of crystallization of natural sulphide-oxide liquids. *Carnegie Inst. Wash. Year Book* 66, pp. 419-427.
- Naldrett, A.J. and Kullerød, G.
1965. Two examples of sulphurization in nature. *Abstract. Econ. Geol.*, v. 60, p. 1563.

1967. A study of the Strathcona mine and its bearing on the origin of the nickel-copper ores of the Sudbury district, Ontario. *Jour. Petrol.*, v. 8, pp. 453-531.

- O'Hara, M.J.
1963. Distribution of iron between coexisting olivines and calcium-poor pyroxenes in peridotites, gabbros and other magnesian environments. *Am. Jour. Sci.*, v. 261, pp. 32-46.
- Phillips, F.C.
1927. The serpentines and associated rocks and minerals of the Shetland Islands. *Geol. Soc. London, Quart. Jour.*, v. 83, pp. 622-652.
- Phillips, A.H. and Hess, H.H.
1936. Metamorphic differentiation of contacts between serpentinite and siliceous country rock. *Amer. Min.*, v. 21, pp. 333-362.
- Ramberg, H., and de Vore, G.
1951. The distribution of Fe and Mg between coexisting olivines and pyroxenes. *Jour. Geol.*, v. 59, pp. 193-210.
- Read, H.H.
1934. On zoned associations of antigorite, talc, actinolite, chlorite, and biotite in Unst, Shetland Islands. *Min. Mag.*, v. 23, pp. 519-540.
- Rose, E.R.
1958. Gordon Lake nickel deposit, Ontario. *Geol. Surv. Can.*, Paper 58-6.
- Scholtz, D.L.
1936. The magmatic nickeliferous ore deposits of East Griqualand and Pondoland. *Trans. Geol. Soc. S. Afrika*, v. 39, pp. 81-210.
- Scoates, R.F.J.
1963. The distribution of copper and nickel and related platinum group metals in orebodies at Gordon Lake, Ontario. Unpubl. M.Sc. thesis, University of Manitoba.

1971. A description and classification of Manitoba ultramafic rocks. *In: Geol. Assoc. Can., Spec. Paper No. 9, Geoscience Studies in Manitoba*, A.C. Turnock, ed., pp. 89-96.
- Shima, M., Gross, W.H. and Thode, H.G.
1963. Sulphur isotope abundance in basic sills, differentiated granites and meteorites. *Jour. Geophys. Res.*, v. 68, pp. 2835-2848.

- Short, M.N.
1940. Microscopic determination of the ore minerals. U.S. Geol. Surv. Bull. 914.
- Skinner, B.J. and Peck, D.L.
1966. The solubility of sulphur in basic magmas (abs.). Econ. Geol., v. 61, p. 802.
- Smith, C.H.
1958. Bay of Islands igneous complex, Western Newfoundland. Geol. Surv. Can. Mem. 290.
1961. Ultramafic intrusions in Canada and their significance to upper mantle studies. Can. Geophys. Bull., v. 14, pp. 157-169.
1962. Notes on the Muskox Intrusion, Coppermine River area, District of Mackenzie. Geol. Surv. Can., Paper 61-25.
- Smith, C.H. and Kapp, H.E.
1963. The Muskox Intrusion, a recently discovered layered intrusion in the Coppermine River area, Northwest Territories, Canada. Symposium on Layered Intrusion, Min. Soc. Amer., Special Publ. 1, pp. 30-35.
- Smitheringale, W.G. and Jensen, M.L.
1963. Sulphur isotopic composition of the Triassic igneous rocks of the eastern United States. Geochim. et Cosmochim. Acta., v. 27, pp. 1183-1207.
- Sørensen, H.
1952. Further studies on ultrabasic rocks in Sukkertoppen District, West Greenland. Medd. fra Dansk Geol. Forening., v. 12, pp. 230-243.
- Tanton, T.L.
1939. Kenora Sheet, Geol. Surv. Can. Map 266A.
- Taylor, H.P., Jr. and Noble, J.A.
1960. Origin of the ultramafic complexes in southeastern Alaska. Trans. Internat. Geol. Cong., Copenhagen, 1960, Part XIII, pp. 175-187.
- Taylor, W.L.W.
1950. Copper-nickel sulphide deposits of the Werner Lake, Ontario and Bird River, Manitoba areas. Unpubl. M.Sc. thesis, McGill University, Montreal.

- Thayer, T.P.
1960. Some critical differences between alpine-type and stratiform peridotite-gabbro complexes. Twenty-first Internat. Geol. Cong., Copenhagen, Repts., Part 13, pp. 247-259.
1967. Chemical and structural relations of ultramafic feldspathic rocks in alpine intrusive complexes. In: *Ultramafic and Related Rocks*, (editor, P.J. Wyllie), John Wiley and Sons, Inc., New York.
- Thode, H.G., Dunford, H.B., and Shima, M.
1962. Sulphur isotope abundances in rocks of the Sudbury district and their geological significance. *Econ. Geol.*, v. 57, pp. 565-578.
- Thode, H.G., Monster, J. and Dunford, B.
1961. Sulphur isotope geochemistry. *Geochim. et Cosmochim. Acta.*, v. 25, pp. 159-174.
- Thompson, J.B., Jr.
1969. Local equilibrium in metasomatic processes. In: *Researches in Geochemistry*, (editor, P.H. Abelson), New York, pp. 427-457.
- Turner, F.J. and Verhoogen, J.
1960. *Igneous and Metamorphic Petrology*. Second Edition, McGraw-Hill, New York.
- Vinogradov, A.P.
1958. Isotopic composition of sulphur in meteorites and in the earth. In: *Radioisotopes in Scientific Research*, v. 2 (R.C. Extermann, Editor), pp. 581-591, Permagon Press, New York.
- Watkinson, D.H. and Irvine, T.N.
1964. Peridotitic intrusions near Quetico and Shebandowan, northwestern Ontario: a contribution to the petrology and geochemistry of ultramafic rocks. *Can. Jour. Earth Sci.*, v. 1, pp. 63-98.
- Whittaker, E.J.W. and Zussman, J.
1956. The characterization of serpentine minerals by X-ray diffraction. *Min. Mag.*, v. 31, pp. 107-126.
- Wilkinson, J.F.G.
1953. Some aspects of the alpine-type serpentinites of Queensland. *Geol. Mag.*, v. 90, pp. 305-321.

- Wilson, H.D.B. and Brisbin, W.C.
1963a. Nature of the granitic crust in the Superior Province. Bull. Geol. Soc. Amer., v. 74, p. 175.
- 1963b. Major structural features in the Canadian Shield. Abstract, Geol. Assoc. Can., Annual Meeting, June, 1963.
- Wilson, H.D.B., Kilburn, L.C., Graham, A.R. and Ramlal, K.
1969. Geochemistry of some Canadian nickeliferous ultrabasic intrusions. Econ. Geol., Mono. 4.
- Wolfe, W.J.
1966. Petrology, mineralogy and geochemistry of the Blue River ultramafic intrusion, Cassiar District, British Columbia. Unpubl. Ph.D. dissertation, Yale University, New Haven, Connecticut, U.S.A.
- Wyllie, P.J.
1969. The origin of ultramafic and related rocks. Tectonophys., v. 7, pp. 437-455.
- Yoder, H.S., Jr. and Tilley, C.E.
1962. Origin of basalt magmas: an experimental study of natural and synthetic rocks systems. Jour. Petrol., v. 3, pp. 342-532.

APPENDIX I

Modal Analyses of Ultramafic Rocks

Modal Analyses of Ultramafic Rocks*

	<u>328¹</u>	<u>1001¹</u>	<u>762¹</u>	<u>440²</u>	<u>442²</u>	<u>444²</u>	<u>446²</u>	<u>447²</u>	<u>46³</u>	<u>194³</u>
olivine	9.1	16.2	12.4	2.9	7.9	1.8	3.2	2.4	11.3	1.7
serpentine (after Olivine)	40.5	38.5	8.2	42.0	32.7	7.6	45.0	29.4	3.3	2.5
magnetite	11.7	19.6	16.9	25.0	6.4	2.9	14.0	13.2	3.4	1.0
orthopyroxene	11.9	2.6	20.7	9.6	22.3	59.3	6.4	-	18.8	26.5
clinopyroxene	1.8	0.4	-	-	-	-	-	4.1	-	-
hornblende	3.1	12.6	39.2	2.5	18.2	5.6	21.3	47.0	51.0	52.4
phlogopite	17.0	-	1.0	7.4	10.3	-	-	-	-	-
talc	-	-	1.2	0.1	-	5.5	-	-	-	-
chrome spinel	2.0	7.9	0.1	7.0	2.2	13.6	9.7	1.7	0.8	-
sulphide	2.9	2.2	0.3	3.5	-	0.2	0.4	2.2	11.4	15.9
calcite	-	-	-	-	-	1.3	-	-	-	-
chlorite	-	-	-	-	-	2.2	-	-	-	-

*Based on a minimum of 1,000 counts per thin section.

¹ 300 level ² 450 level ³ 750 level

Modal Analyses of Ultramafic Rocks*

	<u>382⁴</u>	<u>671⁵</u>	<u>124⁶</u>	<u>134⁶</u>	<u>135⁶</u>	<u>731⁶</u>	<u>210⁷</u>	<u>219⁷</u>	<u>238⁷</u>	<u>711⁷</u>
olivine	17.3	14.5	-	1.2	3.6	6.2	-	3.8	5.3	0.6
serpentine (after olivine)	4.5	24.9	34.6	31.1	26.6	12.1	6.1	30.2	13.4	34.3
magnetite	6.7	10.2	6.3	5.3	8.0	4.9	9.7	13.4	5.9	13.0
orthopyroxene	21.4	6.3	-	6.9	9.0	-	12.4	19.1	13.2	8.5
clinopyroxene	-	-	-	-	-	58.3	5.5	13.5	16.8	4.4
hornblende	44.0	4.4	46.6	41.0	45.0	10.9	58.9	14.8	39.2	35.8
phlogopite	0.2	-	-	-	-	-	-	-	-	-
talc	-	0.2	-	-	-	-	-	-	-	-
chrome spinel	5.4	11.3	2.9	7.2	3.7	4.0	7.4	-	-	-
sulphide	0.5	28.2	9.6	0.1	4.1	3.6	-	5.2	6.2	3.4
calcite	-	-	-	-	-	-	-	-	-	-
chlorite	-	-	-	-	-	-	-	-	-	-

*Based on a minimum of 1,000 counts per thin section.

⁴ 1200 level

⁵ F-peridotite

⁶ A-peridotite - 1050 level ⁷ A-peridotite - 1200 level

Modal Analyses of Ultramafic Rocks*

	<u>706⁷</u>	<u>708⁷</u>	<u>213⁷</u>	<u>215⁷</u>	<u>220⁷</u>	<u>713⁷</u>	<u>598⁷</u>	<u>83⁷</u>	<u>706⁷</u>	<u>588⁷</u>
olivine	3.3	1.5	7.6	7.5	12.9	9.8	5.4	5.1	3.3	7.5
serpentine (after olivine)	7.4	29.5	24.9	28.7	22.7	24.0	6.8	23.5	7.4	3.3
magnetite	6.8	9.2	13.4	8.9	21.0	7.1	5.8	11.8	6.8	3.7
orthopyroxene	-	-	9.3	13.4	2.5	7.9	20.2	0.6	-	-
clinopyroxene	14.3	13.7	-	1.2	18.0	1.0	0.8	29.6	14.3	1.1
hornblende	63.7	3.8	4.8	14.6	9.5	46.5	58.9	8.1	63.7	60.6
phlogopite	-	-	-	0.1	-	-	-	-	-	1.9
talc	-	-	-	-	-	-	-	-	-	-
chrome spinel	-	12.6	8.4	2.4	13.2	3.7	0.7	7.6	-	13.1
sulphide	4.5	19.5	31.6	23.2	0.2	-	1.4	13.7	4.5	8.8
calcite	-	0.2	-	-	-	-	-	-	-	-
chlorite	-	-	-	-	-	-	-	-	-	-

*Based on a minimum of 1,000 counts per thin section.

⁷ A-peridotite - 1200 level

Modal Analyses of Ultramafic Rocks*

	<u>589⁷</u>	<u>591⁷</u>	<u>592⁷</u>	<u>593⁷</u>	<u>594⁷</u>	<u>240⁷</u>	<u>77⁷</u>	<u>469⁸</u>	<u>613⁸</u>	<u>520⁹</u>
olivine	10.4	4.5	3.6	11.1	2.5	5.9	9.3	15.5	3.7	-
serpentine (after olivine)	23.6	31.1	16.7	14.1	5.7	19.9	27.5	22.4	3.4	33.8
magnetite	8.7	13.7	16.4	11.2	1.9	6.9	11.5	13.2	0.2	18.6
orthopyroxene	1.1	8.3	18.6	4.0	-	7.4	-	27.8	84.0	-
clinopyroxene	-	-	-	-	62.3	3.3	12.0	-	-	26.7
hornblende	51.0	33.2	31.3	48.7	8.5	49.0	32.1	4.9	1.9	10.3
phlogopite	-	-	11.3	7.1	9.4	-	-	-	-	-
talc	-	-	-	-	-	-	-	-	-	1.2
chrome spinel	5.2	7.2	2.1	2.1	6.0	5.2	7.6	5.4	3.7	8.4
sulphide	-	2.0	-	1.7	3.7	2.7	-	10.8	3.0	1.0
calcite	-	-	-	-	-	-	-	-	-	-
chlorite	-	-	-	-	-	-	-	-	0.1	-

*Based on a minimum of 1,000 counts per thin section.

⁷ A-peridotite - 1200 level ⁸ A-peridotite - 1350 level

⁹ A-peridotite - 1500 level

Modal Analyses of Ultramafic Rocks*

	<u>616⁹</u>	<u>619⁹</u>	<u>512⁹</u>	<u>516⁹</u>	<u>518⁹</u>	<u>622⁹</u>	<u>626⁹</u>	<u>633⁹</u>	<u>38⁹</u>	<u>79⁹</u>
olivine	5.2	2.6	11.9	5.7	3.2	7.9	1.7	4.5	8.1	9.7
serpentine (after olivine)	4.9	29.9	32.7	3.9	7.9	22.3	11.5	9.7	10.9	13.0
magnetite	4.5	11.7	15.6	6.2	5.9	7.4	1.9	3.0	5.2	3.5
orthopyroxene	39.0	1.7	4.2	21.9	19.9	13.2	15.4	-	9.4	22.9
clinopyroxene	4.3	2.8	8.9	0.5	-	2.0	-	0.6	-	-
hornblende	35.0	25.7	7.1	51.0	50.7	35.3	57.4	73.3	63.5	44.3
phlogopite	-	25.3	-	-	0.2	-	-	6.6	-	-
talc	0.1	-	-	-	-	-	0.5	-	-	-
chrome spinel	6.7	-	4.2	3.1	1.0	5.9	4.7	0.5	2.4	5.8
sulphide	0.3	0.3	15.4	7.7	11.2	5.9	6.9	1.8	0.5	0.8
calcite	-	-	-	-	-	0.1	-	-	-	-
chlorite	-	-	-	-	-	-	-	-	-	-

*Based on a minimum of 1,000 counts per thin section.

⁹ A-peridotite - 1500 level

Modal Analyses of Ultramafic Rocks*

	<u>617⁹</u>	<u>624⁹</u>	<u>627⁹</u>	<u>631⁹</u>	<u>632⁹</u>	<u>538¹⁰</u>	<u>536¹⁰</u>	<u>543¹⁰</u>	<u>534¹⁰</u>	<u>539¹⁰</u>
olivine	11.0	6.8	4.1	4.8	1.9	31.7	14.9	8.0	21.6	17.2
serpentine (after olivine)	27.3	13.6	24.0	10.6	8.8	13.3	7.9	9.8	26.8	37.7
magnetite	4.6	2.1	4.8	3.1	3.8	9.9	7.2	6.0	12.1	17.4
orthopyroxene	8.7	20.2	7.0	10.8	14.0	8.3	50.8	11.8	-	-
clinopyroxene	0.4	0.8	-	0.1	-	-	-	-	-	0.5
hornblende	40.0	45.2	47.0	52.4	60.7	23.4	2.0	51.7	31.0	14.0
phlogopite	-	-	-	-	-	-	-	-	-	-
talc	-	-	-	-	2.8	4.3	0.9	-	-	-
chrome spinel	3.0	6.4	10.9	9.8	2.3	7.5	11.2	7.1	7.8	8.7
sulphide	5.0	4.7	2.2	8.4	5.7	0.6	4.9	5.6	0.7	4.5
calcite	-	-	-	-	-	1.0	0.2	-	-	-
chlorite	-	-	-	-	-	-	-	-	-	-

*Based on a minimum of 1,000 counts per thin section.

⁹ A-peridotite - 1500 level

¹⁰ A-peridotite - 1595 level

Modal Analyses of Ultramafic Rocks*

	<u>642¹⁰</u>	<u>537¹⁰</u>	<u>535¹⁰</u>	<u>540¹⁰</u>	<u>542¹⁰</u>	<u>660¹¹</u>	<u>663¹¹</u>	<u>88¹¹</u>
olivine	2.0	14.0	11.7	12.9	12.1	8.7	6.4	20.7
serpentine (after olivine)	1.1	14.7	7.6	29.9	16.9	28.0	14.9	32.9
magnetite	2.8	10.5	3.0	12.5	9.1	14.4	4.4	25.5
orthopyroxene	27.1	5.7	43.9	4.6	17.0	15.6	30.1	-
clinopyroxene	-	0.7	1.0	0.5	0.4	0.5	-	1.7
hornblende	64.7	30.6	21.4	28.8	36.5	29.0	6.0	0.4
phlogopite	-	-	-	-	-	-	0.4	-
talc	-	-	-	-	-	-	0.6	0.1
chrome spinel	2.2	6.4	10.2	9.8	3.4	3.5	33.5	-
sulphide	0.2	17.4	1.0	1.0	4.6	-	3.4	18.3
calcite	-	-	-	-	-	0.3	0.3	0.4
chlorite	-	-	-	-	-	-	-	-

*Based on a minimum of 1,000 counts per thin section.

¹⁰ A-peridotite - 1595 level

¹¹ A-peridotite - 1650 level

APPENDIX II

Olivine Determinations

Appendix II

Olivine Determinations - % Fo, $2\theta_{174}$

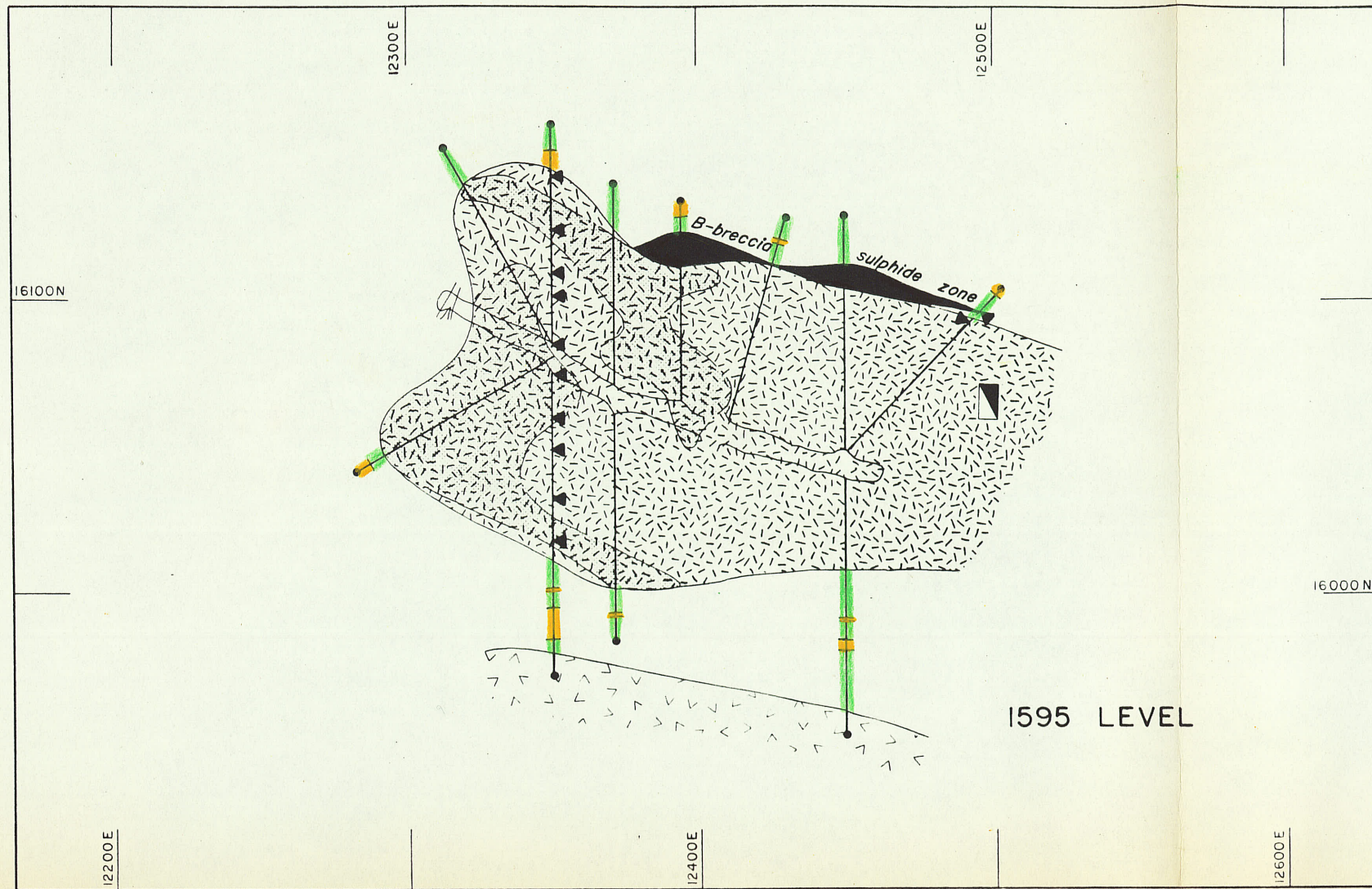
<u>Sample No.</u>	<u>Level</u>	<u>$2\theta_{174}$</u>	<u>Per cent Forsterite</u>
SDG61-328	300	142.22	82.9
SDG61-370	300	142.05	80.8
SDG61-375	300	142.04	80.7
SDG61-415	300	142.14	82.0
SDG61-400	300	141.91	79.0
SDG61-762	300	141.95	79.6
SDG61-1001	300	141.72	76.7
SDG61-163	450	141.85	78.3
SDG61-440	450	142.37	84.8
SDG61-442	450	141.51	74.0
SDG61-444	450	142.33	84.4
SDG61-446	450	142.39	85.1
SDG61-46	750	141.49	73.8
SDG61-194	750	141.85	78.3
SDG61-134	1050	141.99	80.1
SDG61-135	1050	142.06	80.9
SDG61-731	1050	141.94	79.5
SDG61-730	1050	141.90	78.9
SDG61-77	1200	142.06	80.9
SDG61-83	1200	142.02	80.5
SDG61-215	1200	141.77	77.4
SDG61-220	1200	142.05	80.8
SDG61-238	1200	141.70	76.4
SDG61-598	1200	141.94	79.5
SDG61-382	1200	142.25	83.4
SDG61-713	1200	142.16	82.2
SDG61-588	1200	141.68	76.2
SDG61-594	1200	142.00	80.2
SDG61-711	1200	142.06	81.0

<u>Sample No.</u>	<u>Level</u>	<u>$^{20}_{174}$</u>	<u>Per cent Forsterite</u>
SDG61-589	1200	142.31	84.1
SDG61-240	1200	141.72	76.7
SDG61-596	1200	142.17	82.3
SDG61-721	1200	142.08	81.2
SDG61-469	1350	141.82	77.9
SDG61-481	1350	142.03	80.6
SDG61-473	1350	142.14	82.0
SDG60-11	1350	142.05	80.8
SDG60-6	1350	142.14	82.0
SDG61-610	1350	142.02	80.5
SDG61-602	1350	141.96	79.7
SDG60-79	1500	142.02	80.5
SDG61-512	1500	141.76	77.3
SDG61-514	1500	141.79	77.6
SDG61-516B	1500	141.76	77.3
SDG61-626	1500	141.92	79.2
SDG61-616	1500	141.78	77.4
SDG61-633	1500	141.99	80.1
SDG61-518	1500	142.31	84.1
SDG61-622	1500	142.00	80.2
SDG60-38	1500	142.02	80.5
SDG61-629	1500	142.21	82.9
SDG61-624	1500	141.72	76.7
SDG61-536	1595	141.84	78.2
SDG61-538	1595	142.00	80.2
SDG61-543	1595	142.08	81.1
SDG61-534	1595	142.35	84.6
SDG61-539	1595	142.16	82.2
SDG61-642	1595	141.48	73.7
SDG61-535	1595	141.94	79.5
SDG61-542	1595	141.95	79.6
SDG61-537	1595	141.68	76.2


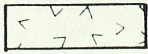

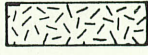

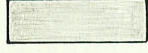


<u>Sample No.</u>	<u>Level</u>	<u>2^θ₁₇₄</u>	<u>Per cent Forsterite</u>
SDG61-540	1595	142.00	80.2
SDG61-663	1650	142.06	81.0
SDG60-88	1650	141.80	77.7
SDG61-660	1650	142.10	81.5
SDG60-103	1650	141.82	77.9
SDG61-648	1650	141.98	80.0
SDG61-666	1650	141.93	79.3
SDG61-671	F-peridotite	141.69	76.1






A - PERIDOTITE

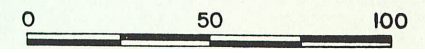
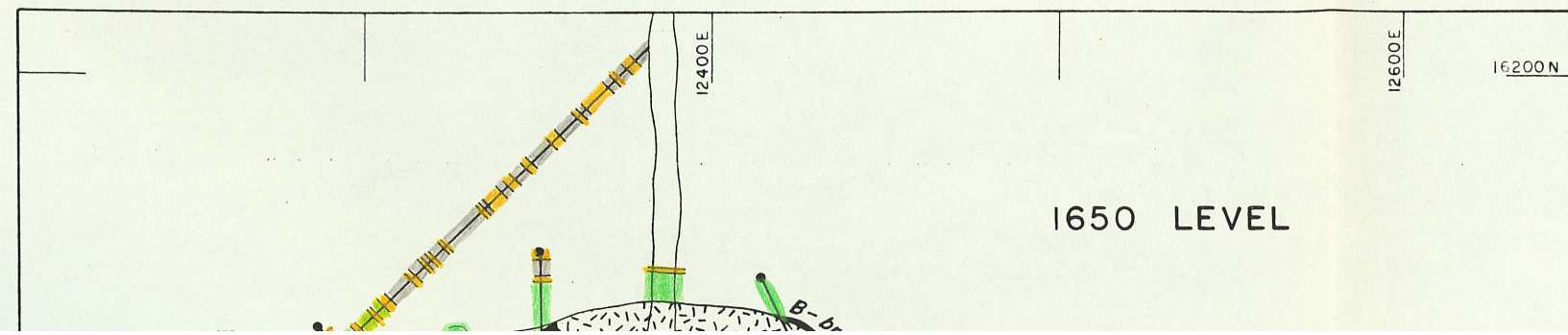
GORDON LAKE, ONTARIO

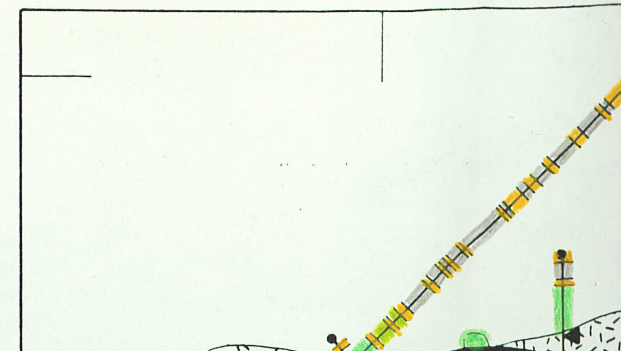
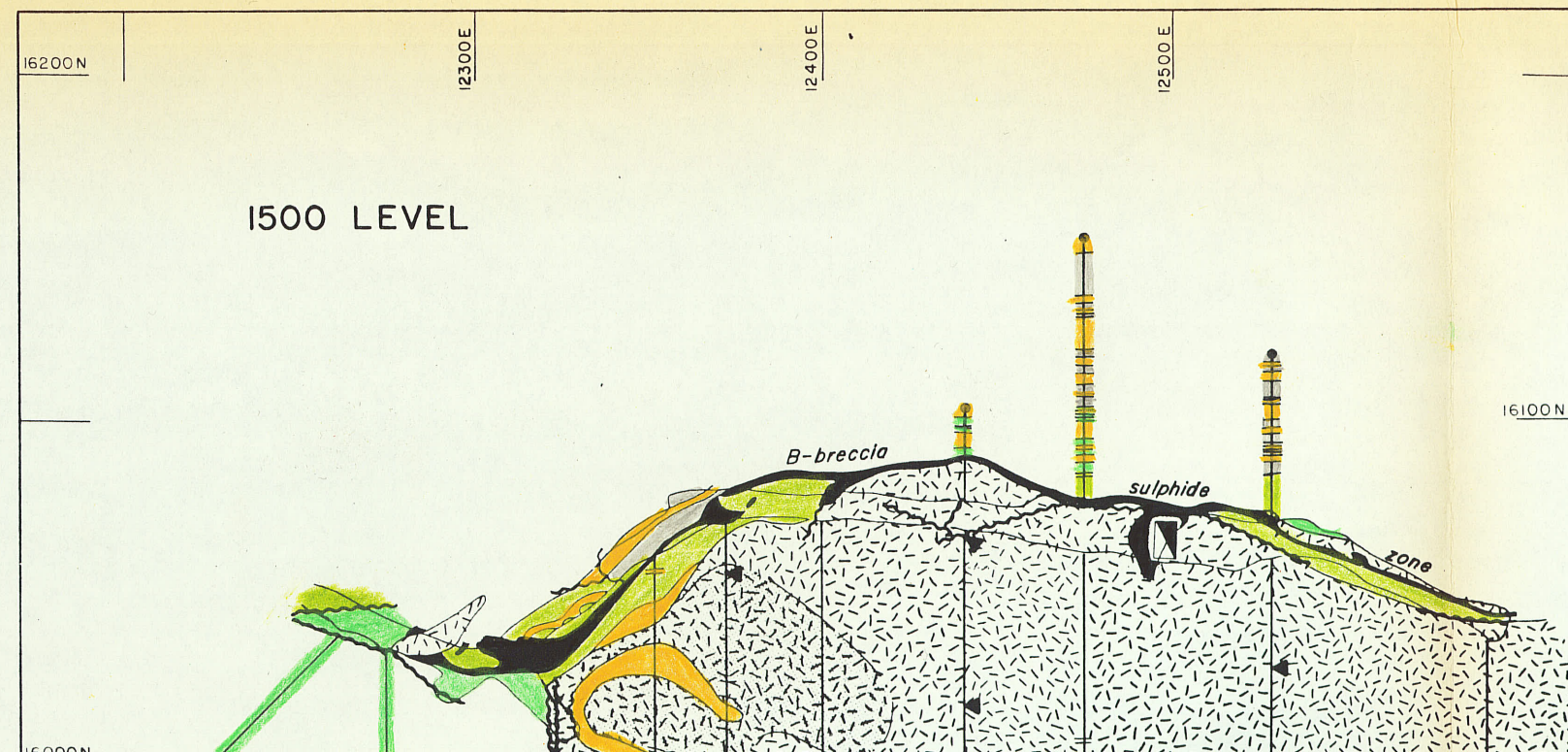
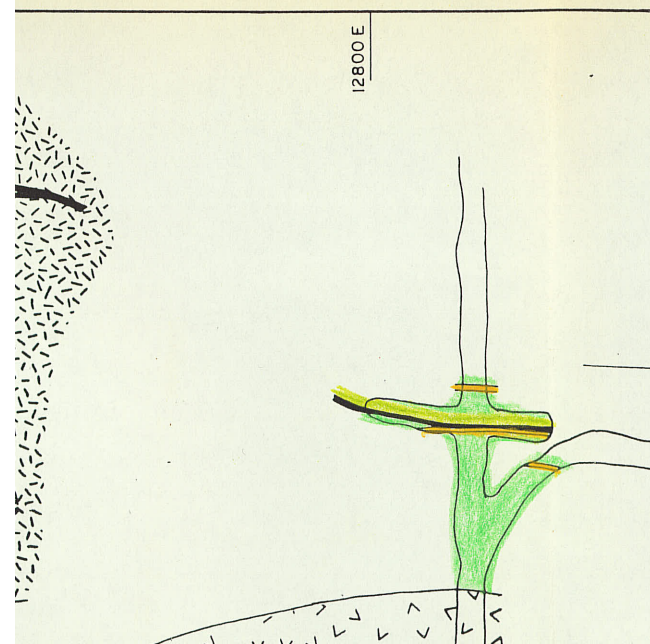
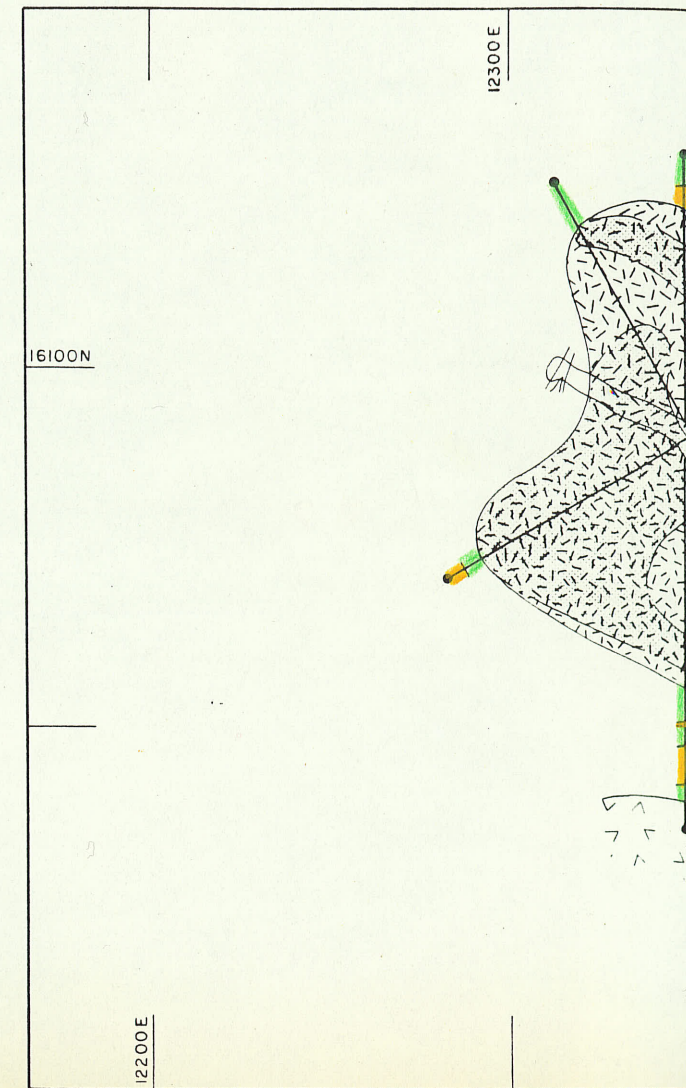
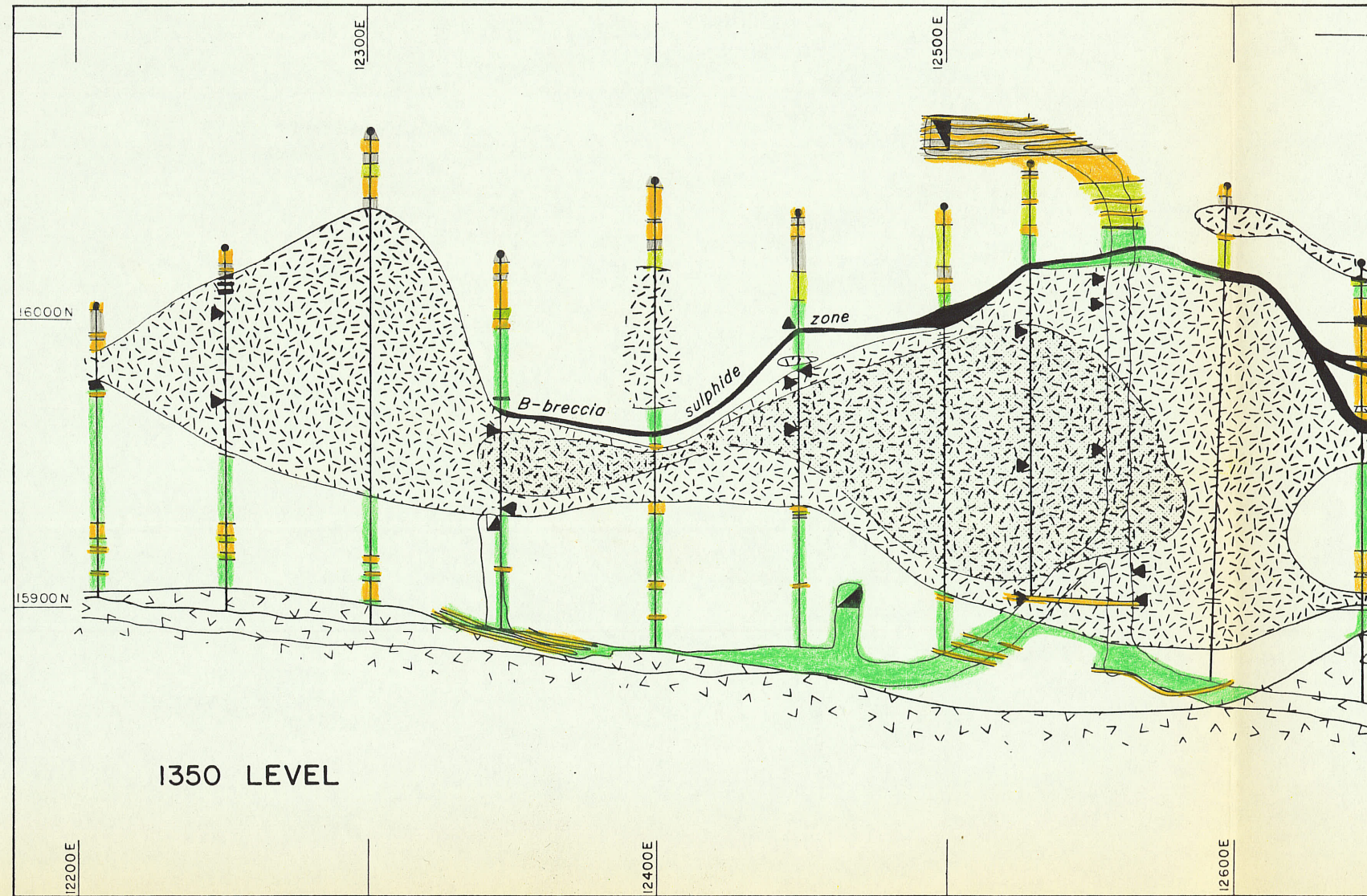
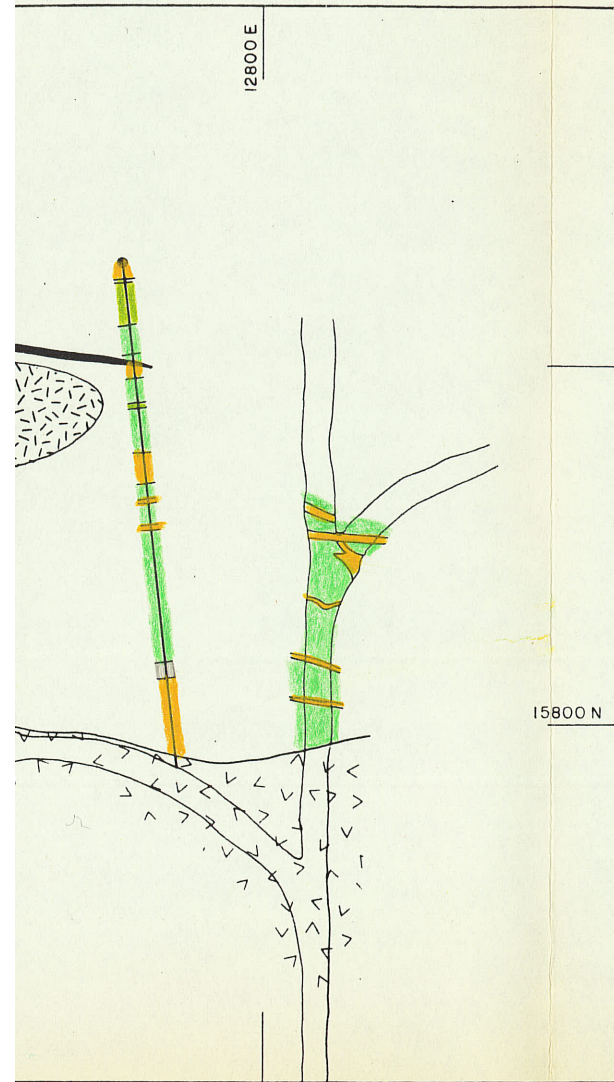


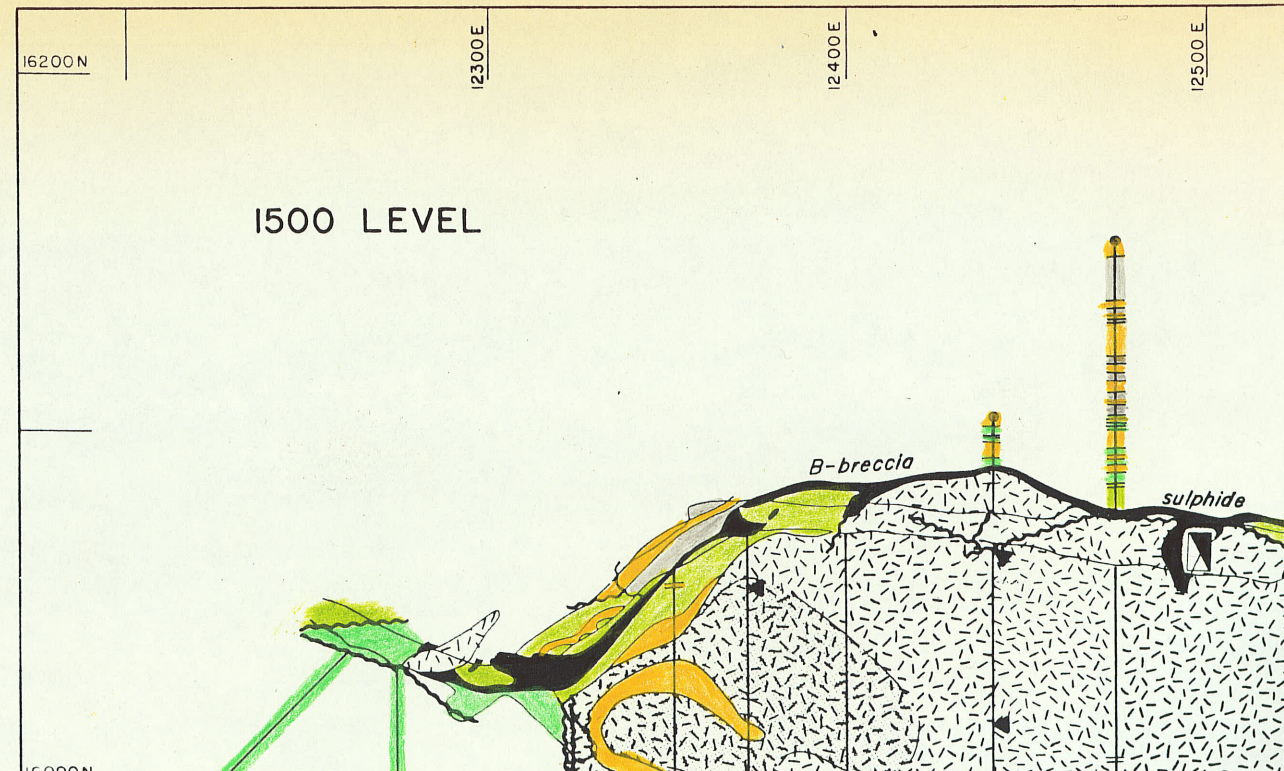
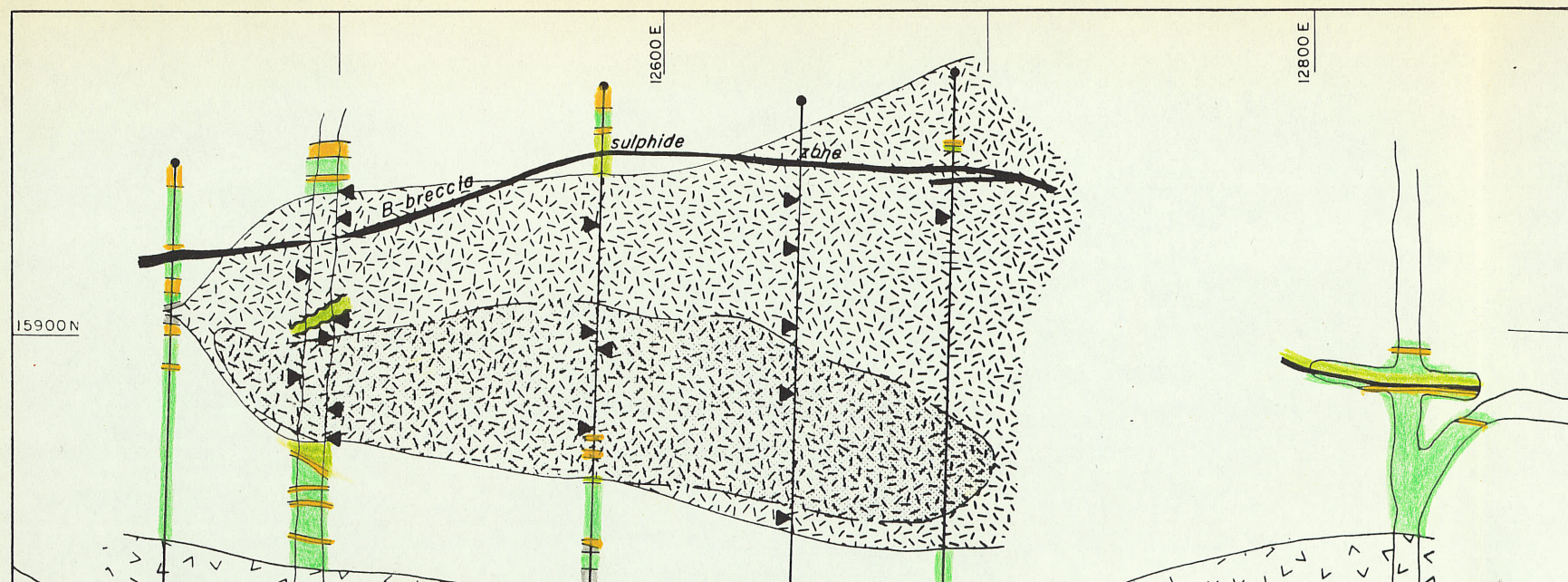
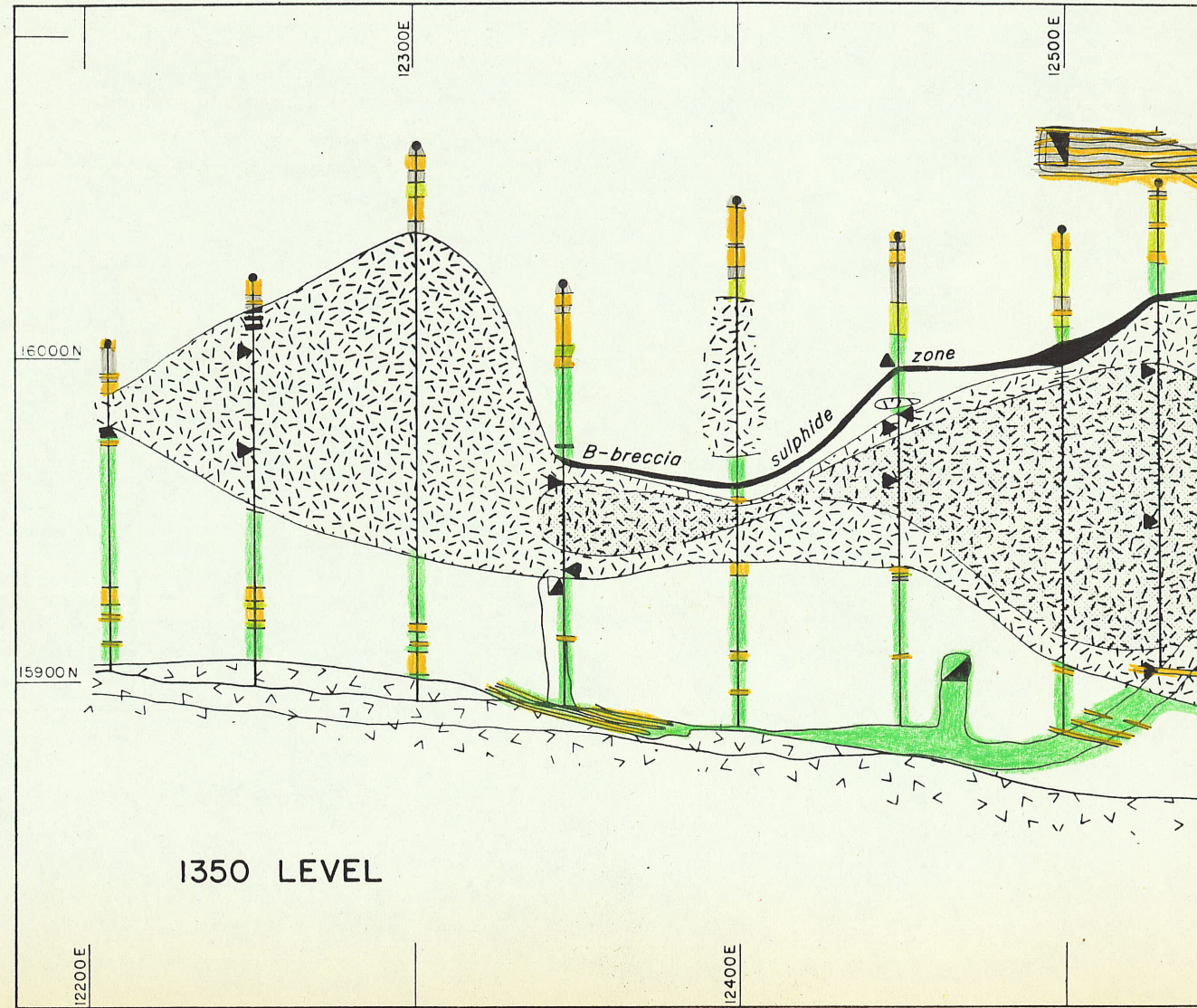
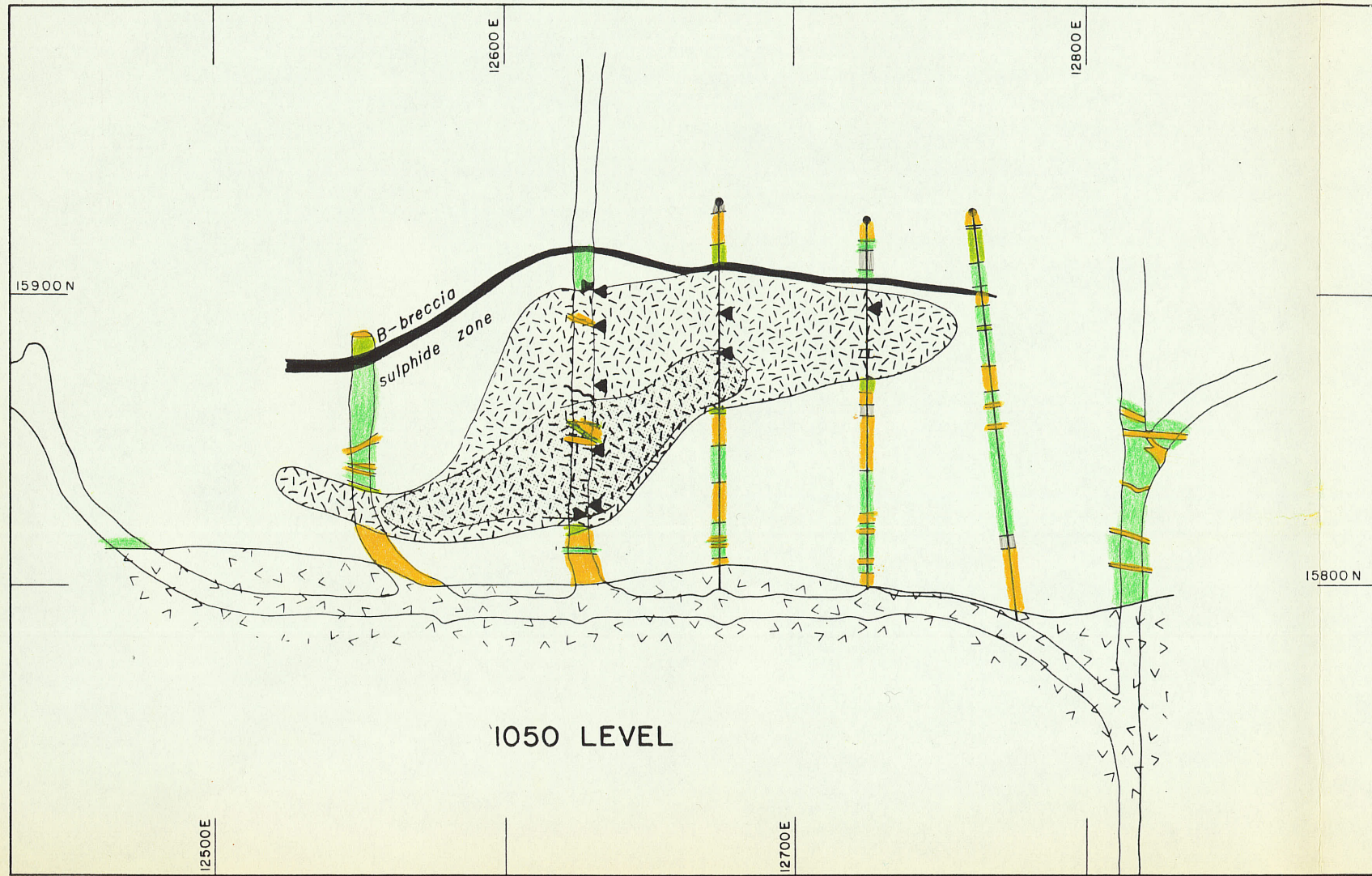
LEGEND

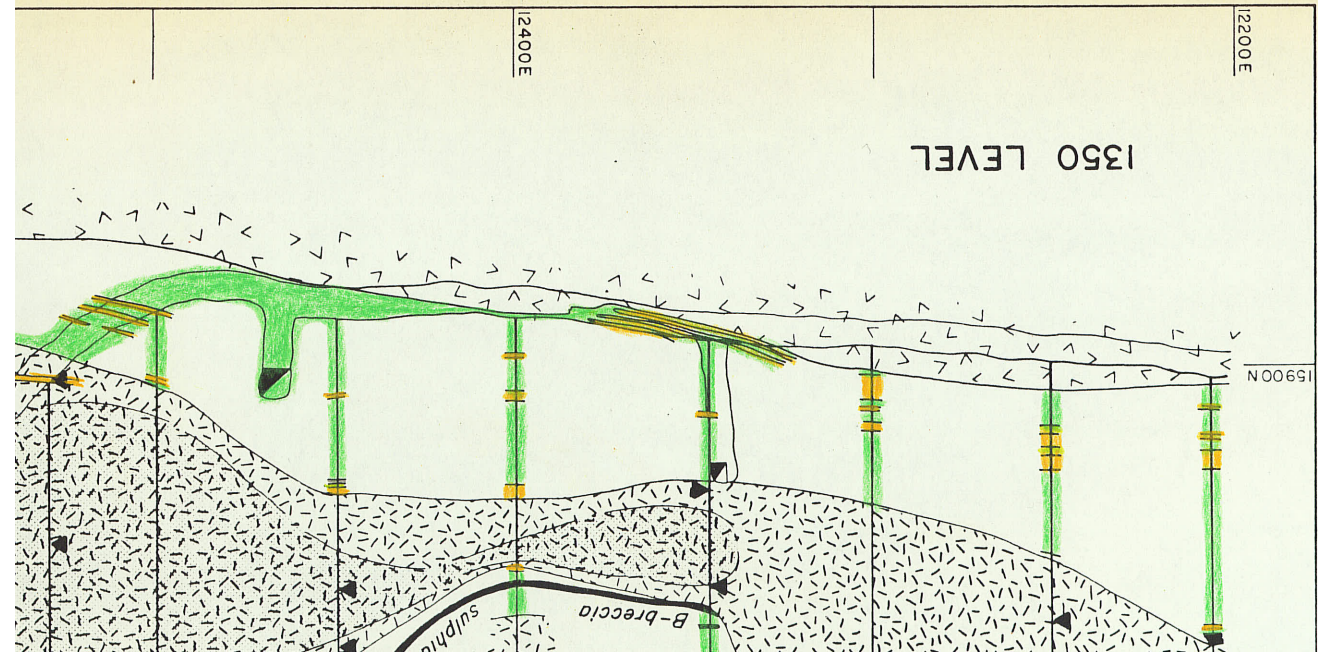
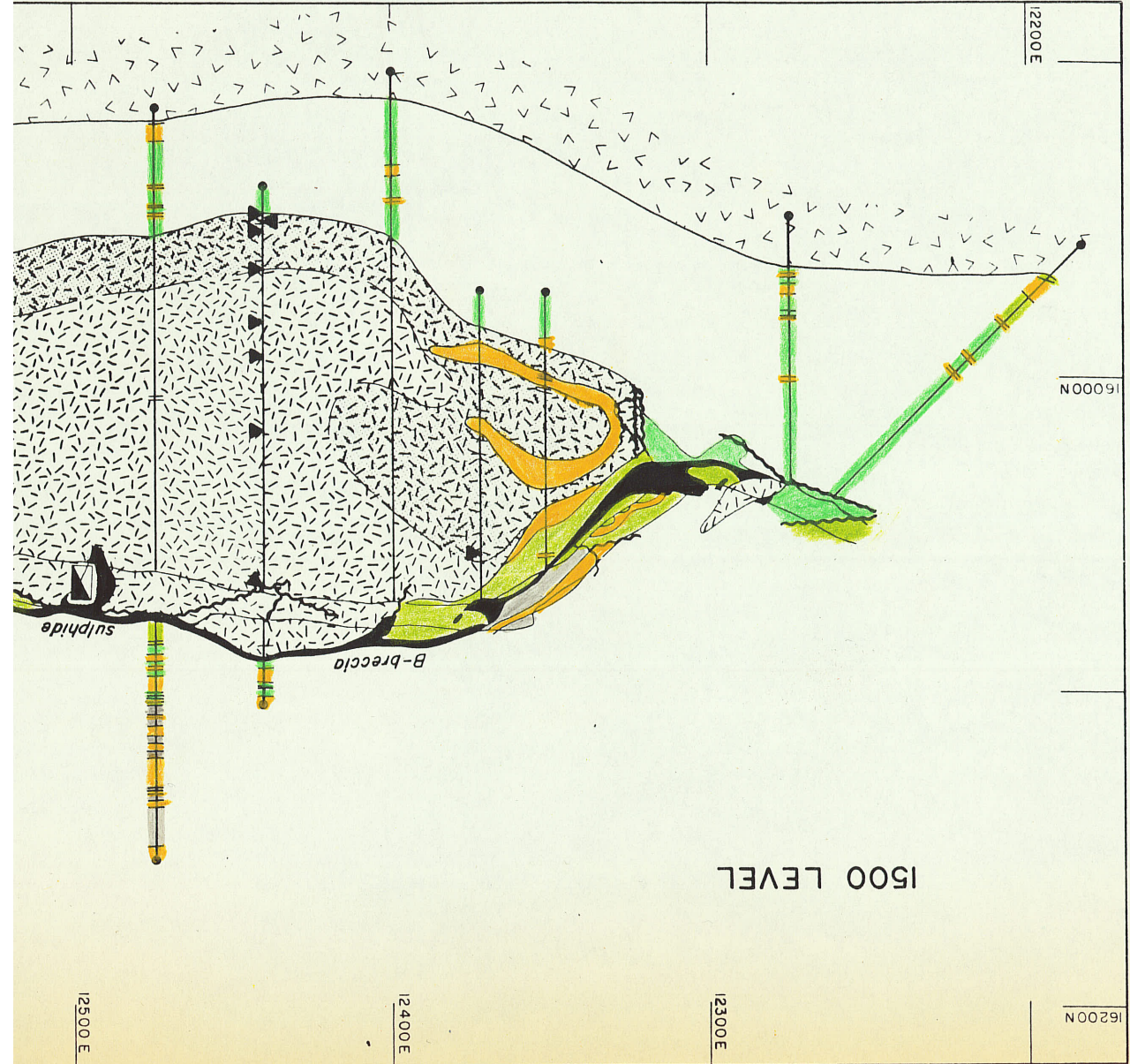
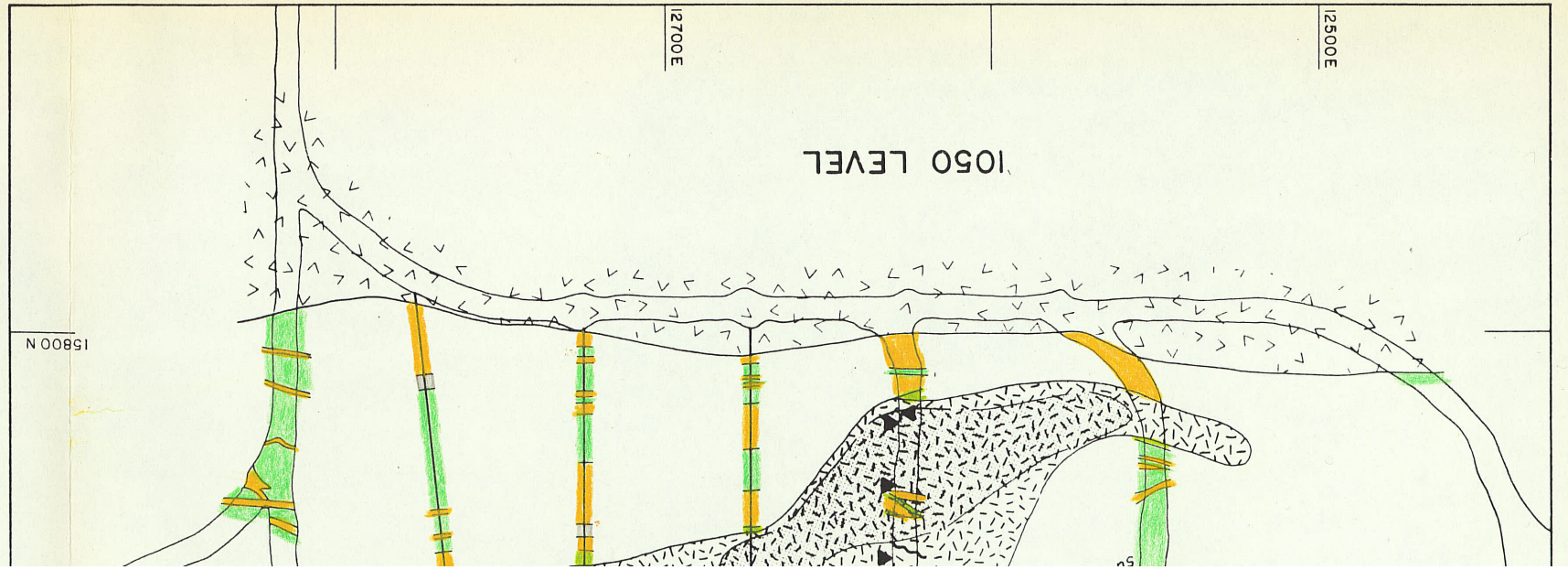
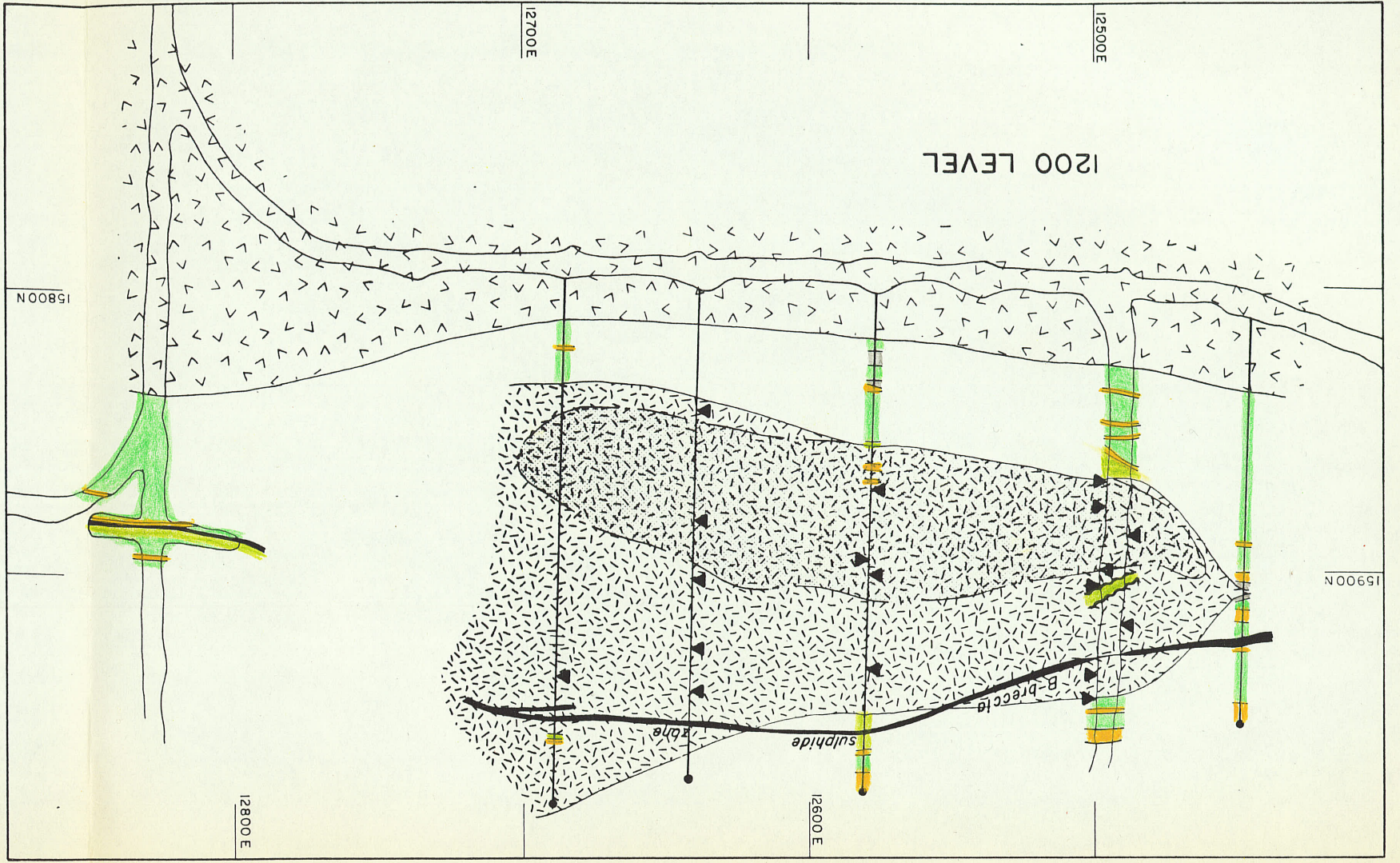
-  PEGMATITE
-  GRANITE
-  SULPHIDE MINERALIZATION (massive, disseminated)
-  ULTRAMAFIC ROCKS (undivided)
-  AMPHIBOLITE
-  AMPHIBOLITE - BIOTITE GNEISS
-  BIOTITE - CHLORITE SCHIST
-  approximate outline of disseminated ore

-  Geological boundary
-  Fault
-  Diamond drill hole
-  Shaft
-  Sample location

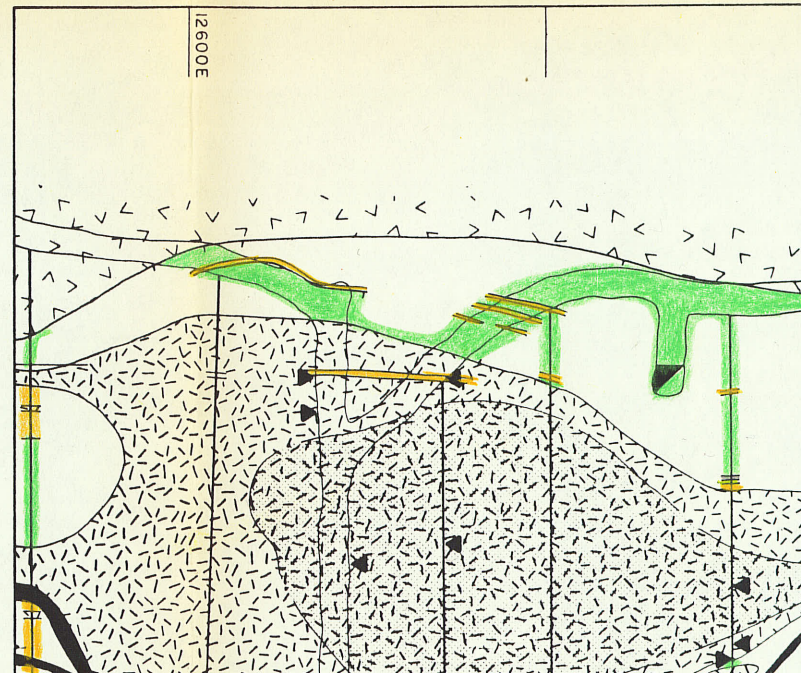
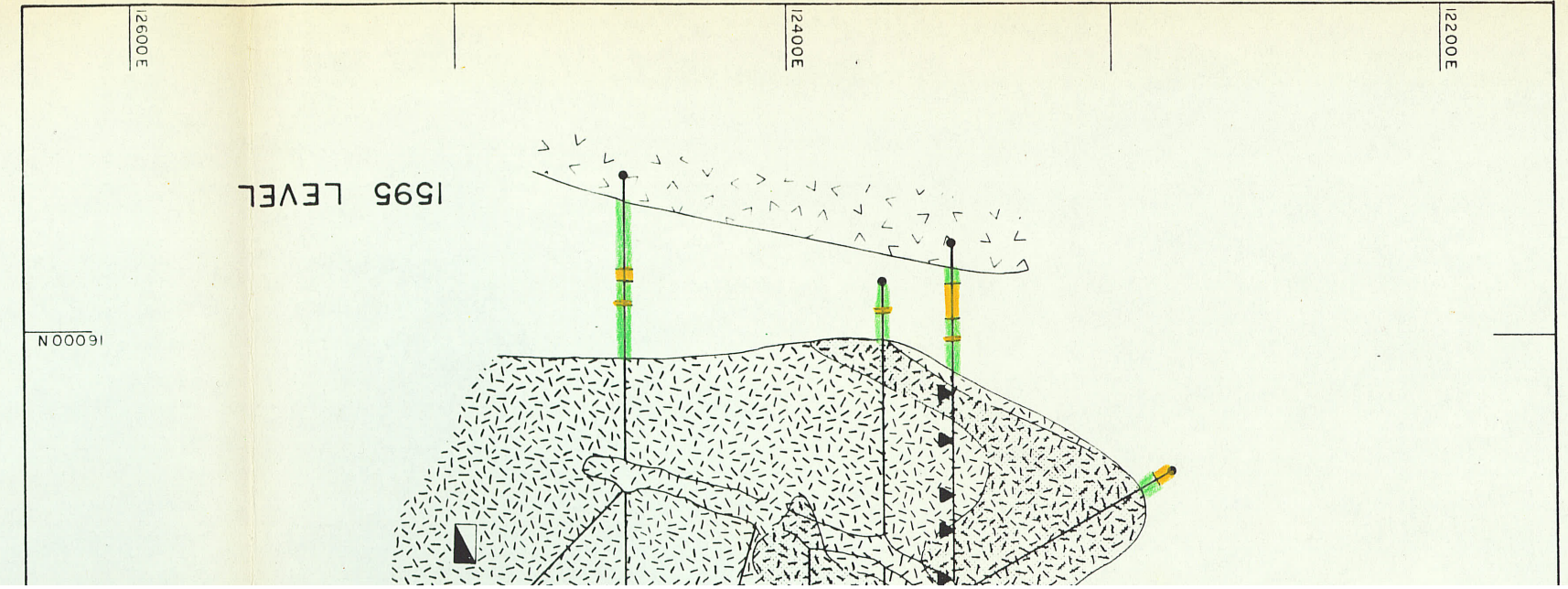
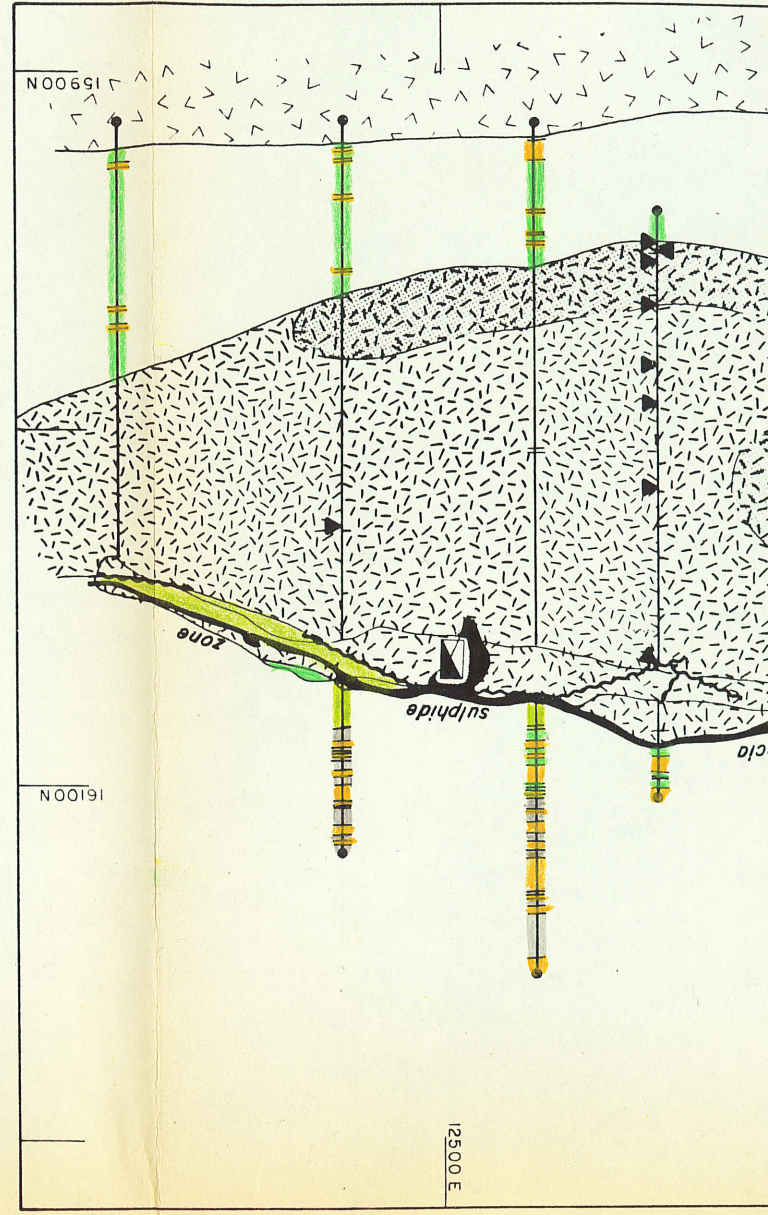
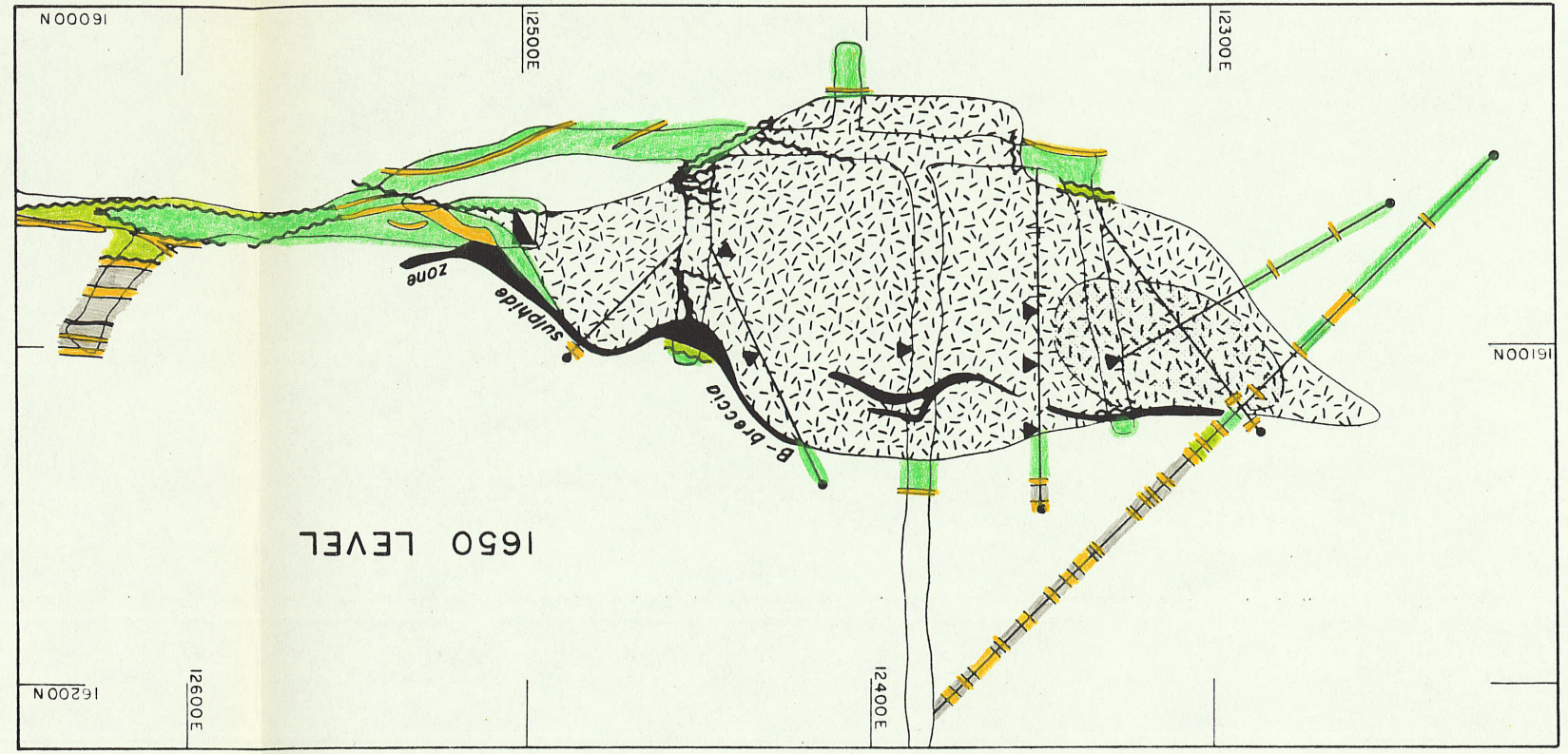








FIGURE



- Geologic
- Fault
- Diamond
- Shaft
- Sample

- GRANITE
- SULPHIDE
- ULTRAM
- AMPHIB
- AMPHIB
- BIOTITE
- approxim

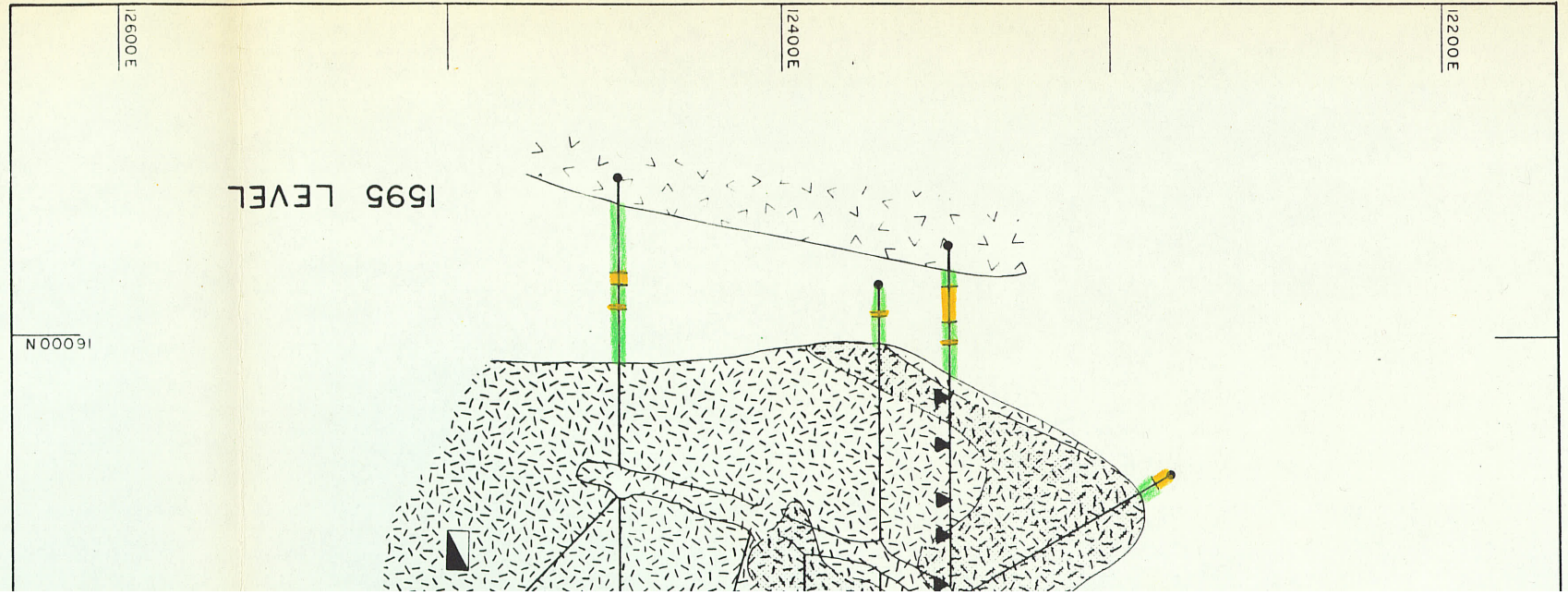
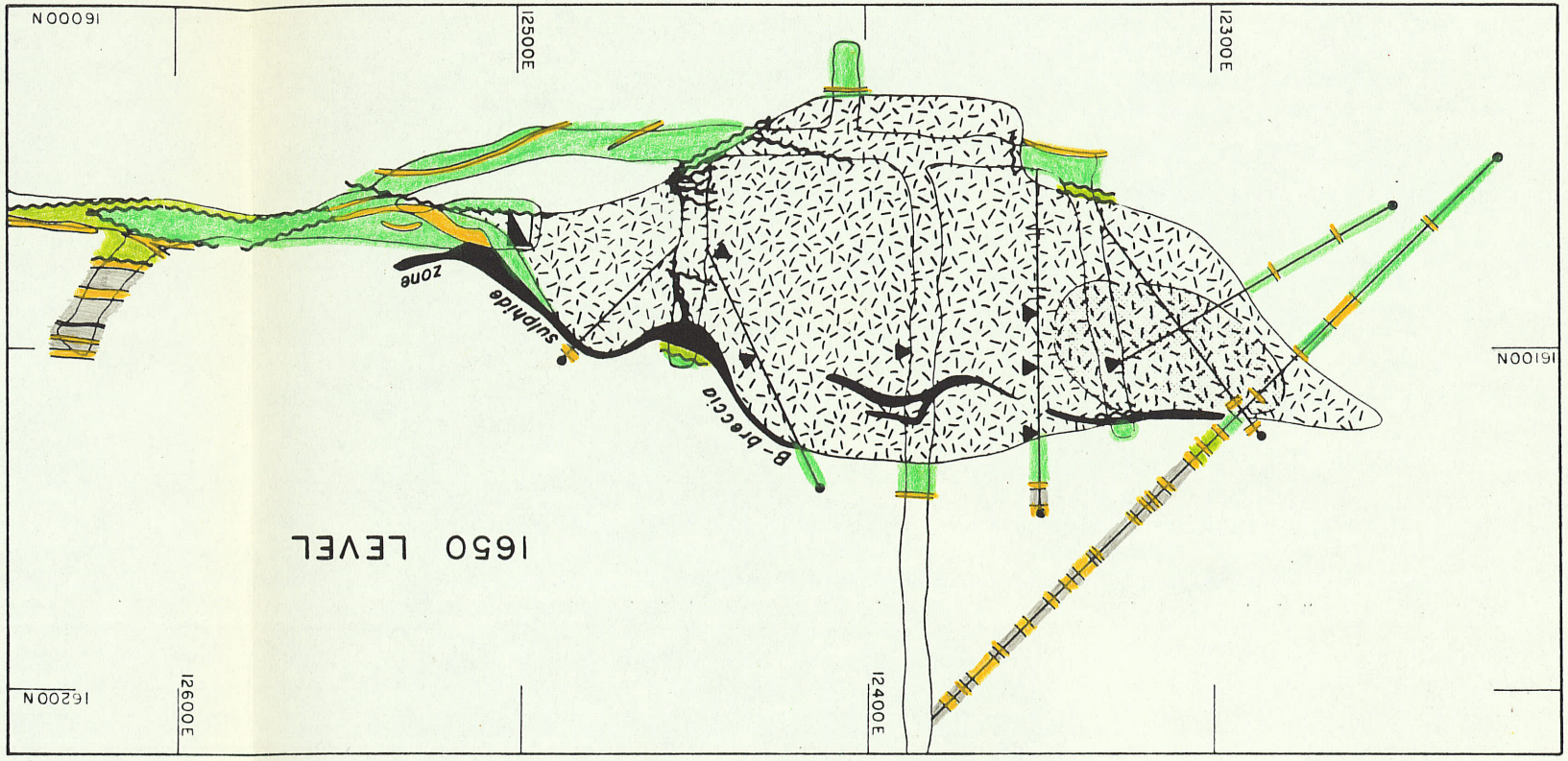
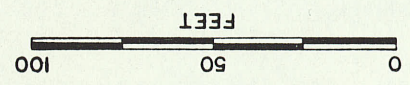


FIGURE 5



- ▲ Sample location
- ◼ Shaft
- Diamond drill hole
- ~~~~~ Fault
- Geological boundary

- approximate outline of disseminated ore
- GRANITE
- ▨ SULPHIDE MINERALIZATION (massive, disseminated)
- ▨ ULTRAMAFIC ROCKS (undivided)
- AMPHIBOLITE
- ▨ AMPHIBOLITE - BIOTITE GNEISS
- BIOTITE-CHLORITE SCHIST